

Investigating the role of the planar cell polarity (PCP) protein CELSR1 in breast cancer

Author: Ladislav Klena

Supervisors: Dr. Caroline Formstone, Dr. Maria Dimitriadi and Professor Jameel Inaal

Submitted to the University of Hertfordshire in partial fulfilment of the requirement of the degree of PhD

August 2023

Acknowledgments

I would like to thank **Dr. Caroline Formstone**, who as my primary supervisor provided exceptional guidance and supported me in the kindest way possible throughout my PhD, thesis writing and beyond, above any expectations

I would also like to thank **Dr. Maria Dimitriadi**, my second supervisor who also provided great support during my PhD, thesis writing process and beyond

I would like to thank **Dr. Maria Braoudaki** for her advice on computational biology and qPCR data experimental procedures and beyond

I would like to thank the **technical team** in the science building for their continued support in the laboratories

I would like to thank **my colleagues, current and previous**, for their continued support and mood lightening capabilities

I would like to thank my **friends and family** for their continued support, and for being fans of my research

Abstract

Planar cell polarity (PCP) is essential for generating highly organized tissue structures and for directional cell movement/migration. The role of PCP in embryogenesis is well-documented, however its role in adult pathologies, such as cancer, is a relatively new field of research. A growing number of publications imply a significant role for PCP proteins in cancer progression and metastasis. PCP is governed by several cytosolic proteins and transmembrane receptors including the G-protein coupled receptor CELSR1. Research studies have raised the hypothesis that CELSR1 acts as a tumour suppressor in breast cancer. Our research aim was to characterise an in-vitro model to understand the molecular/cellular basis of the role of CELSR1 in breast cancer. Computational biology was used to assess CELSR1 expression in breast cancer sub-types and its impact on patient survival. Characterisation of breast cancer cell lines representing increasingly invasive breast cancer was performed through qPCR and western blot analysis to investigate CELSR1 expression and immunocytochemistry to investigate CELSR1 protein distribution. RT-PCR and Sanger sequencing were used to assess differential splicing of the C-terminus of *CELSR1*. Gain and loss-of-function assays were conducted to test the tumour suppressive functions of CELSR1. Bioinformatics analysis has revealed that *CELSR1* expression is increased in the less invasive Luminal A subtype of breast cancer, and that higher expression of *CELSR1* has positive impact on overall patient survival. *In vitro* studies of common breast cancer cell lines revealed that CELSR1 is more highly expressed in less invasive luminal type cell lines, but its expression is reduced in more invasive type cell lines. Furthermore, whilst less invasive breast cancer cell lines exhibit cortical enrichment of CELSR1, CELSR1 becomes localised in intracellular punctate structures adjacent to the nucleus within the highly invasive breast cancer cells. Finally, we find that overexpression of *Celsr1* in highly invasive breast cancer cell lines reduces their migratory ability and proliferation. Taken together, our study is consistent with a role for CELSR1 as a tumour suppressor in breast cancer. Future studies will aim to decipher its mechanism of action.

Contents

1. Introduction	11
1.1. – Cell Polarity	11
1.2. Overview of planar polarity	11
1.2.1. Planar Cell Polarity	12
1.2.2. Wnt-PCP	15
1.2.3 The role of PCP in embryonic development	18
1.2.4 - PCP signalling and the cytoskeleton	19
1.3. – Mammary gland development.....	20
1.3.1. - Mammary gland development <i>in utero</i>	21
1.3.2. – Mammary gland development at puberty.....	21
1.3.3 Mammary gland development during pregnancy and lactation	23
1.3.4. Involution	23
1.4. Evidence of a role for PCP in mammary gland development	24
1.5. Overview of breast cancer	25
1.5.1 Subtypes of breast cancer.....	27
1.5.2 – Immunotherapy in breast cancer.....	30
1.6 Evidence for a role of cell polarity proteins in cancer	31
1.6.1 Apico-basal polarity in cancer	31
1.6.2 Planar cell polarity in cancer	32
1.7 -The CELSR 1 receptor	33
1.7.1. Splice variants of <i>CELSR1</i>	33
1.8 The FZD6 receptor.....	34
1.9 WNT-PCP and cancer	34
1.10 Evidence for a role of FZD6 in breast cancer	36
1.11 CELSR1 receptors in breast cancer.....	37
1.12 EMT	39
1.13 <i>In vitro</i> models of cancer	40
1.13.1 Wild-type control breast epithelial cell line, MCF10A	41
1.13.2 Luminal A and B-type cell lines	41
1.13.3 MCF10A progression series.....	44
1.14 Aims and Objectives.....	45
2 – Materials and Methods.....	47
2.1. – Bioinformatics	47
2.1.1. – Analysis of mRNA expression and copy-number variation (CNV).....	47
2.1.2 - Kaplan-Meier survival plots	47
2.1.3 – UALCAN	47

2.1.4 - GEPIA2.....	48
2.1.5 - Gene set enrichment analysis (GSEA).....	48
2.2. - Cell lines.....	48
2.2.1 - Cell line authentication and mycoplasma testing.....	49
2.3 Ethical Approval for study of human NK cells and breast cancer tissue.....	49
2.4. RNA extraction and quality assessment	50
2.5. RT-PCR and direct sequencing of variant mRNAs	50
2.5.1. Agarose gel electrophoresis for detection of differentially spliced variants and excision of bands.....	51
2.5.2 DNA sequencing and analysis of sequencing data.....	52
2.6. - Quantitative PCR (qPCR)	52
2.6.1. Housekeeping gene selection	52
2.6.2. Multiplex qPCR.....	53
2.7. SDS-PAGE and western blot analysis	53
2.7.1. Preparation of whole cell lysates.....	53
2.7.2 Measurement of protein concentration.....	53
2.7.3. SDS-PAGE	54
2.7.4. - Western blot analysis.....	54
2.7.5 Antibodies for western blots	55
2.8. Immunocytochemistry.....	56
2.8.1. - Antibodies for immunofluorescence	57
2.8.2 Fluorescence microscopy.....	58
2.9 3D spheroid assays.....	58
2.9.1. Matrigel.....	58
2.9.2 – Agarose	58
2.9.3. – Alginate beads in agar moulds.....	59
2.9.5 - Ultra-low attachment plates/spheroid plates	59
2.9.6 – Alginate beads.....	59
2.11 Over-expression of mCelsr1 in breast cancer cell lines	60
.....	62
2.12 - Lentiviral based shRNA knockdown of <i>CELSR1</i>	62
2.12.1 Lentiviral based ShRNAs.....	62
2.12.2 - Lentivirus production using Calcium phosphate method.....	62
2.12.3 – Lentivirus production using Lipofectamine 3000 method.....	63
2.12.4 – Lentiviral titre determination.....	64
2.12.5 Lentiviral transduction	64
2.12.6 – Wound healing assay	65

2.12.7 MTT assay.....	65
2.14 – Figures.....	66
3. RESULTS – <i>IN SILICO</i> CHARACTERISATION OF THE ROLE OF CELSR1 AND FZD6 IN BREAST CANCER	67
3.1 Introduction	67
3.2 <i>CELSR1</i> and <i>FZD6</i> mRNA expression are both altered in breast tumour samples.....	67
3.3 Opposing impact of <i>CELSR1</i> and <i>FZD6</i> on patient survival with different breast cancer sub- types.....	68
3.4 GSEA software predicts positive and negative enrichment of gene pathways when <i>CELSR1</i> and <i>FZD6</i> expression is altered in breast cancer	71
4. RESULTS - CHARACTERISATION OF <i>IN VITRO</i> BREAST CANCER CELL LINES AS POTENTIAL MODELS TO INVESTIGATE CELSR1 AND FZD6 FUNCTION IN BREAST CANCER.....	82
4.1 Introduction	82
4.2 Multiplex qPCR reveals <i>CELSR1</i> mRNA levels are highest in less invasive luminal type cell lines whereas <i>FZD6</i> mRNA levels are highest in more invasive type cell lines, consistent with patient data	83
4.3 Investigation of <i>CELSR1</i> and <i>FZD6</i> protein expression in breast epithelial and breast cancer cell lines.....	85
4.4 Investigation of CELSR1 c-terminal mRNA sequence in breast cancer cell.....	90
4.4.1 RT-PCR analysis suggests that CELSR1-PDZ encoding mRNAs are often truncated and lack the PDZ motif	90
4.4.2 RT-PCR of a 150bp c-terminal sequence reveals the presence of a novel, human-specific PDZ motif containing transcript in foetal tissue and breast cancer cell lines.....	93
4.4.3 RT-PCR analysis of the CELSR1 c-terminus transcripts highlights a duplication of the PDZ motif sequence in genomic DNA which is specific to the Great Apes	95
4.4.4 Investigation of FZD6 mRNA splicing products in breast cancer cell lines failed to identify any differences in breast cancer cell lines	97
4.5 Comparison of CELSR1 and FZD6 antibody staining patterns in breast epithelial and breast cancer cell lines.....	97
4.5.1 – CELSR1-sc and CELSR1-iso antibodies reveal distinct patterns of expression and co- localisation with different cytoskeletal elements in control MCF10A cells.....	97
4.5.2 CELSR1-sc antibody shows cortical enrichment and co-localisation with actin in luminal type common breast cancer cell lines whereas staining becomes more punctate and is eventually lost in the more invasive common cell lines	98
4.5.3 CELSR1 antibody staining reveals cortical enrichment in Luminal type common cell lines but is lost and internalised in basal type common cell lines	98
4.5.4. FZD6 staining of common cancer cell lines reveals cortical enrichment but no co- localisation with CELSR1	100
4.6 MCF10A series	103
4.6.1 CELSR1sc staining in MCF10A series reveals a decrease with increasing invasiveness, but an increasing number of cells stain positive with the CELSR1iso as invasive potential increases	103

5. Results - Assessing the role of CELSR1 in breast cancer using model cell lines and <i>in vitro</i> functional assays	108
5.1 Introduction	108
5.2 Evaluation of different methodologies to generate 3D spheroids from breast cancer cell lines	108
5.2.1. Matrigel.....	109
5.2.2. Agarose	109
5.2.3 Alginate beads in agar moulds.....	109
5.2.4 Ultra-low attachment plates.....	110
5.2.5 Alginate beads.....	111
5.2.6 – On-top Matrigel culture	113
5.3 Investigation of efficiency of commercial shRNAs for CELSR1-specific knockdown in breast epithelial and breast cancer cell lines.....	114
5.3.1 CELSR1-cadherin 3 domain shRNA provides efficient knock-down of CELSR1 protein	114
5.3.2 CELSR1 knockdown with Cad 3 shRNA and 3'UTR shRNA is toxic to BT474 cells	119
5.4 Over-expression of mouse Celsr1 in TNBC -type cell line, MDA-MD-231 cells.....	120
5.4.1 Validation and phenotypic evaluation of CELSR1 gain-of-function experiment.....	122
5.4.2 Functional assays to investigate cell proliferation, cell migration and colony formation .	123
6. DISCUSSION.....	127
6.1 Overview	127
6.2 Assessment of available human breast cancer cell lines as appropriate <i>in vitro</i> models for studying the role of CELSR1 and FZD6 in breast cancer	128
6.3 What is the role of CELSR1 in breast cancer?	131
6.3.1 Does CELSR1 play multiple roles in breast cancer progression?	132
6.3.2 CELSR1 antibody staining of fixed cells shows inconsistencies between antibodies but for CELSR1-sc the immunocytochemistry data reflects the Western blot data	136
6.3.3 CELSR1-iso staining overlaps with the EMT marker, vimentin	136
6.3.4 – Does the CELSR1 PDZ isoform play an important role in breast cancer?	139
6.3.5 Functional studies support a role for CELSR1 as a tumour suppressor	141
6.3.6 3D functional assays.....	143
6.3.7 Enrichment analysis suggest oncogenic/metastatic and tumour protective pathways downstream of FZD6 and CELSR1 receptor signalling respectively	144
6.3.8 Investigation of CELSR1 expression experimentally in patient samples.....	146
6.4 Conclusion.....	147
References	148
Appendix	174

List of Figures

Figure 1 - Planar cell polarity phenotype results in wing hairs oriented away from the fly body towards the distal direction.....	14
Figure 2– Establishment of PCP in vertebrates.	15
Figure 3 -Comparison of WNT signalling pathways..	17
Figure 4 - Convergent extension in neural tube development.....	19
Figure 5 - Showing the 4 stages of human mammary gland development from in utero to post-pregnancy.	26
Figure 6 - Breast cancer progression	27
Figure 7 - Illustration of CELSR 1 and FZD6 GPCRs.	35
Figure 8 - Showing the characteristics of the cell lines used in this project as well as their prognostic significance mirrored to tumours occurring in breast cancer patients.....	43
Figure 9 - Characteristics of the MCF10A series cell lines.....	44
Figure 10 - Various methods used for 3D cell culture.	62
Figure 11 - CELSR1 and FZD6 expression is altered in breast cancer and affects patient survival. ...	70
Figure 12 - Copy number variations vs mRNA expression, survival plots and subtypes..	70
Figure 13 - CELSR1 and FZD6 expression varies across breast cancer subtype.	72
Figure 14 - Gene sets positively enriched by CELSR1.	75
Figure 15 - Significantly positively enriched gene sets by CELSR1.....	77
Figure 16 - Gene sets positively enriched by FZD6.....	80
Figure 17 - Gene sets positively enriched by FZD6.....	81
Figure 18 - qPCR method description.	84
Figure 19 - Multiplex qPCR analysis.....	86
Figure 20 - CELSR1 protein expression analysis by western blot in the common cell lines.....	88
Figure 21 - CELSR1 protein expression analysis by western blot in the MCF10A progression series	90
Figure 22 - EKP variant sequencing figure, showing bands after agarose gel electrophoresis and subsequent Sanger sequencing.	92
Figure 23 - PDZ variant sequencing figure, showing bands after agarose gel electrophoresis and subsequent Sanger sequencing.	94
Figure 24 - PDZ+ variant sequencing figure, showing bands after agarose gel electrophoresis and subsequent Sanger sequencing	96
Figure 25 - Sequence alignments of the Celsr1 C-terminal tail PDZ region across different species	97
Figure 26 - ICC on MCF10A cell lines using the CELSR1sc and CELSR1iso antibodies. . Negative control – secondary antibody only staining of MCF10A cells.....	99
Figure 27 - ICC on Luminal and Basal-type breast cancer cell lines. A, B.	102
Figure 28 - ICC on MDA-MB231 (MB231) with various markers to determine the identity of intracellular puncta which suggest containment of CELSR1.....	102
Figure 29 - - ICC with FZD6 on common cell lines.	104
Figure 30 - ICC on the MCF10A progression series using the CELSR1sc antibody. A-C.	105
Figure 31 - ICC on the MCF10A progression series using the CELSR1iso antibody.	106
Figure 32 - MCF10A progression series quantification of positive CELSR1 staining. A.....	107
Figure 33 - ICC of BT474 cells grown in Matrigel.....	109
Figure 34 - Breast cancer cells forming spheroids on a layer of alginate. A, B.	110
Figure 35 - – Breast cancer cell line spheroids in 1% alginate beads in agar moulds. A.....	111
Figure 36 - Breast cancer cells forming spheroids in ultra-low attachment plates. A.	111
Figure 37 - Imaging of BT474 and T47D spheroids in alginate beads.....	112
Figure 38 - MCF10A spheroid grown on a layer of growth factor reduced Matrigel.....	113
Figure 39 - Phenotypes of MCF10 WT and MCF10A shRNA transfected cells at various densities.	116
Figure 40 - Showing shRNA locations in CELSR1.	117

Figure 41 - ICC of MCF10A KO cells compared to MCF10A WT.....	118
Figure 42 - MCF10A KO ICC quantification and qPCR data.	119
Figure 43 - BT474 transfected with CELSR1 specific shRNAs cells after being placed in selective media (puromycin)	120
Figure 44 - Transfection of mCelsr1-GFP into basal like MDA-MB231 cells	121
Figure 45 - Brightfield and fluorescent images of MDA-MB231 mCelsr1 transfected cells and pcDNA3 control cells.	123
Figure 46 - Western blots of anti-GFP and anti-CELSR1iso antibodies with MDA-MB231 GOF cell samples.....	124
Figure 47 - MTT proliferation assay of MDA-MB231 cells transfected with a pcDNA3 empty vector (control) and with mCelsr1-GFP.....	125
Figure 48 - Scratch assays conducted on MDA-MB231 cells transfected with mCelsr1-GFP.	126

Appendix Figures

AFig 1 – MDA-MB231 cells stained with DAPI and CELSR1iso.	175
AFig 2 – <i>CELSR1 splice variants</i>	176
AFig 3 – Coomassie stained SDS-PAGE gels.....	176
AFig 4 – WB1.....	177
AFig 5 – WB2.....	178
AFig 6- WB3.	179
AFig 7 – WB4.....	180
AFig 8 – WB5.....	181
AFig 9 – WB6.....	182
AFig 10 – WB7.....	183
AFig 11 – WB8.....	184
AFig 12 - WB9.	185
AFig 13 – WB10.....	185
AFig 14 – WB14.....	187
AFig 15 – WB15.....	188
AFig 16 – WB16.	189
AFig 17 - WB17.	190
AFig 18 – WB18.....	191
AFig 19 – WB19.....	192
AFig 20 – MCF10A cells express smooth muscle actin and P63.....	193

Abbreviations

CNV – Copy number variation/s
DCIS – Ductal carcinoma *in situ*
PDZ – PSD95, DLG-A, ZO1 domain
PCP- Planar cell polarity
ABP – Apico-basal polarity
NFKB –NF Kappa B signalling
FGF- Fibroblast growth factor
IDC – Invasive ductal carcinoma
IBC – Invasive breast cancer
TDLU - Terminal duct lobular unit
TNBC –Triple negative breast cancer
ER – Estrogen receptor
PR - Progesterone receptor
EGFR – Epidermal growth factor receptor
EMT- Epithelial to mesenchymal transition
GPCR – G-protein coupled receptor
PD – Pure DCIS
MD- Mixed DCIS
TIF – Tumour interstitial fluid
ECM – Extracellular matrix
TCGA –The cancer genome atlas
GSEA- Gene set enrichment analysis
RT- Room temperature
TPM - Transcripts per million
BRCA- Breast cancer
RACE –Rapid amplification of cDNA ends

1.Introduction

1.1. – Cell Polarity

Cell polarity is essential for generating highly organised tissue structures and its loss has devastating effects both in embryonic and adult tissues (Butler & Wallingford, 2017). Cell polarity also defines tissue function. A major type of cell polarity is apico-basal polarity (ABP). ABP distinguishes the ‘top’ of a cell (apical) from the ‘bottom’ (basal) and is essential for the formation of epithelial tissues including the tubular structures of the body. (Gandalovičová et al., 2016; Wilson, 2011). In the tubes of the breast duct for example, alignment of apical cell interfaces defines the luminal side of the duct, this aspect is responsible for lactation and for the release of milk into the lumen during pregnancy (Neville & Monks, 2018). A further type of cell polarity is defined as front-rear (sometimes also called front-back and anterior-posterior polarity) which drives directional cell migration during embryogenesis and promotes individual and collective cell migration during cancer metastasis (Fenteany et al., 2000; Gandalovičová et al., 2016). Planar polarity is a third type of cell polarity which operates perpendicular to ABP (Fig.1 and Fig.2). Planar cell polarity (PCP) is defined by a specific molecular pathway, depends upon apico-basal polarity for its manifestation and has features in common with front-rear cell polarity. PCP operates across a tissue and orients cell structures and cell behaviours in the tissue plane. Thus, ABP and PCP are characteristic of organised tissues. Loss of ABP is one of the hallmarks of cancer (Hanahan & Weinberg, 2000). How dysfunctional PCP impacts on tumour formation and progression, however, is not well understood. This thesis has sought to identify relevant *in vitro* models with which to study the role of PCP proteins in breast cancer and to investigate how the key PCP protein CELSR1 impacts on the metastatic process of breast cancer.

1.2. Overview of planar polarity

Planar polarity is an essential process for embryonic development (Copp et al., 2013; Nikolopoulou et al., 2017). Currently two molecular pathways of planar polarity have been identified, Fat and Dachshous (Casal et al., 2006) and PCP. Within PCP the same protein components define two further planar polarity systems, namely the core-PCP pathway, and Wnt-PCP. Each planar polarity

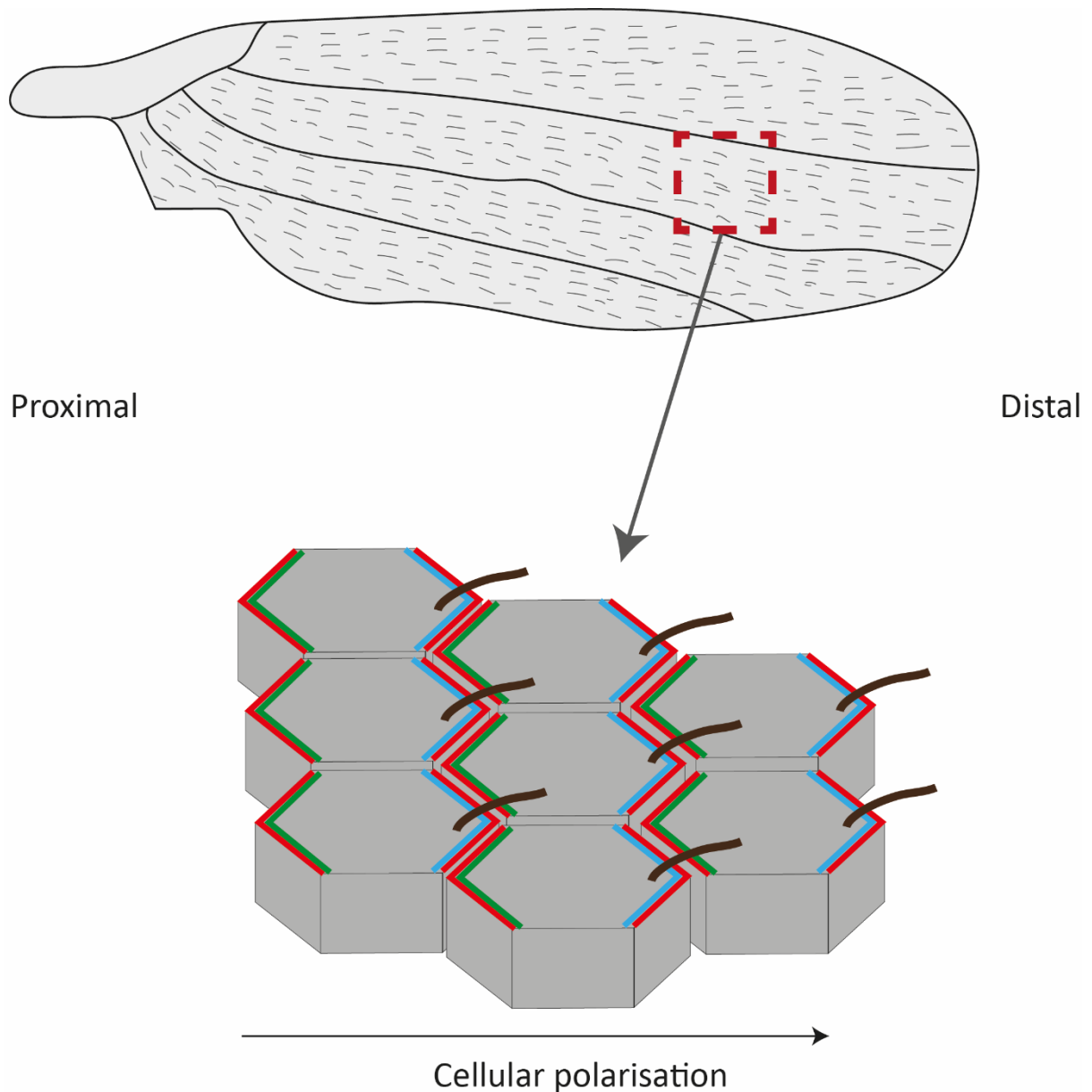
system however is based on the same fundamental premise in that they share common functionality in the alignment of cell effects (cell structures and cell behaviours) along particular body axes. They also generate protein asymmetry at cell-cell interfaces across a tissue which depends upon cadherin-based recognition of transmembrane proteins at the cell surface (Aw & Devenport, 2017; Axelrod, 2020). Without PCP in particular, the neural tube will not close and branching of lung and kidney tubules fails (Brzoska et al., 2016; Kunimoto et al., 2017; L. L. Yates, Papakrivopoulou, et al., 2010; L. L. Yates, Schnatwinkel, et al., 2010). PCP is defined as a molecular pathway that acts in the plane of an epithelium and is evident within epithelia following establishment of apico-basal polarity (Fig. 1 and Fig.2) (Muthuswamy & Xue, 2012). In developing embryos however, PCP proteins facilitate collective cell movement both in the epithelial plane but also in a radial (outside-in) orientation (Panousopoulou et al., 2016). Thus, PCP proteins define organisation within epithelia and alignment of cell/tissue structures and behaviours along specific body axes (Davey & Moens, 2017; Devenport, 2014; Munoz-Soriano et al., 2012). Planar polarity however has not been extensively studied in humans, indeed most of our knowledge of this process comes from animal models of embryonic development. (Casal et al., 2006).

1.2.1. Planar Cell Polarity

Planar cell polarity (PCP) was first described in insects (Lawrence, 1975; Lawrence & Green, 1975). Studies on *Drosophila* revealed mutagenised flies which exhibited disruption of adult wing hair orientation along its proximo-distal wing axis (proximal is closest to the body) (Fig. 1). Identification of the mutated genes revealed a number of membrane-bound and cytoplasmic protein components acting within a single 'core' planar polarity pathway (Feiguin et al., 2001; Lawrence, 1975) including the seven-transmembrane (7TM)-cadherin Flamingo and the 7TM protein Frizzled. Decades on, these core-PCP pathway proteins have been shown to align bristles on the insect notum and abdomen as well as the rotation of the geometrical arrangement of ommatidial units within the *Drosophila* eye (Strutt, 2009). The transmembrane and cytoplasmic PCP proteins enrich to opposing sides of a cell resulting in a visible molecular asymmetry (Feiguin et al., 2001; Lawrence & Green, 1975). Asymmetry

is a hallmark of PCP. Early studies on the *Drosophila* wing noted that protein asymmetry aligned with the axis of PCP defined by wing hair alignment (proximal-distal) (Usui et al., 1999). Thus, the described molecular asymmetry enables visualisation of PCP processes in tissues when PCP protein enrichment to opposing cell interfaces can be labelled (Fig. 1 and Fig. 2). The transmembrane Frizzled receptor is thought to sense shallow pervasive planar polarity cues within a tissue (e.g., Wnt morphogens) whilst the four-transmembrane protein Vang together with Flamingo, amplify the signal within individual cells (W. S. Chen et al., 2008; J. Wu & Mlodzik, 2008). The polarity signal is then transmitted between neighbouring cells across a tissue plane via homodimer bridges formed by Flamingo (Usui et al., 1999). Asymmetry is achieved by the cytoplasmic proteins (Dishevelled, Diego and Prickle) competing and inhibiting each other resulting in their mutual exclusivity to the opposing sides of the cell. Furthermore, cytoplasmic proteins may further activate downstream signalling pathways as shown in Fig 2.

PCP components are evolutionarily conserved. In vertebrates, PCP function has been elucidated by study of amphibian, teleost fish and mouse models (Ossipova et al., 2015; Stubbs et al., 2006; Villasenor et al., 2010; Wada & Okamoto, 2009; J. Wu & Mlodzik, 2017). Vertebrate PCP proteins play a conserved role in the alignment of cell behaviours along specific body axes such as the head-to-tail alignment of neuronal migration in the hindbrain of teleost fish and mice (Sittaramane et al., 2013) and the local coordinated rearrangement of groups of hair follicle cells which results in the global alignment of obliquely oriented hair down-growth along the head-to-tail axis of the mouse back skin (Cetera et al., 2018; Devenport & Fuchs, 2008). The asymmetric enrichment and asymmetric protein:protein interactions of vertebrate PCP proteins are thought to be essentially the same as those of *Drosophila* (Devenport & Fuchs, 2008). On the proximal side of the cell, Vangl (Vang-like) recruits Prickle (Pk) and on the distal side, Frizzled recruits Dishevelled (Dvl) 1-3 (Dsh in *Drosophila*). Dvl then recruits Diversin (Ankrd6), which is a possible orthologue of Diego in *Drosophila* (Fig.2) (W. S. Chen et al., 2008).



Key (*Drosophila* PCP components) -

- Flamingo (*fmi*)/ Starry Night (*stan*)
- Van Gogh/ Strabismus, Prickle
- Frizzled, Dishevelled, Diversin

Figure 1 - Planar cell polarity phenotype results in wing hairs oriented away from the fly body towards the distal direction. Illustration of *Drosophila* wing is shown (top). Lower schematic illustrates the molecular mechanism of PCP establishment in individual wing hair cells – components of PCP are distributed asymmetrically to polarise individual cells (bottom).

The Flamingo homologue, *Celsr1*, generates molecular bridges between neighbouring cells across a tissue along with Frizzled and Vangl (Devenport et al., 2011). Robust enrichment of protein asymmetry provides visual evidence for core-PCP processes in vertebrate tissues as it does in insects (Davies et

al., 2005; Devenport & Fuchs, 2008). Thus, vertebrate, and invertebrate PCP signalling exhibit many shared features.

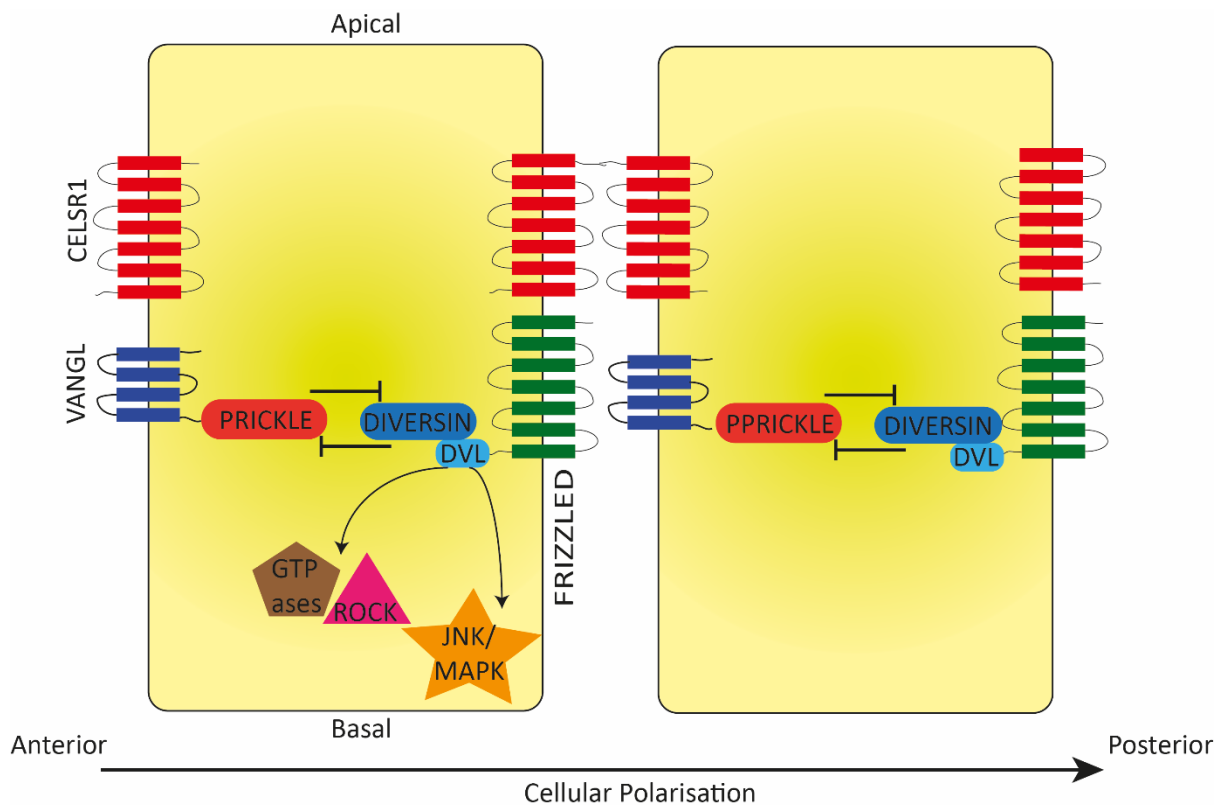


Figure 2 – Establishment of PCP in vertebrates. PCP components enrich to opposing sides of the cell creating asymmetry, which is a hallmark of PCP. The PCP pathway signals downstream to GTPases and JNK/MAPK pathways, which have a role in cell rearrangements

1.2.2. Wnt-PCP

Some PCP proteins are strongly associated with the growth factor and morphogen, Wnt (Barrow, 2011; Corda & Sala, 2017; Daulat & Borg, 2017; B. Gao, 2012; Habas et al., 2001; Humphries & Mlodzik, 2018; Katoh, 2005; Koval et al., 2011; C. Li et al., 2019; Luga et al., 2012; Matsumoto et al., 2010; Naz et al., 2012; vanden Berg & Sassoon, 2009; VanderVorst et al., 2019, 2023; Wada & Okamoto, 2009; J. Wu & Mlodzik, 2017; Y. Yang & Mlodzik, 2015), also known as wingless in *Drosophila* (Lawrence, 1975, 2001). There are a number of Wnt signalling pathways (Fig.3) and Wnt-PCP is defined as a branch of Wnt signalling that is known as non-canonical which provides directional information within a developing tissue. The canonical Wnt signalling pathway however is more broadly involved in tissue growth and fate and is essential for embryonic development and tissue homeostasis in adults

(MacDonald et al., 2009). The canonical pathway is well-studied and is known to play a major role in various human diseases including cancer (VanderVorst et al., 2019, 2023). Canonical Wnt proteins bind to specific Frizzled receptors leading to β -catenin stabilisation and nuclear localisation (hence also called the β -catenin pathway) which impacts on gene transcription to alter cell fate. So far it has not been possible to identify all specific WNT-FZD interactions and the exact pathways which they activate, since FZDs can bind multiple WNT ligands and activate more than one signalling pathway (Alrefaei, 2021; Dijksterhuis et al., 2014). Whilst all 10 FZD receptors activate the canonical (β -catenin) pathway, there are specific FZDs involved in the activation of the and Wnt-calcium pathways (Alrefaei, 2021; Sun et al., 2021) and the WNT-PCP pathway. Among those identified that seem to be specific to the WNT-PCP pathway are FZD1, 2 and 3, FZD6 and FZD7 (Navajas Acedo et al., 2019; Y. Yang & Mlodzik, 2015). It is also important to note that specific WNT ligands are hypothesized to activate different WNT signalling pathways (Alrefaei, 2021; Y. Yang & Mlodzik, 2015). For example, WNT5 and WNT11 have been reported to primarily activate the WNT-PCP pathway and are not involved in the stabilisation of β -catenin (Andre et al., 2015; Veeman et al., 2003) . On the other hand, the WNT-Calcium pathway has been shown to be primarily activated by WNT5, WNT7 and WNT10 (Thrasivoulou et al., 2013). It has been experimentally shown that besides the FZD-WNT interaction, specific co-receptors on the cell surface determine which WNT ligands bind to which FZD receptor as well as the pathway activated (Eubelen et al., 2018). As mentioned, Wnt-PCP utilises a distinct set of Frizzled receptors and provides cells and tissues with directional signals e.g. the orientation and alignment of collective cell movements along specific body axes (B. Gao, 2012; Sepich et al., 2011; Sokol, 2015; Y. Wang et al., 2016; J. Wu & Mlodzik, 2017). Wnt-PCP has been implicated in axon guidance along the head-to-tail axis of the vertebrate central nervous system (Tissir & Goffinet, 2013) but also, intriguingly, in the proximo-distal elongation of vertebrate limbs (Barrow, 2011; B. Gao & Yang, 2013). Study of animal models suggests that Wnt-PCP utilises morphogenetic gradients of specific Wnt ligands as directional cues for collective cell migration (Corda & Sala, 2017; Sebbagh & Borg, 2014; VanderVorst et al., 2018; Y. Yang & Mlodzik, 2015). In *Drosophila* Wnt homologues are proposed to be a source of the pervasive shallow axial gradients amplified by the core PCP components to generate

robust alignment of wing hairs for example across the insect wing (Humphries & Mlodzik, 2018; Simons & Mlodzik, 2008; Y. Yang & Mlodzik, 2015). The main difference between Wnt-PCP and core-PCP at the molecular level appears to be how the PCP-specific Frizzled receptor is utilized. In core-PCP, Frizzled works in concert with Flamingo/Celsr1 at the cell membrane propagating the polarity signal across multiple cell diameters via molecular bridges built by the Flamingo:Celsr1/Frizzled/Vang complex (X. Tang et al., 2020; Usui et al., 1999). In Wnt-PCP however, the Frizzled receptor is thought to act as a receptor for specific Wnt ligands (Y. Yang & Mlodzik, 2015). The role of Celsr1 in Wnt-PCP is less well understood: a recent study suggests that Celsr1 may block the chemoattractive effect of Wnt in neuronal migration in the mouse hindbrain (Hummel et al., 2022) and may act in parallel with Wnt-PCP mechanisms. The exact mechanism by which the Wnt-PCP pathway works remains a matter of debate (J. Wu & Mlodzik, 2017).

A comparison between the canonical and non-canonical (Wnt-PCP) pathways is shown in Fig. 3. The mechanisms by which Wnt ligands interact with Frizzled receptors, especially in Wnt-PCP, are still

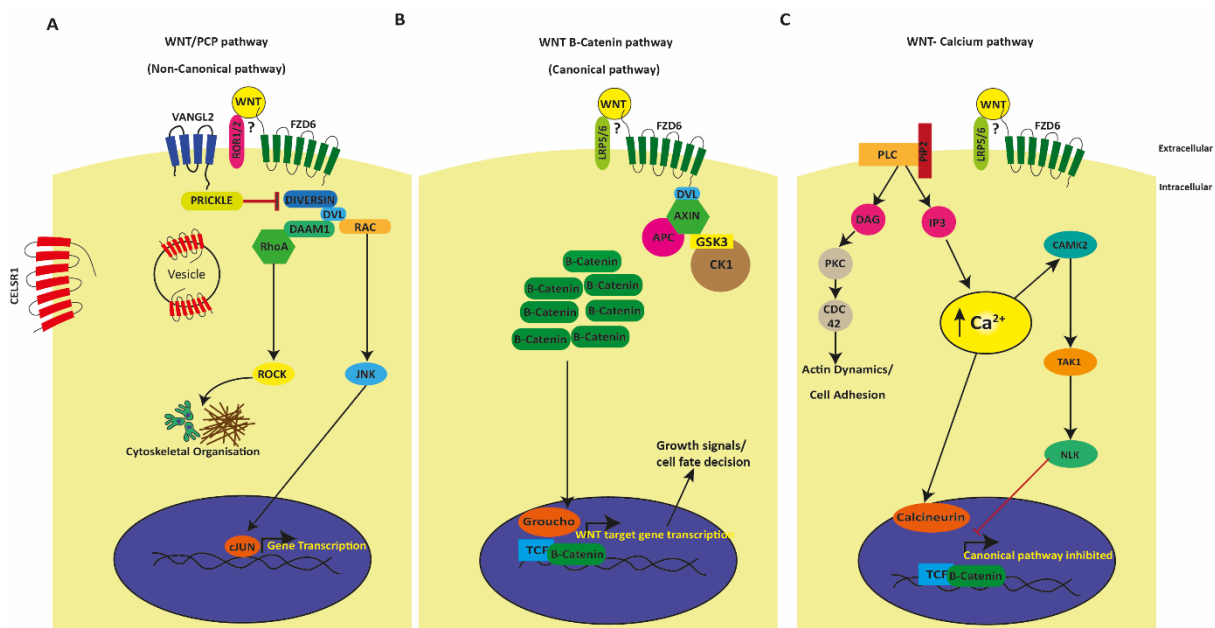


Figure 3 -Comparison of WNT signalling pathways. A. WNT-PCP (Non-canonical) pathway. Involves core PCP components but no beta-catenin. Downstream targets include pathways involved in cytoskeletal organisation and regulation of gene transcription. **B.** WNT- β catenin pathway - activation by FZD ligand leads to β catenin stabilisation, which then activates transcription of genes involved in growth signalling and cell fate determination. **C.** Wnt-Calcium pathway - main factor is intracellular calcium, which regulates pathway activation. Inhibits canonical pathway and regulates actin dynamics, cell adhesion and gene transcription.

unclear. It is well known that Wnt-Frizzled interaction is not monospecific i.e., other membrane co-receptors and components are involved (Eubelen et al., 2018; Gammons & Bienz, 2018; Morgan et al., 2019). Eubelen et al. (2018) has shown the existence of so called “Wnt decoding mechanisms” which distinguish between the otherwise structurally similar Wnt ligands (Miller, 2002). Thus, different co-receptors associated with each Wnt pathway may distinguish their activity and function (Fig.3). Indeed, it is known that transmembrane co-receptors in the different Wnt pathways are not the same (Grumolato et al., 2010; Katoh, 2017).

In summary, in vertebrates Wnt-PCP pathway facilitates collective cell movements to position and/or assemble tissues appropriately in an organised manner (Humphries & Mlodzik, 2018) while the core-PCP pathway promotes the coordinated alignment of tissue structures and cell behaviours in highly organised and complex organs.

1.2.3 The role of PCP in embryonic development

Recent studies suggest that mammalian core-PCP proteins act in 3-dimensions and promote both radial (outside-in) and planar tissue organisation. One example is failure of radial intercalation of thickened trunk ectoderm in the mouse embryo flank to generate the nascent mouse embryonic skin in the *Celsr1* mutant, *Crash*, which precedes failure of the head-to-tail alignment of hair follicle down-growth in the same mutant (Devenport & Fuchs, 2008; Panousopoulou et al., 2016). Notably, hair follicle asymmetry has been shown to be linked to planar cell rearrangements within the hair follicle placode driven by PCP proteins (Cetera et al., 2018). A second example is the failure of convergent extension across the neural plate which precedes failure of apical constriction of midline neural plate cells to generate a midline groove which drives neural fold elevation during neural tube closure (Fig. 4) (Formstone & Mason, 2005). Notably, the same defect in neural tube closure is exhibited by PCP mouse mutants e.g., *Celsr1 Crash/Crash* and a mouse mutant in *Scribble* called circle-tail. *Scribble* is a well-characterised apico-basal polarity determinant discovered in insects. This requirement for 3D ‘tissue’ polarity may explain the severe morphogenetic phenotypes exhibited by mice mutant in PCP genes (Curtin et al., 2003; L. L. Yates, Schnatwinkel, et al., 2010) compared to the adult wing hair and

ommatidial defects observed in *Drosophila melanogaster*. In mammals therefore the term tissue polarity, originally used to define core-PCP function in insects (W. J. Park et al., 1996) may be more suitable to summarise the role of core-PCP proteins in mammalian tissue and organ formation. Moreover, PCP proteins coordinate collective cell behaviours and thus their ability to act in 3-dimensions may explain why their functional disruption in both mouse and humans leads to such severe birth defects in neural tube, lung, and kidney.

1.2.4 - PCP signalling and the cytoskeleton

Since PCP has a fundamental role in morphogenesis and development, it is necessary for it to regulate cell plasticity, such as cell motility and direction. Therefore, PCP has direct control over the cellular cytoskeletal system (Davey & Moens, 2017) . A well characterised developmental event linked to the role of PCP in cytoskeletal regulation is the coordination of convergent extension during neural tube closure (Fig.4) (Curtin et al., 2003; Formstone & Mason, 2005).

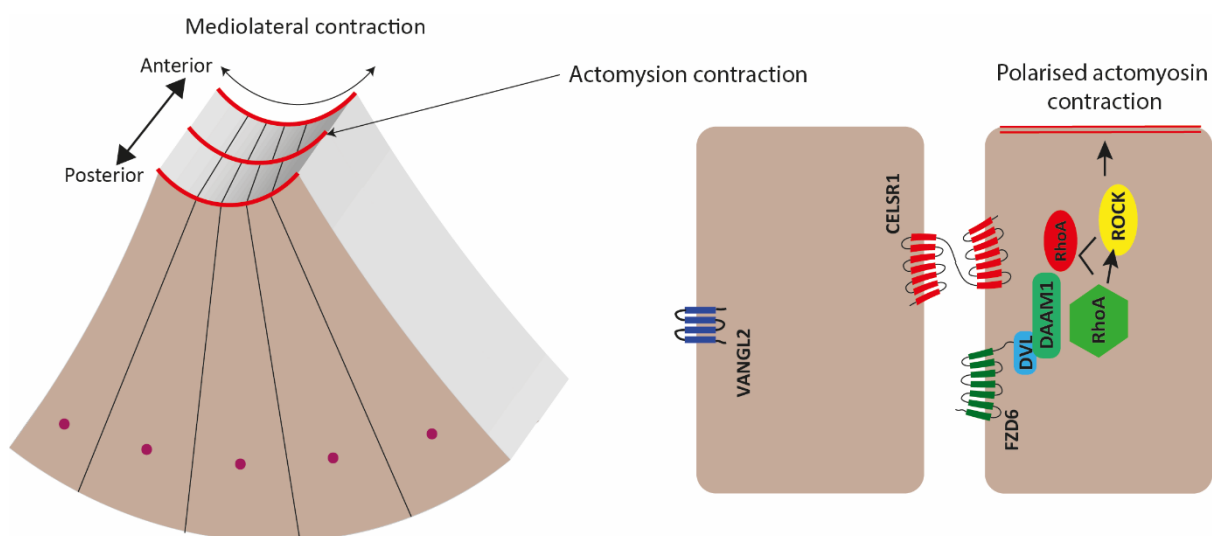


Figure 4 - Convergent extension in neural tube development. PCP regulates polarised actomyosin contraction, which mediates convergent extension during neural tube development. Defects in this pathway result in incomplete neural tube closure, resulting in developmental defects of the neural tube. Left hand schematic shows wedging of the midline neural plate whereas right hand schematic shows asymmetric molecular pathway of PCP leading to actomyosin contraction which PCP coordinates along the head-to-tail axis of the neural tube. Signalling in one cell is shown for simplicity.

It has been shown that PCP is linked to actomyosin contractility and myosin II distribution in the neural plate via Shroom 3 and Rho associated kinase (McGreevy et al., 2015; Nishimura & Takeichi, 2008). PCP also directly regulates RhoA, Rock and Daam1, which are linked to the cytoskeleton (Habas et al., 2001; Nishimura & Takeichi, 2008). Hence, PCP is directly linked to different cellular rearrangements during developmental processes such as cell intercalation (M. Williams et al., 2014). PCP has also been implicated in neural crest cell migration in *Xenopus* and Zebrafish. Here Fzd-Dvl mediate activation of RhoA, which promotes retraction at the rear of the neural crest cell via Rock2 mediated actomyosin contractility, additionally RhoA/Rock also inhibits Rac1, so it becomes polarised towards the leading edge of the cell (Matthews et al., 2008). These events are mainly linked to collective cell migration. PCP also regulates the cytoskeleton in single cell migration in processes such as mouse and zebrafish facial branchiomotor neuron migration (Y. Qu et al., 2010). In this case PCP is linked to filopodial protrusive activity by regulated the actin dynamics, to form actin-based protrusions and hence directional cell migration (Davey et al., 2016). A similar mechanism with the involvement of FZD and VANGL can be seen in migrating breast cancer cells (Luga et al., 2012) although PCP proteins do not connect cancer cells to coordinate their migration in this case.

1.3. – Mammary gland development

Most of our knowledge about mammary gland development comes from animal studies, namely mice, where the developmental process is very similar to the human one. Branching morphogenesis is a phenomenon by which tubular organs in the body are formed during embryonic development in many organisms. This involves organs such as the breast (mammary glands), lungs, kidneys, and the pancreas. (Yates, Papakrivopoulou, et al., 2010; Yates, Schnatwinkel, et al., 2010). The mammary gland is formed as a branching ductal network, via a specific branching morphogenesis process which differs to that of, for example, the lung (Ochoa-Espinosa & Affolter, 2012). The human breast is formed of the parenchyme, which consist of ducts and acini, and the stroma, which consists of adipose tissue (Fig.5) (Javed & Lteif, 2013a).

1.3.1. - Mammary gland development *in utero*

Mammary gland development begins *in utero* and continues until the age of approximately 2 years old, at which time branching morphogenesis ceases. Branching is then reactivated by hormone systems during puberty and pregnancy (Javed & Lteif, 2013a; Macias & Hinck, 2012). Mammary progenitor cells may be detected as early as 4 weeks into gestation (Ewald et al., 2008; Watson & Khaled, 2008). Around E10.5 in mouse embryos (half-way through mouse gestation), two ridges called milk lines or mammary crests are formed (Javed & Lteif, 2013b; Watson & Khaled, 2008). These ridges are an ectoderm which arise from the embryonic ectoderm, the outermost layer of the early embryo. These ectodermal cells then begin to form pairs of placodes, which define the primordial region of the mammary gland (Javed & Lteif, 2013b; Watson & Khaled, 2008). Subsequently, these placode pairs begin to sink into the mesenchyme, forming a mammary bud, also called the primary mammary bud (Javed & Lteif, 2013b; Watson & Khaled, 2008). Then the mammary sprout invades the mammary fat pad precursor and the mammary gland forms ductules, which become tree-like glands just before birth, forming a rudimentary mammary ductal system (Fig. 5). Recent papers highlights the role of cell movement in gland development via live imaging (Ewald et al., 2012; Neumann et al., 2018).

At this point mammary development is temporarily halted until puberty (Andrew & Ewald, 2010; Javed & Lteif, 2013b; Watson & Khaled, 2008). The morphogenetic cues that drive the development of the mammary gland at this stage are secreted by the mammary fat pad precursor cells (Watson & Khaled, 2008).

1.3.2. – Mammary gland development at puberty

A major stage of human mammary gland development occurs at puberty, where branching morphogenesis becomes more evident (Andrew & Ewald, 2010; Ewald et al., 2008). The rudimentary ductal system formed *in utero* now elongates and generates secondary ducts (Fig.5). Terminal ends buds driven by a layer of cap cells at the tip, invade into the fat pad. Terminal end buds are the original cell template for branching morphogenesis and drive the complex branched ductal structure of the breast (Javed & Lteif, 2013a; Macias & Hinck, 2012). The cap cells eventually differentiate into

myoepithelial cells, which become the outer layer of the forming duct (J. M. Williams & Daniel, 1983). Duct elongation occurs via branching morphogenesis, including bifurcation, thus generating a branched structure or the 'mammary tree'. The primary ducts form subsidiary ducts which lead onto terminal duct formation and subsequently, acini formation. A group of these acini is termed a terminal duct lobular unit (TDLU), the first acknowledged site for breast tumour initiation (Javed & Lteif, 2013a; Macias & Hinck, 2012; Wellings & Jensen, 1973). Ewald et.al. (2008) have elegantly shown how collective cell migration and cell rearrangements drive mammary branching morphogenesis. One of the most striking details seen in this study is how similar the mammary gland developmental processes are to those of the initial stages of oncogenesis i.e., hyperplasia and neoplasia (Ewald et al., 2008). The mammary duct elongates via a special form of polarized collective cell migration without forming a leading edge as observed in lung branching morphogenesis (Ewald et al., 2008). The mammary duct TDLU is a multi-layered epithelium, similar to pre-invasive oncogenic stages where the monolayer of the ductal epithelium has generated a multi-layered structure (Andrew & Ewald, 2010; Ewald et al., 2008).

The human breast fully matures at around 18-20 years of age with further remodelling activated during pregnancy, by estrogen (Javed & Lteif, 2013a). At full maturity up to 60% of available space in the mammary fat pad is occupied, leaving the remainder to be utilized during pregnancy and breast-feeding (Macias & Hinck, 2012).

As shown in Fig. 5 the mature mammary gland consists of an inner layer of the breast duct (the lumen) made of luminal epithelial cells which form the secretory alveoli and cists and are the active part for lactation. The ductal monolayer is surrounded by an outer layer is formed of myoepithelial cells, which form a boundary between the luminal cells and the surrounding stroma (Gudjonsson et al., 2005; Péchoux et al., 1999). The Luminal cells provide forces needed for secretion. Research suggests that myoepithelial cells arise from a common precursor which also generates luminal epithelial cells (Gudjonsson et al., 2005; Péchoux et al., 1999). It has been shown that myoepithelial

cells act as regulators of tissue polarity and provide regulatory signals to maintain a highly organised tissue structure in the breast (Gudjonsson et al., 2005; P  choux et al., 1999).

1.3.3 Mammary gland development during pregnancy and lactation

The penultimate stage of mammary gland remodelling is during pregnancy and lactation (Fig.5). This process is induced by prolactin and progesterone, which induce alveologensis and gland maturation, and results in the differentiation of alveoli, which are responsible for milk secretion (Brisken et al., 1998; Lydon et al., 1995). The JAK/STAT pathway is activated downstream of the Prolactin/Prolactin receptor (Cui et al., 2004; Han et al., 1997; Wagner et al., 2004). Prolactin secreted from the pituitary gland stimulates the secretion of progesterone from the ovary. Prolactin and progesterone then act together to initiate a complex cascade of downstream signalling, which eventually results extensive side branching of the mammary ducts and lactation. Prolactin initiates the JAK/STAT pathway by binding to a set of receptors – Integrin, SIRPA and PRLR. Progesterone activates the progesterone receptor. The activated JAK/STAT pathway and progesterone receptor induce the transcription of several genes including *Rankl*, which synthesises RANKL, which then binds to the RANK receptor and activates alveologensis through NFKB. The JAK/STAT pathway/RANK also induce the transcription of *Wsp* (whey acidic protein) and *Csnb* (casein beta), leading to the production and secretion of milk (Beleut et al., 2010; Fernandez-Valdivia et al., 2008; Han et al., 1997; Mukherjee et al., 2010; Schramek et al., 2010).

1.3.4. Involution

Involution is the final stage of breast morphogenesis after lactation (Fig.5). It is initiated by a lack of demand for milk and resets the breast architecture to pre-lactation status. Involution happens in two phases. The first phase is characterised by apoptosis and detachment of alveolar cells, which are shed into the lumen. This occurs within 12 hours of lack of demand (for milk). There are no significant morphological changes, and this stage is still reversible by re-establishing demand. The second stage occurs at 48 after demand ceases. This phase is characterised by breakdown of the ECM

and activation of proteases which leads to large scale apoptosis. This phase is non-reversible and results in complete cessation of lactation. Total remodelling of the breast architecture occurs resulting in pre-lactation morphology (Balogh et al., 2006; D’Cruz et al., 2002). According to research the earliest stages of involution involve lysosomal membrane permeabilization (Fernandez-Valdivia et al., 2009). Research has shown that the initiation of mammary involution occurs at a local level (M. Li et al., 1997). The Stat switch plays a significant role here, where STAT3 suppresses STAT5 pro-survival signalling and promotes pro-apoptotic signalling pathways (Chapman et al., 1999; Clarkson et al., 2006; Creamer et al., 2010). The second phase of involution is marked by the activation of matrix metalloproteinases (MMPs) and serine proteases (Fata et al., 2001; Sympton et al., 1994). Interestingly it has also been reported that post-lactational involution, which includes extensive remodelling of the breast architecture can resemble wound healing and tumorigenesis (Clarkson & Watson, 2003). It has been shown that post-lactational ECM can create the ideal tumour microenvironment (McDaniel et al., 2006; Schedin, 2006).

1.4. Evidence of a role for PCP in mammary gland development

The core-PCP pathway is proposed to regulate the collective cell movements of branching morphogenesis in the lung during embryo development (Yates, Papakrivopoulou, et al., 2010; Yates, Schnatwinkel, et al., 2010) however little is understood about their potential role in mammary gland development. Moreover, PCP genes are usually switched off in tissues during the post-natal period but might be reactivated during the coordinated breast tissue remodelling that occurs during puberty or lactation . One study has looked at the role of VANGL2 (Hatakeyama et al., 2014). VANGL2 is reported to play a significant role in normal mammary gland development via both the Wnt-PCP and core PCP pathways. In this study, gene knockdown of VANGL2 has a significant impact on normal breast development (Smith et al., 2019). A further study reported on roles for WNT morphogens in Wnt-PCP during mammary gland development and suggested that WNT5A promotes developmental processes in the mammary gland (Kessenbrock et al., 2017).

Intriguingly, one mechanism of breast lumen development and re-modelling during lactation involves radial intercalation (Neumann et al., 2018). PCP proteins are reported to be involved in radial intercalation in vertebrate organ development (Ossipova et al., 2015; Stubbs et al., 2006) including establishment of the epidermis of the developing mouse skin (Panousopoulou et al., 2016). Study of the role of PCP in the development of other tubular organs e.g., kidney tubules, pancreatic ducts, tracheal tube, and oviducts (Shi et al., 2014) have raised additional hypotheses relevant to the impact of PCP on breast development. For example, in the mouse oviduct *Celsr1* has been found to be important in establishing ciliary polarity to enable the correct functioning of the oviduct and also in maintaining correct tissue morphology (Shi et al., 2014). PCP is also necessary for kidney branching morphogenesis, as PCP mouse mutants have been found to have defects in ureteric bud branching morphogenesis (Brzoska et al., 2016; L. L. Yates, Papakrivopoulou, et al., 2010). Yates et al. have reported actin polymerisation defects in these mutants, showing that PCP regulates branching morphogenesis in the kidney via cytoskeletal rearrangements (Yates, Papakrivopoulou, et al., 2010).

1.5. Overview of breast cancer

Cancer is the second leading cause of death worldwide with breast cancer being the second most common cancer (WHO, 2018). In the UK, breast cancer is the second most common cancer accounting for 7% of all cancer deaths (CRUK, 2017). It is a debilitating disease with long-lasting effects even after treatment for many individuals. Ductal carcinoma in situ (DCIS) (also called non-invasive or intra-ductal cancer) is a precursor of invasive breast cancer (IBC) consisting of pervasive lesions originating from normal breast tissue (Burstein et al., 2004). DCIS has also been defined as a neoplastic proliferation of epithelial cells confined to the ductal-lobular system (Carraro et al., 2014). The first model of DCIS development was published by Wellings and Jensen (1973). These authors proposed that the terminal duct lobular unit (TDLU; Fig. 6) of the breast undergoes a series of abnormal events. Subsequent study defined an initial step as ductal hyperplasia (the enlargement of an organ due to abnormal, excessive cell proliferation) which leads to DCIS (Burstein et al., 2004; Duggal et al., 2013).

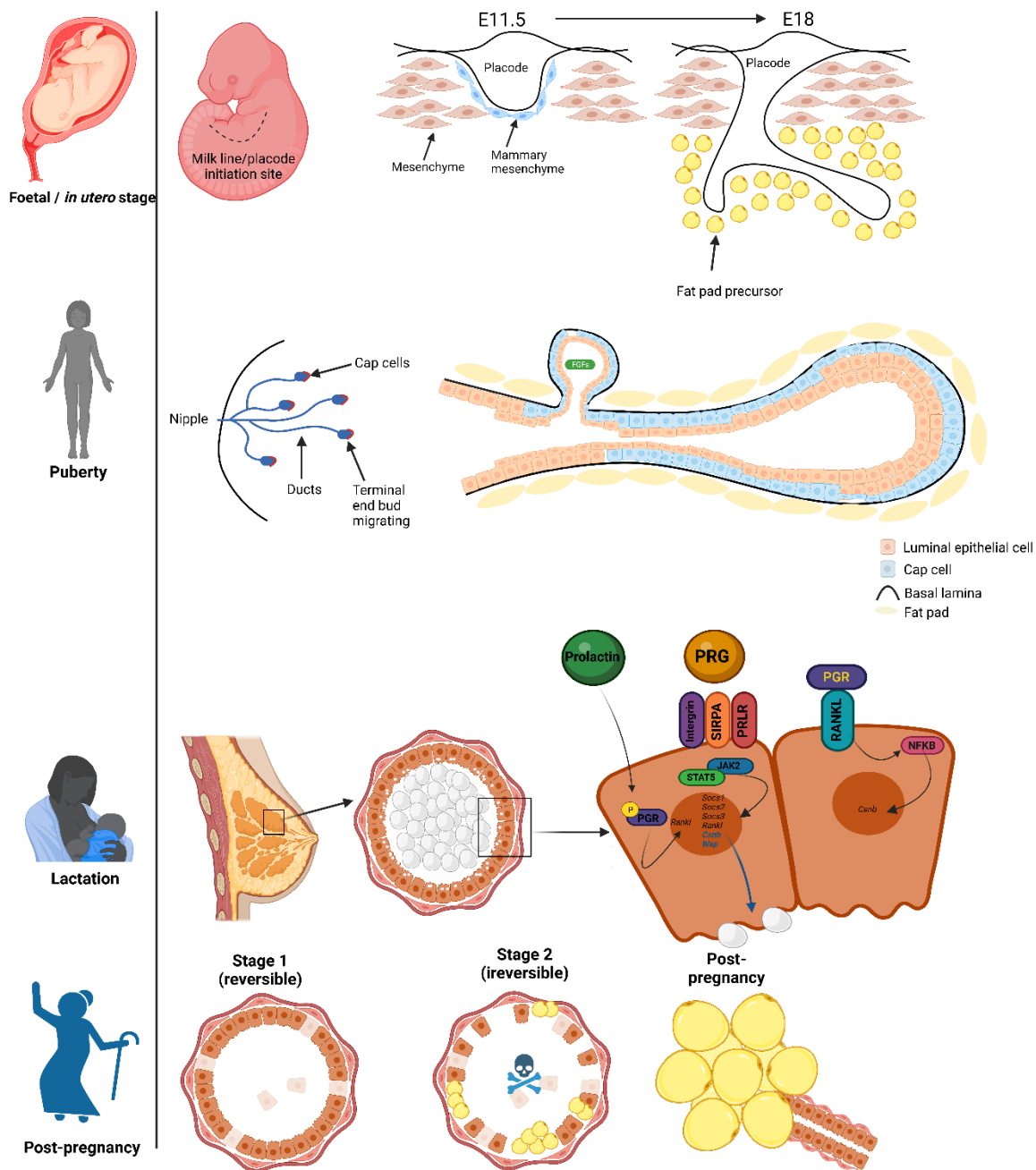


Figure 5 - Showing the 4 stages of human mammary gland development from *in utero* to post-pregnancy. (1) Foetal/*in utero* stage – shows how the placode invades into the pre-mammary fat pad *in utero* (more detail in text). (2) Puberty stage – Left image shows multiple mammary duct branching points in the breast. Right image shows enlarged image of an elongating duct with cap cells at the leading edge and Fibroblast Growth Factor (FGF) promoting branch outgrowth. (3) Lactation stage – During this stage the mammary gland branches rapidly to aid lactation. Lactation is controlled by the signalling mechanism shown on the rightmost image (details in text). (4) – Post-pregnancy stage – 3 stages of involution. Left – Stage 1 - is reversible with minimal alveolar cell shedding into the lumen. Middle – Stage 2 – is irreversible as it involves extensive apoptosis of luminal alveolar cells. Right – Stage 3 – is the final stage where the architecture of the breast returns to puberty-like stage with and mostly consists of adipocytes. Created using biorender.com

Interestingly, most known changes in gene expression occur during the transformation from normal breast tissue into DCIS, rather than during the transformation of DCIS to IBC (Burstein et al., 2004). The exact mechanism of DCIS development is poorly understood however, as is the relationship between DCIS and IBC. It is known that 14% to 50% of DCIS lesions progress to IBC if left untreated (Carraro et al., 2014). Triple Negative Breast Cancer (TNBC), also known as basal-like, is the most aggressive type of IBC.

1.5.1 Subtypes of breast cancer

1.5.1.1 Luminal A/B (ER+)

Luminal type breast cancer accounts for 2/3 of all breast cancer cases in the world (Goldhirsch et al., 2011). Luminal cancer mainly occurs in the duct but can also be lobular or mixed, there are also less common forms, such as cribriform, mucinous or tubular (Colleoni et al., 2012).

The luminal subtype can be further classified into Luminal A and Luminal B. From among these two, Luminal A is the most common subtype, accounting for >50% of all breast cancer cases (Yersal & Barutca, 2014). Generally Luminal A breast cancers have low mitotic activity, a low histological grade, low degree of nuclear pleomorphism and therefore have a 'good' prognosis (Carey, 2010; Yersal &

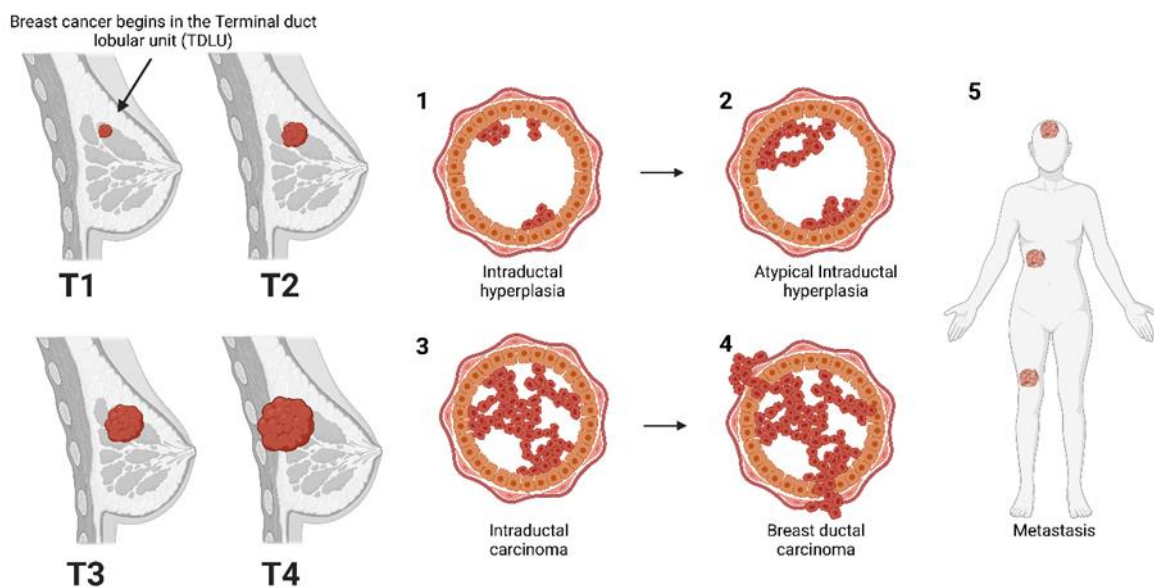


Figure 6 - Breast cancer progression. Showing the different clinical stages of breast cancer (left). Different stages of cellular and cancerous abnormalities are shown on the right. T1-T4 – Indicates breast cancer stage based on tumour size

Barutca, 2014). This cancer type is also characterised by low expression of genes linked to cancer proliferation and high levels of the growth factor receptor, oestrogen receptor (ER), making luminal A cancers a good candidate for ER-based endocrine therapy where ER expression is high (Kennecke et al., 2010; Sotiriou et al., 2003).

Luminal B breast cancers account for the lower number of cases (~20%) (Creighton, 2012). Compared to Luminal A breast cancer, Luminal B comes with a worse prognosis reflected by a higher histological grade, proliferative index and generally higher aggressiveness (Creighton, 2012; Ellis et al., 2008). By far the greatest difference between Luminal A and Luminal B is the expression of genes involved in cancer proliferation, such as cyclin E1, *n-MYB*, and *CCNE1* (Reis-Filho et al., 2010). Additionally, Luminal B tumours exhibit an increased expression of growth receptor signalling genes, such as human epidermal growth factor receptor type 2, HER2+ (~30% luminal B tumours over-express HER2) (Loi et al., 2009). Growth factor pathways such as the Fibroblast Growth Factor receptor (FGFR) and phosphoinositide-3-kinase (PI3K) have also been implicated to contribute to increased proliferation and poor prognosis in luminal B breast cancer (Tran & Bedard, 2011). Luminal B breast cancers do not respond to endocrine therapy as well as do luminal A breast cancers, however luminal B tumours respond better to neoadjuvant chemotherapy (Bhargava et al., 2010; Esserman et al., 2009; Paik et al., 2004; Tran & Bedard, 2011).

1.5.1.2 *HER2-positive (HER2+)*

The human epidermal growth factor receptor-2 (HER2) is a tyrosine kinase receptor encoded by the *ERBB2* gene (*ERBB2 Gene - GeneCards | ERBB2 Protein | ERBB2 Antibody*, n.d.). HER2+ breast cancers account for ~20% of all breast cancer cases (Tsuetsui et al., 2003). As the name suggests HER2+ breast cancers exhibit increased expression of the *HER2* gene. Activation of the HER2 receptor leads to the activation of downstream second messenger pathways, which activate pro-cancer transcription pathways (Barnes & Kumar, 2004; Bazley & Gullick, 2005; Moasser, 2007). These include angiogenesis, proliferation, metastasis, and survival pathways (Barnes & Kumar, 2004; Bazley & Gullick, 2005; Gutierrez & Schiff, 2011; Moasser, 2007). As a result, HER2+ cancers are more aggressive than Luminal

type breast cancer. HER2+ cancers also have a high rate of p53 mutations and half of all cases are also ER-positive, however the levels of ER are on the lower end of the perceived scale (Nicoletto & Ofner, 2022; Tsutsui et al., 2003). HER2+ breast cancers are generally resistant to endocrine therapy, however they respond well to doxorubicin, which is an antibiotic chemotherapy drug with multiple mechanisms of action including inhibiting DNA synthesis, altering metabolism or promoting oxidative stress (Ross et al., 2003). Trastuzumab, also known as Herceptin, is currently the 'go to' treatment for patients with HER2+ breast cancer (Cameron et al., 2017). Herceptin is a drug which targets the fourth extracellular EGF domain of HER2+, preventing receptor dimerization, which in turn causes cell cycle arrest (Gemmete & Mukherji, 2011).

1.5.1.3 Basal-like

Finally, the most aggressive of all breast cancer subtypes, the basal-like subtype accounts for up to 37% of all cases (Rakha et al., 2009). Typical features of basal-like breast cancers include a high histological grade, high mitotic and proliferative rate, disorganised structure with necrotic and fibrotic zones, and are highly metastatic, especially to sites such as the brain and lungs (Heitz et al., 2009). Metastasis of basal-like breast cancers to the brain accounts for 15%-30% of cases, unlike the less aggressive types of breast cancer which metastasize to the bones, for example (C. Anders & Carey, 2008; Jin et al., 2018). A peculiarity of basal-like tumours is that they express increased levels of myoepithelial cell markers and lack all the three previously mentioned receptors – ER, PR and HER2 – and are therefore named triple-negative. As expected, basal-like cancers possess a high rate of p53 (*TP53*) mutations. It is important to note that not all basal-like breast cancers are triple-negative and not all triple-negative cancers are basal-like (Kreike et al., 2007). Basal-like breast cancer is defined by the expression of basal myoepithelial markers (Dai et al., 2017). Several genes and signalling pathways have been linked to promoting invasiveness, survival and migratory capabilities in basal-like cancers. These include MAPK, NF- κ B, PI3K and AKT (Criscitiello et al., 2012). Studies have shown that around three-quarters of *BRCA1* related breast cancers belong to the basal subtype and also possess abnormalities in Epidermal growth factor receptor (EGFR) and P-cadherin (Foulkes et al., 2004).

Currently, chemotherapy is the best available treatment option for basal like breast cancer as no targeted options are available (Alluri & Newman, 2014). Nevertheless, targeted treatment options for basal-like breast cancers are in active development and include inhibitors of angiogenesis, PARP or EGFR inhibitors (Alluri & Newman, 2014).

Breast tumour cell-cell remodelling, and directional migration are thought to be key to attaining a metastatic state. Because PCP defines directional information to promote cell-cell rearrangements and directional migration, it is important to look at what role this tissue polarity system might play in breast cancer.

1.5.2 – Immunotherapy in breast cancer

Metastatic breast cancer, including TNBC is usually difficult to treat, with aggressive therapeutic measures in needed to combat the equally aggressive cancer. The lack of specific treatment targets for highly aggressive breast cancer (such as TNBC) calls for alternative treatment methods, with better outcomes and less side effects (Zhu et al., 2021a). One of these methods is immunotherapy, which uses the patient's own immune system to defeat metastatic cancer (Waldman et al., 2020). Specifically, this means enhancing or re-activating the immune system in such a way as to increase cancer elimination capabilities. Among the various types of immunotherapies, the most common method for the treatment of metastatic breast cancer are immune checkpoint inhibitors (Emens, 2018). Cancer cells evade immunosurveillance by activating the immune checkpoint pathway, suppressing the immune response (Darvin et al., 2018). One of the best known and most widely used immune checkpoint inhibitors in metastatic breast cancer are PD-1/PD-L1 inhibitors (Emens, 2018; Waldman et al., 2020; Zhu et al., 2021b). The PD-1/PD-L1 axis is a negative regulator of T cell activity by activating the immune checkpoint and switching 'off' T cell responses. The programmed cell death protein 1 (PD-1) promotes self-tolerance and inhibits immune responses (Han et al., 2020). PD-1 is expressed mainly on T cells, NK cells, B lymphocytes, macrophages and other immune cell types (Han et al., 2020). It is involved in a protective signalling pathway to prevent dangerous, out of control cells from causing autoimmunity. Cancer cells have the capacity to activate the PD-1 signalling axis to

essentially disable immune cells from destroying them. Inhibiting this regulatory axis enables immune cells, namely T-cells to be maintained in order to boost cancer cell destruction (Zhu et al., 2021b). The best known of these inhibitors, targeted mainly at TNBC include pembrolizumab and atezolizumab (Emens, 2018; Zhu et al., 2021b). Other immune checkpoint inhibitors researched for use in breast cancer patients include CTLA-4 inhibitors, as well as other types of immunotherapies, including CAR-T cells and personalised vaccines (Emens, 2018; Zhu et al., 2021b).

1.6 Evidence for a role of cell polarity proteins in cancer

Loss of ABP is a hallmark of cancer (Hanahan & Weinberg, 2000; M. Lee & Vasioukhin, 2008). Studies on the role of apico-basal polarity proteins (ABPs) in cancer suggest that once dismantled, ABPs are re-employed to promote cancer cell migration (Gandalovičová et al., 2016; Halaoui & McCaffrey, 2015). These findings raise the hypothesis that core-PCP proteins have a similar fate during tumourigenesis (Halaoui & McCaffrey, 2015).

1.6.1 Apico-basal polarity in cancer

Cell polarity pathways are partially lost or rewired during the EMT process (Gandalovičová et al., 2016). EMT is usually triggered by transcription factors, such as Snail/slug, twist or ZEB (Aigner et al., 2007; Barberà et al., 2004; J. Yang et al., 2004). Hallmarks of EMT include the suppression of epithelial genes, a switch from E-cadherin to N-cadherin ('cadherin switch') and the increased expression of the intermediate filament vimentin. It has been shown that the transcription factors, which induce EMT suppress components of the ABP pathway to down-regulate ABP. For example, it has been shown that SNAIL can suppress CRUMB3 and thus eliminate the CRUMBS and PAR complex from the apical cell membrane (Whiteman et al., 2008). SNAIL has also been shown to suppress the ABP determinant LGL, the result of which is the induction of invasive behaviour (Kashyap et al., 2012). Lgl as well as Patj and Crumbs have been found to be suppressed by the transcription factor Zeb1 (Aigner et al., 2007). Deregulation of ABP proteins in cancer can affect single and collective cell migration differently. ABP proteins interact with Rho GTPases, which regulate cellular components

that elicit cellular motility (Gandalovičová et al., 2016). One such example is the interaction between cdc42 and the par complex, which promotes migratory polarity via the activation of aPkc (Z. Li et al., 2005; Parker et al., 2014). Another complex involved in promoting cancer invasiveness is the SCRIBBLE complex, which promotes cell migration by increasing Rac1 and Cdc42 activity (Elsum et al., 2013; Feigin et al., 2014). Scribble does this by redirecting Rac1 and Cdc42 to the cell front (Dow et al., 2006). Another member of the scribble complex, Dlg, also plays a role in facilitating directed cell migration during cancer invasion by relocating to the leading edge and interacting with Pkca (O'Neill et al., 2011). Lgl also contributes to regulating invasive cell migration by interacting with non-muscle myosin and removing it from the leading edge, which results in the uninhibited formation of actin filaments and focal adhesions, thus facilitating migration (Dahan et al., 2012).

1.6.2 Planar cell polarity in cancer

The impact of PCP proteins on breast cancer progression is little understood. The field of PCP and cancer is therefore an emerging one. A recent study showed that PRICKLE1 and its interacting partner Epithelial Cell-Transforming Sequence 2 Oncogene (ECT2) appear to be reactivated during tumorigenesis, promoting metastasis (Daulat et al., 2019). Given the importance of collective cell movements for embryogenesis, reactivation of developmentally expressed proteins in cancer cells could provide an important driver for similar cell behaviours, albeit dysregulated, during cancer progression. Dysregulation of master developmental signalling pathways such as Wnt/ β -catenin or Notch (Kamdje et al., 2017; Micalizzi et al., 2010) is well-known in cancer progression. As described in the section above, mis-localisation of SCRIBBLE can promote cancer invasiveness. The PCP component VANGL2 is commonly dysregulated in breast cancer (Puvirajesinghe et al., 2016). VANGL2 also associates with SCRIBBLE and ensures its correct localisation (vanden Berg & Sassoon, 2009). Mutations in VANGL2 prevent this and enable SCRIBBLE to be hijacked for the benefit of the cancer cells (vanden Berg & Sassoon, 2009). VANGL2 also associates with Rac1, and when either is lost cell adhesion defects arise (Lindqvist et al., 2010). VANGL and FRIZZLED have been extensively studied in Wnt-PCP driven (breast) cancer, which will be discussed in greater detail below. The goal of this project

is to investigate the roles of two transmembrane receptors of the PCP pathway, Frizzled 6 and CELSR1, in relation to breast cancer. The spotlight is specifically on Frizzled and CELSR receptors because published literature suggests that they play opposing roles in breast cancer, as outlined below.

1.7 -The CELSR 1 receptor

Cadherin EGF LAG seven-pass G-type receptors (Celsr/CELSR) are atypical 7-pass transmembrane cadherins (Fig.7) sitting within the cadherin and G-protein coupled receptor (GPCR) superfamilies. Within the latter, they are a member of the Adhesion-GPCR sub-family (Morgan et al., 2019). There are three CELSR genes in humans (CELSR1-3) which are conserved in other vertebrate species (Eaton, 1997; Hardin et al., 2013; Maung & Jenny, 2011). Celsr proteins are atypical cadherins because they do not associate with β -catenin and participate in cell recognition rather than cell adhesion. Indeed, a key role for Celsr proteins in transmission of cell polarity across a field of cells stems from their ability to mediate homophilic interactions: they form intercellular homodimers with Celsr proteins on opposing cell interfaces, most likely through their N-terminal cadherin repeats (Fig.7) (Usui et al., 1999). Celsr1 protein is large (~400 kDa) in size and contains several evolutionarily conserved motifs. The extensive extracellular domain is comprised of 9 extracellular cadherin repeats, Epidermal growth factor -like (EGF-like) domain repeats and Laminin G (LAM) repeats, a hormone receptor domain, a GPCR autoproteolysis (GAIN) domain followed by 7-transmembrane (7-TM) repeats and finally a long cytoplasmic tail (Basta et al., 2023; Formstone et al., 2010). To date, the 3D structure of CELSR1 has not been published. However, a 3D structure of cadherin domains 4-6 determined by x-ray crystallography has recently been deposited in the protein data bank under the accession no. 7SZ8 (RCSB PDB - 7SZ8: *Crystal Structure of Human CELSR1 EC4-7*, n.d.).

1.7.1. Splice variants of CELSR1

Various splice variants of *CELSR1* exist and are evolutionarily conserved (Formstone et al., 2010; Morgan et al., 2019; Y. Qu et al., 2010). In humans they are defined by the differentially spliced c-terminal tail region and denoted as the EKP (AA seq.) variant and PDZ (GSNETSI – AA seq.) variant

(Gene: *CELSR1* (ENSG00000075275) - Summary - Homo_sapiens - Ensembl Genome Browser 110, n.d.).

The PDZ variant is of particular interest since PDZ domains are known to be involved in downstream protein interaction in cell signalling (Lee & Zheng, 2010). Currently and to the best of our knowledge, it is not known what factors the CELSR1 PDZ domain interacts with or is linked to.

1.8 The FZD6 receptor

Frizzled seven-transmembrane receptors (Fig.7) sit within the GPCR superfamily and are well known for their role as receptors for Wnt ligands. They belong to class F of GPCRs with a conserved cysteine-rich domain (CRD) and charged residues in the N-terminal and C-terminal loops (Koval et al., 2011; Schulte & Wright, 2018; Zeng et al., 2018). Frizzled receptors are proposed to 'sense' underlying shallow gradients along a body axis and to amplify this signal and, together with Vang and Celsr1, make it more robust. PCP proteins act downstream to organise the actin cytoskeleton leading to alignment of cell structures and cell behaviours. This will be discussed in the next section.

One Frizzled receptor (Fz6) is known to work together with Celsr1 during mammalian embryonic skin development (Devenport & Fuchs, 2008; Hobbs & Formstone, 2022; Oozeer et al., 2017; X. Tang et al., 2020). CELSR1 and FZD6 have also been shown to associate in the secretory pathway, where they were found in the same transport vesicles and delivered to the surface together (X. Tang et al., 2020). Oozeer et. al. (2017) reveal that CELSR1 and FZD6 play a role in orienting planar cell divisions in the mammalian embryonic skin. Devenport lab paper reveals a role for Fz6 in local collective cell movements that drive hair placode formation (Cetera et al., 2018).

1.9 WNT-PCP and cancer

The role of WNT signalling in cancer progression is well-established (Katoh, 2005, 2017; Klaus & Birchmeier, 2008). Mutations in several components of the canonical WNT pathway are associated with several cancers (e.g., colon cancer), however, few studies have considered the non-canonical WNT-PCP pathway (Klaus & Birchmeier, 2008). Several components of the WNT-PCP pathway have been found to be upregulated/overexpressed in certain human cancers, including WNT5a, Frizzled

receptors and ROR2 (Katoh, 2005). Specifically, upregulation of WNT5a and WNT11 has been found to promote breast cancer migration/invasiveness and cell motility and tumour metastasis, respectively (VanderVorst et al., 2018). A review by Daulat and Borg (2017) lists other Wnt-PCP ligands, which were implicated in breast cancer progression, including WNT7 (Daulat & Borg, 2017).

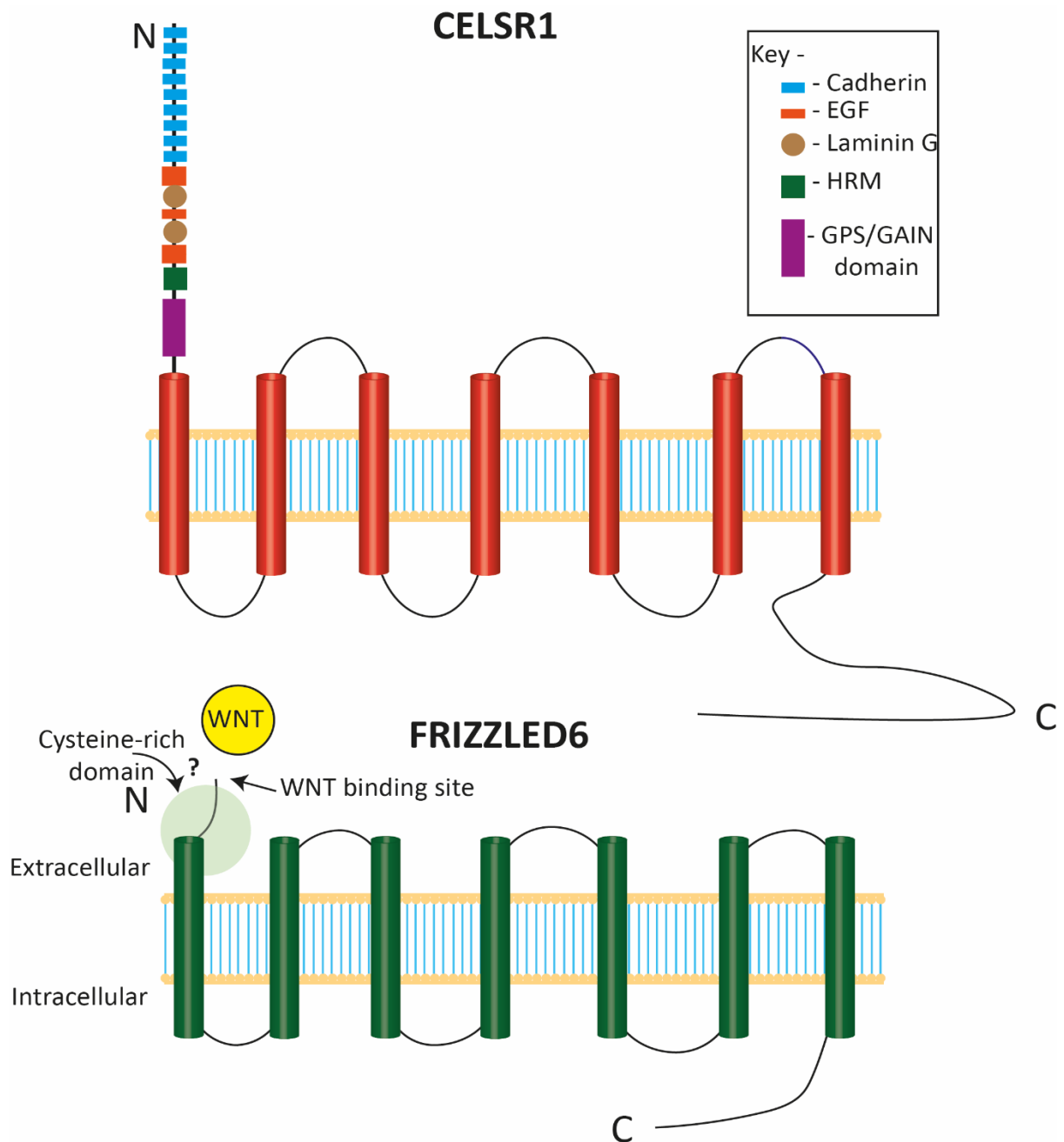


Figure 7 - Illustration of CELSR 1 and FZD6 GPCRs. '?' denotes the uncertainty whether WNT ligands are involved when FZD6 works together with CELSR1

Thus upregulation/overexpression of non-canonical WNT ligands may trigger aberrant PCP signalling, possibly independent of *Frizzled* upregulation and the loss of *CELSR1*. Many studies have

also suggested that the tumour microenvironment (i.e., non-neoplastic cells) has a significant role in cancer progression (Allinen et al., 2004; Bombonati & Sgroi, 2011; Carraro et al., 2014; Duggal et al., 2013). Notably, fibroblast derived exosomes promote Wnt-PCP signalling to drive breast cancer cell metastasis (Luga et al., 2012). However, while Luga et. al. showed a link between fibroblasts and Wnt-PCP, they did not show a direct link between core-PCP and breast cancer.

VANGL has been implicated in WNT-PCP driven breast cancer (Hatakeyama et al., 2014). VANGL dependent WNT signalling is initiated by a WNT5A binding to the Frizzled6 receptor and recruiting DVL. VANGL and DVL then work together acting as scaffolds to activate downstream effectors that mediate actin cytoskeletal rearrangements leading to increased cell motility (Hatakeyama et al., 2014; MacMillan et al., 2014; Wald et al., 2017). Upon activation Frizzled has been also shown to enrich to the leading edge, where it interacts with integrins and the microtubule associated protein APC through DVL, regulating cell-cell adhesions in human breast cancer cell lines (Matsumoto et al., 2010). VanderVorst et.al. (2023) elegantly show how VANGL overexpression contributes to WNT-PCP driven invasiveness of breast carcinoma (VanderVorst et al., 2023). WNT-PCP could be an important consideration for this project, since WNT-PCP this may be promoted by cells of the microenvironment.

1.10 Evidence for a role of FZD6 in breast cancer

Recently human Frizzled (FZD) receptors have been reported to be dysregulated in cancer (VanderVorst et al., 2019). There are 10 FZD receptors in mammals (FZD1-FZD10) and of these FZD6, FZD7 and FZD8 have been implicated in breast cancer invasiveness and are proposed as potential candidates for targeted therapy (King et al., 2012; Pohl et al., 2017; Simmons G. E. et al., 2014). The FZD6 and FZD3 receptors work within core PCP (Dong et al., 2018; Ghimire & Deans, 2019). Several studies report on the role of the FZD6 receptor in cancer with one study focussing on breast cancer (Cantilena et al., 2011; Corda et al., 2017; Q. L. Wu et al., 2009; C. Xu et al., 2019). How dysregulation of FZD6 function is linked to increasing the metastatic potential of cancers, however, is yet unclear but a plausible hypothesis put forward by several research groups is that FZD6 acts as a protooncogene

(Cantilena et al., 2011; Corda et al., 2017; Corda & Sala, 2017; Katoh, 2005; Neta et al., 2011; Saramaki et al., 2006; C. Xu et al., 2019). For example, Corda & Sala (2017) lists all cancers in which gene copy number or RNA levels of *FZD6* were found to be aberrant. They report that all studies to-date on *FZD6* in breast cancer patients demonstrated either gene amplification or overexpression. Moreover, *FZD6* has been reported to be frequently overexpressed in TNBC which may contribute to metastatic progression (Corda & Sala, 2017). Corda & Sala (2017) also demonstrated that *FZD6* is frequently overexpressed in the highly aggressive TNBC subtype compared to normal tissue, and that expression levels progressively increase with the more invasive subtypes of breast cancer. They also showed that when *FZD6* is knocked down in a luminal type cell line, the effect on cell migration is insignificant. However, when *FZD6* was knocked down the more aggressive HER2+ and TNBC subtype-like cell line, the rate of cell migration was significantly slowed. These data are consistent with a role for *FZD6* in promoting cancer progression. *In vivo*, *FZD6* depleted cells injected into the mammary fat pad did not slow down tumour growth however, indeed the injected mice exhibited fewer metastases to secondary sites (Corda et al., 2017). Immunohistochemistry (IHC) on breast cancer patient biopsies also revealed high levels of *FZD6* staining in TNBC. The study has also shown that breast cancer patients with *FZD6* overexpression have a worse prognosis when it comes to relapse and distant-metastasis free survival (Corda et al., 2017).

Another member of the Frizzled family, *FZD3*, has additionally been shown to be significantly overexpressed in breast cancer and therefore could additionally impact on cancer progression and invasiveness (Corda & Sala, 2017). *FZD3* and *FZD6* are shown to cooperate in embryonic development e.g. in the developing central nervous system (Dong et al., 2018; Ghimire & Deans, 2019). The functional redundancy observed during development raises the hypothesis that *FZD6* and *FZD3* may act together in breast cancer.

1.11 CELSR1 receptors in breast cancer

In breast cancer, Liao et.al. (2012), identified gene copy number gains of *CELSR1* in two subtypes of DCIS which are pure DCIS (PD) - DCIS without an invasive component (Muggerud et al., 2010)- and

mixed DCIS (MD) - invasive with an *in-situ* component. A further study on *CELSR1* copy number aberrations in DCIS reported that *CELSR1* was more commonly amplified i.e., copy number was increased, in non-progressive (benign) DCIS and lost in progressive (metastatic/invasive) DCIS (Geradts et al., 2016). These authors proposed a protective role of *CELSR1* in breast cancer progression and invasiveness when *CELSR1* copy number or RNA levels are amplified (Geradts et al., 2016). Notably this outcome is opposite to that proposed for *FZD6* (Corda et al., 2017; Corda & Sala, 2017). Additionally, Geradts et al (2016) proposed that loss of *CELSR1* copy number contributed to progressive DCIS (Geradts et al., 2016). Another recent study has elegantly shown that how *CELSR1* could be a biomarker to distinguish between the luminal and HER2+/basal subtypes of breast cancer, by analysing proteins secreted into the tumour interstitial fluid (TIF) (Terkelsen et al., 2021). This study has shown that there are clusters of specific proteins secreted into the TIF which distinguish between low-grade and high-grade tumours. Protein-protein interaction networks from differentially analysed TIF proteins revealed two interesting findings, first, that *CELSR1* levels are markedly upregulated in Luminal vs. TNBC type breast cancer. Secondly, its interaction partners included *SHROOM3*, which is linked to cell shape changes, and *SFRP1*, which is linked to WNT signalling and cell polarity (*SFRP1 Gene - GeneCards | SFRP1 Protein | SFRP1 Antibody*, n.d.; *SHROOM3 Gene - GeneCards | SHRM3 Protein | SHRM3 Antibody*, n.d.). The study has found that *CELSR1* and *BCAM* were significantly upregulated in Luminal type breast cancer compared to TNBC, which was also confirmed by IHC on Luminal and TNBC type tissue samples. The authors of the study have suggested the potential use of this expression signature as a biomarker.

The exact molecular mechanism by which invasiveness is linked to loss and gain respectively of *CELSR1* and *FZD6* expression in invasive breast cancer is not yet fully understood, indeed published data suggests that they may play opposing roles. Given their developmental roles, where *CELSR1* and *FZD6* co-operate to directionally align cell structures and cell behaviours in highly organised epithelia along both planar and superficial-basal tissue axes (Devenport & Fuchs, 2008; Panousopoulou et al., 2016). One possibility is that their opposing dysfunction in cancer may first promote disorganisation of epithelia, which is the most prominent hallmark of cancer, followed by promotion of tumour

metastasis. With regard to the former, failure of tissue intrinsic outside-in (radial) oriented cell intercalation in the mouse *Celsr1* mutant Crash leads to aberrant multi-layering of the early surface epithelium (Panousopoulou et al., 2016).

1.12 Epithelial-Mesenchymal Transition (EMT)

Epithelial-to-mesenchymal transition (EMT) is a reversible process where highly adhesive epithelial cells switch to a more migratory character and which may eventually lead, via gene transcriptional changes, to a highly differentiated cell type with a distinct function to the original epithelial cell (Kalluri & Weinberg, 2009). EMT mostly requires a delamination process i.e., a detachment from the basement membrane. EMT processes are required during embryonic development, tissue remodelling and wound healing. EMT is therefore a normal process that is observed in the developing/healing human tissues (Kalluri & Weinberg, 2009). EMT also has a reverse process termed MET (mesenchymal-to-epithelial transition) where mesenchymal cells regain epithelial characteristics (Kalluri & Weinberg, 2009; M. Park et al., 2022). There are three different categories of EMT. Type I EMT is observed during embryonic development e.g. delamination of neural crest cells to generate the peripheral nervous system (Kalluri & Weinberg, 2009; Y. Wang & Zhou, 2011). Type II EMT is primarily observed during wound healing (Kalluri & Weinberg, 2009). While in type I EMT, MET is vastly observed, Type II EMT can result in tissue fibrosis during the regenerative process (Marconi et al., 2021). Type III EMT is the primary mechanism by which cancer cells gain the ability to migrate to secondary sites and therefore becoming metastatic (Kalluri & Weinberg, 2009). EMT is one of the main hallmarks of cancer (Hanahan & Weinberg, 2000, 2011). In general, a major characteristic of EMT is the suppression of E-Cadherin, a key epithelial cell adhesion protein, which occurs via loss of E-cadherin gene transcription. EMT is also characterised by the expression of mesenchymal markers (Kalluri & Weinberg, 2009; M. Park et al., 2022), the most prominent of which include N-cadherin and Vimentin. Vimentin is a type III intermediate filament of the cytoskeleton, which interacts with other cytoskeletal proteins to regulate cell adhesion, motility, and migration (Usman et al., 2021). Up-regulation of vimentin in increasingly invasive cancer cells is therefore

associated with their increased migratory ability (Usman et al., 2021). EMT is a complex process that is usually initiated via a combination of different signalling pathways and factors (Y. Wang & Zhou, 2011). TGF- β is seen as the main inducer and enhancer of EMT in more aggressive types of breast cancer. TGF- β ligand binds to TGF β cell surface receptors and activates downstream Smad effectors which move into the nucleus and induce transcription of *Snail*, a master regulator of EMT (Y. Wang & Zhou, 2011). Other regulators of EMT include *Slug* and *Twist*. These factors regulate the EMT program by initiating metastasis and activating stem cell traits. Other activators of EMT include WNT, mediated via FZD receptors, receptor-tyrosine kinases (RTKs), the Notch signalling pathway, the hypoxia pathway and TNF- α signalling (Kalluri & Weinberg, 2009; Y. Wang & Zhou, 2011). An elegant study on breast cancer EMT has also shown that partial EMT, rather than full EMT, is necessary for successful metastasis and colonisation of the lungs. This study has shown that only breast cancer cells in partial EMT state have significantly colonised the lungs, compared to breast cancer cells which have undergone full EMT and had no impact on lung metastasis (Lüönd et al., 2021).

1.13 In vitro models of cancer

Mammalian cell lines are widely used and effective models of human development and disease. Their use in cancer research is standard practice for testing various hypotheses and theories before moving onto *in vivo* and human/clinical studies. One of the first model cell lines was established over 80 years ago (Gey et al., 1952) and the number of available breast cancer cell lines has been increasing ever since, representing different subtypes of breast cancer (Holliday & Speirs, 2011). The main two questions or issues with using breast cancer cell lines as *in vitro* models of breast cancer are (1) How representative are these cell lines of cancer heterogeneity? (2) When cultured outside their native environment, cells lose access to the ECM and complex tumour microenvironment, thus how well representative is this model of an actual tumour? Molecular profiling has enabled researchers to classify breast tumour into distinct subtypes which has been translated into various breast cancer cell lines. There is no official classification of breast cancer cell lines, however publications and reviews have made a useful attempt to match them to their corresponding patient tumour subtype (Dai et al.,

2017; Y. Qu et al., 2015).(Dai et al., 2017). Breast cancer cell lines have been classified into the 4 molecular subtypes introduced in section 1.4.1. – Luminal A, Luminal B, HER2+ and Basal. Growing cells in 2D makes them behave differently than what one would observe *in vivo*, nevertheless it remains the most common way of culturing cancer cell lines for functional assays (Section 1.4.1.) Jensen & Teng, 2020). Hence one of the objectives of this study was to optimise a 3D *in vitro* cell culture model system for use as a functional assay system. This is especially important as PCP can function in 3-dimensions. 3D spheroid modelling is, however, more costly and time consuming to establish, optimise and maintain. It also requires more expertise and sometimes more specialised equipment and reagents. The following cell lines have been used in this study (Fig.8).

1.13.1 Wild-type control breast epithelial cell line, MCF10A

According to ATCC the MCF10A cell line is an epithelial cell line derived from a 36-year-old female patient with benign fibrocystic disease (MCF 10A - CRL-10317 | ATCC, n.d.; Soule et al., 1990). The MCF10A cell line is intended to act as a 'healthy' breast cell line, in that it is not tumorigenic, though it is immortal (Puleo & Polyak, 2021; Soule et al., 1990). These cells lack any sort of invasive or oncogenic characteristics and fail to initiate tumorigenesis even when induced (Puleo & Polyak, 2021) The MCF10A cell line is classified as basal simply because it lacks all three receptors – ER, PR and HER2+ (Kao et al., 2009). The MCF10A cell line is a powerful tool and is hence used to study normal mammary gland functions (Qu et al., 2015; Puleo & Polyak, 2021). The MCF10A cell line is also a parental cell line for the MCF10A cancer progression series.

1.13.2 Luminal A and B-type cell lines

1.13.2.1 T47D

According to ATCC the T47D cell line is a breast epithelial cell line derived from a pleural effusion of a 54-year-old female patient (*T-47D - HTB-133 | ATCC, n.d.*). The T47D cell line is an infiltrating ductal carcinoma. It is ER-positive, PR-positive and HER2+ - negative, making it a Luminal A subtype (Dai et al., 2017; Kao et al., 2009; Neve et al., 2006; Yu et al., 2017). This cell line has mutations in the

TP53 and PIK3C pathways, it also does not express the hypoxia and wound-healing gene signatures (Kao et al., 2009). From observations these cells grow slower and form uniform colonies until contact inhibition occurs.

1.13.2.2. BT474

According to ATCC the BT474 cell line is an epithelial cell line obtained from a solid source of an invasive ductal carcinoma from a 60-year old female patient (*BT-474 - HTB-20 | ATCC, n.d.*). The BT474 cell line is ER-positive, PR-positive and HER2+ - positive, making it a Luminal B type cell line (Dai et al., 2017; Kao et al., 2009). Similar to T47D cells, BT474 cells exhibit a slower growth rate and form uniform colonies until confluency.

1.13.2.3. Basal-like cell lines

Basal-like cell lines typically exhibit highly invasive features, including motility, and are also usually triple negative (characterised by the absence of all three receptors -ER, PR and Her2+). Again, cell lines can be basal-like but not triple negative and vice versa. Dai et.al. (2017) and others further classify the Basal subtype into Basal A and Basal B. Basal A cell lines are basal-like in that they are enriched for a plethora of basal markers, including integrins and cytokeratins. Basal B cell lines, also called normal-like and claudin-low are characteristic for over-expressing genes associated with aggressive and invasive features. Basal B cell lines are usually of mesenchymal type.

1.13.2.4 MDA-MB436

According to ATCC the MDA-MB436 cell line is a cell line of the mammary gland derived from a pleural effusion and is an adenocarcinoma (Dai et al., 2017; *MDA-MB-436 - HTB-130 | ATCC, n.d.*). This cell lines lacks all three receptors (ER, PR and Her2+) and is classified as a basal and triple negative subtype (Dai et al., 2017; Kao et al., 2009). Dai et.al. (2017) classify the MDA-MB436 cell line as Basal (triple negative) A with mutations in TP53 as well as the PTEN and PIK3CA pathways and wound healing and hypoxia gene signatures. The phenotypical characteristics of these cell lines are distinct in that they have a spindle-like appearance and rather than grow in clusters/colonies, these cell lines spread

individually all over the area when grown in 2D. Furthermore, their growth rate is much faster than any of the Luminal type cell lines.

1.13.3.5 MDA-MB231

According to ATCC the MDA-MB231 cell line is a breast cancer epithelial cell line derived from a pleural effusion and is an adenocarcinoma (Dai et al., 2017; *MDA-MB-231 - HTB-26 | ATCC*, n.d.). It is a Basal B (triple negative) cell line and is therefore the most aggressive and invasive cell line used in this study (Dai et al., 2017; Kao et al., 2009). The phenotypical characteristics of these cell lines are the same as those of MDA-MB436 cell lines except that MDA-MB231 cells grow even faster. They also possess TP53, PTEN and PIK3CA mutations as well as mutations in the hypoxia and wound healing gene signatures (Kao et al., 2009).

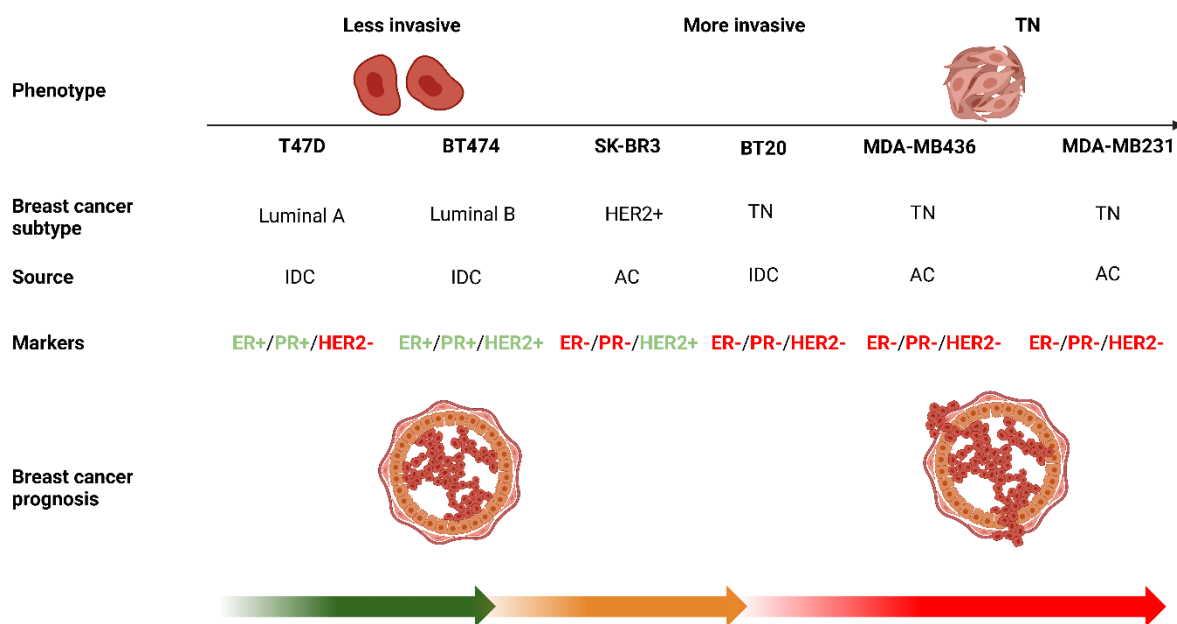


Figure 8 - Showing the characteristics of the cell lines used in this project as well as their prognostic significance mirrored to tumours occurring in breast cancer patients. Coloured arrows denote worsening prognosis – Green – Good, Orange – Poor, Red – Worst. IDC -Intraductal carcinoma, AC – Adenocarcinoma, ER +/- - Estrogen receptor positive/negative, PR +/- - Progesterone receptor positive/negative, HER2+/- - HER2 +/- - Human epidermal growth factor receptor 2 positive/negative.

1.13.3 MCF10A progression series

The MCF10A series cell lines were also incorporated into this study to assess whether they could also be a good model to study the role of CELSR1 in breast cancer in addition to the common cell lines described in the introduction. The advantage of the MCF10A series cell lines is that they have a common genetic makeup since they all come from the same parental cell lines (Y. Qu et al., 2015). NeoT is the least invasive in this series with AT1 also representing a low invasive benign type. DCIS.com through to Ca1.A, D and H show increasing invasive behaviour (Y. Qu et al., 2015; Santner et al., 2001). These cell lines are characterised by features of increasing invasive characteristics as seen in Figure 9. These include an increase in HRAS expression, which is a well characterised oncogene involved in regulating cell division. Another feature is the decrease in function and expression of the tumour suppressor TP53. Finally, the MCF10A progression series also shows an increase in P-AKT expression, which is associated with oxidative stress, evading apoptosis, and motility (Fig.9).

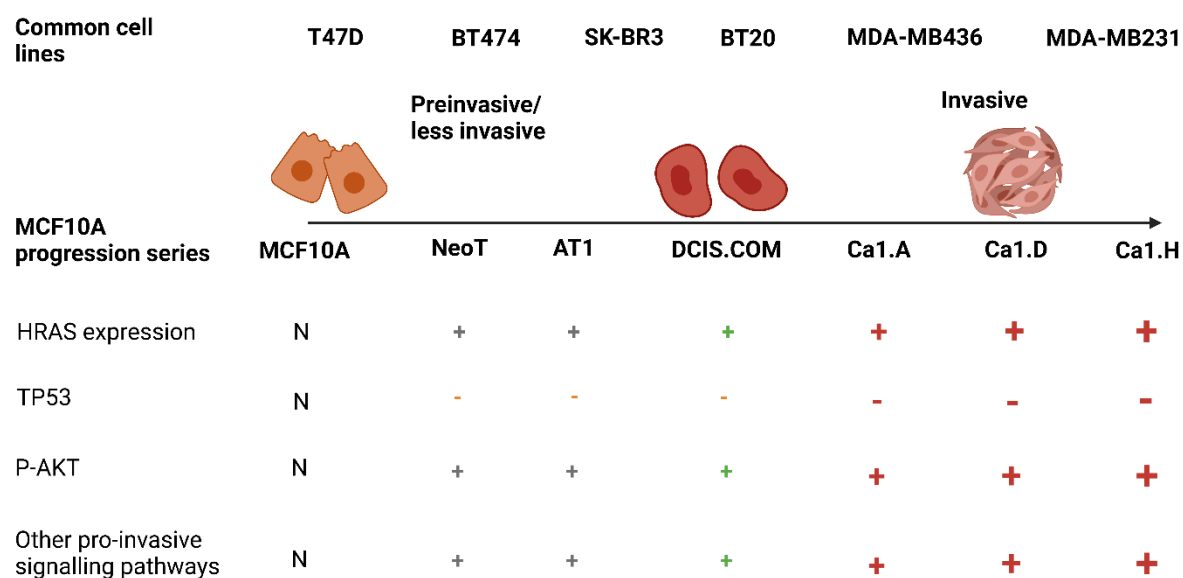


Figure 9 - Characteristics of the MCF10A series cell lines. Common cell lines included on top for comparison

1.14 Aims and Objectives

This thesis has sought to identify relevant *in vitro* models to study the role of PCP proteins in breast cancer and to investigate how the key PCP protein CELSR1 impacts on the metastatic process of breast cancer.

The aims and objectives of this study are:

1. Gain insight into the genetic variation and function of CELSR1 and FZD6 in breast cancer patients by using a computational approach.

- (a) Comparison of CNVs, mRNA and protein expression using the large-scale breast cancer patient datasets (such as TCGA), including different subtypes of breast cancer.
- (b) Correlation of patient survival analysis to determine whether *CELSR1* and *FZD6* mRNA expression has an effect on breast cancer patient survival.
- (c) Gene set enrichment analyses to determine whether *CELSR1* and *FZD6* enrich gene sets involved in signalling pathways which might contribute to or protect against breast cancer invasiveness and aggressiveness.

2. To characterise relevant breast cancer cell lines to act as potential *in vitro* models to study PCP in breast cancer

- (a) Multiplex qPCR to assess the relative mRNA expression of *CELSR1* and *FZD6* in relation to control.
- (b) SDS-PAGE and western blot analysis using a commercial FZD6 antibody, a CELSR1 isoform specific (against PDZ region) and CELSR1 commercial antibodies to assess protein expression.
- (c) RT-PCR, gel electrophoresis and Sanger sequencing to conduct differential splicing analysis of the C-terminal tail region of CELSR1 and FZD6
- (d) Immunocytochemistry of breast cancer cell lines using commercial FZD6 and CELSR1 antibodies as well as a custom-made isoform specific CELSR1 antibody to determine sub-cellular localisation and staining pattern of CELSR1 and FZD6 in human breast cancer cell lines

3. To assess the role and significance of CELSR1 in breast cancer using model cell lines and *in vitro* functional assays

(a) Knock- down of CELSR1 in MCF10A and BT474 cell lines using CELSR1-specific shRNAs and assessing any phenotypic changes

(b) Overexpression of mouse Celsr1 in highly aggressive basal-type TN MDA-MB231 breast cancer cell lines and conducting functional assays including MTT, migration and colony formation assays to determine any tumour suppressive functions of CELSR1 *in vitro*.

(c) 3D spheroid assays, together with ICC and 3-dimensional imaging techniques to study how cell polarity might change in non-transformed breast cancer cell lines as well as cells with loss-of-function and gain-of-function of CELSR1.

2 – Materials and Methods

2.1. – Bioinformatics

2.1.1. – Analysis of mRNA expression and copy-number variation (CNV)

The cBioPortal for cancer genomics was used to access TCGA Pan-cancer and METABRIC datasets - <https://www.cbioportal.org/> (Cerami et al., 2012; Curtis et al., 2012; J. Gao et al., 2013; J. Liu et al., 2018). CNV and mRNA expression data for *CELSR1* and *FZD6* was downloaded and compared. Loss/gain CNV events and mRNA expression z-scores were analysed. Calculations and scoring was conducted in Microsoft Excel. SHAL DEL – deletion of one copy, Diploid -both copies, Gain – additional copy. CNV events for matching patient samples were compared for *CELSR1* and *FZD6*. The effect of CNVs on mRNA expression was then assessed. This was done by downloading mRNA expression z-scores and comparing them to each CNV event.

2.1.2 - Kaplan-Meier survival plots

To assess the clinical relevance of *CELSR1* and *FZD6* in breast cancer, Kaplan-Meier survival plots were generated using KM plotter (Lánczky & Győrffy, 2021). Overall survival plots were generated using the mRNA gene-chip datasets. The Affy ID for *CELSR1* was 41660_at, for *FZD6* 203987_at. Patients were split using the ‘auto select best cutoff’ option. Plots were generated for all breast cancer subtypes without further specification; no other settings were changed. Next, we wanted to see whether the significance of *CELSR1* expression on overall survival changes with increasing invasive potential of major breast cancer subtypes. The same analysis was conducted as described above; however, the breast cancer subtype was specified using the Subtype-StGallen option. Survival plots were generated for Luminal A, Luminal B, HER2+ and Triple negative subtypes.

2.1.3 – UALCAN

The University of ALabama at Birmingham CANcer data analysis Portal – UALCAN, was used to determine *CELSR1* and *FZD6* expression in different subtypes of breast cancer (Chandrashekar et al.,

2017, 2022). The TCGA breast invasive carcinoma dataset was probed, and the graphical outputs downloaded.

2.1.4 - GEPIA2

GEPIA2 was used to assess the significance of CELSR1 and FZD6 as a tumour suppressor and oncogene in breast cancer, respectively (Z. Tang et al., 2019). A body map was generated to see how gene expression varies from normal to cancerous tissue followed by a comparison of expression between different types of cancer.

2.1.5 - Gene set enrichment analysis (GSEA)

The cBioportal (Cerami et al., 2012; J. Gao et al., 2013) for cancer genomics and the Gene set enrichment analysis software (GSEA) (Mootha et al., 2003; Subramanian et al., 2005) were used to assess how CELSR1 and FZD6 expression in invasive breast cancer affect various signalling pathways and cellular processes related to oncogenesis and metastasis. TCGA Pan-cancer significant mRNA expression (RNAseq) data was downloaded for *CELSR1* and *FZD6* in 'tsv.' format. All fields except 'Gene' and 'Log2 Value' were deleted. The file was then saved as '.rnk' to facilitate compatibility with the GSEA software. The 'rnk.' data file was loaded into GSEA. A GSEA pre-ranked analysis was conducted using the 'h.all.v2022.1.Hs.symbols.gmt' gene set, with the 'Collapse/Remap' option set to 'No_Collapse'. No other settings were changed. Enrichment results with an FDR of <25% were considered significant as recommended by GSEA software.

2.2. - Cell lines

Breast cancer cell lines representing invasive and non-invasive cancer were selected as potential models for this study. All cell lines except MCF7 and MCF10A were a kind gift from Dr.George Poulgiannis (Institute of Cancer Research, London). MCF7 cells were obtained in-house (original source: ECCAC). MCF10A cells (immortalized "normal" breast cell line) were a kind gift from Dr.Katiuscia Bianchi (QMUL, London). With the exception of the MCF10A parental/series, all cell lines were grown in DMEM (Gibco - high glucose, GlutaMAX™ supplement, pyruvate – Fisher Scientific

3196602) at 37°C, 5% CO₂. The media was changed every Monday and Friday each week. N.B. – Initial growth of each cell line was supplemented with 1% Pen/Strep (Fisher scientific - 11568876), all subsequent passages were grown without pen/strep. The SK-BR3 cell line proved susceptible to contamination, therefore 1% Pen/Strep was used more frequently. MCF10A, AT1 and NeoT cells were grown in Gibco DMEM/F12 nutrient mix media (Fisher Scientific - 11554546) supplemented with 100ng/mL cholera toxin (Merck - C8052-5MG), 5% horse serum (Fisher Scientific - 12694207), 10 µg/mL insulin (Merck - I9278-5ML), 20 ng/mL human epidermal growth factor (Fisher scientific - 10193743), 0.5 µg/mL hydrocortisone (Fisher scientific - 17199911) and 1% Pen/Strep (as above) at 37°C, 5% CO₂. MCF10A-Ca1.a, Ca1.d, Ca1.h and DCIS.COM were grown in Advanced DMEM (Fisher Scientific - 11510436) supplemented with 5% horse serum (as above), 1% Pen/Strep (as above) and 2mM L-glutamine (Fisher scientific - 15410314). Cell aliquots were store in liquid nitrogen in FBS and 10% DMSO.

2.2.1 - Cell line authentication and mycoplasma testing

Media from cultured cells was routinely tested for mycoplasma by technical staff at the University of Hertfordshire. Cell lines chosen as models were authenticated by short tandem repeat (STR) profiling. This technique results in a unique DNA ‘fingerprint’ specific to each cell line and is done by amplifying polymorphic markers using PCR. STR profiling was outsourced to the UK Health Security Agencies (UKHSA) cell line profiling services.

2.3 Ethical Approval for study of human NK cells and breast cancer tissue

NHS HRA ethics approval (19/SC/0451) and University of Hertfordshire ethics approval (LMS/PGR/NHS/02939) were granted for the purpose of obtaining and using breast cancer patient samples in this study. Patient samples were obtained from the Breast Cancer Now tissue bank, London. Initially 3 samples of DCIS, TNBC and normal breast tissue were obtained for the characterisation of RNA and protein species. Fixed tissue slides of the same quantity were also obtained for immunofluorescence assays.

2.4. RNA extraction and quality assessment

Cells were cultured for RNA extraction as outlined in 2.2 above. Culture media was aspirated and cells were washed once with ice-cold 1X PBS. Total RNA was extracted using the Absolutely Total RNA Purification Kit (Agilent Technologies – 400800) as per manufacturer's instructions, by adding lysis buffer to the flask. Extracted RNA was stored at -20°C. The quantity and quality of extracted RNA was assessed using the CLARIOstar Plus reader (BMG lab tech) at 220-400 nm wavelength. MARS data analysis software (BMG lab tech) was used for analysis. RNA samples with A260/A280 ratio of ~2 were deemed to be high quality extracts. Agarose gel electrophoresis (1.5% TBE gel run for 90 min. at 100v) was also used for qualitative assessment by observing 2 clear 18s and 28s rRNA bands.

2.5. RT-PCR and direct sequencing of variant mRNAs

cDNA was synthesised from RNA using a High-Fidelity cDNA synthesis kit (Merck – 5081955001) using the random hexamer primer protocol with an internal control as per manufacturer's instructions using 100µg RNA. Primers were designed based on the sequence of known differentially spliced genes from Ensembl genome browser (A. D. Yates et al., 2020) and NCBI gene (Agarwala et al., 2018). Primers for RT-PCR - *CELSR1*(1) F - 5' TCCGCCACCACCAGGGCC 3', R- 5' TGTGGGGTGACGGGCTTG 3'; *CELSR1*(2) F- 5' CTGGGCTCTGGCGGCCCC 3', R - 5'TGTGGGGTGACGGGCTTG 3'; *FZD6* (1) F -5' ACTCAAGTCACTTGGGC 3', R - 5' GCGGCAATACTCTGGTC 3'; *FZD6*(2) F - 5' TTCATCCAAGCCATGTGG 3', R- 5'AAAGTTTACGACAAGGTG 3'. Primers for nested PCR included *CELSR1* F - 5'CTGACGCTGACG GAGCAGACG 3', R - 5' GTGATGCCGCAGCCTGTG 3'. Endpoint PCR was carried out using the GoTaq PCR core System I kit (Promega - M7660) as per manufacturer's instructions in an Eppendorf mastercycler nexus gradient thermal cycler. Cycling conditions were adjusted during the optimisation phase for each primer pair and are detailed in Table 1. A negative control with no template was included. The positive control was human CS20 embryonic spinal cord cDNA obtained from the Human Developmental Biology Resource (HDBR Newcastle – NHS HRA Ethics Ref. 18/NE/0290). RT-PCR products were analysed by agarose gel electrophoresis and DNA sequencing on both cDNA strands.

Table 1 - RT-PCR cycling conditions

<u>Stage</u>	<u>Temperature (°C)</u>	<u>No. of cycles X Time</u>
Initial denaturation	95	2 min.
Denaturation	95	30 x 1 min. each
Annealing	65 (Primer pair 1)	
	66 (Primer pair 2)	
Extension	72	
Final extension	72	5 min.

2.5.1. Agarose gel electrophoresis for detection of differentially spliced variants and excision of bands

PCR products were analysed by agarose gel electrophoresis using a standard laboratory horizontal midi-gel tank. Samples were loaded on a 1.5% agarose gel made in Tris-Borate EDTA (TBE), which was run at 100V for 90 minutes. The gel was post-stained with GelRed Nucleic Acid Gel Stain (Cambridge Bioscience - BT41003) 1:30 solution in deionized water for 30 mins by gentle rocking. Stained gels were viewed under UV light, and images acquired using an InGenius 3 manual gel documentation system and GeneSys software (Syngene).

For Sanger sequencing, PCR was performed as described as in 2.5.0. PCR reactions using the same primers were pooled per sample and a volume of 150-200 μ L loaded on a gel made with wells of a larger width. PCR fragments were separated using a 2% agarose gel made with TBE to better resolve bands as they were within <100bp of each other. The gel was run for about 2 hours. Gels were post-stained as described above but for 1-2 hours, as a 2% gel was used. After staining, the gel was viewed on a UV table and individual bands were excised using an extra sharp scalpel. Excised fragments were purified using the QIAquick Gel extraction kit (Qiagen – 28704) as per manufacturer's instructions. The final eluate and primers were quantified using the CLARIOstar Plus reader (BMG lab tech). Purified PCR fragments were verified by agarose gel electrophoresis on a 1.5% gel made in TBE, at 100V for 90 minutes, post-stained with GelRed as described above.

2.5.2 DNA sequencing and analysis of sequencing data

Sequencing primers together with excised and purified DNA fragments were diluted according to Source Bioscience's (Cambridge) Sanger sequencing sample submission requirements (10ng/μL DNA, 3.2pmol/μL sequencing primers). Purified fragments were submitted to Source Bioscience for Sanger sequencing as per their instructions. cDNA fragments were sequenced on both strands.

Sequencing data was analysed in FinchTV chromatogram viewer software (Geospiza Research Team - <https://digitalworldbiology.com/FinchTV>). Manual quality control was conducted for each sequence and blank "Ns" were replaced with the most appropriate base according to the chromatogram. Final forward and reverse sequences were translated using ExPASy translate tool (<https://web.expasy.org/translate/>). Multiple sequence alignment of amino acid sequences was done using EMBL-EBI Clustal Omega (<https://www.ebi.ac.uk/Tools/msa/clustalo/>); Human splice variant and mouse sequences from NCBI Gene were included in the multiple alignment as a reference. Final alignments were prepared using JalView (Waterhouse et al., 2009) and colour-coded using ClustalX based on amino acid features.

2.6. - Quantitative PCR (qPCR)

2.6.1. Housekeeping gene selection

The relative quantification method ($\Delta\Delta C_t$) was used to assess the levels of expression of *FZD6* and *CELSR1* in our human breast cancer cell line models. Initially, the GeNorm kit (Primerdesign – ge DD 6) was used to assess the most relevant housekeeping gene for our cell lines. The following candidate genes were selected within the kit – *ACTB*, *18S*, *YWHAZ*, *GAPDH*, *ATPSYNTH*, *CYT-C*. The second set of genes analysed were obtained as ready-made assays from ThermoFisher Scientific based on studies suggesting these as ideal housekeeping genes for cancer-based qPCR were (Kiliç et al., 2014; Tilli et al., 2016) *PUM1* (ThermoFisher scientific - Hs00472881_m1) and *CCSER2* (ThermoFisher scientific - Hs00397623_mH).

2.6.2. Multiplex qPCR

Taqman primers and Taqman probes were obtained as pre-designed multiplex qPCR assays from ThermoFisher Scientific with the following dye combinations - *CCSER2* FAM-MGB (Hs00397623_mH), *FZD6* VIC-MGB (Hs01092009_m1) and *CELSR1* JUN-QSY (Hs00947709_m1). The Oasig Lyophilised qPCR Master Mix (PrimerDesign - oasig-standard-150) was used without ROX (a background control). The reaction was set-up according to the manufacturer's instructions consisting of the master mix, predesigned primer/probe mix and water. This was the main mix which was first added to each well. The template was added to each well separately at a concentration of 100ng/ μ L. The qPCR run was set up according to the Oasig Lyophilised qPCR mastermix user manual, with 40 cycles. The reference sample used was MCF10A cDNA.

2.7. SDS-PAGE and western blot analysis

2.7.1. Preparation of whole cell lysates

Cells were grown as described (2.2.0), media was aspirated, and cells were washed with cold 1X PBS. Whole cell lysates were prepared using a custom-made cell lysis buffer as reported by Formstone et.al. (2010) – 20mM Tris-HCL pH8, 2mM EDTA, 2% Triton X-100 and 1 tablet of protease inhibitors per 10mL (Fisher Scientific – 15672129). 1 mL of ice cold cell lysis buffer was added directly to a T-25 or T-75 flask on ice, respectively. The flask was left for 10 minutes after which lysis was aided by scraping the cells and washing down then sides of the flask. DNase I (ThermoFisher Scientific – 180-015) was then added. The lysate was then centrifuged at 15,000 RPM for 20 minutes at 4°C. The supernatant was aliquoted and stored at -20°C.

2.7.2 Measurement of protein concentration

Prior to SDS PAGE, total protein was quantified by Bradford assay using the Pierce Detergent Compatible Bradford Assay Kit (ThermoFisher Scientific – 23246). A standard curve was prepared, and the standard microplate procedure was followed as per manufacturer's instructions. All samples

including the standard curve were prepared in triplicate. The 96-well microplate was read using a CLARIOstar Plus reader (BMG lab tech) at 595nm. MARS data analysis software (BMG lab tech) was used to analyse the data. A curve fitting algorithm was used to plot a quadratic standard curve, which was used to determine the total protein ($\mu\text{g}/\text{mL}$) in each sample. The average of each triplicate was used as the final total protein at $\mu\text{g}/\text{mL}$.

2.7.3. SDS-PAGE

SDS-PAGE was carried out using a 7.5% or 10% polyacrylamide gel made with ProtoGel 30% Soln. 37:5:1 (Geneflow - A2-0074), ProtoGel resolving buffer Tris/SDS (Geneflow - B9-0012), ProtoGel stacking buffer Tris/SDS (Geneflow - B9-0014), TEMED (Biorad – 1610800) and 10% ammonium persulfate + TEMED. Protein samples were diluted in deionized water to a final concentration of $1\mu\text{g}/\mu\text{L}$. Samples ($10\mu\text{g}$) were then prepared in SDS PAGE treatment buffer as described by Formstone et.al. (2010) – 4M urea, 3.8% SDS, 20% v/v glycerol, 75mm Tris-HCL pH 6.8, 5% v/v 2-mercaptoethanol and bromothymol blue. Samples were then denatured at 95°C for 5 minutes. Human NK cells were used as a positive control for FZD6 (a kind gift from Dr Diana Hernandez, Anthony Nolan Trust). The sample/treatment buffer mixture ($20\mu\text{l}$) was loaded into individual wells, and the gel run at 180 V for approximately 2 hours in 1X tank buffer (25mM Tris Base, 192.4mM Glycine, 3.46mM SDS). Precision Plus Protein™ All Blue Prestained Protein Standards (Biorad - 1610373) were used as a size marker.

2.7.4. - Western blot analysis

Following SDS-PAGE, the gel was equilibrated in transfer buffer (25 mM Tris, 192 mM glycine, 20% v/v methanol) for 15 minutes. The gel was then placed in a western sandwich for wet transfer to a $0.45\mu\text{m}$ nitrocellulose blotting membrane (Fisher Scientific – 10600114), which was carried out for 2 hours in transfer buffer at 80v and 4°C . Following transfer, membranes were blocked in 5% BSA/milk PBST (1X PBS, 0.1% Tween-20) for 1 hour at RT or overnight at 4°C . Primary antibody was made in 1% BSA/milk PBST. The membrane was then incubated in primary antibody overnight at 4°C or 2 hours RT with gentle agitation. Next, primary antibody was removed, and membranes were washed 3x with PBST for 5 minutes. Membranes were then incubated with secondary antibody, also made in 1%

BSA/milk PBST, at room temperature for 1 hour with gentle agitation. Finally, secondary antibody was removed, and membranes were washed 3x with PBST for 5 minutes. The membrane was placed on the imager stage and covered in Pierce™ ECL Western Blotting Substrate (32109 – ThermoFisher Scientific) or Novex™ ECL Chemiluminescent Substrate Reagent Kit (ThermoFisher Scientific - WP20005) and left for 1 minute. Chemiluminescent imaging was carried out with a myECL Imager or the iBright 1500 imaging systems (both ThermoFisher scientific). Band size was estimated using the overlay method which enabled the ladder to be overlaid over the chemiluminescent blot. Images were exported and edited/labelled using a combination of iBright image analysis software, Fiji, Biorad ImageLab, Adobe Photoshop and Adobe Illustrator.

2.7.5 Antibodies for western blots

Primary and secondary antibodies used for western blots are detailed in the table below –

Table 2 - Antibodies used for western blots

<u>Antibody</u>	<u>Type</u>	<u>Dilution</u>	<u>Manufacturer</u>
Frizzled 6 rabbit mAb	Primary	1:1000	Cell signalling technology - 5158
Celsr1 pB (CELSR1iso)	Primary	1:1000	Generated by Formstone lab
CELSR1 (CELSR1sc)	Primary	1:100	Santa Cruz Biotechnology – sc-514376
GAPDH	Primary	1:5000	Merck Millipore – AB2310
Actin	Primary	1:5000	Merck Millipore – MAB1501
Beta-actin monoclonal antibody	Primary	1:2000	Fisher Scientific - 15597191
Transferrin	Primary	1:500	Fisher Scientific - 11533723
Vimentin Antibody	Primary	1:50	DSHB – 40E-C
EEA1 monoclonal antibody	Primary	1:1000	ProteinTech - 68065-1-Ig
HRP conjugated anti-mouse	Secondary	1:1000	Cell signalling technology - 7076
HRP conjugated anti-rabbit	Secondary	1:1000	Fisher Scientific - 103796640
HRP conjugated anti-rabbit	Secondary	1:1000	Cell signalling technology - 7074S

HRP linked anti-chicken antibody	Secondary	1:1000	Merck - A9046
----------------------------------	-----------	--------	---------------

2.8. Immunocytochemistry

Cells were grown in T-25 or T-75 flasks until confluent. Cells were then washed with 1X PBS, trypsinised and seeded at 50,000 cells/well in 2,4 or 8-well chamber slides (Fisher scientific – 16240681). Media was changed every Monday and Friday where necessary. Cells were fixed when they reached 80-90% confluency. Media was aspirated from the wells and cells were washed with 1X PBS. Cells were covered in 4% methanol-free formaldehyde in 1X PBS (ThermoFisher – 28906). Following a 15-minute incubation at RT, formaldehyde was removed, and cells were washed twice with 1X PBS. Chamber slides with fixed cells were then either stored sealed in sterile 1X PBS at 4°C until further processing or immediately processed further.

PBS was aspirated from the chamber slide wells. Fixed cells were incubated in PBS/1% Triton X-100 for 15 minutes with gentle agitation and subsequently incubated in a blocking solution - 10% goat serum (Fisher Scientific - 11475055) in PBS/1% Triton X-100 for 30 minutes at RT with gentle agitation. The blocking solution was aspirated, and cells were incubated in primary antibody (in 10% goat serum PBS/1% Triton X-100) overnight at 4°C with gentle agitation. Dilutions for each antibody are shown in Table 3. Primary antibody dilutions were vortexed to mix and centrifuged at 13,000 rpm to exclude large protein aggregates prior to pipetting into each chamber. Next day, the antibody solution was aspirated, and cells were washed 3 times with PBS/1% Triton X-100 for 5 minutes. For secondary antibody alone controls, cells were incubated in block without primary antibody. All cells were subsequently incubated in secondary antibody (prepared as for primary) for 1hr at RT with gentle agitation. Cells were then again washed 3x with 1X PBS/1% triton for 5 minutes. Where indicated cells were incubated with Alexa Fluor 488 Phalloidin (ThermoFisher Scientific - A22287) according to the manufacturer's instructions (2 drops per mL). Chambers were then gently removed leaving only the slide. A few drops of 4',6-diamidino-2-phenylindole (DAPI) in 1X PBS were applied to each slide and left for 5 minutes. Excess liquid was gently dabbed off with tissue paper. To mount the slides a few drops of SlowFade diamond antifade mountant (ThermoFisher Scientific - S36967) or

in-house made anti-fade mountant (*Anti-Fade Mounting Medium - Jackson ImmunoResearch, n.d.*) were applied to the slide and coverslip was gently dropped downwards at a 45° angle. The coverslip was sealed using nail varnish. The slides were protected from light and stored at 4°C overnight allowing the nail varnish to dry.

2.8.1. - Antibodies for immunofluorescence

Primary and secondary antibodies used for ICC are detailed in the table below –

Table 3 - Antibodies used for immunocytochemistry

<u>Antibody</u>	<u>Type</u>	<u>Dilution</u>	<u>Manufacturer</u>
Frizzled 6 rabbit mAb	Primary	1:1000	Cell signalling technology - 5158
Frizzled 6	Primary	1:250	R&D systems - AF3149
Celsr1 pB (CELSR1iso)	Primary	1:1000	Generated by Formstone lab
Celsr1 pA	Primary	1:1000	Generated by Formstone lab
CELSR1 (CELSR1sc)	Primary	1:100	Santa Cruz Biotechnology - sc-514376
Vimentin Antibody	Primary	1:50	DSHB – 40E-C
EEA1 monoclonal antibody	Primary	1:1000	ProteinTech - 68065-1-Ig
CD63 antibody	Primary	1:1000	Merck - SAB4700215-100UG
YL 1/2	Primary	1:250	BioRad - MCA77G
Cytokeratin	Primary	1:1000	
Anti-Laminin	Primary	1:800	Merck - L9393
Anti-caspase 3	Primary	1:500	R&D systems - AF835
PARD3/Par3	Primary	1:1000	R&D systems - MAB8030-SP
Anti mouse Alexa Fluor 488	Secondary	1:1000	ThermoFisher scientific - A-11001
Anti goat Alexa Fluor 488	Secondary	1:1000	ThermoFisher scientific - A-11055
Anti-rat Alexa Fluor 568	Secondary	1:1000	ThermoFisher scientific - A-11055
Anti rabbit Alexa Fluor 598	Secondary	1:1000	ThermoFisher scientific - A-11012
Anti mouse Alexa Fluor 647	Secondary	1:1000	ThermoFisher - A-21242

2.8.2 Fluorescence microscopy

Fluorescent images were obtained using a Zeiss Axioimager M2 microscope fitted with an Axiocam 503 imaging device using Zeiss ZEN software (Zeiss Microscopy). Cell fluorescence was visualised using an EC Plan-Neofluar 63X (1.25) oil objective. The following channels were used for various fluorophores - DAPI (Ex. -353, Em.-465), Alexa Fluor 488 (Ex.-493, Em.-517), Alexa Fluor 568 (Ex.- 577, Em.-603), Alexa fluor 594 (Ex.-280, Em.-618) and Alexa fluor 647 (Ex.-653, Em.-668). The ZenBlue (Zeiss) software was used for image acquisition and subsequent analysis.

2.9 3D spheroid assays

2.9.1. Matrigel

BT474 and MDA-MB231 cells grown as described in 2.2.0. above and resuspended in media pre-cooled on ice and mixed with Matrigel (Corning - 356234) at final concentration of 100,000 cells/mL as per manufacturer instructions. 200 μ L of the cell-matrigel mixture was then pipetted onto sterile glass coverslips which had been positioned in the centre of a 6-well plate. The mixture was allowed to solidify for 1 hour at 37 °C in a humidified cell culture incubator and 5% CO₂ before media was added. Cell spheres were allowed to form typically for 7 days in a humidified cell culture incubator at 37°C/ 5% CO₂.

2.9.2 – Agarose

Agarose was used as a substrate for the cells to grow upon as described previously (Jaiswal et al., 2017a). Briefly, molecular biology grade agarose (Fisher scientific -10766834) was mixed with 1X PBS to create a 1.6% solution and heated on a hot plate inside a biosafety cabinet until the mixture simmered and agarose dissolved. The wells of a 96 well U-bottom plate or 8-well chamber slide were then coated with the agarose whilst still molten. The plate/slide was placed under a UV lamp inside the biosafety cabinet for 1 hour for sterilisation. Cells were then seeded at varying densities (depending on the cell type) onto the agarose within each well to form spheroids and maintained in

complete DMEM for 7 days or until the spheroids reached a desired diameter of about $\sim 300\mu\text{M}$ measured by GXCapture software (GT Vision UK).

2.9.3. – Alginate beads in agar moulds

Cells were grown in alginate beads solidified in agar moulds as described previously (Cavo et al., 2018). Briefly, 1% technical agar (Fisher scientific - 11793523) in 25mM HEPES and CaCl_2 buffer was autoclaved to sterilise, poured in a 6-well plate, and allowed to solidify. A Pasteur pipette was used to create 3 holes in the agar plug for each well. Ultra-pure alginate (IFF Nutrition Norge AS d/b/a NovaMatrix - Pronova SLG100-GMP) was resuspended in HEPES buffer to create a 2% stock solution. Cells were mixed with alginate or a 50:50 alginate Matrigel mix to a density of 100,00 cells and pipetted into the agar moulds. The plate was then placed into a tissue culture incubator at 37 °C to allow for gelation of the alginate which involves diffusion of CaCl_2 ions from the agar into the alginate for 1 hour and 15 minutes. The alginate beads were then carefully removed from the agar plug and placed in suspension in a 96-well plate. Media was added, and cells were grown within the alginate beads for a week initially.

2.9.5 - Ultra-low attachment plates/spheroid plates

Cells were cultured in Corning® Elplasia® ultra-low attachment plates (24-well) as per manufacturer's instructions. Briefly, the plates were wetted with 500 μL media and spun at 500 RPM for 1 minute to get rid of any air bubbles in the micro-grooves. This was followed by seeding 5000 cells per well. Spheroids were cultured for 7 days or until they reached 250-300 μm in diameter, after which they were processed as described previously (Gonzalez et al., 2021).

2.9.6 – Alginate beads

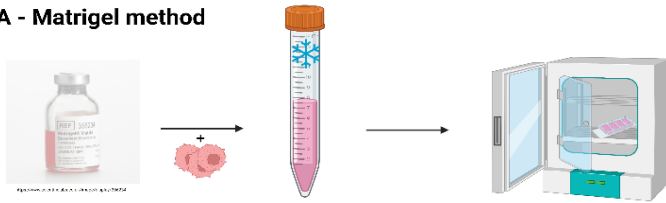
Cells were grown in 1.2% ultra-pure alginate beads (IFF Nutrition Norge AS d/b/a NovaMatrix - Pronova SLG100-GMP) as described previously (Jaiswal et al., 2017b). Briefly, cells were trypsinised and diluted to a desired concentration of a total of 10^6 cells/mL. The cells were spun down, and trypsin/media removed. The cells were then mixed with 1mL of the 1.2% alginate without creating air

bubbles. The mixture was drawn into a 1mL syringe with a 21-g needle. The mixture was slowly ejected to generate small drops of cell/alginate mixture over a petri dish with 20 mL sterile CaCl₂ solution. Upon contact the droplets immediately solidified and formed small beads. These were then placed into an incubator for 15 minutes to allow further gelation. After the beads were washed twice with 0.9% NaCl and once with complete media. Complete media was then added to the dish to cover the beads and cultured in a humidified incubator with 5% CO₂ at 37° C for up to two weeks depending on cell type.

2.11 Over-expression of mCelsr1 in breast cancer cell lines

A full-length mouse Celsr1 cDNA tagged at the C-terminus with eGFP and cloned into a pCDNA3.1 mammalian expression vector (Formstone et al., 2010) was stably transfected into breast cancer cell lines. As the pCDNA3.1 expression plasmid contained a gentamycin (G418) antibiotic resistance gene, an antibiotic G418 sulphate (ThermoFisher Scientific - 10131035) kill curve was first performed on MDA-MB-231, BT474 and MCF10A cells to determine an appropriate antibiotic concentration for selective cell growth following transfection. Cells were then seeded in a 12-well plate according to the manufacturers protocol for Lipofectamine 3000 transfection (ThermoFisher Scientific -L3000001). 0.5 ug of mCelsr1 expression plasmid/empty vector was transiently transfected into each cell type following the manufacturer's protocol. After 2 days transfected cells were analysed using an EVOS FL fluorescent microscope (Invitrogen) with the GFP filter to check for GFP-positive cells. If fluorescent cells were observed then cells were immediately trypsinised, pooled if multiple wells were transfected with the same plasmid for the same cell type, and seeded into a 20cm dish in media containing sufficient G418 to kill non-expressing cells. Cells were allowed to form colonies for 1-2 weeks depending on the cell line periodically checked for colonies exhibiting green fluorescence. Most of the media was then removed and GFP-positive colonies were marked with a circle on the outside of the bottom of the dish. Marked colonies were then picked by coincident scraping and sucking up using a pipette and pipette tip and transferred into a 6 well plate.

A - Matrigel method

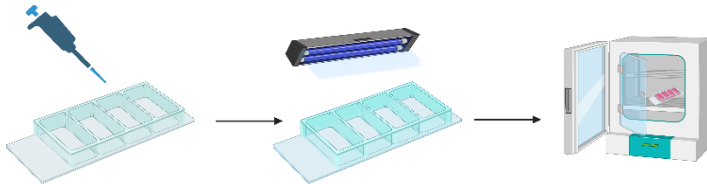


1. Cells were mixed with Matrigel on ice

2. The Matrigel cell mix was then deposited into wells of a chamber slide.

3. The chamber slide was then placed in an incubator for 15 minutes for matrigel to undergo gelation, after which DMEM was added and cells were incubated for 7 days

B - Agarose method



1. The surface of the wells was coated with agarose and let to solidify

2. The agarose coated chamber slide was placed under a UV lamp for 1 hour

3. A desired number of cells was plated into each well with complete media and cells were incubated for 7 days

C - Alginate beads in agar mould method



1. The agar-CaCl₂ was poured into the wells of a 6-well plated

2. A Pasteur pipette was used to create 3 holes in each well

3. A desired number of cells in complete DMEM was mixed with 1.2% ultrapure alginate and pipetted into each mold

5. The plate was incubated for 1h15m to allow calcium ions to diffuse from the agar into the molds.

6. The beads were taken out from the molds using a spatula and placed into a 96-well plate with complete media and incubated for 7 days

D - Ultra-low attachment plates



1. The ULAP plate was 'wetted' with media and spun at low speed to remove air bubbles
2. A desired number of cells in complete DMEM was pipetted into each well and the plate was placed into an incubator with 7 days

E - Alginate bead method

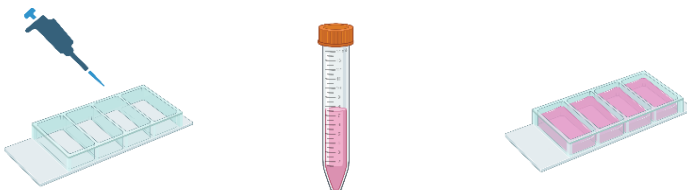


1. A desired number of cells was spun down and the pellet resuspended in 1.2% alginate
2. The petri dish was placed into an incubator for 15 minutes to allow for complete gelation of the beads

3. The alginate-cell mixture was drawn up into a syringe with a needle and was then slowly ejected dropwise into a petri dish containing a CaCl₂ solution

4. Beads were then washed 3x with 1XPBS and complete media. Beads were then incubated in complete media for 7 days

F - EHS on-top culture



1. The surface of the wells was coated 50uL EHS and left to solidify in an incubator

2. A desired number of cells was resuspended in assay medium and plated on top of the solidified EHS. Spheroids were grown for up to 14 days in an incubator

Figure 10 - Various methods used for 3D cell culture. A-E - Method titles are self-explanatory. Details in text. Created with biorender.com

Once cells were confluent within the 6-well plate cells were grown up in a T-75 flasks for freezing down, as described below. Multiple vials were frozen as individual vials of frozen cells were grown on for protein and functional analysis but only passaged once before disposal due to DNA recombinant events in the cancer cell lines which silenced or removed the mCelsr1 expression plasmid.

2.12 - Lentiviral based shRNA knockdown of *CELSR1*

2.12.1 Lentiviral based ShRNAs

Small hairpin RNAs (shRNA) for *CELSR1* were bought 'off-the-shelf' as validated shRNAs (SHCNLV) from Sigma/MERCK. *CELSR1* shRNA containing MISSION pLKO.1 plasmids with puromycin antibiotic resistance were either purchased as lentiviral particles (3rd gen) generated by transient transfection, or MERCK provided us directly with shRNA containing lentiviral transduction particles. shRNAs sequences were 5' AGGAGGTGCAACCTGTATATA 3' (TRCN0000273659) which was located within and targeted the 3'UTR and 5' CCAGAAATACTCGCTGAGCAT 3' (TRCN0000011238) which was located within the Cadherin3 domain of *CELSR1*, see Figure 40 in Chapter 3. The MISSION® pLKO.1-puro non-mammalian shRNA Control Plasmid DNA (SHC002) was used as a negative control.

2.12.2 - Lentivirus production using Calcium phosphate method

To generate lentiviral particles HEK293 cells were grown in a T-175 flask until confluent. Cells were then trypsinised and seeded at a density of 2.3×10^5 cells per well in a 6-well plate. Once the cells reached around 50-80% confluency, the transfection procedure was started. On day one, the shRNA containing plasmid was transiently transfected into cells using the CalPhos Mammalian transfection kit (Takara- 631312) along with the MISSION® Lentiviral Packaging Mix (Sigma-Aldrich - SHP001) which containing viral packaging plasmids, following the manufacturer's instructions. On day 2, after an overnight incubation, the calcium phosphate containing medium was removed and cells were washed once with 1X PBS and 2 mL of fresh media was added. Media used was specific for each cell line as

described. The cells were incubated for an additional 48 hours. On day 4, the virus containing medium was collected and stored at 4°C. Media was replaced fresh and virus expressing cells shed virus into the media for an additional 24 hours. On day 5 the second batch of virus containing medium was collected and pooled with the first. The pooled media was centrifuged at 1500rpm for 7-minutes and the supernatant transferred into fresh falcon tubes. A small quantity of raw supernatant was retained for estimation of viral titre. Following sterile filtration of supernatant using a 0.45µM filter. The supernatant was ultra-centrifuged at 26,000 RPM at 4°C for 2 hours to sediment the viral particles which were subsequently re-suspended in 150µL sterile 1XPBS following aspiration of the supernatant. 10-20µL aliquots were made, placed on dry ice, then stored at -80° C. The viral titre of the concentrated particles was determined using qPCR as described below. All plasticware in contact with lentivirus particles were treated with 10% bleach solution before disposal by autoclaving.

2.12.3 – Lentivirus production using Lipofectamine 3000 method

HEK293 cells were treated as outlined in 2.12.2 above and Lipofectamine 3000 transfection reagent (ThermoFisher Scientific -L3000001) was used together with the lentiviral packaging mix protocol according to the manufacturer's instructions. Briefly, the transfection cocktail was made according to the two protocols optimised for a 6-well plate. The transfection cocktail was added to the wells and cells were incubated overnight. On day two the media was removed and replaced with fresh media which was left on cells for a further 24 hours. On day 3 the virus containing media was harvested and stored at 4°C: fresh media was added to the cells. On day 4 the virus containing media was harvested for a second time, pooled with the first and stored at 4°C. A small quantity of media was put aside for viral titration. The remaining media was subject sterile filtration using a 0.45µm filter followed by ultracentrifugation at 26,000 RPM at 4°C for two hours to concentrate the viral particles. The supernatant was aspirated, and the viral pellet was resuspended in 150µL of sterile 1XPBS, 50µL aliquots were made. The viral titre of the concentrated particles was determined using qPCR as described below. All plasticware in contact with lentivirus particles were treated with 10% bleach solution before disposal by autoclaving.

2.12.4 – Lentiviral titre determination

Viral titration was performed using the qPCR Lentivirus Titre Kit (abm-LV900) following the manufacturers protocol. Briefly the ABI Quantstudio 7 Flex instrument (Applied Biosystems - ThermoFisher Scientific) was used with the SYBR green channel, as the kit included SYBR based probes. The final desired viral titre was calculated using abm's calculator available to download here - <https://www.abmgood.com/qpcr-lentivirus-titration-titer-kit.html> .

2.12.5 Lentiviral transduction

shRNA plasmids contain a puromycin resistance gene and thus a puromycin kill curve was performed on cell lines to determine the minimum concentration of puromycin required to kill cells which do not express the shRNA plasmid. The protocol for MISSION lentiviral transduction particles (SHCLNV, /MERCK) was followed. Number of viral transduction particles required was calculated by using the equation in the manufacturer's protocol – this was dependent on the number of cells seeded per well and the multiplicity of infection (MOI) desired (5 and 20 MOI were used). Briefly, 24 hours prior to transduction, cells were plated in a 96-well plate and incubated until they reached 50-80% confluency. The lentiviral stock/viral particles were thawed on ice. Hexadimethrine bromide (Merck-H9268) in 1X PBS was added to cells at a concentration of 8µg/mL to enhance transduction. The calculated volume of lentiviral particles corresponding to either 5 or 20 MOI was added to each well. After 24 hours, media was changed and after a further 24 hours cells were tryprinised and moved into a 6-well plate with complete DMEM including 0.0005 mg/mL puromycin. Cells were grown until stable colonies had formed. Three to five colonies for each MOI were picked per cell line and expanded on into 6 well plates. Once cells were confluent, they were trypsinised and grown on into a T-25 flask and multiple aliquots frozen in liquid nitrogen as described before, but with the addition of 0.5 µg/mL puromycin.

2.12.6 – Wound healing assay

Control and experimental cells were seeded in triplicate in a 6-well plate at 200,000 cells per well. Once cells reached confluency (typically 48 hours after seeding), a uniform horizontal scratch was performed using a sterile yellow P200 tip. Another scratch was performed in the same well vertically resulting in a cross scratch. This was done to maximize the number of imaging points and minimize uneven scratch areas. Media was aspirated following the scratching process and cells were washed once with 1X PBS to remove cell debris. PBS was aspirated and replaced with fresh media. Each scratch was photographed at 3 different time points, 0h, 24h, and 48h, using an Olympus CKX41 inverted microscope fitted with a GXCAM HiChrome-MET camera, at 4X magnification (0hr). The cell-free area within the wound scratch was then measured using Fiji Image J (Schindelin et al., 2012) using a specialised plugin for wound healing assays (Suarez-Arnedo et al., 2020). Mean of 3 scratch sites per well x technical repeats for each of n=3 samples were calculated in excel and n=3 values for biological replicates plotted on a graph using GraphPad Prism. One-way ANOVA with Tukey's multiple comparisons test was done for statistical analysis.

2.12.7 MTT assay

Cell proliferation was assessed using the MTT assay kit (Abcam - ab211091) following the manufacturers protocol. Briefly, 10,000 cells were seeded in each well of a 96-well plate in quintuple, which included 5 control wells which contained media only and no cells. Once cells had reached 70% confluency, media was aspirated and replaced with 50µL fresh media + 50µL MTT reagent. The plate was covered with foil and incubated at 37°C 5% CO₂ for 3 hours. After 3 hours the MTT reagent was carefully removed and replaced with MTT solvent, which had been pre-warmed to 37°C. The plate was again covered and shaken on an orbital shaker for 15 minutes at RT at moderate speed. Finally, absorbance readings were taken at OD= 590 nm taken using a ClarioStar plate reader (BMG Labtech). An unpaired students t-test was conducted for statistical analysis.

2.14 – Figures

All figures were created using a combination of Adobe Illustrator 2020, Adobe photoshop 2020, Microsoft Powerpoint and Biorender (www.biorender.com). Where the figures were created solely by the author, Biorender is not mentioned.

3. RESULTS – IN SILICO CHARACTERISATION OF THE ROLE OF CELSR1 AND FZD6 IN BREAST CANCER

3.1 Introduction

Computational biology has become a significant part of cancer research over the last decade and plays an important role in modern day cancer research. Large ‘omics’ datasets derived from extensive in-depth patient studies have granted cancer researchers access to a wealth of data, which can be instrumental in the design of *in vitro* experiments. This project has utilised bioinformatics tools to determine the significance CELSR1 and FZD6 have in invasive breast cancer. mRNA expression levels, patient survival data and gene set enrichment were all analysed, both generally across breast cancer but also across subtypes of breast cancer.

3.2 CELSR1 and FZD6 mRNA expression are both altered in breast tumour samples

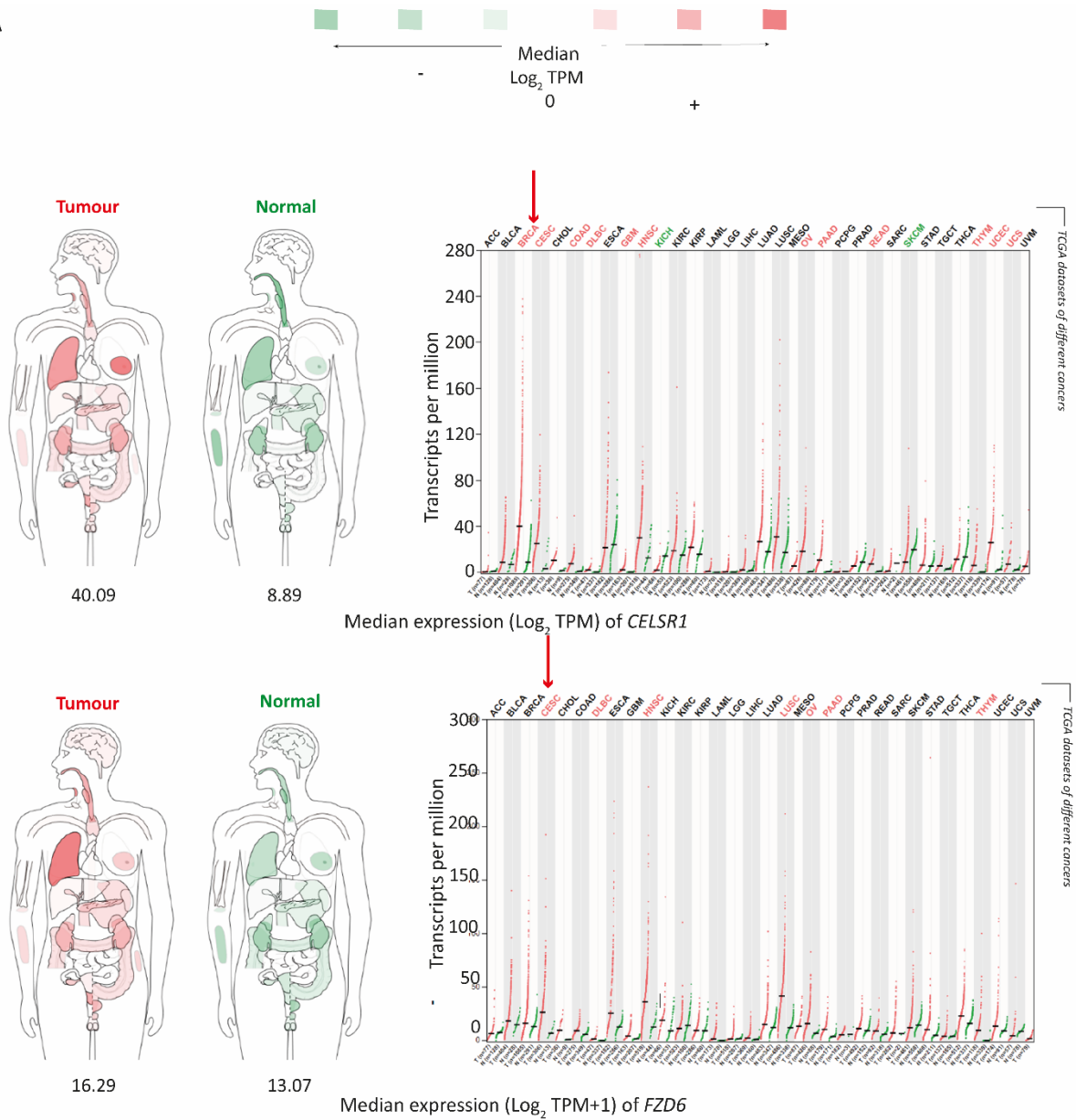
In order to verify that *CELSR1* expression is altered in patients with breast cancer, GEPIA2 and UALCAN were used to probe the TCGA database for mRNA expression data. A body map and a corresponding graph, showing *CELSR1* and *FZD6* expression in all TCGA datasets (breast cancer – BRACA - is highlighted with a red arrow) were generated. In Fig. 11 *CELSR1* expression was found to be increased in breast tumours (40.09 TPM -Log₂ median) compared to normal healthy controls (8.89 TPM - Log₂ median). From among all the different types of cancer, *CELSR1* expression was most altered in breast cancer compared to *FZD6*. The lower panel of Fig.11A shows how *FZD6* expression is altered and it can be seen that there is a small difference between *FZD6* expression in tumour (16.29 TPM - Log₂ median) and normal healthy controls (13.07 TPM -Log₂ median) is 3.22 TPM -Log₂ median. In contrast, the difference between tumour and normal controls for *CELSR1* is 31.2 TPM -Log₂ median. These data are reflected in the intensity of colour for breast in the body map schematics (Fig.11A) which overall provides a useful visualisation of *CELSR1* and *FZD6* expression levels in healthy versus tumour tissue for each organ: *FZD6* levels are highest in lung tumours (Fig.11A). Next, we looked at

mRNA expression data for breast cancer generated by UALCAN. Fig. 11B shows *CELSR1* expression levels are significantly higher in breast tumours (26.7 TPM -median) compared to normal (12.42 TPM – median) controls, whereas *FZD6* expression levels are significantly lower in breast tumours (20.41 TPM – median), compared to normal controls (24.26 TPM - median), but with a smaller *P* value than for *CELSR1*.

3.3 Opposing impact of *CELSR1* and *FZD6* on patient survival with different breast cancer sub-types

Previous publications have reported increased *CELSR1* gene copy-number in less invasive breast cancers and decreased *CELSR1* gene copy number in more invasive breast cancers (Geradts et al., 2016; Liao et al., 2012) whereas the opposite was reported for *FZD6* (Corda et al., 2017; Corda & Sala, 2017). Our analysis of invasive breast cancers (TCGA-pancancer database) confirmed that up to 30% of patient samples exhibit *CELSR1* copy number loss and *FZD6* copy number gain (Fig.12A). Since copy-number variations are not always reflected in mRNA expression levels, mRNA data mining was performed. It was found that mRNA z-score (the number of standard deviations from the mean) decreases with reduced copy-number for *CELSR1* in invasive breast cancer and increases with copy number gains for *FZD6*: changes in copy number were significant in both cases when compared to diploid tumour samples (Fig.12B). Interestingly, *CELSR1* mRNA levels decreased in instances where *CELSR1* copy-number was gained. Low expression of *CELSR1*, on the other hand, had a negative impact on patient survival. In comparison, although *FZD6* expression is not so drastically altered in breast cancer patients (Fig. 12), high expression has a significantly negative impact on the survival of breast cancer patients.

A



B

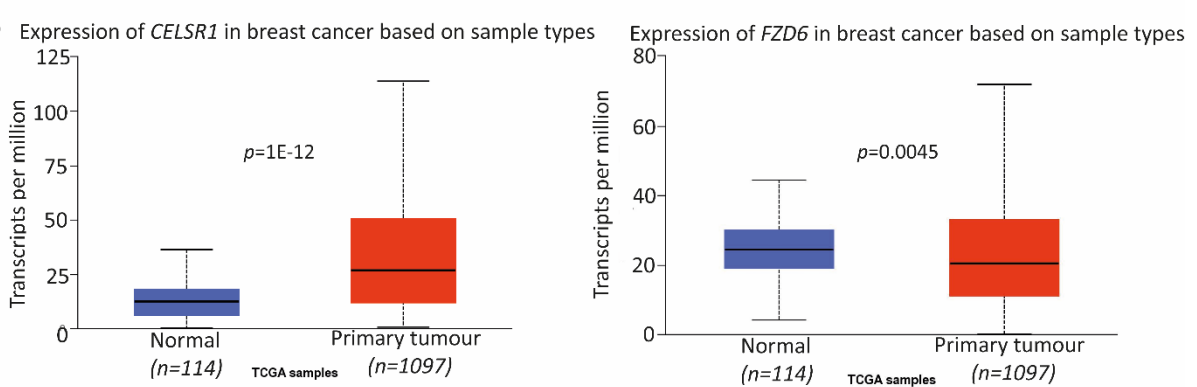


Figure 11 - *CELSR1* and *FZD6* expression is altered in breast cancer and affects patient survival. A. Body map and dot plot showing increased levels of *CELSR1* in breast cancer patients compared to healthy individuals (top). *FZD6* expression levels are slightly increased in breast cancer patients compared to healthy individuals. All expression levels are in transcripts per million (TPM). **B.** UALCAN data showing significantly higher mean expression of *CELSR1* in cancer patients compared to healthy controls. *FZD6* mean expression is significantly lower in tumour patients compared to healthy controls, but expression is more varied. Student-t test (all data for this figure was downloaded directly from the respective websites - <http://gepia2.cancer-pku.cn/> and <https://ualcan.path.uab.edu/>). P values are indicated

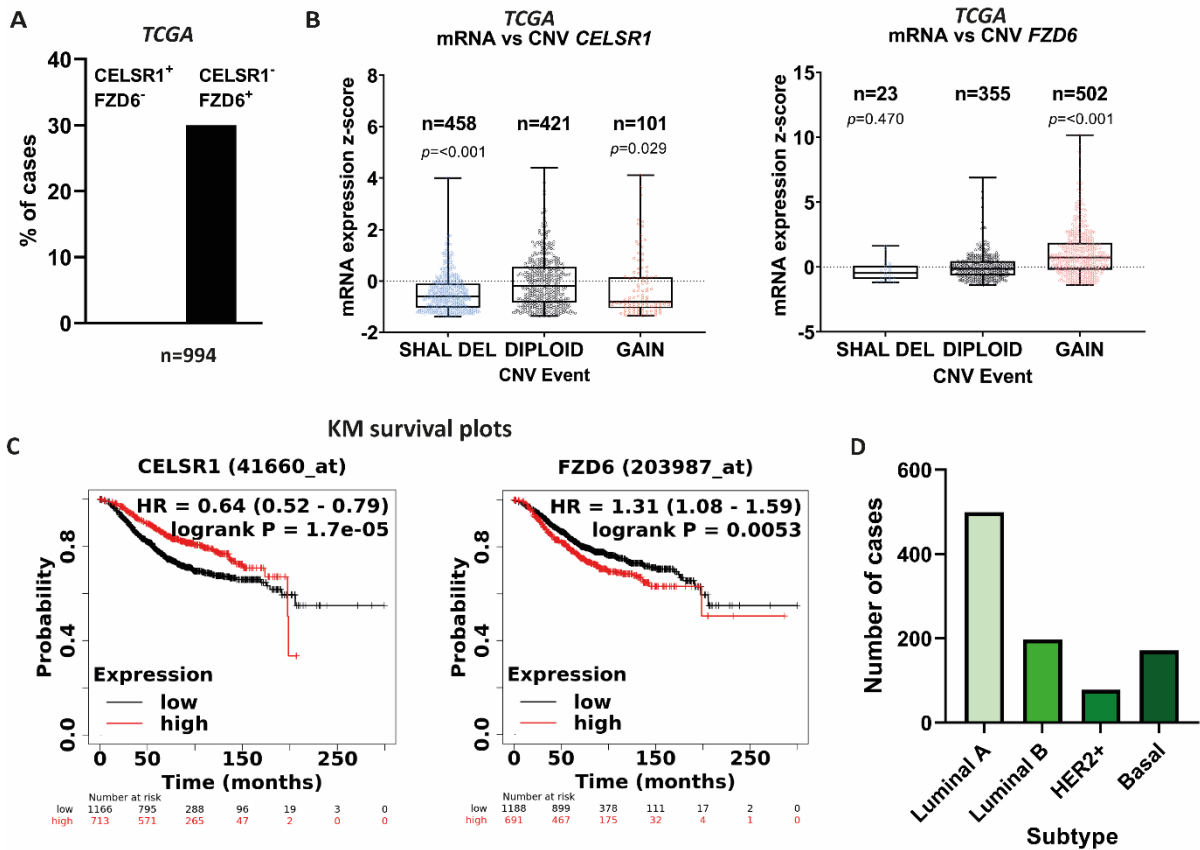


Figure 12 - Copy number variations vs mRNA expression, survival plots and subtypes. A. Total % of patients from TCGA BRCA that *CELSR1* gain/*FZD6* loss and *CELSR1* loss/*FZD6* gain. **B.** mRNA expression z-score vs. CNVs in the TCGA database. *CELSR1* mRNA expression increases from deletion CNV to diploid but then decreases with a gain CNV. *FZD6* mRNA expression increases from deletion through to gain. **C.** Kaplan- Meier survival plots showing that differing expression levels of *CELSR1* (left) and *FZD6* (right) significantly affect the overall survival (OS) of breast cancer patients. High expression levels of *CELSR1* have a positive impact on patient survival compared to *FZD6*. **D.** Breast cancer subtype distribution of the TCGA dataset taken from cBioPortal. Luminal A breast cancer is most common, followed by Luminal B, Basal and finally HER2+. P values are indicated.

The TCGA dataset comprises different breast cancer sub-types, with luminal the most commonly represented followed by basal (triple-negative) sub-types and then HER2+ sub-

types (Fig.12D). Break-down of expression data for each sub-type revealed that *CELSR1* expression levels were significantly increased in the less invasive Luminal subtype but significantly decreased in the more aggressive HER2+ and triple-negative (TNBC) subtypes (Fig. 13A). *FZD6* expression was significantly increased in TNBC, which is consistent with previous studies (Corda et al., 2017; Corda & Sala, 2017). Assessment of patient survival for each sub-type however revealed no statistically significant differences for *CELSR1* or *FZD6* (Fig.13C) although high levels of *CELSR1* and low levels of *FZD6* were nearing significance for a better prognosis in Luminal A sub-types. It was also surprising that HER2+ and basal subtypes showed a 'switch' in *CELSR1* expression levels associated with patient survival, with a trend for higher expression of *CELSR1* associated with a worse outcome for survival. This was compared to a trend for higher *CELSR1* expression associated with a better outcome for survival in patients with the less aggressive Luminal A and Luminal B subtypes (Fig.13C). Taken together, these data confirm that *CELSR1* expression is significantly increased in Luminal breast cancer sub-types, which is associated with better survival outcomes for patients. In more invasive breast cancer however the situation is reversed, and survival outcomes appear worse when *CELSR1* expression levels are higher. Conversely, low *FZD6* expression in less aggressive breast cancer shows a trend for better survival outcomes, whilst high *FZD6* expression is strongly associated with more invasive breast cancer.

3.4 GSEA software predicts positive and negative enrichment of gene pathways when *CELSR1* and *FZD6* expression is altered in breast cancer

TCGA BRCA data downloaded from cBioPortal using the GSEA software can be used to predict which defined sets of genes are significantly enriched between two biological states, which in this case is breast cancer exhibiting *CELSR1* and *FZD6* gene copy number variations/mRNA expression levels and diploid breast cancer. This is possible through the

computational analysis of thousands of gene expression patterns across hundreds of cancer specimens.

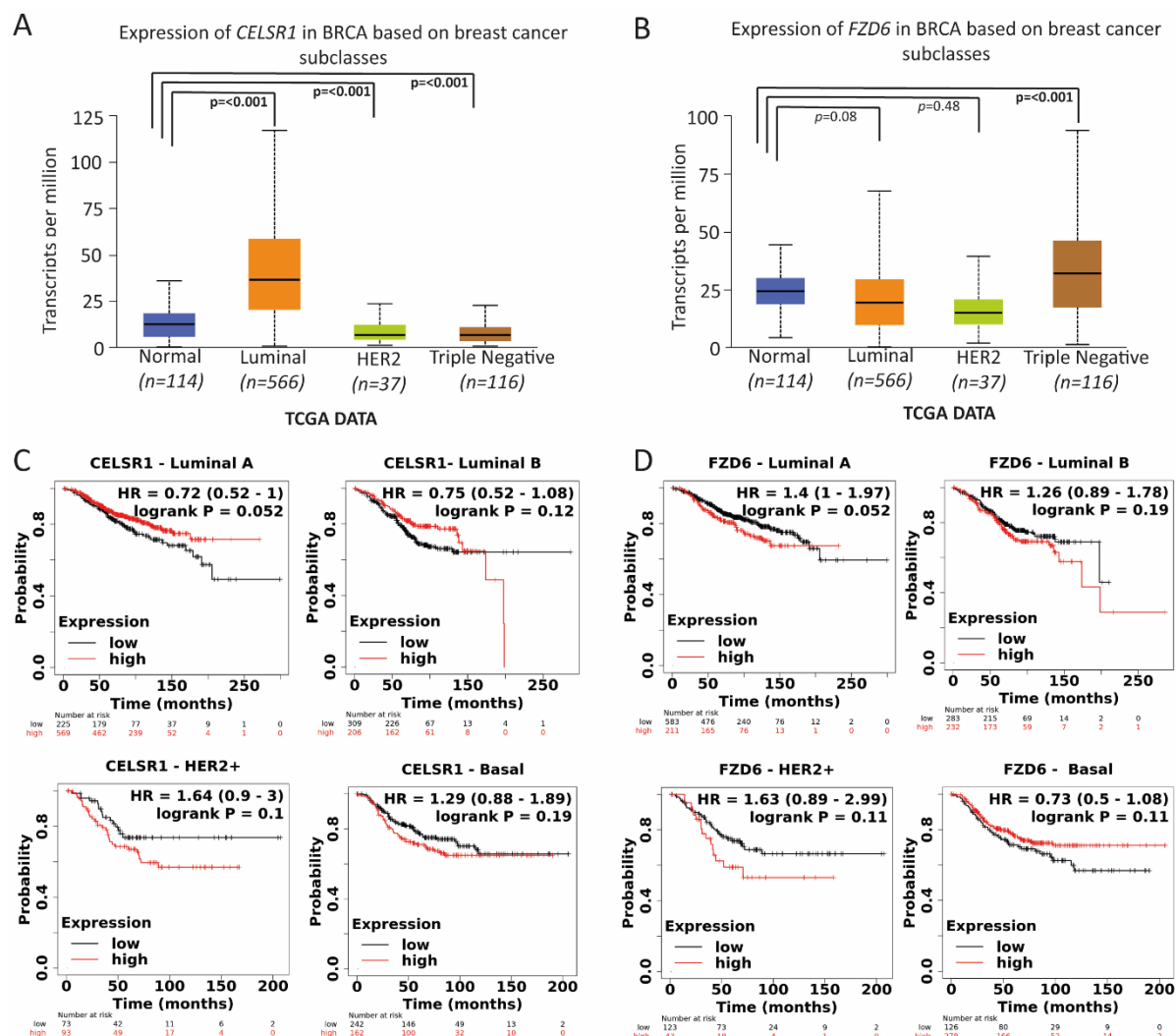


Figure 13 - *CELSR1* and *FZD6* expression varies across breast cancer subtype. A. UALCAN expression data showing *CELSR1* in expression in the TCGA BRCA dataset (in TPM) based on different subtypes of breast cancer. There is a significant increase in expression between normal and luminal type breast cancer, while in HER2+ and triple-negative types *CELSR1* expression levels drop below the normal healthy control. **B.** While *FZD6* levels are lower in luminal and HER2+ compared to normal samples, there is a significant increase in the triple-negative breast cancer compared to healthy controls. **C.** Kaplan-Meier survival plots for different subtypes of breast cancer (from the least aggressive Luminal A to the most aggressive Basal subtype) based on *CELSR1* and *FZD6* expression levels. The logrank P test p value increases with subtype aggressiveness for *CELSR1* KM plots. There is no direct pattern seen with *FZD6* KM plots. P values are indicated

The stated goal of GSEA is to identify genes sets related to various signalling pathways in a list of ranked genes and determine if there is statistically significant difference. Significant gene enrichment is defined by a probability (P) value of <0.05 and a false discovery rate (FDR) of $<25\%$. Such enrichment profiles could direct research studies towards particular cancer signalling pathways linked to changes in *CELSR1* and *FZD6* expression which may help uncover their potential role in breast cancer progression.

Several gene sets with potential protective effects were found to be positively enriched in the TCGA breast cancer datasets when *CELSR1* expression was altered in patients presenting with different breast cancer sub-types, as shown in Fig. 12D. Luminal sub-types were most highly represented within the TCGA database (Fig.12D) which is consistent with the positive enrichment of gene sets involved in early and late estrogen response (Fig.14). Gene sets regulating mitotic spindle stability were also found to be positively enriched, which is of interest as *CELSR1* is known to play a role in mitotic spindle orientation (Oozeer et al, 2017). However, MYC targets were also found to be enriched positively.

Gene set enrichment analysis revealed negative enrichment of multiple gene sets involved in signalling pathways linked to oncogenesis, metastasis, and drug resistance (Fig.15). Notable in this group are pathways linked to angiogenesis and epithelial-to-mesenchymal transition (EMT) which are strongly associated with cancer metastasis (Fantozzi et al., 2014). Another gene set negatively enriched by *CELSR1* includes the kRas signalling pathway. kRas signalling in cancer is well known to contribute to breast cancer metastasis (Galiè, 2019; R. K. Kim et al., 2015). The hypoxia pathway is also negatively regulated by *CELSR1*. Hypoxia is known to contribute to breast cancer metastasis, angiogenesis, and resistance to drug therapy (Muz et al., 2015). TNF- α via NF κ B signalling, is also linked to hypoxia, increases metastasis, and correlates with poor prognosis in breast cancer

(Mercogliano et al., 2020; Xia et al., 2018). The reactive oxygen species (ROS) pathway influences the tumour microenvironment, particularly having an effect on metastasis, angiogenesis and inducing cancer cell survival pathways (Aggarwal et al., 2019). Interferon alpha (INF- α) at high levels has been reported to increase the metastatic potential of breast tumours (Provance & Lewis-Wambi, 2019). Metastasis promoting pathways, such as IL6/JAK/STAT3 (which is known to promote EMT, cell proliferation and suppression of apoptosis) and aberrant IL2/STAT signalling (which increases metastasis, survival, and proliferation of cancer) are also significantly deregulated (Halim et al., 2020; Manore et al., 2022). Components in the coagulation pathway, such as tissue factor, have been implicated in breast cancer metastasis (Belting et al., 2005). Components of apical junction signalling have been attributed to have tumour suppressive and tumorigenic effects in cancer, (González-Mariscal et al., 2020). As a PCP protein, altered *CELSR1* expression might be expected to disrupt AB cell polarity (Shi et al., 2014). Interestingly, the WNT β -catenin signalling pathway, even though negatively regulated was not altered significantly. Upregulation of WNT β -catenin signalling is well characterised in promoting breast cancer metastasis (Klaus & Birchmeier, 2008; MacDonald et al., 2009; Pohl et al., 2017).

Of particular interest was the opposition of oxidative phosphorylation (positively enriched) and glycolysis (negatively enriched). Tumour cells notoriously use glycolysis to drive tumour growth, the so-called Warburg effect (Heiden et al., 2009). It is highly interesting therefore that *CELSR1* is associated with the downregulation of glycolytic datasets.

Gene set enrichment analysis was also conducted for TCGA BRCA data for *FZD6*. In contrast to *CELSR1*, it was found that *FZD6* was significantly associated with positive enrichment of gene sets involved in oncogenic and metastatic signalling processes (Fig.16).

These included gene sets linked to E2F target genes involved in promoting cancer cell survival and metastasis (Hollern et al., 2019; Yan et al., 2019).

Gene sets positively regulated by CELSR1

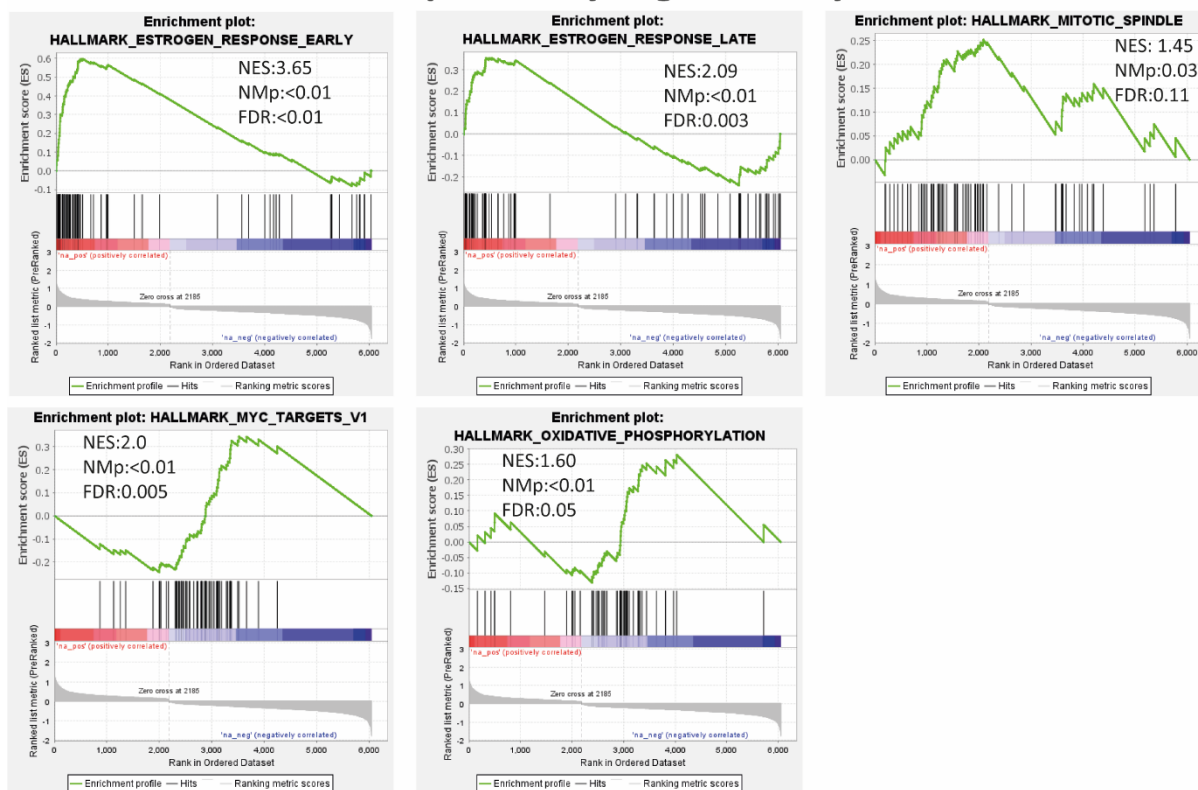


Figure 14 - Gene sets positively enriched by *CELSR1*. The following gene sets are significantly positively upregulated by *CELSR1* in invasive breast cancer. NES – Normalized expression score, NMP – Nominal p value, FDR – false discovery rate (significant if <25%).

Another positively enriched gene set is linked to fatty acid metabolism. Cancer cells need energy to survive and are well known to ‘hijack’ metabolic pathways for their own benefit (Koundouros & Poulogiannis, 2019). Fatty acids are known to act as secondary messengers in the oncogenic process, as well as having an involvement in progression and metastasis, and the ability to remodel the tumour microenvironment (Koundouros & Poulogiannis, 2019; Snaebjornsson et al., 2020). Abnormal mTOR signalling is well characterised in breast cancer and is known to promote tumour cell proliferation and metastasis (Hare & Harvey, 2017; Zou et al., 2020). Both MYC targets and oxidative phosphorylation are significantly enriched by

FZD6 and *CELSR1* (Fig.15 and Fig.16). MYC is known to be overexpressed in basal like breast cancer and to contribute to oncogenesis and resistance to therapy (Fallah et al., 2017; J. Xu et al., 2010).

Gene sets negatively enriched by CELSR1

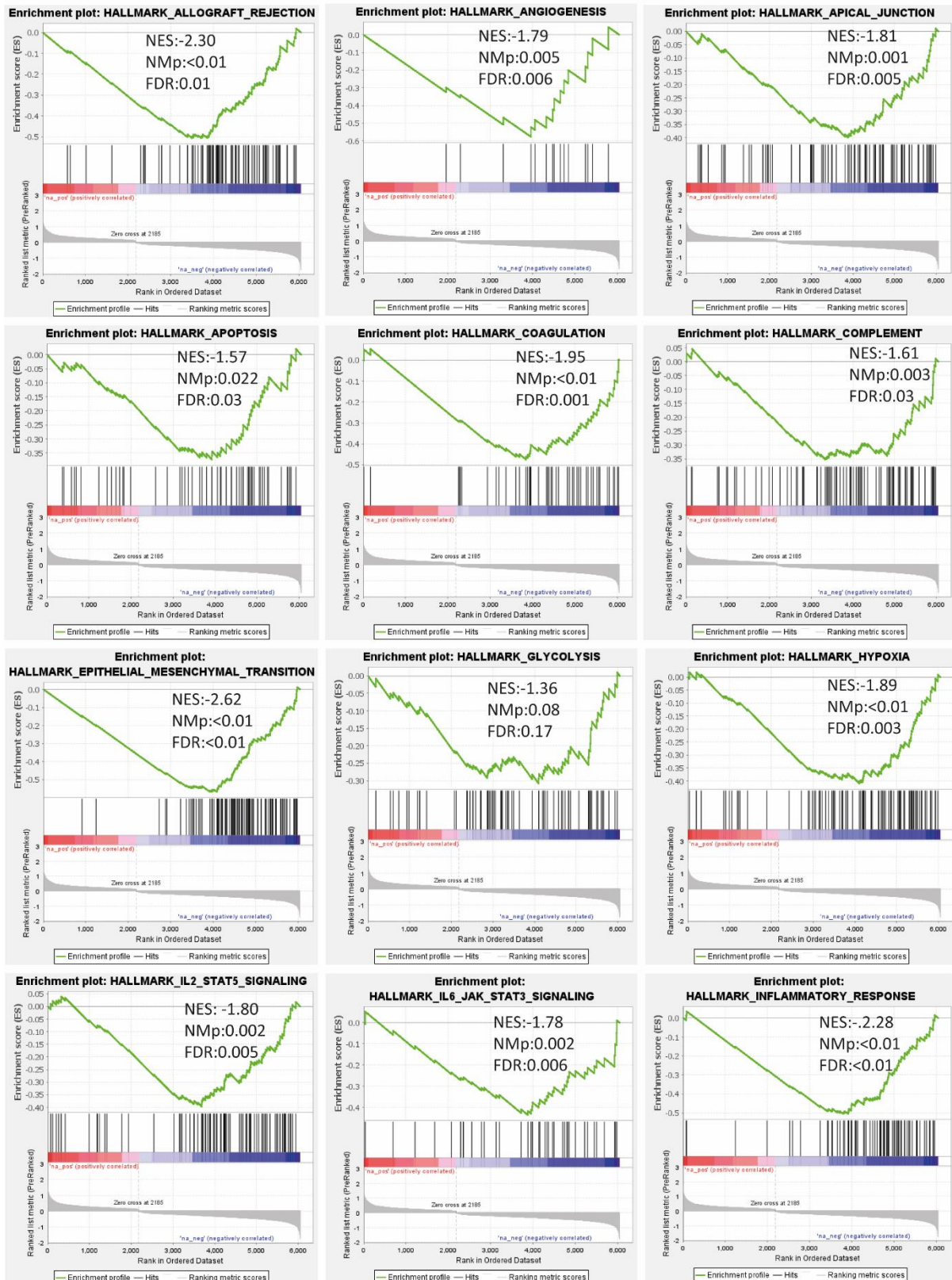


Figure 15 - Significantly positively enriched gene sets by *CELSR1*. ES – Normalized expression score, NMP - Nominal p value, FDR – false discovery rate (significant if <25%).

Gene sets negatively enriched by CELSR1

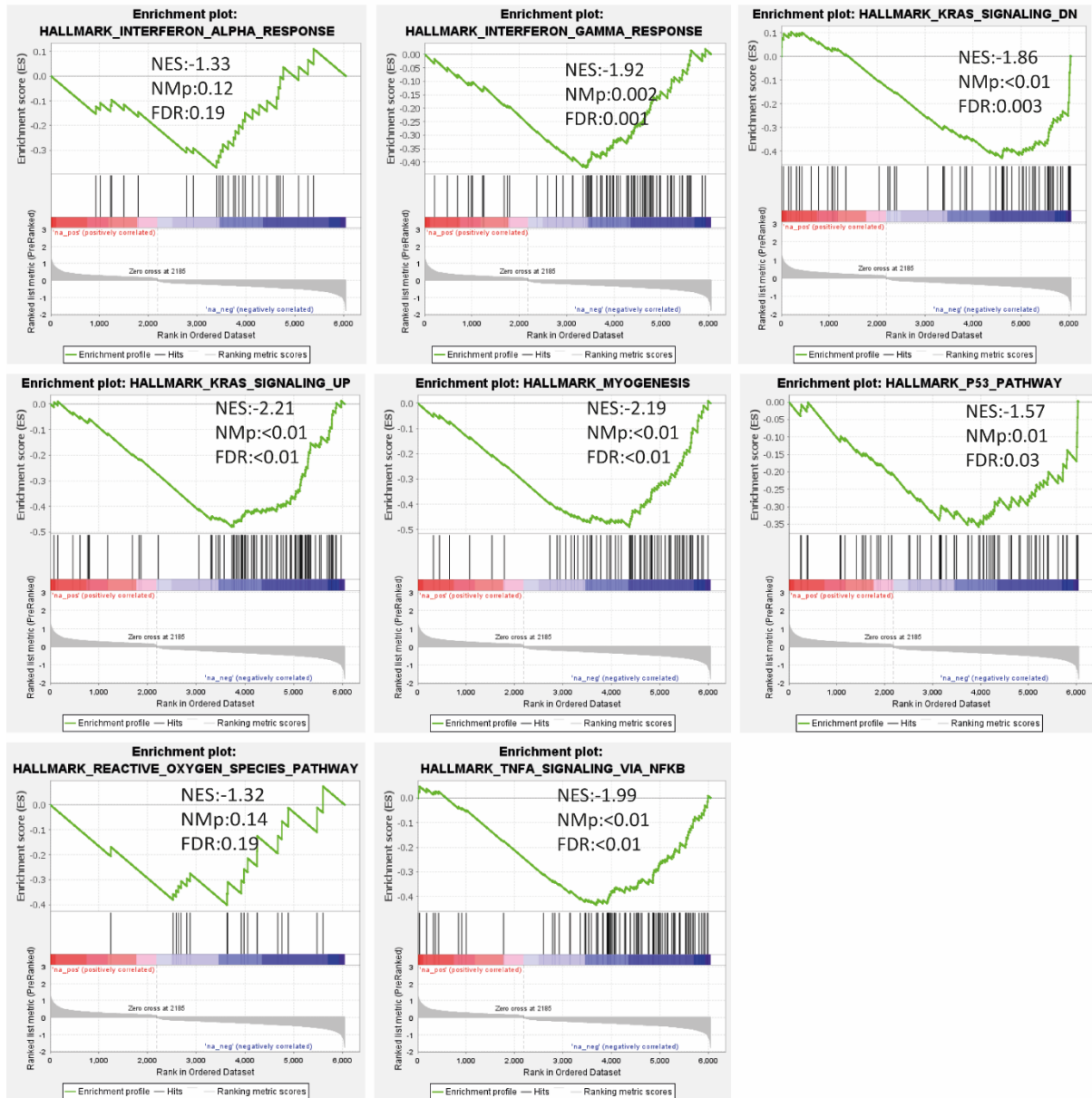


Figure 15 cont. - Significantly positively enriched gene sets by *CELSR1* cont. NES – Normalized expression score, NMP - Nominal p value, FDR – false discovery rate (significant if <25%).

Overexpression of *MYC* in breast cancer is also linked to metastasis and generally a poor prognosis, sustaining cancer cell growth and regulating metabolic pathways, which are usually ‘hijacked’ to fuel cancer cell proliferation (Fallah et al., 2017; J. Xu et al., 2010). Notably, oxidative phosphorylation pathway has been associated with a worse prognosis in breast cancer (Evans et al., 2021). *Fz6* functions alongside *Celsr1* in mouse embryo skin in orientation of spindle alignment (Oozer et al., 2017). To complete the picture, gene sets

negatively enriched by *FZD6* were investigated (Fig. 17). Surprisingly, only a few of these are relevant to directly regulating the tumour environment. Moreover, and as for *CELSR1*, negatively enriched gene sets included those linked to apical junctions, EMT, KRAS and TNF- α /NF κ B signalling. Loss of apical junctions is intimately connected to EMT. Both down-regulate cell adhesion, which is one of the hallmarks of metastasis, therefore positive regulation and maintenance of cell adhesions is important to prevent cancer from spreading (Brennan et al., 2010; González-Mariscal et al., 2020). As reported EMT is negatively regulated by both *CELSR1* and *FZD6*. This fits with our hypothesis about the role of *CELSR1* in luminal breast cancer. Specifically, its known role in cellular and tissue organisation in the sense that *CELSR1* prevents cell plasticity and maintains cell-cell adhesions. This is an interesting phenomenon considering that *FZD6* has been characterised as an on oncogene and reported to positively regulate EMT (Corda et al., 2017; Corda & Sala, 2017). However, the oncogenic role of *FZD6* has been reported in already invasive breast cancer. It should be noted that the GSEA analysis has been conducted on all types of breast cancer. Therefore, the fact that *FZD6* is exhibiting negative regulation of EMT might reflect non-invasive luminal subtypes of cancer where its role might be unknown.

KRAS signalling and TNF- α /NF κ B signalling are well characterised in promoting oncogenesis and metastasis (Galiè, 2019; R. K. Kim et al., 2015; Mercogliano et al., 2020; Sero et al., 2015). However, it has been also reported, that in TNBC increased KRAS signalling might be beneficial (Tokumaru et al., 2020). Altogether the gene enrichment data highlight several downstream signalling pathways affected by changes in *CELSR1* and *FZD6* gene expression in breast cancer patients, which can be investigated further using *in vitro*-based assays.

Gene sets positively enriched by FZD6

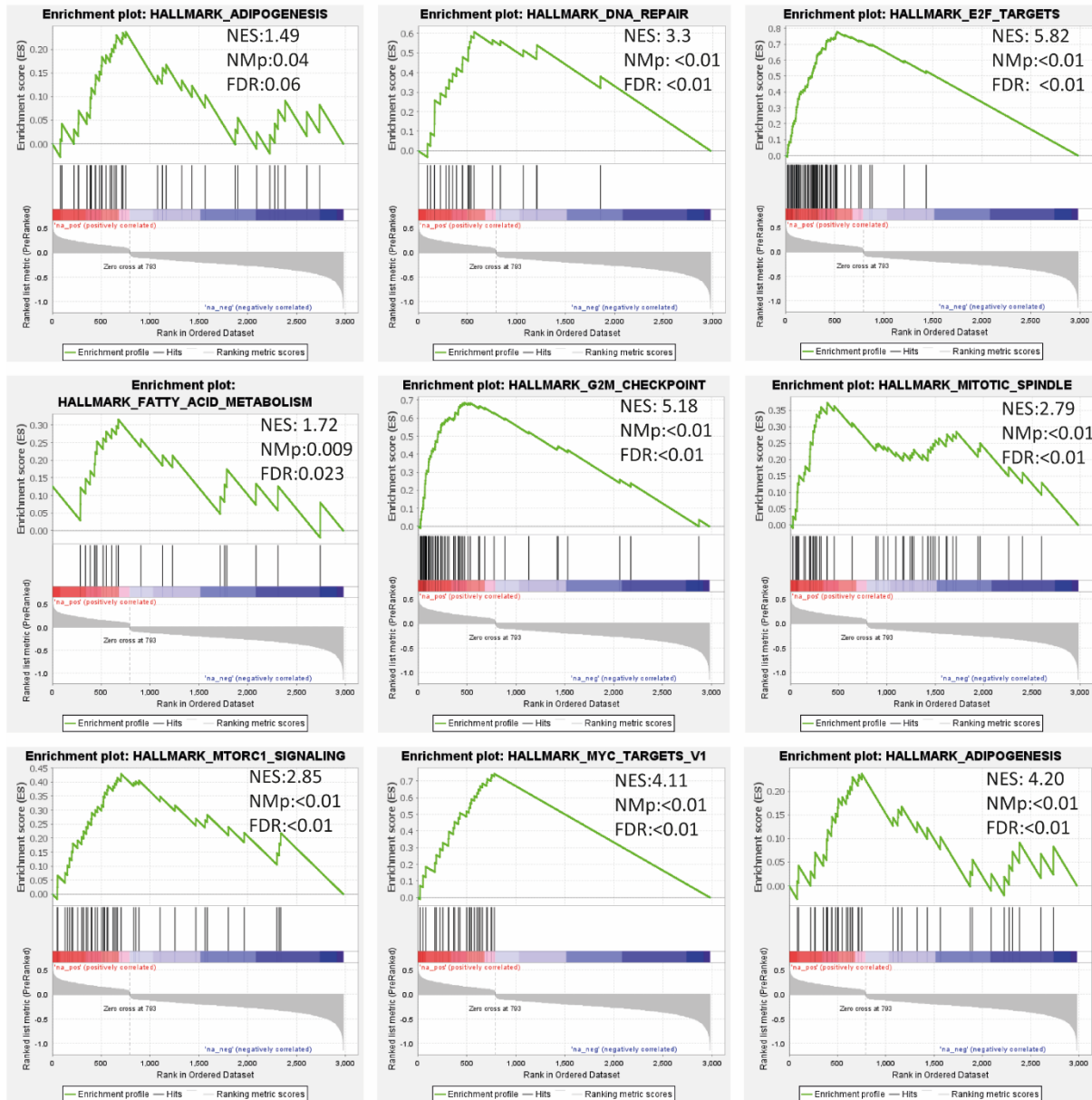


Figure 16 - Gene sets positively enriched by FZD6. The following gene sets are significantly positively upregulated by FZD6 in invasive breast cancer. NES – Normalized expression score, NMP - Nominal p value, FDR – false discovery rate (significant if <25%).

Gene sets negatively enriched by FZD6

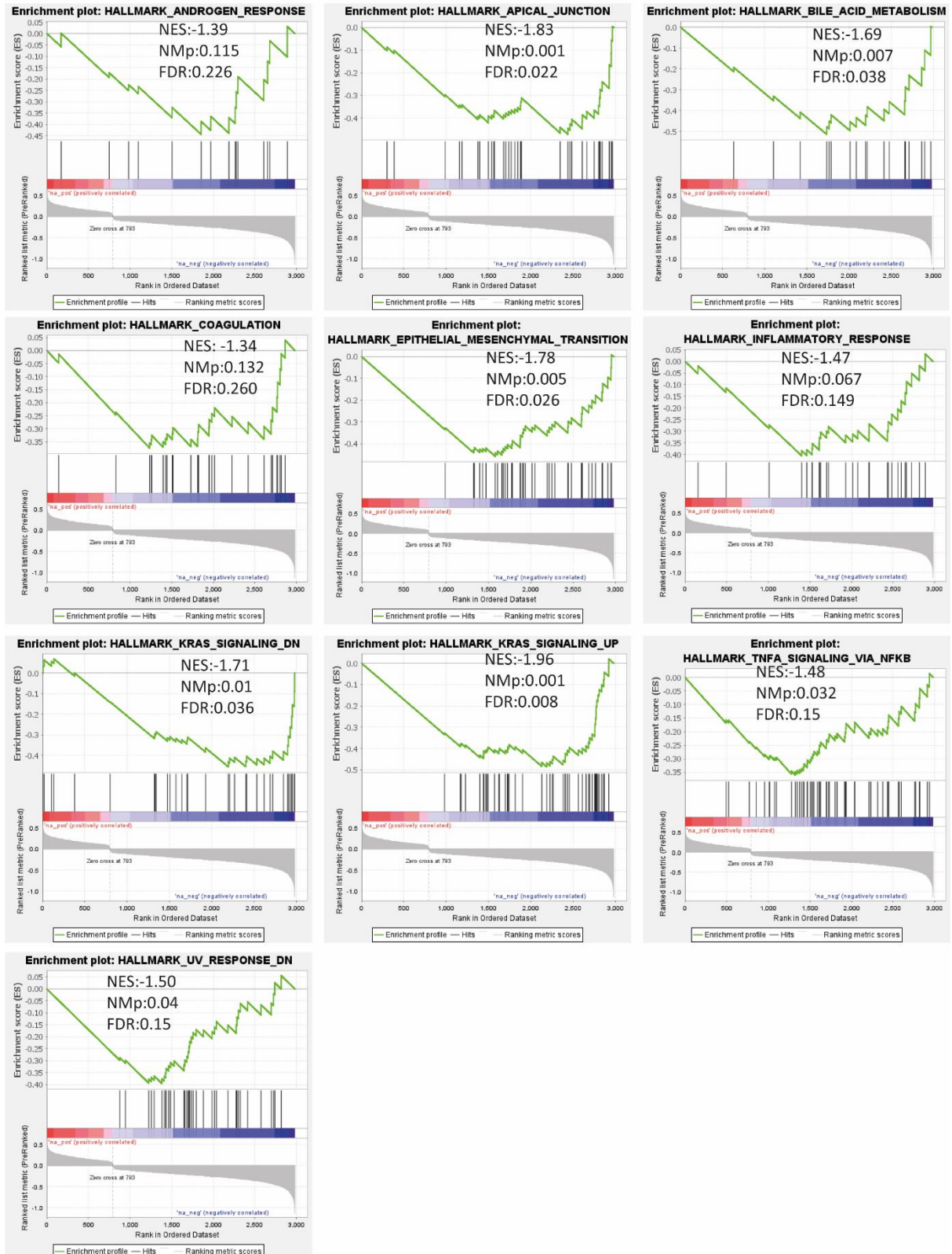


Figure 17 - Gene sets positively enriched by FZD6. The following gene sets are significantly positively upregulated by *FZD6* in invasive breast cancer. NES – Normalized expression score, NMp - Nominal p value, FDR – false discovery rate (significant if <25%).

4. RESULTS - CHARACTERISATION OF *IN VITRO* BREAST CANCER CELL LINES AS POTENTIAL MODELS TO INVESTIGATE CELSR1 AND FZD6 FUNCTION IN BREAST CANCER

4.1 Introduction

Mammalian cell lines are popular *in vitro* tools to model disease states, to test the effect of drugs and to investigate gene function without the need to source human tissue or conduct *in vivo* studies, which generally carry a greater ethical and financial burden. Mammalian cell lines are not grossly expensive and relatively easy to culture. Moreover, in recent decades, techniques which better reflect the *in vivo* situation, such as 3D culture and organoids, have become available.

A number of cell lines exist as *in vitro* models for breast cancer. These are cell lines originally derived from patients (hereafter called common cell lines) and cell lines engineered from a parent immortal MCF10A breast epithelial cell line as a cancer progression series (Imbalzano et al., 2009; Puleo & Polyak, 2021). Since the second aim of the project herein was to identify *in vitro* models to understand the role of CELSR1 in breast cancer progression, a number of cell lines were selected for study. Selection of common cell lines originally derived from patients was mainly based upon previously published work on *FZD6* in breast cancer (Corda et al., 2017). A range of cell lines was chosen to represent and act as models of the main subtypes of breast cancer – Luminal A, Luminal B, HER2+ and Basal/TNBC (Fig.8). The matching subtype and molecular characteristics reflect the nomenclature of Dai et.al. (2017). The MCF10A cancer progression series, which contain the same genetic background, provides an interesting alternative to common cell lines originally derived from patients (Fig.9).

To characterise these cell lines as suitable *in vitro* models, qPCR and RT-PCR with direct DNA sequencing, western blotting and immunocytochemistry was performed.

4.2 Multiplex qPCR reveals *CELSR1* mRNA levels are highest in less invasive luminal type cell lines whereas *FZD6* mRNA levels are highest in more invasive type cell lines, consistent with patient data

In order to be able to better compare *in vitro* data with that from patients multiplex PCR was performed so mRNA levels for *CELSR1* and *FZD6* could be compared in the same cell line samples. As a result, the TaqMan qPCR system was chosen. The TaqMan method is a more sensitive qPCR method since sequence-specific probe is used (unlike for example SYBR green, which binds to any dsDNA). The probe binds to a specific nucleotide sequence and sits in the midst of the forward and reverse primers (Fig.18). During qPCR cycling, the probe binds first followed by the primers. Once the extension cycle begins, the Taq polymerase synthesising the new strand moving along the sequence strikes the quencher off the fluorescent probe. This allows the reporter to emit a fluorescent signal, which is detected by a special camera and recorded by the instrument. The instrument in our lab allows for multiplexing, where up to 5 different fluorescent probes can be used in a single well i.e., a quantplex reaction. The experiment was designed to be a triplex reaction, with *CELSR1*, *FZD6* and the normalisation gene *CCSER2* being amplified in the same well.

When setting up the Taqman system, the GeNorm kit was initially used to assess the ideal housekeeping control. The following genes were tested – *ACTB*, *18S*, *YWHAZ*, *GAPDH*, *ATPSYNTH* and *CYT-C*. Different sample concentrations were investigated, and data was analysed using the GeNorm algorithm. However, none of the housekeeping genes proved to be stably expressed across all samples (data not shown).

Furthermore, the GeNorm kit and analysis software became discontinued by suppliers, so they were ceased to be used in this study. To facilitate ideal housekeeping gene selection, we then studied the literature and found that several publications suggested ideal housekeeping genes for breast cancer research (Kiliç et al., 2014; Tilli et al., 2016).

PUM1 and *CCSER2* were subsequently selected for pilot studies. Each cell line was tested with each housekeeping gene at varying sample cDNA concentrations ranging from 10ng/μL to 100ng/μL. Through these pilot experiments we determined the ideal housekeeping gene, which was the one that

was most stably expressed throughout all samples, which was *CCSER2*. I also determined the optimal cDNA concentration to use in future experiments.

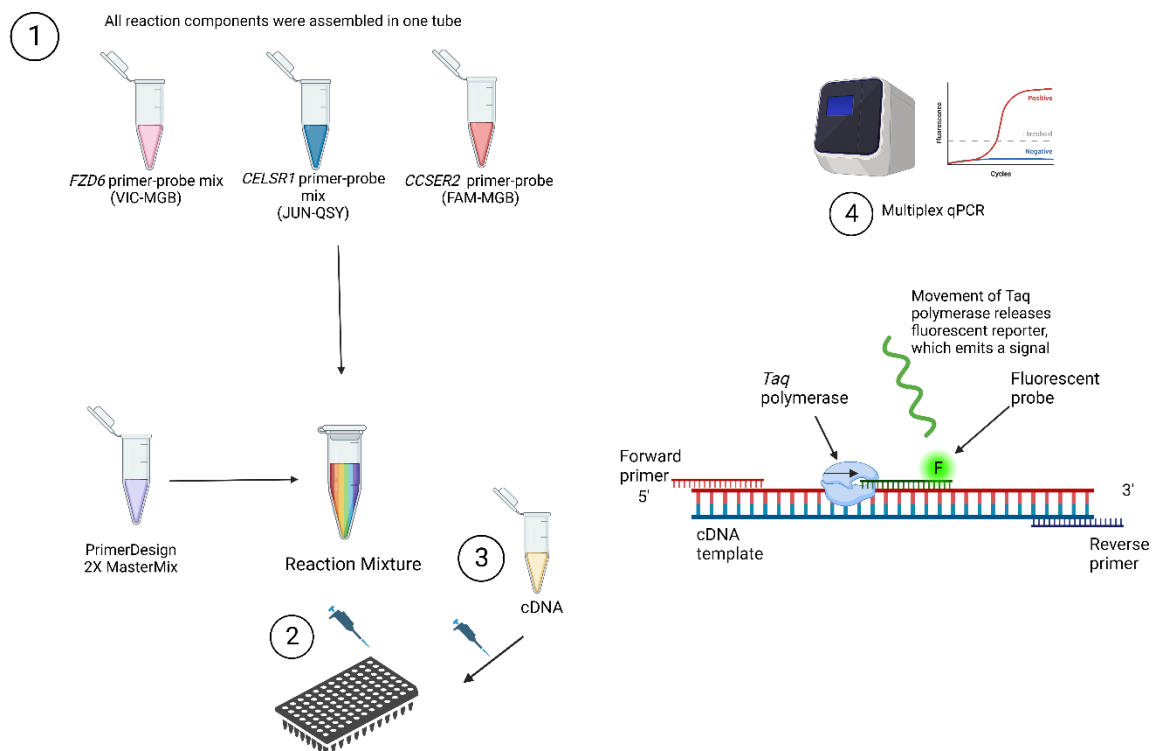


Figure 18 - qPCR method description. 1-3 – Experimental setup. 4. qPCR method detail

Multiplex quantitative PCR was then conducted in order to assess the relative expression levels of *CELSR1* and *FZD6* in the common breast cancer cell lines originally derived from patients. The MCF10A cell line (healthy epithelial control) was used as the reference sample across breast cancer cell lines (where a double delta cT value of 1 denotes normal expression and anything above or below is over or under expression, respectively). To calculate the $\Delta\Delta cT$ value from raw data, the following calculation steps were followed -

1. \bar{X} of technical replicates for each biological replicate
2. \bar{X} of technical replicate means for each biological replicate

3.
$$\frac{cT_{samples} - cT_{normaliser}}{cT_{reference} - cT_{reference\ normaliser}} = \Delta\Delta cT$$

4. $2^{-\Delta\Delta cT} = Yaxis$

It was found that both T47D and BT474, which are Luminal type cell lines, exhibited the highest levels of *CELSR1* expression (Fig.19A). This data correlates well with the TCGA patient data, which demonstrates that *CELSR1* expression was increased in Luminal type breast cancer (Chapter 1, Fig.13A). For the more invasive basal MDA-MB436 and MDA-MB231 cell lines *CELSR1* expression was significantly decreased when compared to the Luminal type cell lines. Once again, this corresponds well with the TCGA patient data, which demonstrates that compared to healthy patients and those with Luminal type breast cancer, patients with basal types have significantly lower *CELSR1* expression (Chapter 1, Fig.13A). *FZD6* expression levels were consistently lower than the MCF10A control, nevertheless, *FZD6* expression was significantly higher in the more invasive MDA-MB436 and MDA-MB231, basal type cell lines, compared to the less aggressive, luminal type cell lines (Fig.19B). Again, this data agrees with the patient data for *FZD6* expression (Fig. 13B, Chapter 1). Altogether these data reveal that *CELSR1* and *FZD6* exhibit opposing levels of mRNA expression in breast cancer cell lines consistent with patient analyses.

4.3 Investigation of *CELSR1* and *FZD6* protein expression in breast epithelial and breast cancer cell lines

Next, an assessment of *CELSR1* and *FZD6* protein expression in the commonly used breast cancer cell lines was performed using Western blot analysis. Three *CELSR1* antibodies were trialled. The first was a polyclonal antibody which was raised against the C-terminal PDZ isoform of avian *Celsr1*. The second was a polyclonal antibody raised against the avian *Celsr1* C-terminal EKL isoform. Both these antibodies were generated by Dr Caroline Formstone whilst at King's College London and generate expected patterns of protein expression for *Celsr1* protein in the avian neural tube and avian inner ear (C. Formstone, personal communication; Appendix, AFig. 2). The final antibody was a commercial polyclonal *CELSR1* antibody raised against the C-terminal tail of human *CELSR1* (residues 2684-2809), which is termed *CELSR1sc* hereafter.

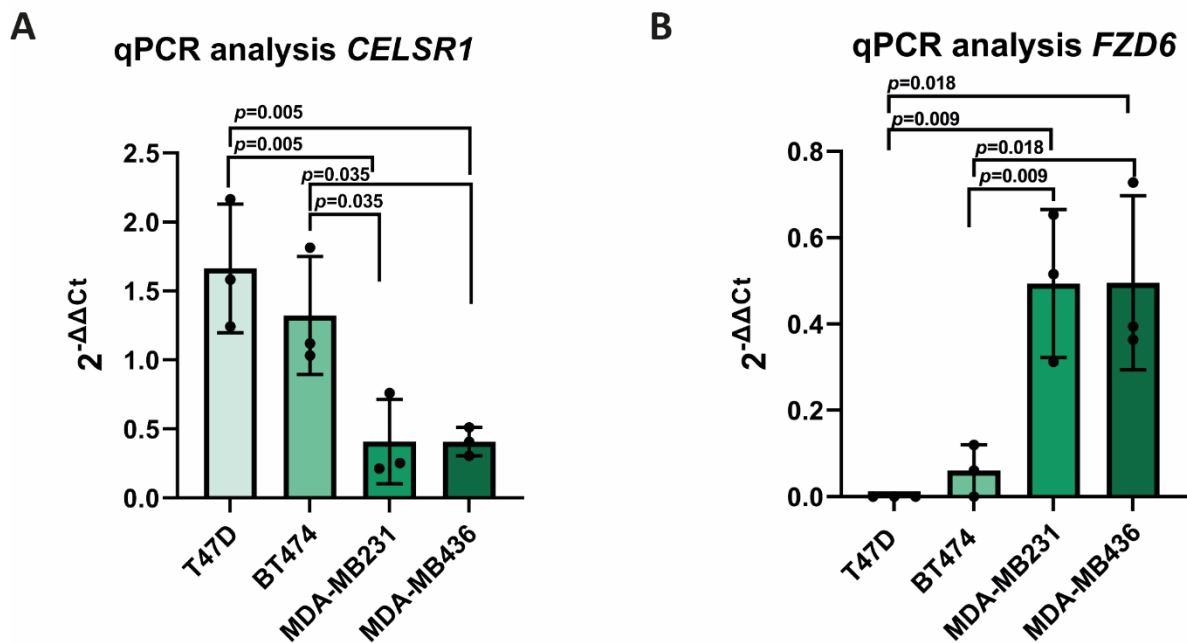


Figure 19 - Multiplex qPCR analysis. A. *CELSR1* expression in common cell lines normalised to the MCF10A cell line. One-way ANOVA with Tukey's multiple comparisons test shows a significant difference between *CELSR1* expression in luminal type cell lines compared to basal. **B.** *FZD6* expression in common cell lines normalised to MCF10A. All cell lines exhibit lower *FZD6* expression (<1) than MCF10A control. The same statistical test shows significantly lower *FZD6* expression in luminal breast cancer cell lines and higher expression in basal cell lines. Biological replicates are shown, mean of 4 technical replicates per experiment, n=3 independent experiments. One way ANOVA with Tukey's multiple comparisons test was used for statistical analysis. Mean, SD and P value are indicated

The *CELSR1*sc residues did not overlap with those of PDZ being located just upstream within the cytoplasmic tail of *CELSR1* (Fig.20A). In some cases, *CELSR1* protein expression was assessed against that of *FZD6* on the same Western Blot. Actin levels were also examined and GAPDH and transferrin were used as loading controls. The protein concentration of all samples was quantified using a Bradford assay and protein samples were diluted prior to loading so that the same amount of protein (10 μ g) was loaded for each sample.

Western analysis of commonly used cell lines was performed using the *CELSR1*-SC antibody. A band of the expected size, as reported for mouse *Celsr1* (400KDa) (Formstone et al., 2010; Oozeer et al., 2017) was observed with the most prominent band consistently in T47D cells and much fainter bands in MDA-MB4-36/231 cell lines (Fig.20B shows a representative blot from n=3 experiments where the same amount of protein loaded for each cell line, for each independent blot, as shown by

the Coomassie stained image). Notably, the profile of CELSR1sc staining was consistent with qPCR data (Fig.19). For these blots a Coomassie stained gel was used to show consistent loading as actin and GAPDH staining did not work, despite multiple attempts. Sample aggregation at the top of the gel indicated an issue with protein resolution and incomplete/non-existent separation, resulting in low molecular weight proteins being absent. After investigation of equipment and reagents, it was determined that multiple freeze thaw cycles resulted in protein precipitation, which caused the issue. We resorted to a more sophisticated approach of making whole cell lysates, by adding treatment buffer on the day of lysis (see Materials and Methods section 2.7.1) and storing individual single-use aliquots.

The avian Celsr1 PDZ and EKL antibodies were tested independently but both simultaneously with FZD6 antibody on the same blots. A 400KDa protein of the expected size was observed with Celsr1-PDZ antibody but not with Celsr1-EKL. A representative western blot (n=3 independent blots) is shown for the presumptive CELSR1 PDZ protein isoform (hereafter, CELSR1iso) along with FZD6, actin and GAPDH in Fig.20C. It was observed that a 400Kda CELSR1iso band was detected in multiple cell lines with Luminal type T47D exhibiting a band of low intensity compared to BT474 cells, which was consistently higher in n=3 blots (Fig.20B). Moreover, lower level CELSR1iso bands were also observed in the more aggressive Basal type cell lines (e.g. MDA-MB231 Fig.20B). The opposite was found for FZD6, with T47D cells exhibiting lowest staining of FZD6 protein (expected size of 80kDa) and MDA-MB 436/231 cell lines the strongest staining bands (Fig.20B). Actin levels did not appear to alter across the different cell lines consistent with the loading of the same amount of protein into each well. low levels of staining for CELSR1iso in T47D cells was highly surprising as it did not reflect mRNA expression data obtained by qPCR where T47D showed the highest RNA levels for *CELSR1* (Fig.19).

Altogether, CELSR1-sc and FZD6 antibodies revealed a progressive decrease in CELSR1 protein expression from the least invasive to the most invasive of the commonly used breast cancer cell lines, which was consistent with mRNA expression data. The CELSR1-iso antibody, although recognising an expected 400KDa protein, exhibited a distinct pattern of protein expression with consistently higher

staining levels in the BT474 breast cancer cell line and bands of lower relative staining in the most invasive cell lines. CELSR1 protein levels were also investigated in the genetically similar MCF10A progression series. CELSR1-sc antibody staining revealed a gradual reduction in the intensity of the 400KDa CELSR1 band with increasing invasiveness of the cancer cell line (arrow, Fig.21A).

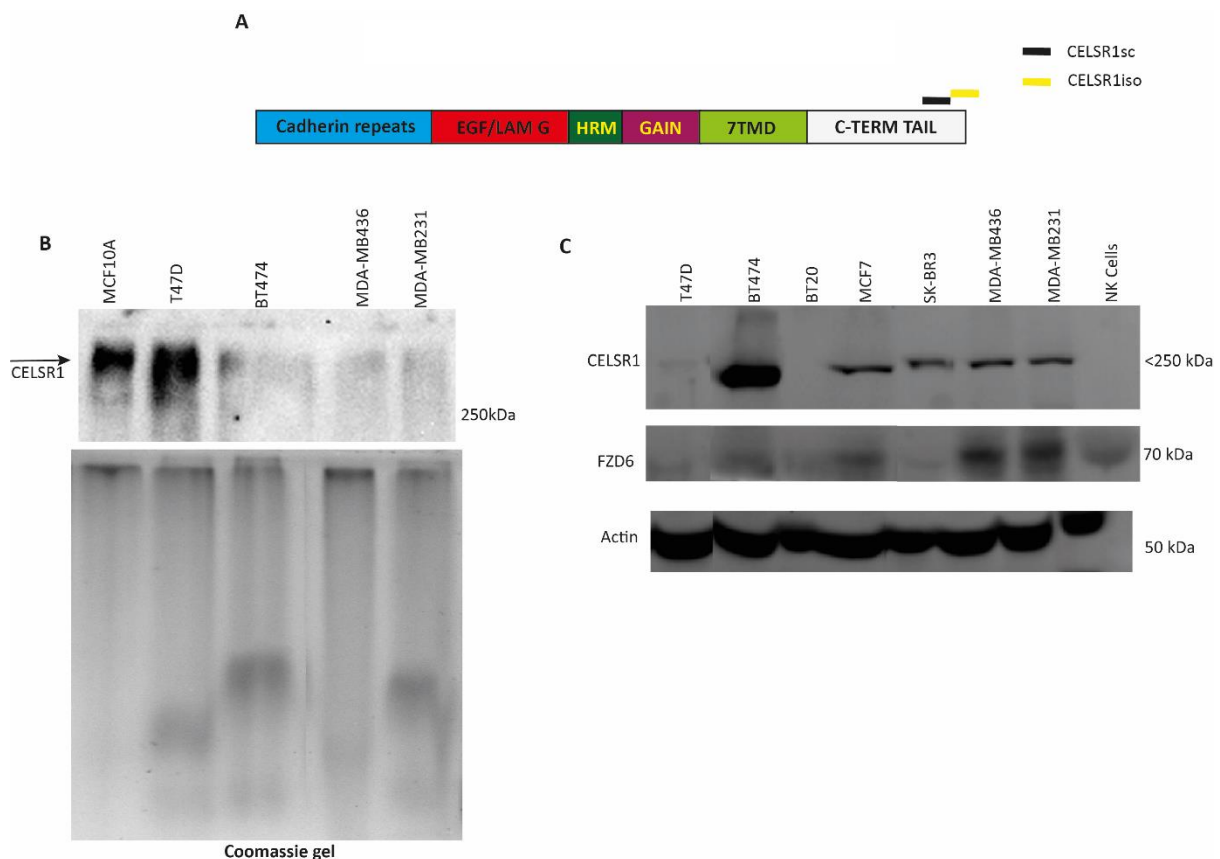


Figure 20 - CELSR1 protein expression analysis by western blot in the common cell lines. A. Schematic of CELSR1 protein with location of antibody recognition within the cytoplasmic tail marked by black colour line (Celsr1-sc) and yellow colour line (Celsr1-iso). **B.** Western blot on common cell lines (Luminal and Basal) using CELSR1sc antibody. Arrow indicates Celsr1 band at approximately 400Kda. A Coomassie stained gel loaded at the same time as the gel that was blotted shows the amount of protein loaded for each lane. Blot is representative of n=3 blots. **C.** Western blot on common cell lines (Luminal and Basal) using CELSR1iso antibody, FZD6 antibody and actin and loading control. A 400Kda CELSR1 protein can be seen , an 80 kDa band is see for FDZ6. Blot is representative of n=3 independent experiments for CELSR1iso antibody and n=1 for FZD6 antibody. The same amount of protein was loaded in each lane for all blots. Sizes of protein ladder are shown

Sometimes, a slightly smaller band appeared in lanes where the 400Kda band was lost (highest arrow, Fig.21A) although the specificity of this band for CELSR1 is not known. Mouse Celsr1 is known

to be cleaved to a p85 product (Oozeer et al., 2017) thus the band at 75Kda may represent a cleaved CELSR1 protein (lower asterisk, Fig.21A). Western blot shown in Fig.21B is representative of n=3 independent blots for Celsr1-sc, actin and GAPDH loading controls are shown. In other blots we did observe a faint band in AT1 cells (Appendix, AFig.19). For CELSR1-iso antibody only one useful blot was achieved which unfortunately was broken along the line where the CELSR1 band was located. Dark bands were observed around 400kDa with AT1 and DCIS.com showing darker staining than NeoT. Some staining was also seen in Ca1A and D but not in the most invasive cell line Ca1H (Fig.21B). Again, despite multiple attempts loading controls did not work for these blots, thus a Coomassie stained gel loaded with the same amount of protein at the same time as the blotted gel was loaded is shown. The DCIS.com lane from the Coomassie gel shown in Fig.21B looked very different to the other samples which highlighted a possible issue with the protein samples, which might explain the lack of success with loading control antibody staining and CELSR1 antibodies in general. Subsequent comparison of Coomassie gels which reflect multiple freeze-thawing of the same protein samples revealed progressive loss of banding patterns in the samples and an increase in the density of protein at the top of the gel (Appendix, AFig.3). It is possible therefore that freeze-thaw of protein samples resulted in protein aggregation and subsequent loss of protein movement into the gel, so that after the third freeze-thaw little or no protein was present on the membrane following Western blot resulting in no antibody staining.

Altogether these data reveal some consistency between the common cell lines and the MCF10A breast cancer series. Less invasive cell lines show stronger staining bands with Celsr1-sc consistent with qPCR data. For Celsr1-iso antibody however, the darkest staining bands are observed in the mid-range invasive cell lines i.e. BT474 and AT1, DCIS.com. Better quality Western blots are needed for Celsr1-iso and loading controls for all blots in order to verify these intriguing findings.

4.4 Investigation of CELSR1 c-terminal mRNA sequence in breast cancer cell lines

4.4.1 RT-PCR analysis suggests that CELSR1-PDZ encoding mRNAs are often truncated and lack the PDZ motif

The CELSR1-iso antibody was raised against a C-terminal Celsr1 PDZ isoform (Appendix, Fig.2; C. Formstone, personal communication). Whilst qPCR showed that T47D expressed the highest levels of *CELSR1* mRNA, Western blot analysis revealed a dark stained band of 400Kda in BT474 luminal type cells but not T47D luminal type cell line (Fig.19).

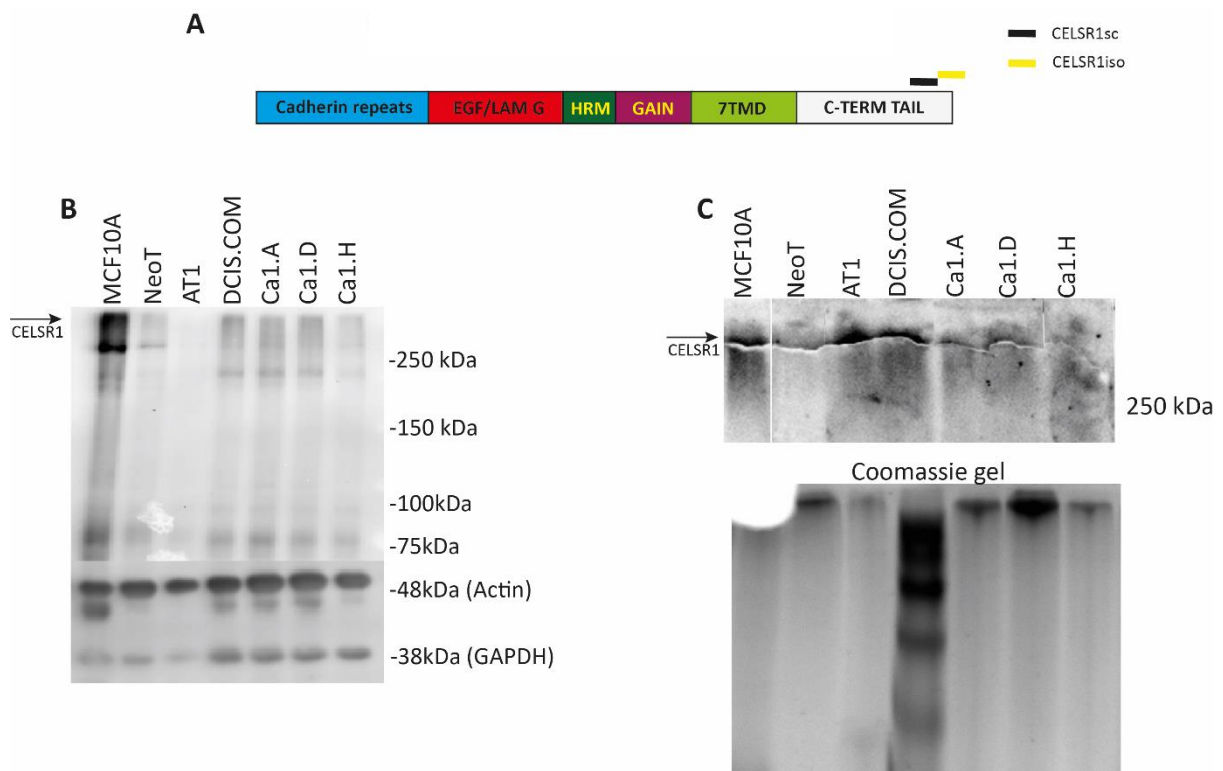


Figure 21 - CELSR1 protein expression analysis by western blot in the MCF10A progression series. A. Western blot of the MCF10A progression series with the CELSR1-sc antibody. Top panel shows antibody specificity. PDZ – MDCK-PDZ cells, MDA-MB231 and BT474 cells were used as controls. Bands of expected size can be seen across most cell lines <400kDa. MCF10A cells show the strongest staining intensity. Band intensity drops in NeoT and is almost absent in AT1 cells. DCIS.COM, Ca1.A and Ca1.D cell lines show similar band intensity, while in Ca1.H cell lines band intensity is low. Actin and GAPDH were used as loading controls. **B.** Western blot of the MCF10A progression series using the CELSR1iso antibody. Top image shows antibody specificity. The western blot produced non-specific bands only. n=3 independent experiments

As cancer cells are well known to recombine genomic DNA and this is particularly true of cancer cell lines (Creeden et al., 2021), the presence of mRNA containing the PDZ isoform was investigated in the commonly used cell lines, using reverse transcriptase (RT)-PCR and direct sequencing analysis. Moreover, all commonly used cell lines were studied in parallel in order to investigate any changes in CELSR1 c-terminal isoform expression across less invasive and highly invasive cell lines. We used immortal control MCF10A breast epithelial cells as a cell line control and human foetal ectoderm-derived cDNA as an *in vivo* control. Primers were designed to amplify the c-terminal tail region of *CELSR1*. Two specific splicing products for Celsr1-PDZ and Celsr1-EKP isoforms were expected as these had been previously identified in other vertebrate species (C. Formstone, personal communication). Individual and nested primers were designed to amplify a short stretch of *CELSR1* c-terminal mRNA using the same reverse 3'UTR primer and different forward primers, primer pair 1 (PP2) and primer pair 3 (PP3). Nested PCR was necessary to consistently amplify PCR products from the foetal cDNA control. A larger cDNA which encompassed most of the CELSR1 C-terminal tail was also amplified via RT-PCR generated using forward primer PP1 with the reverse 3'UTR primer. Direct sequencing of all PCR bands amplified was performed.

Two PCR bands were consistently observed using primer PP1 (entire CELSR1 cytoplasmic tail) whereas three PCR bands were consistently observed for PP2 and PP3 primers (PCR fragment spanned the extreme C-terminal sequence encompassing the spliced isoforms), from more than n=10 independent RT-PCR experiments for each primer pair (Figs. 22-24).

DNA sequence alignment analysis of the smaller of the PP1 PCR products encompassing the entire cytoplasmic tail of CELSR1 (890bp) revealed that it encoded the expected CELSR1 SDSEKP variant (Fig. 22C) with 100% sequence similarity observed for BT474 and BT20 cell lines when compared to the NCBI *CELSR1* reference sequence. MCF10A control cDNA sequence was not amplified for this primer pair. Notably, the C-terminal region was truncated in T47D, SK-BR3 and 231 cell lines (Fig.22C and Fig.23C), with an in-frame stop codon identified within the sequence amplified for T47D. Direct sequencing of the smaller band for the PP2 product, which amplified around 100bp across the

c-terminal splice region (Fig.23) confirmed the SDSEKP variant and revealed that all *CELSR1* cDNA products amplified were scrambled across the C-terminal coding sequence except for the spliced domain and 3'UTR (Fig.23C). Further nested PCR with the PP3 primer and using the PP2 PCR products as template also amplified EKP containing bands (smallest band) but with the expected C-terminal sequence across all cell lines shown in Fig.24, although direct sequencing of T47D products using nested PCR was not achieved (Fig.24). These data suggest that PP1 and PP3 forward primers consistently amplify a valid *CELSR1* cDNA product, whilst PP2 possibly shows variable priming ability.

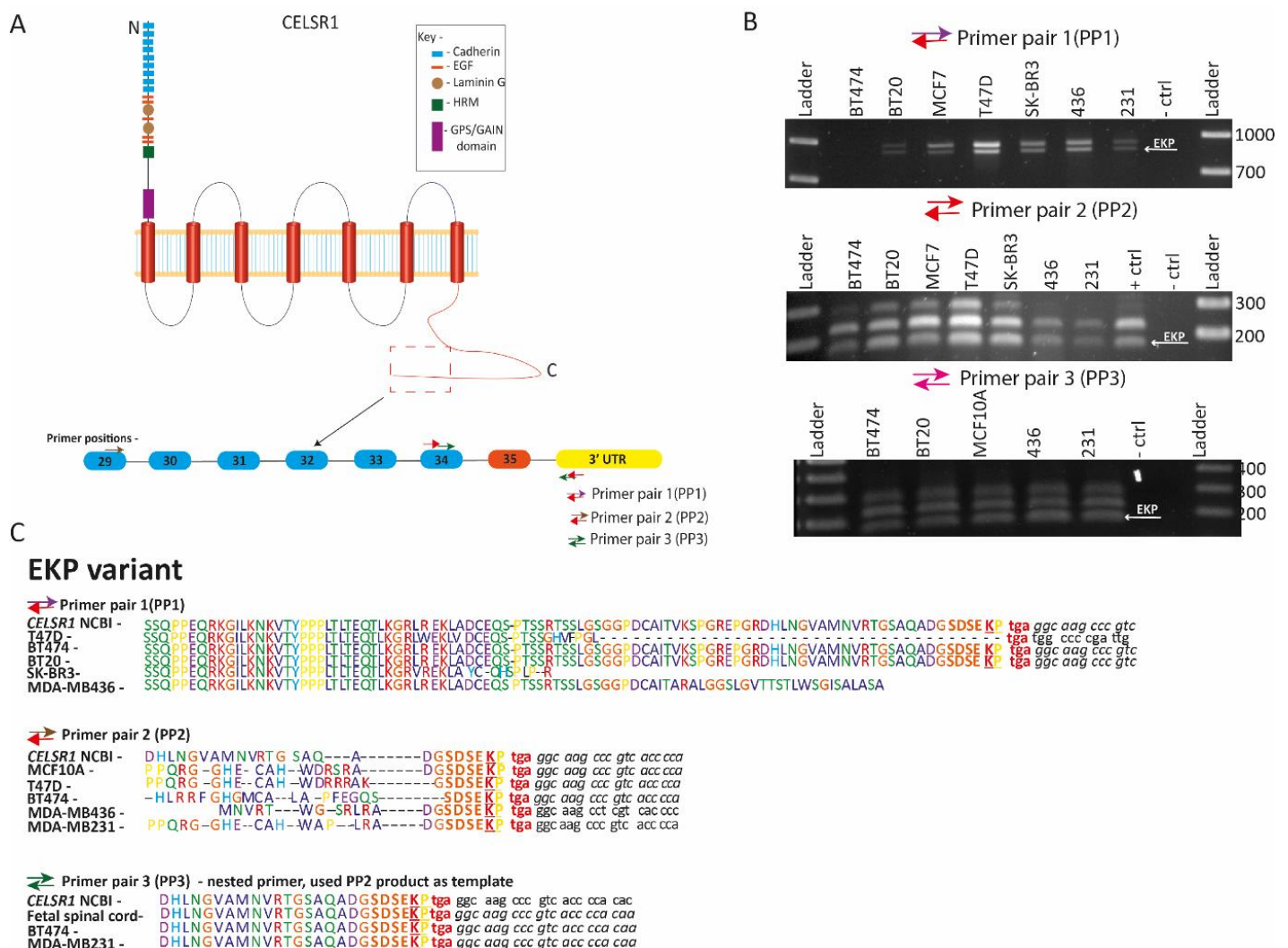


Figure 22 - EKP variant sequencing figure, showing bands after agarose gel electrophoresis and subsequent Sanger sequencing. A. Schematic of primer positions. **B.** Top – Agarose gel electrophoresis using PP1, Middle – Agarose gel electrophoresis using PP2, Bottom – Agarose gel electrophoresis using PP3. White arrow indicates the EKP band. **C.** Top – Sequencing results using PP1, Middle – Sequencing results using PP2, Bottom – Sequencing results using PP3. Individual amino acids are colour coded using Clustal X. *Italicised* nucleotide sequence indicates similarity. n=3. Besides T47D cells, most sequences were constructed with forward sequence only. N=3 independent experiment

Sequence alignment for the largest of the two PP1 products (entire cytoplasmic tail PCR; 890bp band) revealed that it encodes the expected SDSEGNETSI (PDZ domain binding motif) variant (Fig. 22) with 100% sequence similarity to the NCBI *CELSR1* reference sequence for all cell lines used (Fig.22). Direct sequencing of the middle PP2 PCR product (~300bp) revealed it also encoded the SDSEGNETSI product, however, similarity to the reference sequence was found for MCF10A cells only (Fig.22) again suggesting variable priming of PP2 in the breast cancer cell lines.

The C-terminal spliced domain and 3'UTR remained largely intact however (Fig.22). The middle band of nested PCR sequences generated with PP3 revealed a PCR product in the foetal control and BT474 cells which were similar to the NCBI reference for the GSNETSI variant. MDA-MB231 sequences were profoundly different however, except again for the C-terminal splice domain, which was intact (Fig.22C). We were not able to generate DNA sequence from the T47D PP3 middle band.

Altogether, RT-PCR data confirms the existence of the *CELSR1*-PDZ mRNA in breast cancer cell line exists in the breast cancer cell lines including the T47D luminal-type cell line. PP2 primer products suggest that there is a truncated *CELSR1* protein upstream of the C-terminal splice region, which may explain why the *CELSR1*-iso antibody does not recognise a *CELSR1* protein by Western blot analysis. However, this result will need to be confirmed using an alternative PCR primer.

4.4.2 RT-PCR of a 150bp c-terminal sequence reveals the presence of a novel, human-specific PDZ motif containing transcript in foetal tissue and breast cancer cell lines

Intriguingly, RT-PCR with both PP2 and PP3 (nested) forward primers amplified a third band that was the largest in size (Fig.24). Direct sequencing of the PP3 generated PCR product from foetal cDNA and MCF10A controls revealed a different, and novel, PDZ motif (GSNETSI) containing transcript (Fig.24C). This product had not been amplified in any other vertebrate species (C. Formstone, personal communication), suggesting it is human-specific. This sequence contains the PDZ sequence but also contains additional nucleotides upstream of the PDZ motif which encode a potential novel in-frame protein domain upstream of the PDZ motif (Fig.24C).

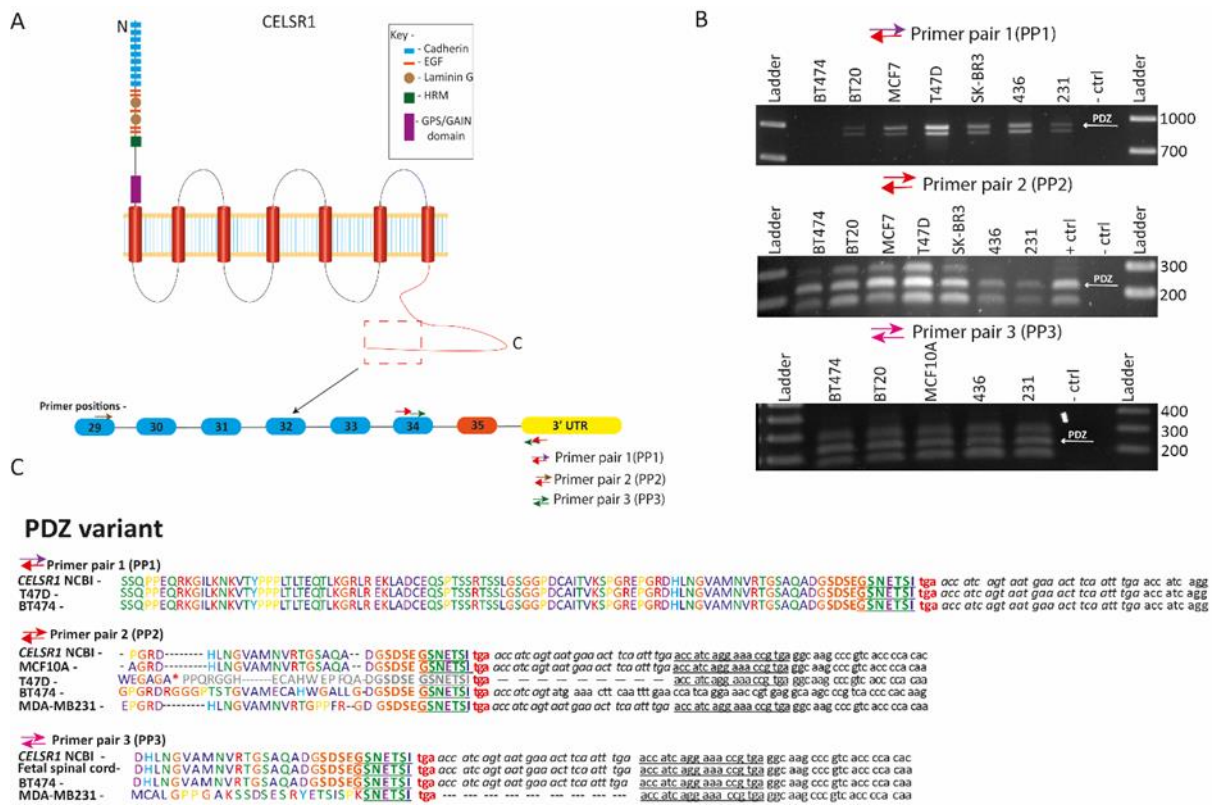


Figure 23 - PDZ variant sequencing figure, showing bands after agarose gel electrophoresis and subsequent Sanger sequencing. A. Schematic of primer positions. **B.** Top – Agarose gel electrophoresis using PP1, Middle – Agarose gel electrophoresis using PP2, Bottom – Agarose gel electrophoresis using PP3. White arrow indicates the PDZ band. **C.** Top – Sequencing results using PP1, Middle – Sequencing results using PP2, Bottom – Sequencing results using PP3. Individual amino acids are colour coded using Clustal X. *Italicised* and underlined nucleotide sequence indicates similarity. n=3. Besides T47D cells, most sequences were constructed with forward sequence only. *Greyed out sequence is SDSEGSNETSI sequence. n=3 independent experiments

A BLAST search using the novel DNA sequence yielded no hits (even with stringency settings being lowered). This transcript was named *CELSR1* PDZ+. PP3 amplified band from T47D again did not generate useful sequence, however BT474 sequence showed local change in sequences compared to the foetal cDNA control, in particular a triplet of amino acids between the conserved SDSE motif and the PDZ motif were different: GRC (foetal) was changed to KRS (BT474). Profound sequence alterations were observed in MDA-MB231 cells which included a duplication of the PDZ motif (Fig.24C). Altogether these data raise the possibility that two distinct *CELSR1*-PDZ C-terminal domain containing proteins exist in humans. Moreover, a PDZ+ product could not be sequenced from T47D cDNA which could also explain the absence of the 400Kda *CELSR1*-iso antibody in this cell line. It

is possible that CELSR1-iso antibody recognises either or both of the CELSR1-PDZ products identified by RT-PCR.

4.4.3 RT-PCR analysis of the CELSR1 c-terminus transcripts highlights a duplication of the PDZ motif sequence in genomic DNA which is specific to the Great Apes

The organisation of c-terminal splicing of *Celsr1* across species is conserved, the PDZ motif exon is upstream of the EKP exon, and the two exons are consistently separated by nine nucleotides (Fig.25). RT-PCR and direct sequencing of PDZ and PDZ+ containing cDNAs however revealed a duplication of the nucleotide sequence encoding the PDZ alternatively spliced exon, with the **TGA** stop codon triplet retained in the first copy of the duplicated sequence (highlighted in red, Appendix, Fig.2).

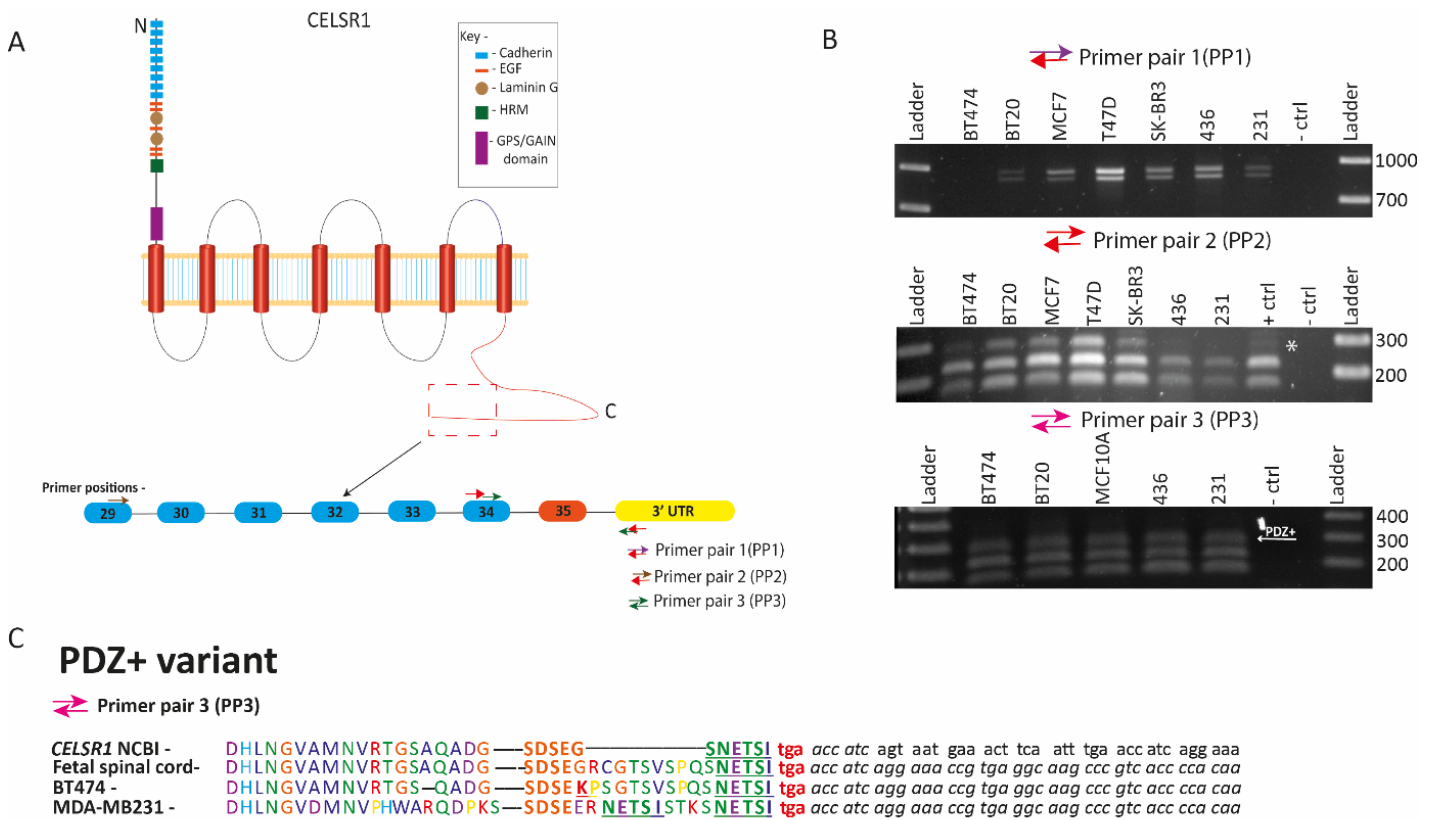


Figure 24 - PDZ+ variant sequencing figure, showing bands after agarose gel electrophoresis and subsequent Sanger sequencing. A. Schematic of primer positions. **B.** Top – Agarose gel electrophoresis using PP1, Middle – Agarose gel electrophoresis using PP2, Bottom – Agarose gel electrophoresis using PP3. White arrow indicates the PDZ+ band. **C.** Top – Sequencing results using PP1, Middle – Sequencing results using PP2, Bottom – Sequencing results using PP3. Individual amino acids are colour coded using Clustal X. *Italicised* nucleotide sequence indicates similarity. Besides T47D cells, most sequences were constructed with forward sequence only. n=3 independent experiments

Thus, the duplicated sequence was found in the 3'UTR sequence of the PDZ motif containing cDNAs (Fig.23), the start of the 3'UTR sequence observed in EKP cDNAs is italicised in Fig.22. BLAST searches of different mammals revealed that this duplication had occurred in the Great Apes (Fig. 25). Notably, the PDZ exon sequence duplication was not observed in the 3'UTR of the PDZ+ cDNAs (Fig.24). Sea mammals revealed CELSR1 intron between the 'SDSE' containing exon and the 'PDZ motif' containing exon also failed to identify nucleotide sequence encoding the novel 'GRCGTSVS' sequence upstream of the PDZ motif in the PDZ+ PCR product.

<i>Homo sapiens</i> (Human)	GGCAGTAATGAAACTTCAATT TGA ACCATCAGTAATGA-----	38
<i>Pan troglodytes</i> (Chimpanzee-G)	GGCAGTAATGAAACTTCAATT TGA ACCATCAGTAATGAAACTTCAATTGA	51
<i>Macaca mulatta</i> (Macaque-OW)	GGCAGTAATGAAACTTCAATT TGA -----	24
<i>Callithrix jacchus</i> (Common Marmoset-O)	-----AATGAGACC-----TCCATT--	15
<i>Aotus nancymaae</i> (Night Monkey-O)	-----AATGAAACC-----TCCATCT--	16
<i>Sus scrofa</i> (Pig)	GGCAGTAACGAAACTTCAATT-----	21
<i>Felis catus</i> (Cat)	GGCAGCAACGAAACCTCAAT TGA -----	24
<i>Canis lupus familiaris</i> (Dog)	GGCAGTAATGAGACTTCAAT TGA A-----	25
<i>Mus musculus</i> (Mouse)	GGCAGTAATGAAACTTCAATT TGA A-----	25

Figure 25 - Sequence alignments of the Celsr1 C-terminal tail PDZ region across different species. TGA indicates the stop codon for the PDZ spliced exon. G - Great Apes, OW – Old world monkey, O – Other/New world monkey

4.4.4 Investigation of FZD6 mRNA splicing products in breast cancer cell lines failed to identify any differences in breast cancer cell lines

FZD6 is reported to contain 5'UTR splice variants, which were also investigated using RT-PCR (Gene: *FZD6* (ENSG00000164930) - Splice Variants - *Homo_sapiens* - Ensembl Genome Browser 110, n.d.). However, no splice variants were detected, a constant band around the expected size was observed in all cell lines (data not shown).

4.5 Comparison of CELSR1 and FZD6 antibody staining patterns in breast epithelial and breast cancer cell lines

Next, the distribution of CELSR1 and FZD6 proteins in fixed cell lines in 2D culture was investigated using immunocytochemistry (ICC).

4.5.1 – CELSR1-sc and CELSR1-iso antibodies reveal distinct patterns of expression and co-localisation with different cytoskeletal elements in control MCF10A cells

CELSR1 protein distribution was first investigated in healthy, immortal MCF10A cells. MCF10A cells showed enrichment of CELSR1-sc staining at the interface between expressing cells (white arrows) and co-localisation with actin (Fig.26B), as expected for a Celsr1 protein which contains cadherin repeats and thus undergoes homophilic adhesion and protein enrichment at expressing cell-cell interfaces (Devenport & Fuchs, 2008; Formstone et al., 2010). Secondary antibody alone controls are also shown (Fig.26A). CELSR1-iso immunostaining however did not co-localise with actin (Fig.26C).

Instead CELSR1-iso antibody-stained filamentous structures (white arrow, Fig.26C and 26D) that often 'wrapped' around part of the nucleus. They also sometimes appear to connect one cell with another (Fig.26C, D). To investigate these filamentous and bridge-like structures MCF10A cells were co-stained with a range of cytoskeletal markers (Fig. 25C-D). Co-localisation with CELSR1-iso antibody was predominant only with an antibody against vimentin, a type of intermediate filament (white arrows, Fig.26F).

4.5.2 CELSR1-sc antibody shows cortical enrichment and co-localisation with actin in luminal type common breast cancer cell lines whereas staining becomes more punctate and is eventually lost in the more invasive common cell lines

Luminal type T47D and BT474 cell lines showed enrichment of CELSR1-sc staining at the interface between expressing cells (white arrows) and co-localisation with actin (Fig.27D, F), similar to MCF10A cells (Fig.26). Staining was less tightly associated with actin staining at the cell membrane however in BT474 cells compared to T47D cells (Fig.27D-G). The more invasive 231 cells did not show any specific staining (Fig.27H, I). Altogether this data is consistent with the RNA and western blot data for CELSR1 which demonstrates gradual loss of CELSR1 expression as cell lines become increasingly invasive in type (Figs. 19, 20 and 21).

4.5.3 CELSR1 antibody staining reveals cortical enrichment in Luminal type common cell lines but is lost and internalised in basal type common cell lines

CELSR1-iso antibody staining of T47D cells did not generate a specific staining pattern (Fig.27) consistent with Western analysis (Fig.20). In BT474 cells CELSR1-iso immunostaining was contained within punctate structures (white asterisk) suggesting internalisation of protein into vesicles (Fig.27G). Again, co-localisation with actin was not observed (Fig. 27G). Co-immunostaining with vimentin was not performed. CELSR1-iso staining of MDA-MB231 cells also revealed punctate staining (Fig.27I) but puncta were much larger and always adjacent to the nucleus.

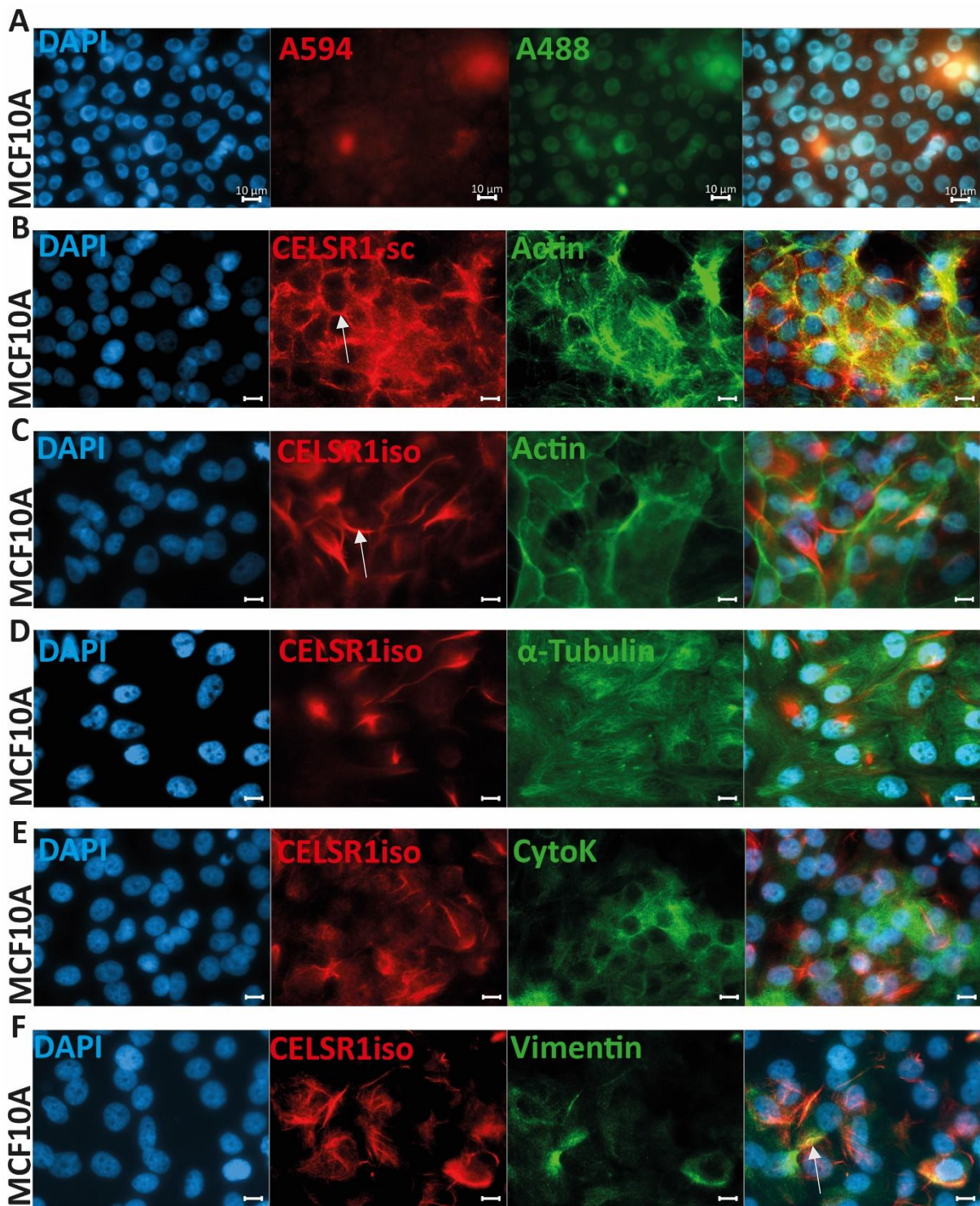


Figure 26 - ICC on MCF10A cell lines using the CELSR1sc and CELSR1iso antibodies. **A.** Negative control – secondary antibody only staining of MCF10A cells. **B.** CELSR1sc stained MCF10A cells reveal cortical enrichment of CELSR1 indicated by white arrow. **C.** CELSR1iso staining of MCF10A cells reveals bridge-like structures enwrapped around the nucleus, connecting individual cells – indicated by white arrow. There is no co-localisation with actin. **D.** MCF10A cells stained with CELSR1iso co-stained with α -Tubulin did not reveal any co-localisation. **E.** MCF10A cells stained with CELSR1iso co-stained with CytoK also did not reveal any co-localisation. **F.** MCF10A cells stained with CELSR1iso co-stained with Vimentin revealed a certain degree of co-localisation. n=3 independent experiment. Scale bar 10 μ m.

CELSR1-iso was also observed in filamentous structures in MDA-MB231 cells (arrow, Fig.27I). To better understand the large puncta in MDA-MB231 cells co-immunostaining was performed with antibodies that label various intracellular vesicles. CELSR1-iso and CELSR1-sc staining did not co-localise with early endosomes (EEA-1) or lysosomes (LAMP-1), respectively (Fig.28 A, E) but did show some limited overlap with CD63, a marker for multi-vesicular bodies and/or exosomes (Fig.28B).

Together with the findings in MCF10A cells, immunostaining of breast cancer cell lines is consistent either with CELSR1-iso staining a variant pattern of CELSR1 protein distribution or alternatively, that the CELSR1-iso antibody is recognising a different protein to CELSR1.

4.5.4. FZD6 staining of common cancer cell lines reveals cortical enrichment but no co-localisation with CELSR1

MCF10A cells stained with FZD6 revealed cortical enrichment, but no co-localisation with CELSR1 (Fig. 29). In the Luminal type T47D cells FZD6 staining seems weaker, but cortical enrichment can still be seen. In this case, there is also no co-localisation with CELSR1iso antibody. Intense FZD6 staining and cortical enrichment is observed in BT474 cells. Taken together, this data reveals interesting structures in control MCF10A and luminal type cell lines when stained with the CELSR1iso antibody. CELSR1sc antibody staining shows cortical enrichment in healthy and luminal type cell lines. Both CELSR1sc and CELSR1iso antibodies reveal punctate staining in the basal-type cell lines with varying sizes of intracellular puncta, suggesting protein entrapment.

Co-staining with appropriate markers did not reveal the identity of these intracellular bodies, although low levels of co-localisation were observed with the MVB/exosome marker CD63. However, CELSR1iso shows co-localisation with vimentin in basal-type cell lines.

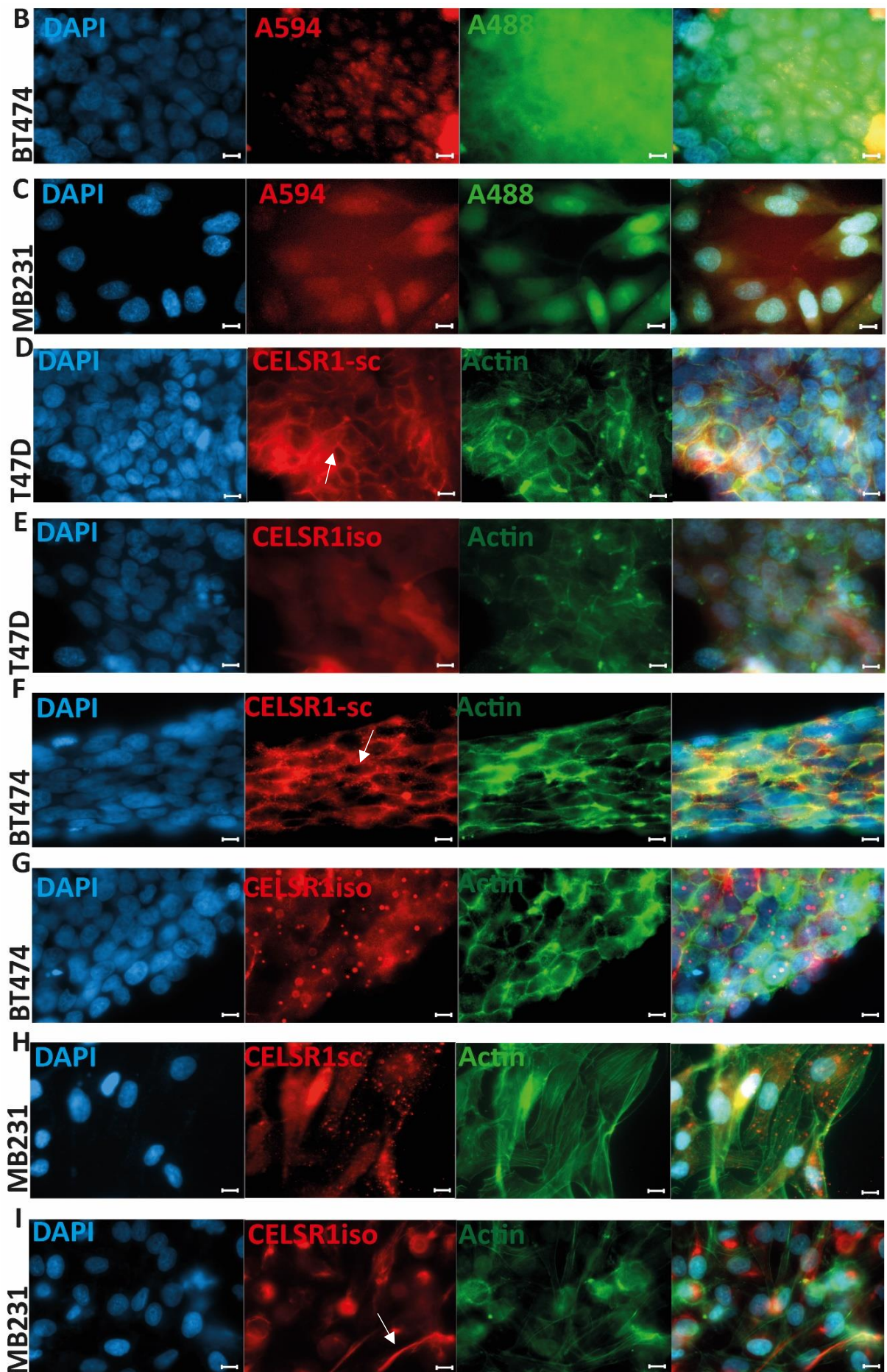


Figure 27 - ICC on Luminal and Basal-type breast cancer cell lines. A, B. Negative controls – secondary antibody only .**C.** CELSR1sc staining of T47D cells revealed cortical enrichment of CELSR1. **D.** CELSR1iso staining on T47D cells did not produce any results. **E.** CELSR1-sc staining on BT474 cell lines revealed cortical enrichment. **F.** CELSR1iso staining on BT474 cell lines shows a speckly pattern and is most likely non-specific. **G.** CELSR1-sc staining of MDA-MB231 cell lines shows punctate staining, suggesting that CELSR1 might be contained in intracellular vesicles. **I.** Like E, CELSR1iso staining suggests that CELSR1 is contained in intracellular vesicles, however in this case large puncta can be observed. N=3 independent experiments. Scale bar 10µm.

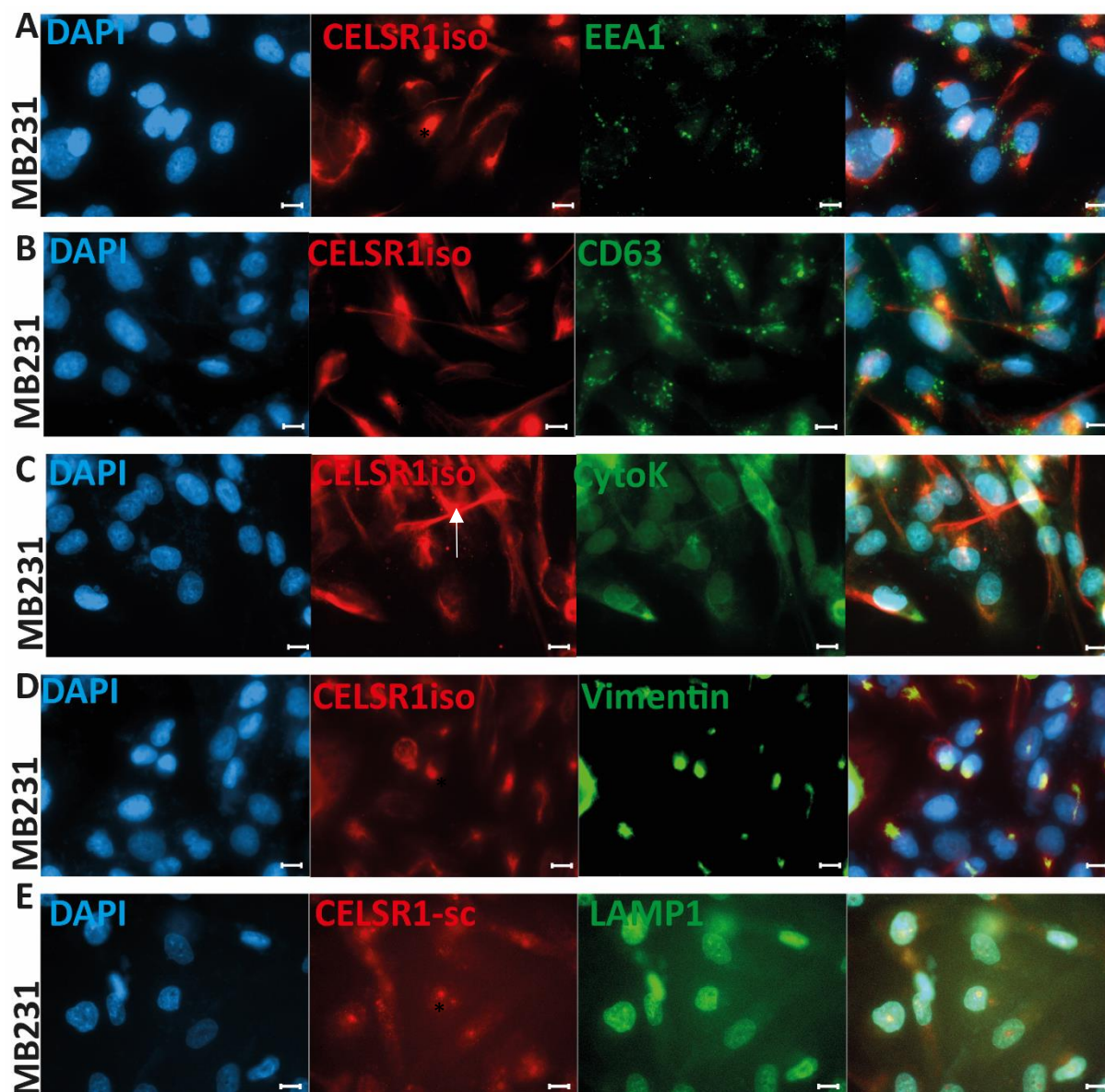


Figure 28 - ICC on MDA-MB23 (MB231) with various markers to determine the identity of intracellular puncta which suggest containment of CELSR1. A., B., D., E. Large intracellular puncta are marked with an asterisk. **C.** Bridge-like structure connecting two cells is marked with a white arrow. N=3 independent experiments. Scale bar is 10µm.

4.6 MCF10A series

The MCF10A series cell lines are a series of genetically engineered cell lines stemming from the parental MCF10A cell line.

4.6.1 CELSR1sc staining in MCF10A series reveals a decrease with increasing invasiveness, but an increasing number of cells stain positive with the CELSR1iso as invasive potential increases

Co-immunostaining with the CELSR1-sc antibody and actin in benign type NeoT and AT1 cells revealed enrichment at cell-cell interfaces and cortical localisation with actin (Fig.30A, B). This was progressively lost in the more invasive DCIS.COM and Ca1.A cell lines and is nearly completely absent in the most invasive Ca1.D and Ca1.H cell lines (Fig.30F, G). This change was quantified by counting the number of stained cells in n=3 images for each cell lines (Fig.32A).

Number of CELSR1-sc positive cells counted is significantly lower in the Ca1.A, D and H cell lines when compared to the MCF10A parent cells.

Immunostaining with the CELSR1-iso antibody revealed a strong staining pattern in NeoT compared to AT1 cells which was not consistent with Western blot data (Compare Fig 31 with Fig. 21A). A similar restriction of protein expression to small puncta adjacent to the nucleus in both AT1 cells (low invasive potential) and Ca1.A cells (higher invasive potential) (Fig.31C, E). Notably, vimentin staining becomes cortical in AT1 cells but co-localises with CELSR1-iso in puncta in Ca1.A cells (Fig.31 C, E). In DCIS type cells and the most invasive CA1.D and Ca1.H cells CELSR1-iso staining, along with vimentin, appears more filamentous (Fig.31D, F and G). Again, numbers of cells staining for CELSR1-iso was quantified. DCIS.com cells showed a significant increase in the total number of CELSR1iso positively stained cells compared to the MCF10A parent cell (Fig.32B).

Altogether these data reveal that in the MCF10A cancer progression series, CELSR1-sc expression is progressively lost as invasive potential increases and is consistent with western blot data (Fig.32A). CELSR1-iso staining however exhibits highly dynamic and inconsistent pattern of staining through the MCF10A series overall but does becomes more consistently more filamentous in the most

invasive cell types. ICC staining pattern for CELSR1-iso does not match the Western blot pattern (compare Fig.30 with Fig.21B).

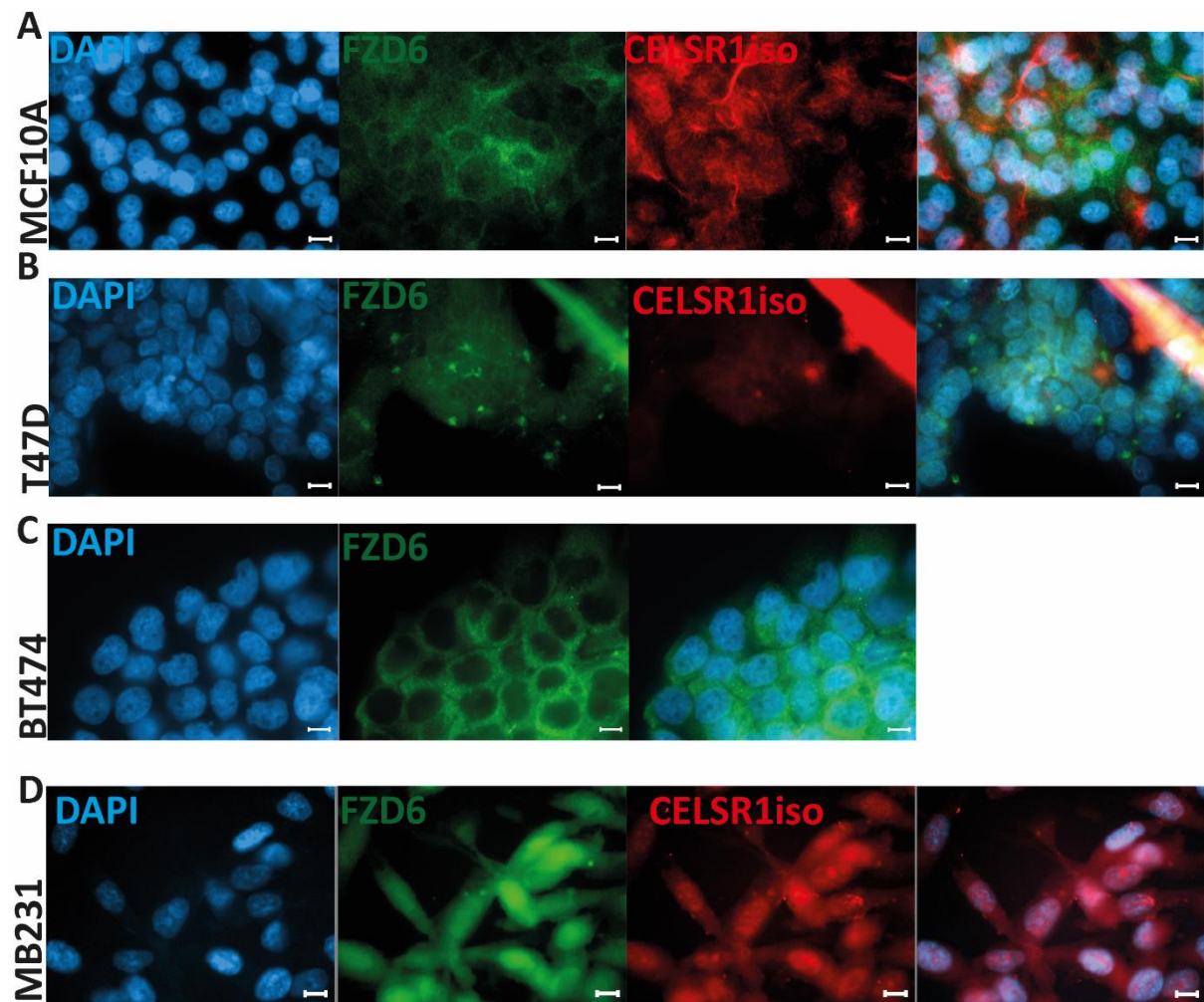


Figure 29 - ICC with FZD6 on common cell lines. A. MCF10A cell lines. **B.** T47D cell lines. **C.** BT74 cell lines. No data with CELSR1sc is available. **D.** MDA-MB231 cell lines. n=3 independent experiments

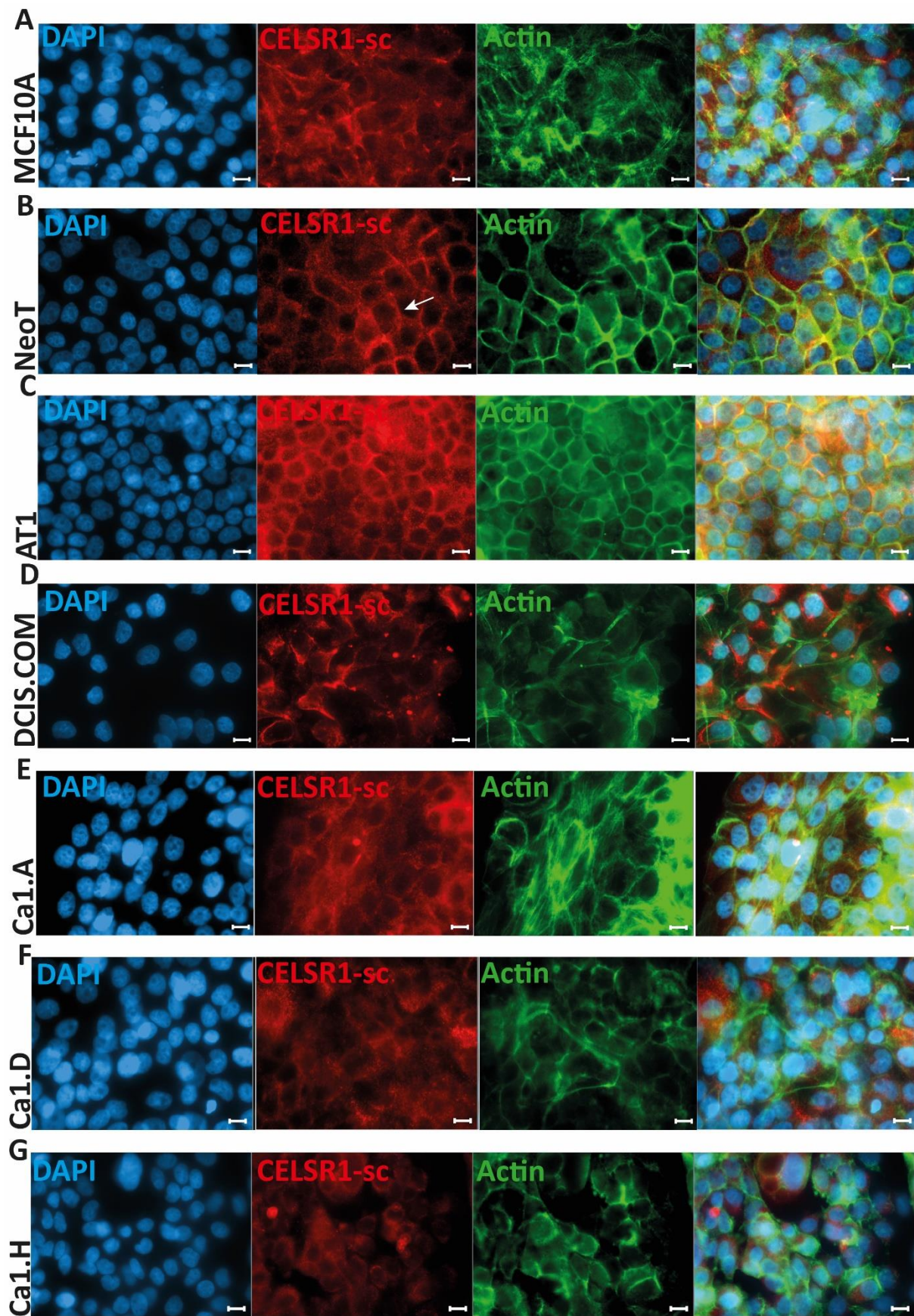


Figure 30 - ICC on the MCF10A progression series using the CELSR1sc antibody. A-C. MCF10A, NeoT and AT1 cells shows cortical enrichment of CELSR1. **D-G.** In DCIS.COM cell lines cortical enrichment seems to get lower and progressively disappears in Ca1.A, D and H cell lines. n=3 independent experiments

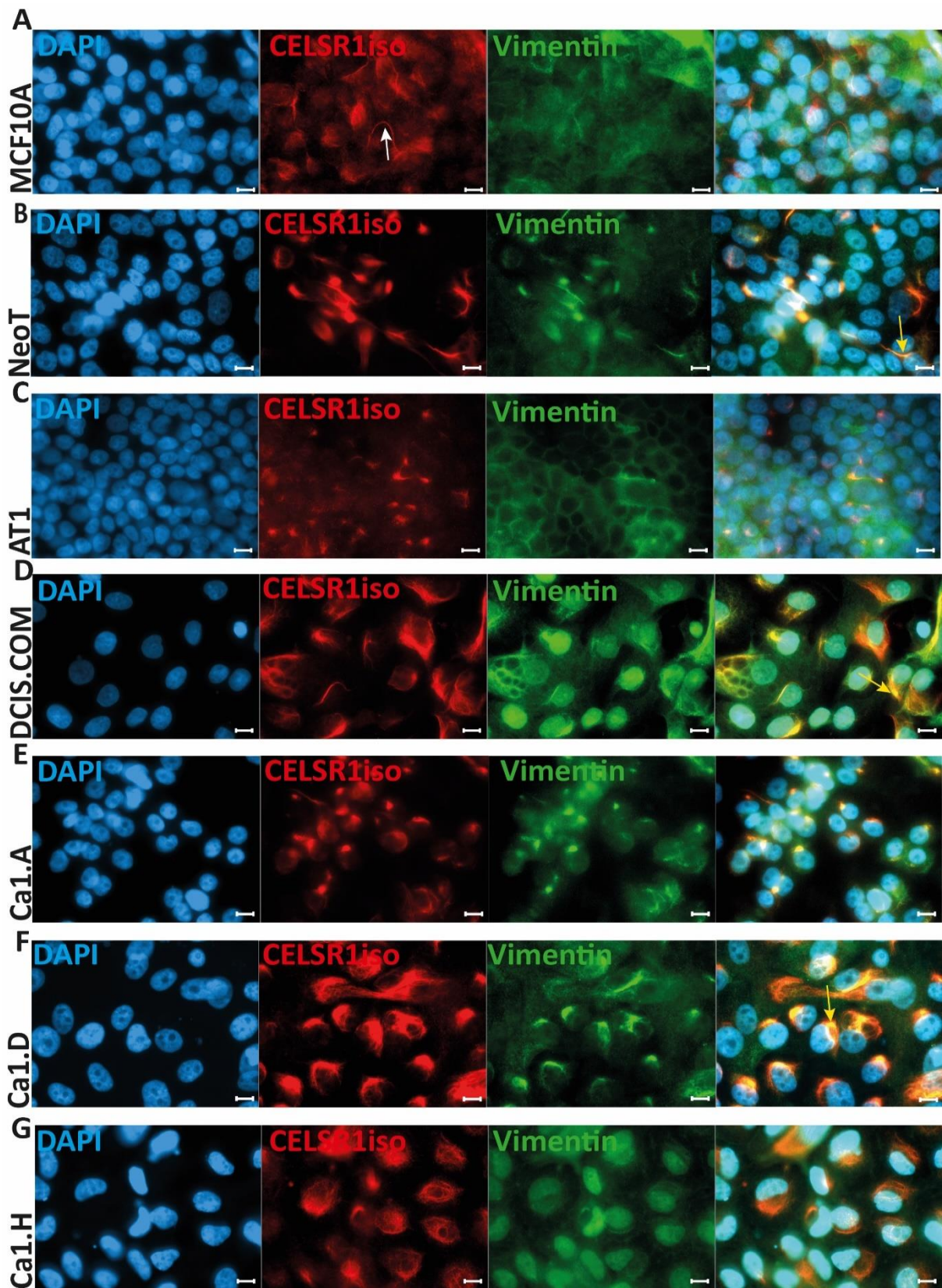
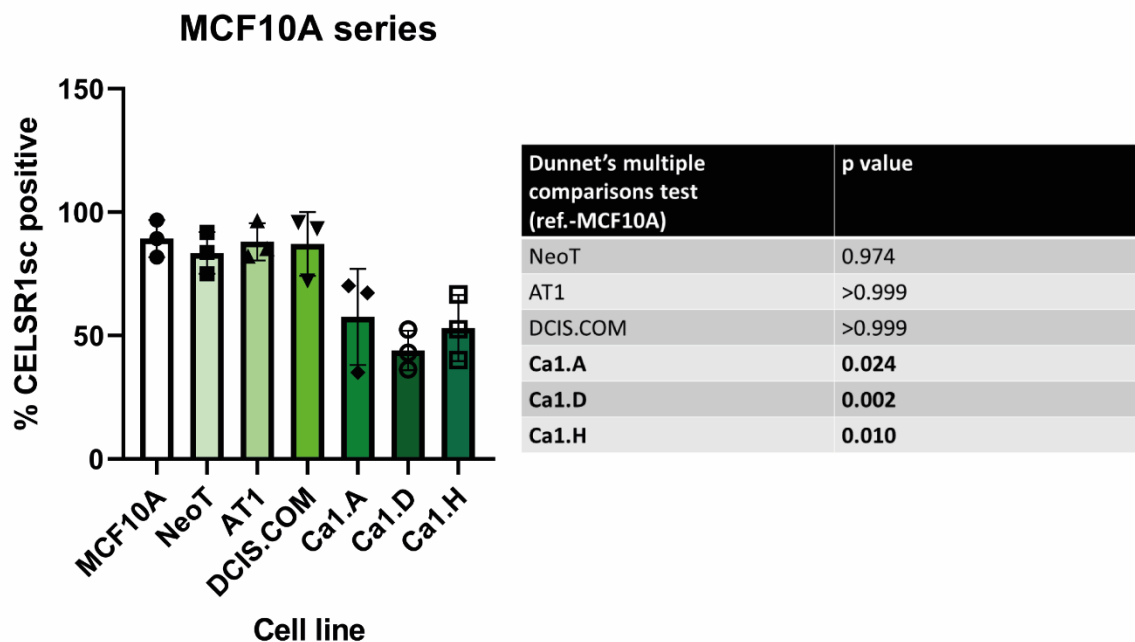


Figure 31 - ICC on the MCF10A progression series using the CELSR1iso antibody. MCF10A cells co-stained with vimentin showing CELSR1 bridges (white arrow) and nuclear enwrapment. B-D. NeoT, AT1 and DCIS.COM cells also exhibit CELSR1 bridges and nuclear enwrapment. Colocalisation with vimentin is also evident. E-G. Ca1.A, Ca1.D and Ca1.H cells CELSR1iso staining seems to be more intense as well as more localised to the nucleus rather than bridge-like. Yellow arrows show colocalization with vimentin in merged images. n=3 independent experiments

A



B

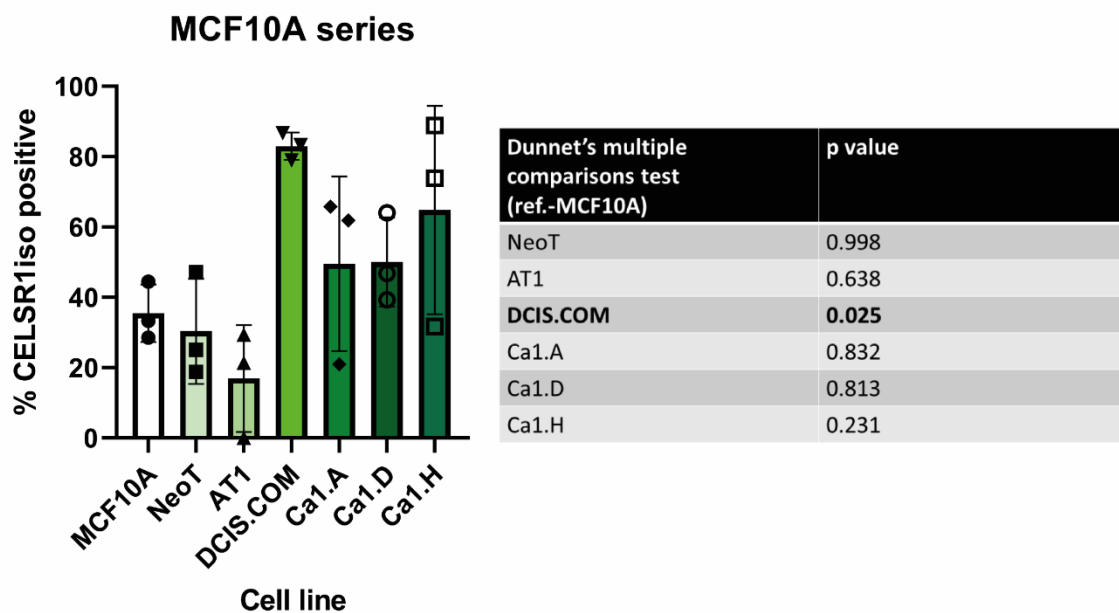


Figure 32 - MCF10A progression series quantification of positive CELSR1 staining. **A.** Graph showing the percentage of CELSR1sc positively stained cells from the total. CELSR1sc positive staining is significantly lower in the Ca1.A, D and H cell lines as shown by one-way ANOVA with Dunnet's multiple comparisons test (compared to MCF10A). **B.** Graph showing the percentage of CELSR1iso positively stained cells from the total. The % of CELSR1iso positively stained cells significantly increases in DCIS.COM cells. There is also a positive trend in the Ca1.A, D and H cell lines, however it is not statistically significant as shown by one-way ANOVA with Dunnet's multiple comparisons test (compared to MCF10A). n=3 independent experiments. P values provided in tables

5. Results - Assessing the role of CELSR1 in breast cancer using model cell lines and *in vitro* functional assays

5.1 Introduction

In Chapter 3 bioinformatic analysis was used to assess the significance of *CELSR1* and *FZD6* in breast cancer and in Results Chapter 4 several human breast cancer cell lines were characterised to identify an appropriate *in vitro* model for use in functional assays. The project then moved onto setting up relevant functional assays which could be used to interrogate the role of PCP proteins in breast cancer. Functional assays for this thesis were focused on CELSR1 given that Western blot and ICC data presented in Chapter 2 mainly represented CELSR1, and also because of the scarcity of published studies focusing on CELSR1 in cancer. In preparation for gain-of-function and loss-of-function assays for CELSR1 3D spheroids were derived using breast epithelial and breast cancer cell lines, using various substances such as synthetic and natural hydrogels and special surfaces. This is because in this environment breast cancer spheroids better resemble tubular structures of the mammary gland. This is important for this project since cell polarity is directly involved in the formation of mammary ducts. Therefore, 3D models will not only better mimic an *in vivo* environment, ICC was also conducted and fluorescent imaging involving z-stacks performed. Initial studies which investigated both a gain-of-function of Celsr1 protein in highly invasive MDA-MB-231 cells and loss-of-function in control and luminal type breast cancer cells were also initiated.

5.2 Evaluation of different methodologies to generate 3D spheroids from breast cancer cell lines

A variety of synthetic and natural hydrogels as well as special surfaces were tested to determine and optimise an ideal method to generate 3D spheroids. It is well known that monolayer cell culture is not natural for a cell that usually integrates with a 3D cell community *in vivo* and interacts with ECM in this context. In 2D, cells are forced to adapt to a non-native environment. 3D cell culture better

mimics and *in vivo* environment without the costly and lengthy procedures associated with using animal models.

5.2.1. Matrigel

Matrigel was cultured with BT474 cells, but large spheroids did not form. ICC staining using DAPI and CELSR1iso antibodies on the small 3-5 cell spheroids that were generated, was successful (Fig.33). Despite the good quality of the staining pattern, the small size of the spheroids generated and the high cost of Matrigel, led to the abandonment of this method.

5.2.2. Agarose

Next, an agarose layer method was trialled using MCF10A, BT474 and MDA-MB231 cells. Although cells formed large 3D spheroids (Fig.34), it proved difficult to conduct ICC because the spheroids were partly embedded in the agarose. During the ICC procedures, the cells dispersed and were lost. This method was therefore also not taken further forwards.

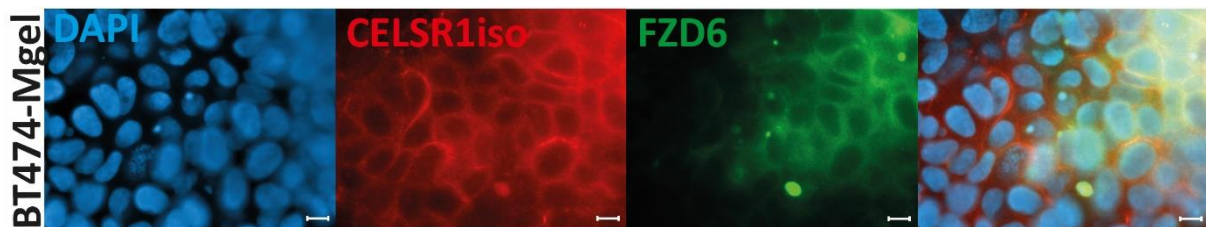


Figure 33 - ICC of BT474 cells grown in Matrigel. Scale bar is shown. Scale bar 5µm

5.2.3 Alginate beads in agar moulds

This method involved BT474 and 231 cells being embedded in beads which were then allowed to gel within special agar moulds containing calcium chloride as the gelling agent. This method proved to be very time-consuming owing to the lengthy preparation steps needed to create the agar moulds. Unfortunately, once ICC was attempted the beads ‘disappeared’ during the staining/wash steps, so this method was also abandoned. Nevertheless, 3D spheroids were generated (Fig.35).

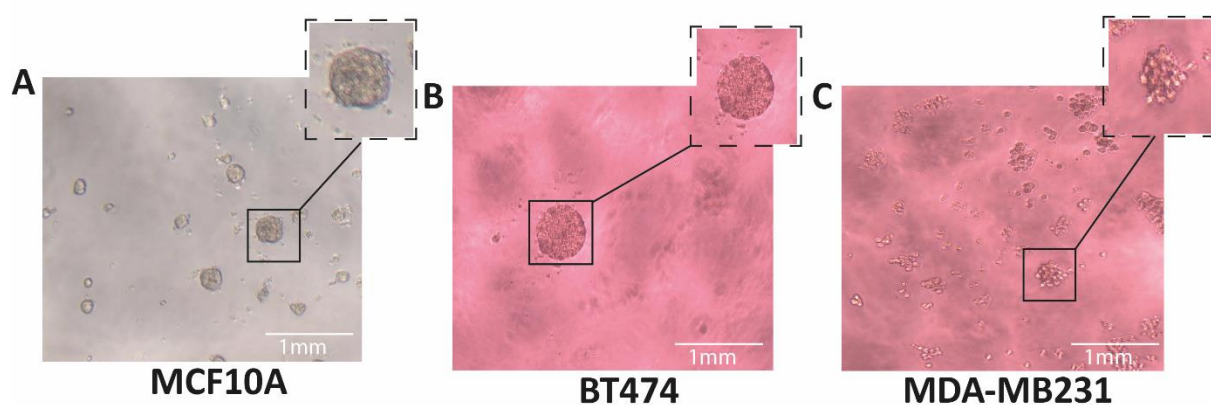


Figure 34 - Breast cancer cells forming spheroids on a layer of alginate. A, B. MCF10A and BT474 cells form rigid spheroids. **C.** MDA-MB231 cells forming 'loose' spheroids. Images in dashed line boxes show enlarged images of spheroid in original image. Scale bar 1mm.

Further reading uncovered the possibility that the absence of calcium and magnesium in ICC solutions, which are necessary to maintain the cross-linked structure of the alginate, might have caused the ICC to fail.

5.2.4 Ultra-low attachment plates

In this method ultra-low attachment plates were used. Elplasia™ plates from Corning contain a special surface covering for the microwells contained within the plate. The method was very simple as the only step required a desired number of cells to be plated per well (in a 6 or 24-well Elplasia plate). The cells were then left for 7 days to form spheroids of desired size (Fig.36). The main issue with this method was that as the spheroids were not being grown in a matrix, they were simply suspended in media, it was difficult to handle them without disturbing their 3D structure. Again, during ICC, despite careful handling, spheroids were lost or destroyed. One observation was that spheroids of cancer cells which lacked adhesive properties (i.e., highly aggressive MDA-MB23 cells) were much more easily disrupted.

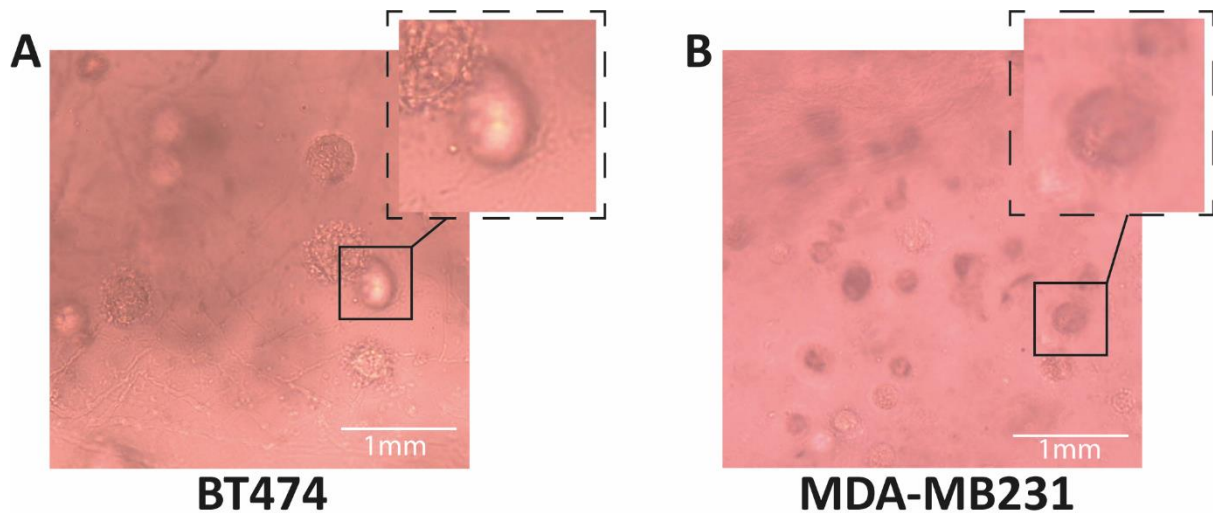


Figure 35 – Breast cancer cell line spheroids in 1% alginate beads in agar moulds. A. BT474 cells forming spheroids. **B.** MDA-MB231 cells forming spheroids. Images in dashed line boxes show enlarged images of spheroid in original image. Scale bar 1mm

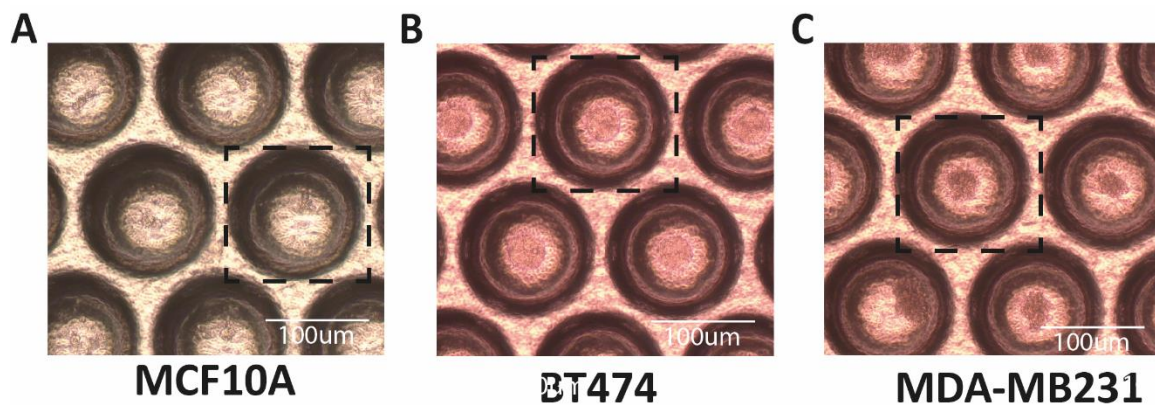


Figure 36 - Breast cancer cells forming spheroids in ultra-low attachment plates. A. MCF10A cells forming individual spheroids per well. **B.** BT474 cells forming individual spheroids per well. **C.** MDA-MB231 cells forming individual spheroids per well. Dashed lined boxes highlight a single spheroid. Scale bar 1mm.

5.2.5 Alginate beads

The penultimate method involved a simple alginate bead method which used Hanks balanced salt solution with calcium and magnesium (HBSSCM) to preserve the alginate cross-linking and which then allowed ICC to be successfully performed. Fig. 37 shows successful ICC using CELSR1iso/CELSRsc, phalloidin and DAPI (Fig.37). ICC staining of T47D cells shows clear phalloidin staining (Fig.37C, D),

although a lumen could not be defined. However, the distribution pattern of CELSR1 antibody staining was hard to assess (Fig.37). Images were taken using an Apotome fluorescent microscope and thus the quality is perhaps lower than they would be using a confocal microscope.

Altogether these experiments suggested that, at least in our hands, the simplest and most optimal method to generate 3D spheroids is the alginate bead method (4.2.5). This method allowed for decent quality images to be taken. This method was therefore considered to be most suitable for future assays on *CELSR1* shRNA knockdown and *CELSR1* over-expression models described in the next sections.

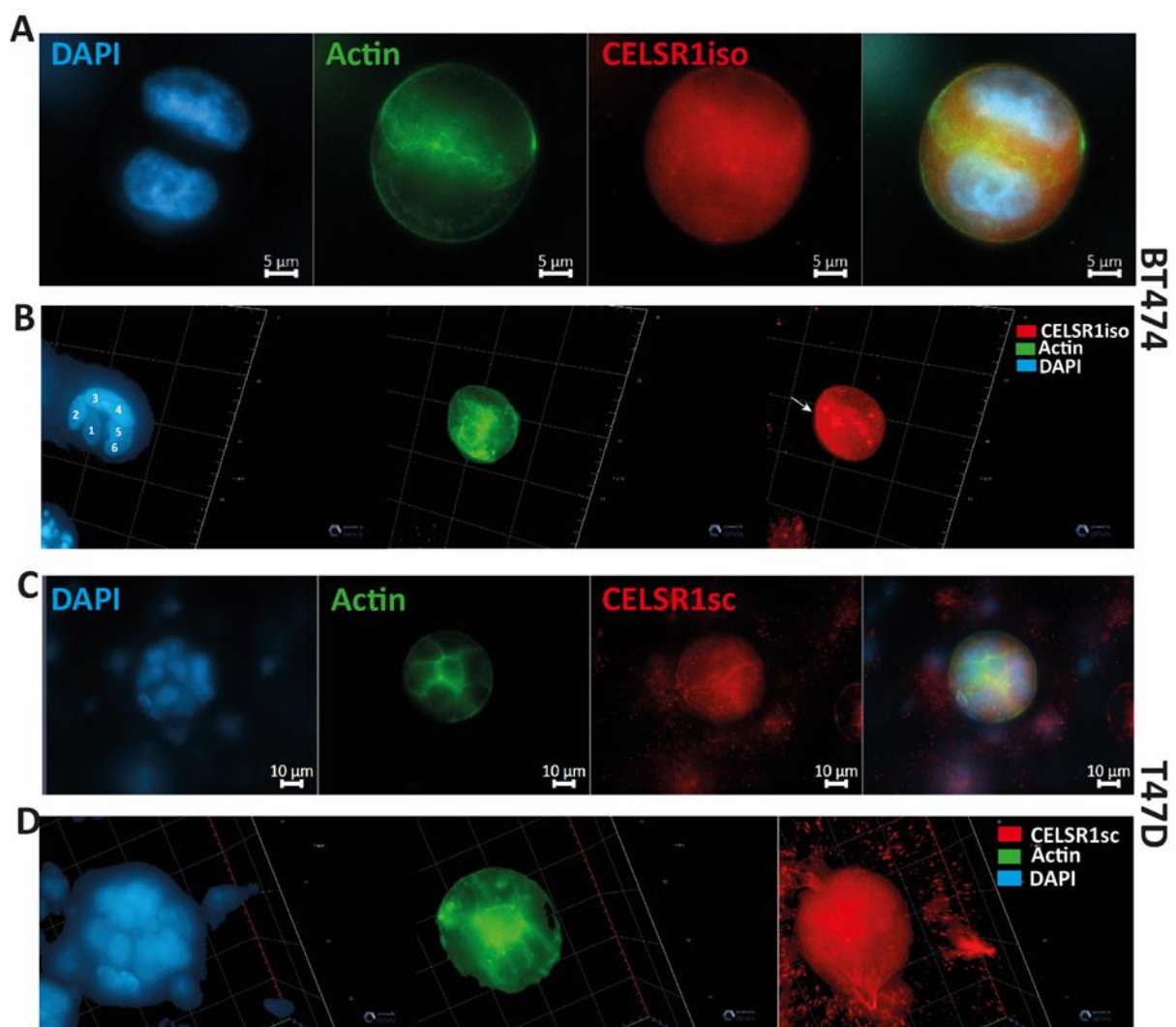


Figure 37 - Imaging of BT474 and T47D spheroids in alginate beads. A. 2D images of a BT474 spheroid stained. **B.** Z-stack of a BT474 spheroid with the individual nuclei numbered **C.** 2D images of a T47D spheroid. **D.** Z-stack of the spheroid in C. n=2 independent experiments. Scale bar is 10μm.

5.2.6 – On-top Matrigel culture

‘On-top’ culture with growth factor reduced Matrigel was conducted for MCF10A cells in order to attempt a 3D structure with a hollow lumen, resembling a mammary duct. Growth factor reduced Matrigel was used since epidermal growth factor (EGF) was already included in the MCF10A media composition. This 3D spheroid strategy was of particular interest as it could enhance studying PCP in breast cancer, since as mentioned before, PCP works in 3 dimensions. Using ‘On top’ culture MCF10A cells formed spheroids, however most of them merged together so immunostaining was not very clear. Only one spheroid generated a hollow lumen (Fig. 38). In future, MCF10A cells would be seeded at lower density to increase the chances of single spheroids being generated.

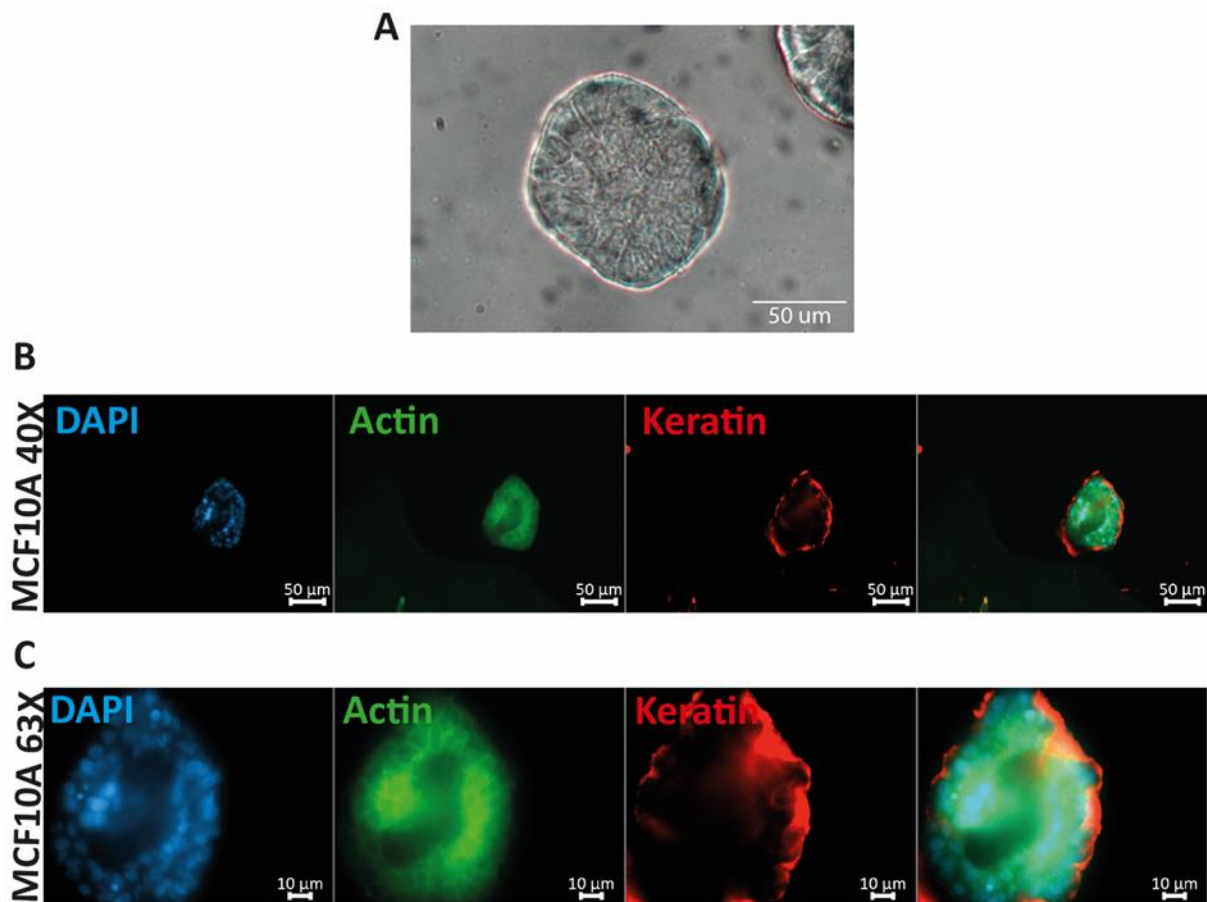


Figure 38 - MCF10A spheroid grown on a layer of growth factor reduced Matrigel A. Brightfield images of a single spheroid after 8 days of culture. B. ICC of a single spheroid in 2D. A lumen appears to have formed C. B at 63X magnification. Scale bars are shown. N=1. Scale bar is 50μm (A) and 10μm (B, C)

5.3 Investigation of efficiency of commercial shRNAs for CELSR1-specific knockdown in breast epithelial and breast cancer cell lines

As demonstrated by qPCR and western blots in Chapter 2, the MCF10A cell line and the luminal BT474 cell line both exhibit sufficient levels of CELSR1 protein to warrant knock-down studies. In addition, MCF10A is a control epithelial cell line and BT474 a benign type breast cancer cell line which represents Luminal type breast cancer, which was found to express high levels of *CELSR1 mRNA* in patient samples (Chapter 1, Fig.19). Hence, these two cell lines were chosen to attempt *CELSR1* knockdown. Two commercially available and validated (Sigma Aldrich) small hairpin RNAs (shRNAs) were selected and tested in these pilot studies. We selected shRNAs rather than siRNAs (small interfering RNAs), since shRNAs provide a stable knockdown, rather than a transient one by siRNAs. Therefore, the use of shRNAs increases experimental accuracy and results in more robust data. The details of the shRNAs are in Table 4 and a schematic showing their location within the third cadherin domain and the 3'UTR of CELSR1 is shown in Figure 39A. A control shRNA was provided as a plasmid with a packaging mix. However, it could not be generated at sufficient titre for infection despite concentration by ultracentrifugation. Wild-type MCF10A cells were therefore used as a control for Western blot and ICC experiments.

Table 4 - Showing the NM ID, clone ID and location within CELSR1 of the shRNAs used

<u>NM ID</u>	<u>Clone ID</u>	<u>CELSR1 Location</u>
NM_014246	TRCN0000273659	3'UTR
NM_014246	TRCN0000011238	Cadherin domain 3

5.3.1 CELSR1-cadherin 3 domain shRNA provides efficient knock-down of CELSR1 protein

A lentivirus containing a shRNA against the third cadherin domain of CELSR1 (Fig.39A) was used to infect MCF10A cells at 20,000 cell per infection. shRNA infected colonies were then grown in selective puromycin antibiotic to select clones that had stably integrated the shRNA construct into their genomes. Once clones had been expanded, cell lysates were submitted to qPCR and Western

analyses. qPCR analysis revealed equivalent levels of *CELSR1* mRNA expression in both MCF10A WT cells and MCF10A KD cells. Western blotting confirmed *CELSR1* knockdown using both *CELSR1*-sc and *Celsr1*-iso antibodies (Fig.39B, C, D). Thus, knock-down experiments are consistent with *CELSR1*sc and *CELSR1*iso antibody specificity for Western blot analyses. However, loading controls on the same blot as *CELSR1* antibody staining will be needed to confirm specificity.

Notably, a phenotypic change in the appearance of cadherin 3 shRNA containing cells (MCF10A KD) compared to MCF10A wild-type (WT) cells was observed when these cells were grown in 2D culture (Fig.39). At low density MCF10A KD cells failed to form extensive adhesive cell-cell contacts and appeared filamentous in structure, compared to WT MCF10A cells (Fig.39A). However, at high density MCF10A KD cells had formed cell-cell adhesion and appeared somewhat similar to WT MCF10A cells (Fig.39C).

ICC analysis in 2D confirmed *CELSR1* KD using *CELSR1*-sc antibody as antibody staining was lost in each of 3 MCF10A KD clones analysed compared to WT MCF10A cells (Fig.40), quantification of *CELSR1*-sc antibody staining in KD cells is shown (Fig.41). Conversely, *CELSR1*iso staining was significantly increased (Fig.40D, F, H), which is quantified in Figure 41A. Thus, *CELSR1*iso must be binding to another, unknown, protein in fixed MCF10A cells in 2D culture. Thus, these data invalidate *CELSR1*iso antibody as a tool to distinguish *CELSR1* via ICC in MCF10A cells.

Notably, the *CELSR1*iso antibody defined a small population within WT MCF10A cells (Fig.26 ,Chapter 2). Stable KD of *CELSR1* using the cadherin-4 shRNA significantly increased the number of *CELSR1*iso antibody expressing cells however (quantified in Fig.42B). Given that *CELSR1*-iso co-localised with vimentin in MCF10A cells, which is an intermediate filament associated with mesenchymal cell types (Chapter 2, Fig.26) it was hypothesized that *CELSR1* KD drives an epithelial-mesenchymal transition (EMT) in MCF10A breast epithelial cells. Further study revealed that WT MCF10A cells predominantly expressed p63 and smooth muscle actin (Appendix, AFig.20). Coupled to the ICC data which shows that around 20-30% of WT MCF10A cells stain with *CELSR1*iso (Fig.42B) which strongly co-localises with vimentin, it was further hypothesized that the MCF10A cells used in

this study represented a population of precursor cells that can generate myoepithelial cells in culture. Given that at least one 3D MCF10A spheroid generated via 'on top' Matrigel culture could form a lumen, it is further postulated that the WT MCF10A cells can also generate luminal type cells supporting the idea that these cells represent a precursor population. However, we cannot rule out at this point that the WT MCF10A cells are mostly myoepithelial cells with a few luminal cells. Further experiments are needed to characterise the WT MCF10A population used in this study.

A 3'UTR shRNA was also used to infect WT MCF10A cells, but cells did not proliferate and eventually died.

Taken together these CELSR1 KD data validate the Cad3 CELSR1 shRNA and reveal that knockdown occurs at the protein level. CELSR1iso antibody is validated for western blot but not for ICC. These pilot CELSR1 KD experiments also pave the way for fruitful investigation of CELSR1 function in vitro in the future.

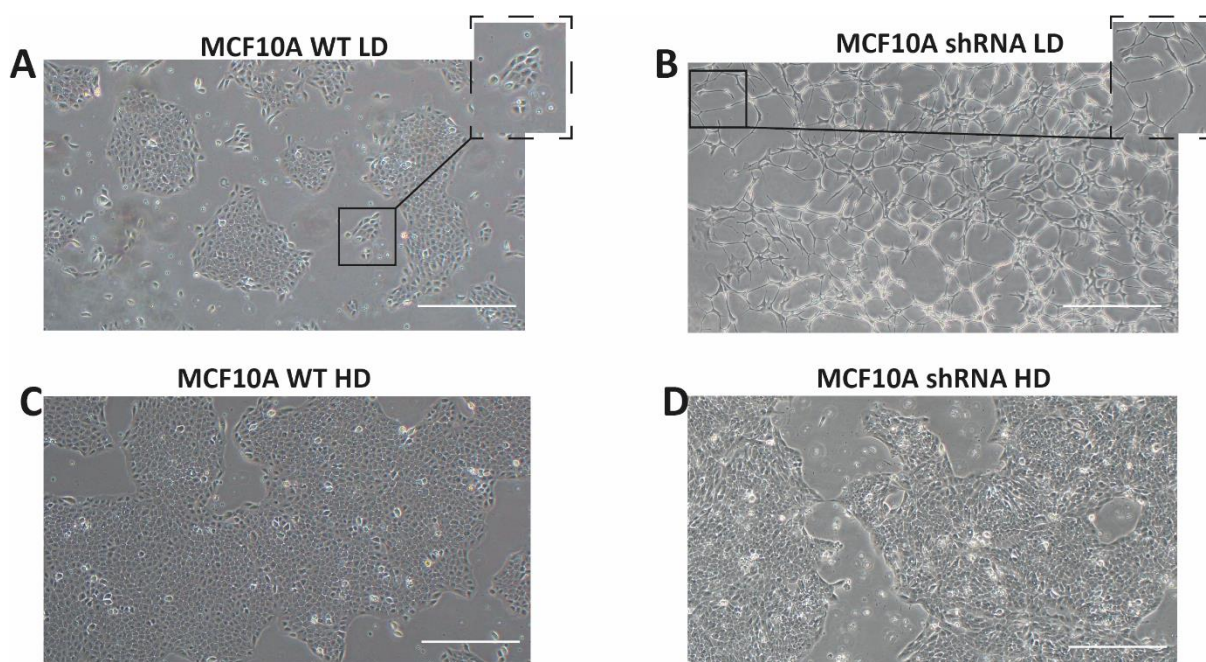


Figure 39 - Phenotypes of MCF10 WT and MCF10A shRNA transfected cells at various densities. A,C. MCF10A WT at lower density (top) and higher density (bottom). **B, D.** MCF10A shCad3 cells at lower density (top) and higher density (bottom). Scale bar is 1mm.

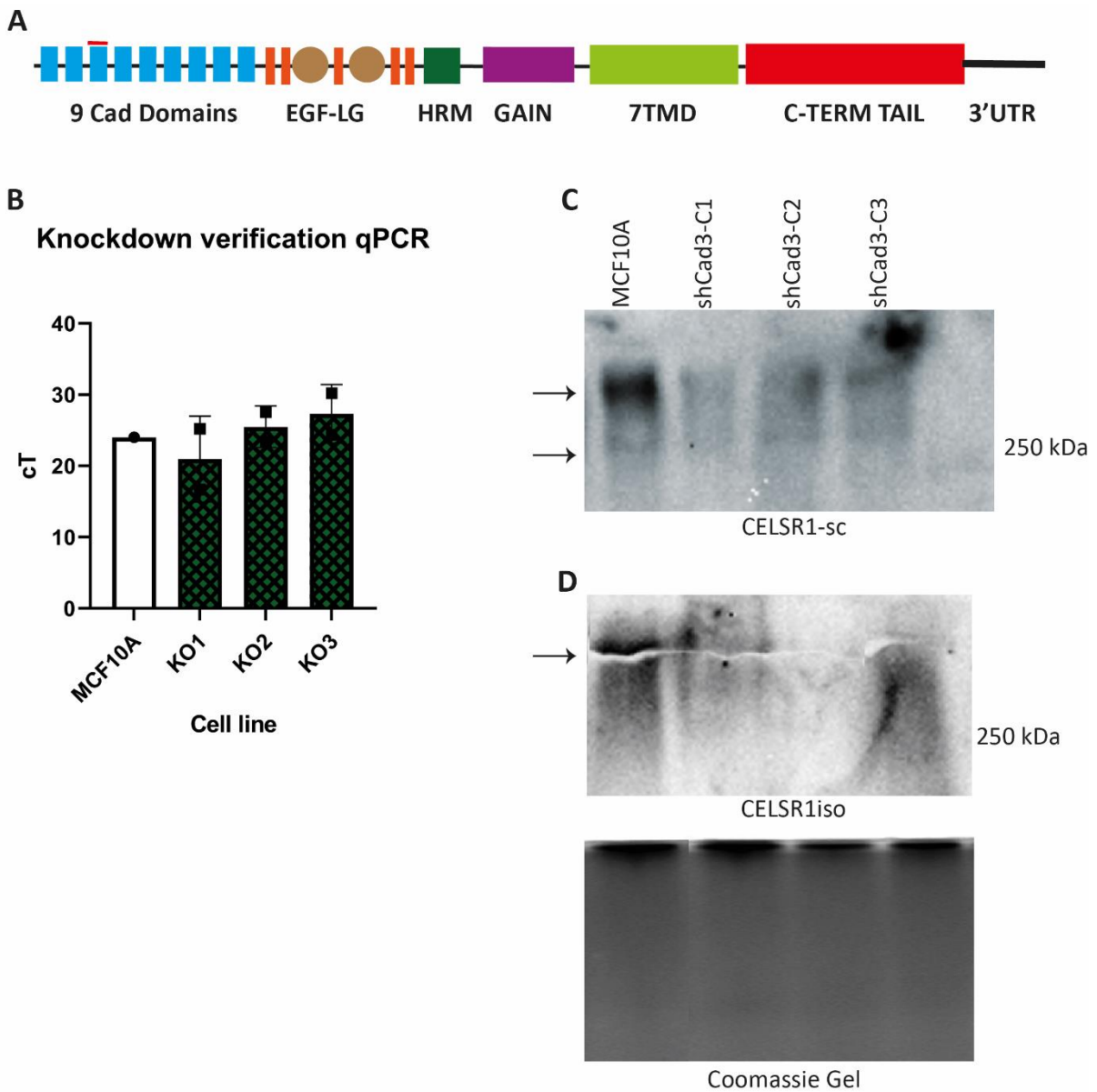


Figure 40 - Showing shRNA locations in CELSR1. A. Positions of shRNAs tested within the CELSR1 protein structure. Cad = Cadherin, EGF = EGF-like receptor = GAIN = Gain domain 7 TM = 7-transmembrane domain **B.** Absence/presence qPCR with MCF10A KO cells compared to MCF10A WT cells. cT = Cycle-threshold, higher cT indicates lower mRNA expression and vice versa. All three clones have more or less similar mRNA levels according to qPCR. N=1 (3 technical replicates). Mean + SD are shown. **C.** WB with CELSR1-sc antibody shows reduction of CELSR1 in the shCad3 cells compared to MCF10A wt cells. The lower band marked by an arrow act as a loading control. **D.** WB with CELSR1iso antibody shows reduction/absence of CELSR1 in shCad3 cells compared to MCF10A wt cells. The Coomassie gel below acts as a loading control. N=1 independent experiment (B), N= 5 independent experiments (C, D)

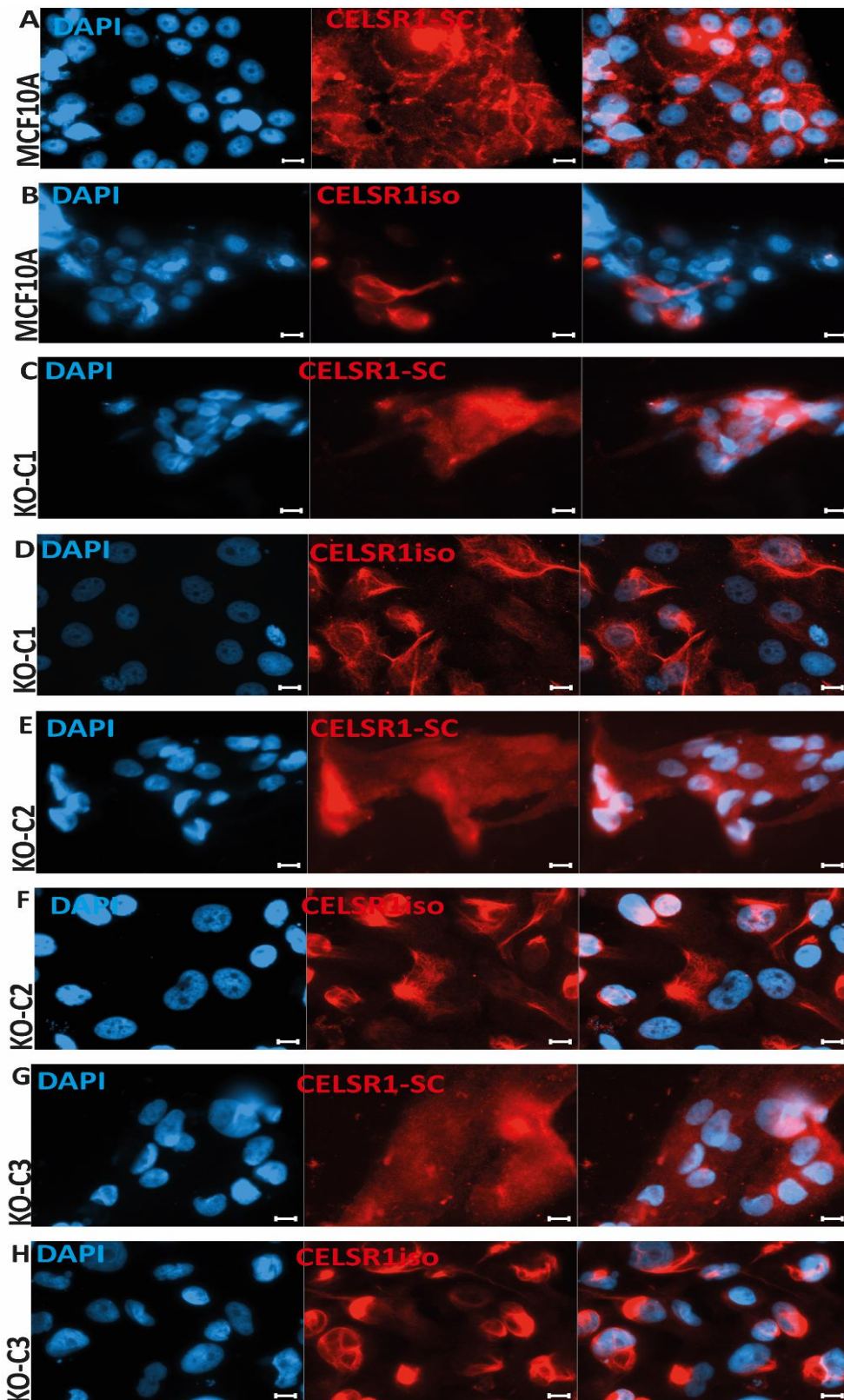


Figure 41 - ICC of MCF10A KO cells compared to MCF10A WT. A. A cortical staining pattern is observed with MCF10A WT cells stained with CELSR1sc. **B.** Bridge like structures can be observed when MCF10A WT cells are stained with CELSR1iso as. **D, F , H.** CELSR1iso staining of 3 clones of MCF10A KO cells. **C, E, G.** CELSR1sc staining is absent from the 3 MCF10A KO clones n=3 independent experiments. Scale bar is 5 μ m

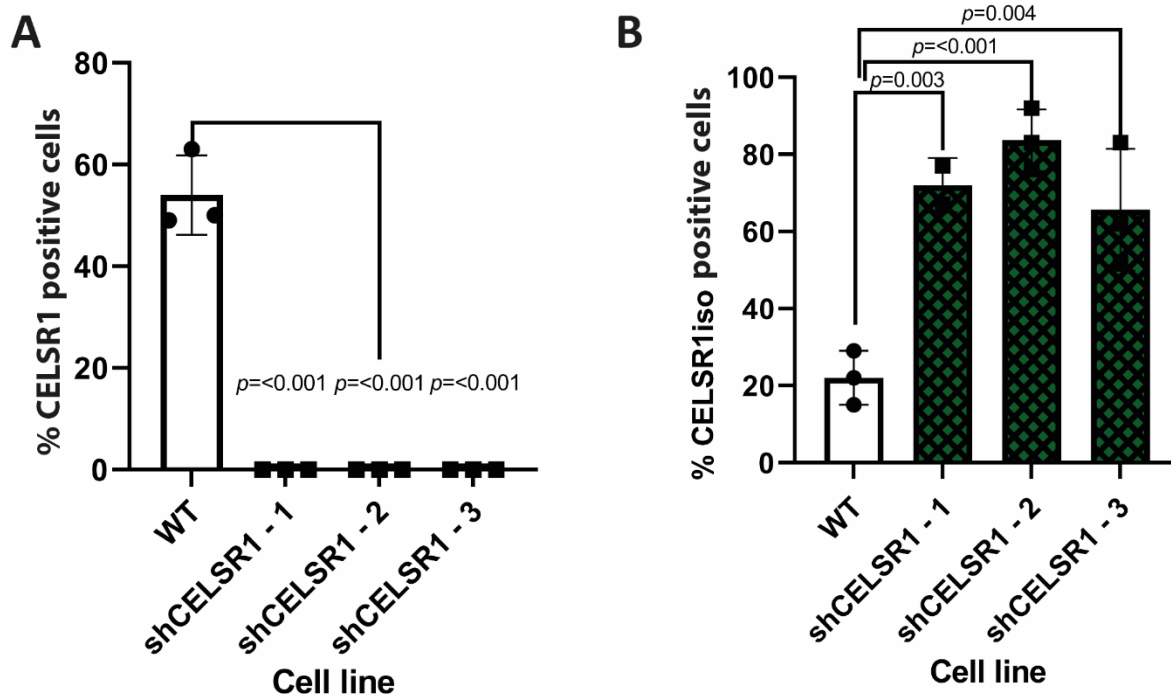


Figure 42 - MCF10A KO ICC quantification and qPCR data. **A.** (Left) Percentage of CELSR1iso positive cells compared to the total (DAPI). All three clones of MCF10A KO cells exhibit significantly greater CELSR1iso staining than MCF10A WT cells. (Right) Percentage of CELSR1sc positive cells compared to the total (DAPI). All three clones of MCF10A KO cells exhibit significantly lower CELSR1sc staining than MCF10A WT cells. One-way ANOVA with. N=3 independent experiments

5.3.2 CELSR1 knockdown with Cad 3 shRNA and 3'UTR shRNA is toxic to BT474 cells

Knockdown of BT474 cells was conducted as for MCF10A cells, using both Cad3 and 3'UTR specific shRNAs. However, in both cases, once the cells were moved into selective puromycin containing medium, they died (Fig.43). This was repeated for the Cad shRNA, and on subsequent attempts the BT474 cells again died (Fig.43). They initially formed colonies however they later became spherical and detached from the surface of the tissue culture well.

BT474 cells transfected with the 3'UTR specific shRNA did not proliferate and eventually died (Fig.43) supporting what was observed in MCF10A cells, that this shRNA is somehow toxic to the cells.

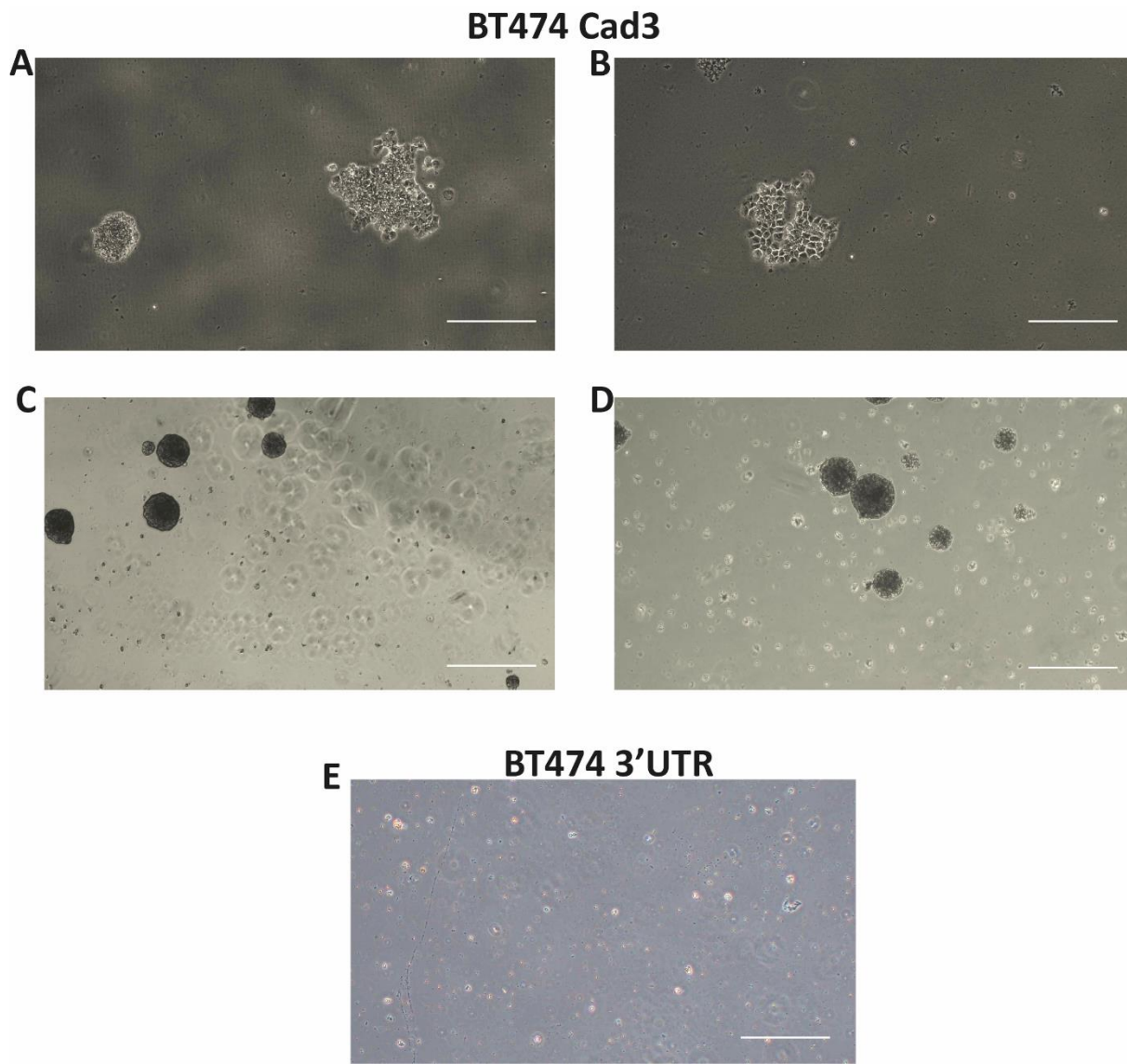


Figure 43 - BT474 transfected with CELSR1 specific shRNAs cells after being placed in selective media (puromycin). A. The colony on the right looks normal, but on the left cells round up and detach. **B.** Normal looking colony of BT474 cells in initial stages of growth. **C, D.** After some time, cells rounded up, died, and detached. **E.** BT474 cells transfected with 3'UTR specific shRNA. Scale bar is 1mm.

5.4 Over-expression of mouse Celsr1 in TNBC -type cell line, MDA-MD-231 cells

In Chapter 2 it was demonstrated that CELSR1 mRNA and protein expression is significantly reduced in the highly invasive TNBC-type MDA-MB231 cell lines (Chapter 2, Fig.19 and Fig.20). ICC has also shown that in MDA-MB231 cell lines CELSR1 staining disappears (using CELSR1-sc antibody, Chapter 2, Fig.27H). These findings are consistent with the hypothesis that CELSR1 might be a tumour

suppressor. Therefore, to assess if and to what extent CELSR1 could be a tumour suppressor, an available full-length mouse Celsr1 (mCelsr1) cDNA tagged 19 at the C-terminus with GFP (in-house) was overexpressed in the basal TNBC-type MDA-MB231 cell line. The GFP fusion was made in-frame with the SDSE motif, which in the CELSR1 cDNA is located immediately before the variant C-terminal spliced domains (C. Formstone, personal communication). mCelsr1 is closely related to CELSR1 at the protein level and was thus considered a valid substitute for the human protein. mCelsr1 however is known to exist as a 400kda full length protein and a smaller cleaved protein at around 80kd, which contains the cytoplasmic tail (Oozeer et al., 2017).

A mammalian expression construct pCDNA3.1 containing a full-length cDNA encoding mouse Celsr1-GFP was transiently transfected into MDA-MB231 cells using Lipofectamine 3000 as shown in Fig.44 and cells which had stably integrated the construct into their genomic DNA were selected for using Geneticin (G418).

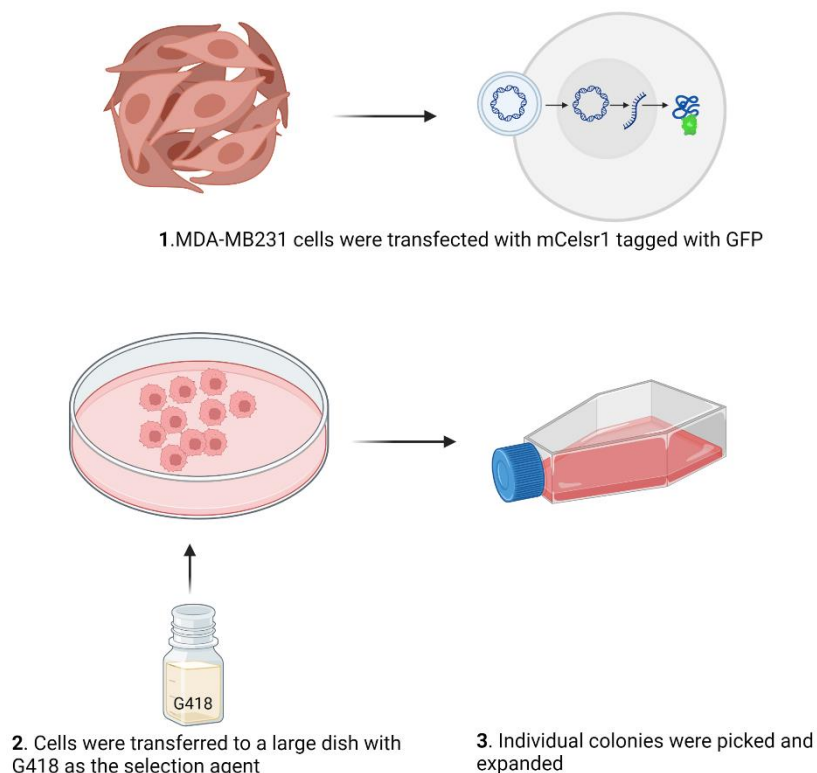


Figure 44 - Transfection of mCelsr1-GFP into basal like MDA-MB231 cells

5.4.1 Validation and phenotypic evaluation of CELSR1 gain-of-function experiment

The transfected cells were periodically checked under a fluorescent microscope to confirm protein expression via GFP fluorescence. Fluorescent colonies were picked and expanded. Any phenotypic changes were documented (Fig.45). PCR was used to verify the successful transfection of empty pcDNA3 vector into the same parental population of MDA-MB231 cells, which was used as a transfection control (Fig.46A). T7 (5' TAATACGACTCACTATAGGG 3') and SP6 (5' TACGATTTAGGTGACTATAG 3') primers were used to generate a PCR band of the expected size (data not shown). Western blots were then performed on both control and experimental cells, using an anti-GFP antibody to visualise the GFP-tagged mCelsr1 protein (Fig.46A). Protein bands of expected size were observed for two clones expressing the mCelsr1-GFP protein but not in control cells. Addition of a GFP tag to mCelsr1 increases the expected size of cleaved mCelsr1 protein to 110 kDa. A band of this size is observed on Western blots (black arrow, Fig.46A) but at lower intensity to a band of 75Kda (asterisk, Fig.46A) One possibility is that the cleaved 110Kda mCelsr1 protein product is processed further to 75KDa in the MDA-MB231 cells, which may mean loss of the GFP tag from the C-terminus of the protein.

Cells were passaged on for functional assays and checked for GFP fluorescence throughout. However, fluorescence was lost after more than 3 passages suggesting that MDA-MB231 cells had completely or partially recombined the mCelsr1 construct. The transfection was therefore repeated, and fluorescent colonies grown to confluence in G418 once again, before being frozen down in multiple aliquots. One aliquot of transfected cells was then regrown and only passaged once before functional assays were performed to circumvent loss of mCelsr1-GFP expression during the course of the functional experiments.

Detailed analysis of stable mCelsr1-GFP expressing MDA-MB231 cells in 2D culture (first and second transfection) revealed that GFP was strongly expressed in large, punctate intracellular structures (Fig.45 A, B). The extent of cell-cell contacts and adhesive surfaces in mCelsr1-expressing cells compared to control cells was not observed to be altered via light microscopy. It was expected

that mCelsr1-GFP would be enriched at the cell surface of MDA-MB231 cells as was observed in canine kidney cells (C.Formstone, personal communication). However, fluorescent imaging of live MDA-MB231 cells revealed that mCelsr1 was in cytoplasmic vesicles (Fig.45). It is unclear if low levels of mCelsr1 GFP are shortly expressed at the cell surface or mCelsr1-GFP has a fast-recycling rate at the membrane of MDA-MB231 cells.

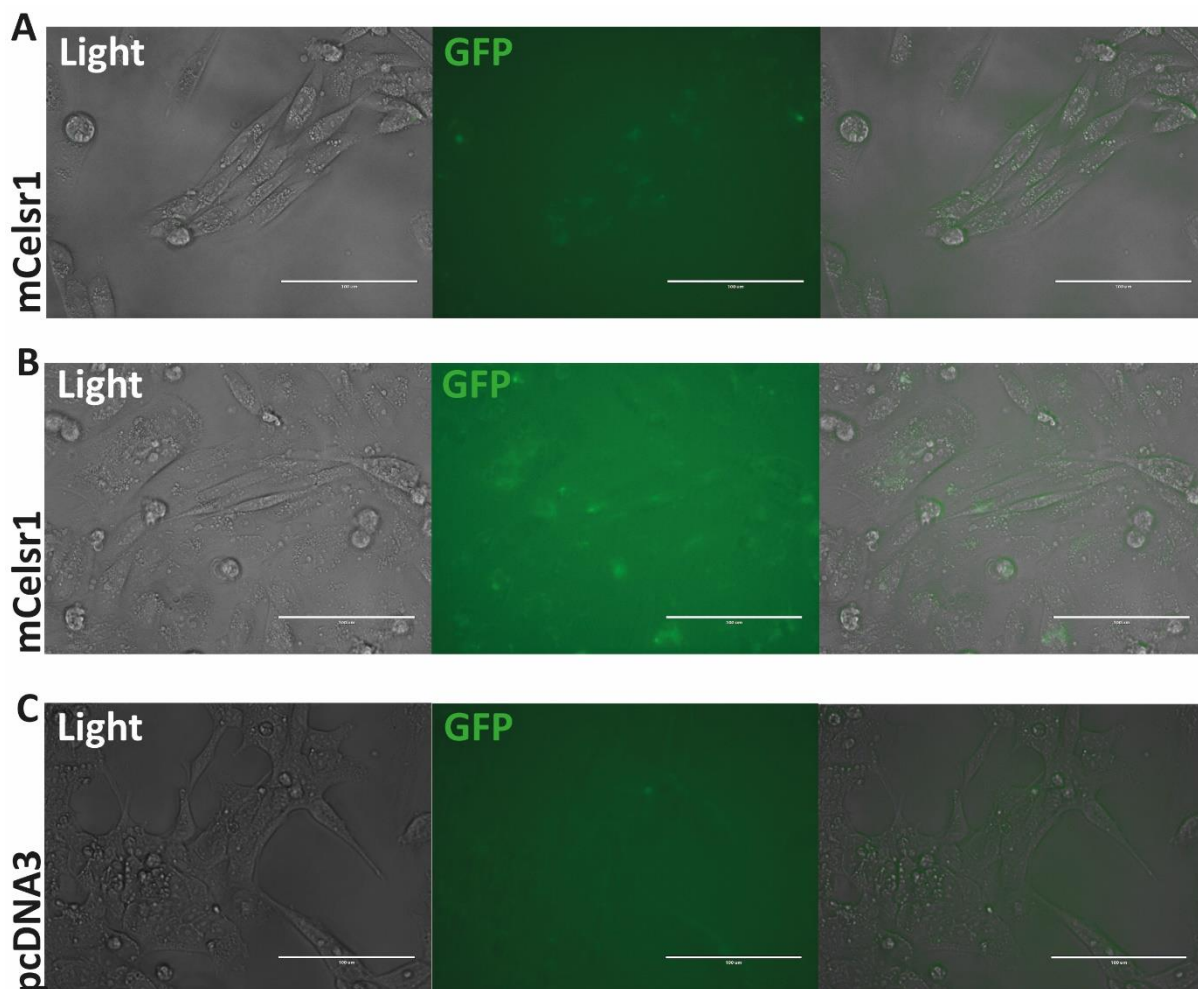


Figure 45 - Brightfield and fluorescent images of MDA-MB231 mCelsr1 transfected cells and pcDNA3 control cells. A, B. Images of two independent MDA-MB231 mCelsr1 clones. **C.** Images of MDA-MB231 pcDNA3 control cells. Final image is merge of brightfield and GFP. Scale bar is 100 μ m.

5.4.2 Functional assays to investigate cell proliferation, cell migration and colony formation

Two functional assays were conducted to investigate whether forced expression of mCelsr1-GFP in MDA-MB231 cells altered their growth and/or their invasive potential.

Firstly, the MTT assay was conducted to investigate whether forced expression of mCelsr1 affected cell proliferation. The MTT assay is a colorimetric assay, which measures cell proliferation by relying on a reduction reaction of the MTT reagent to purple formazan by mitochondria. Fig. 47 shows that in compared to control pcDNA3 cells, mCelsr1-expressing MDA-MB231 cells were significantly less proliferative. Secondly, a scratch assay was used to investigate migratory ability. mCelsr1 expression was observed to reduce the migratory ability of invasive type MDA-MB231 cells.

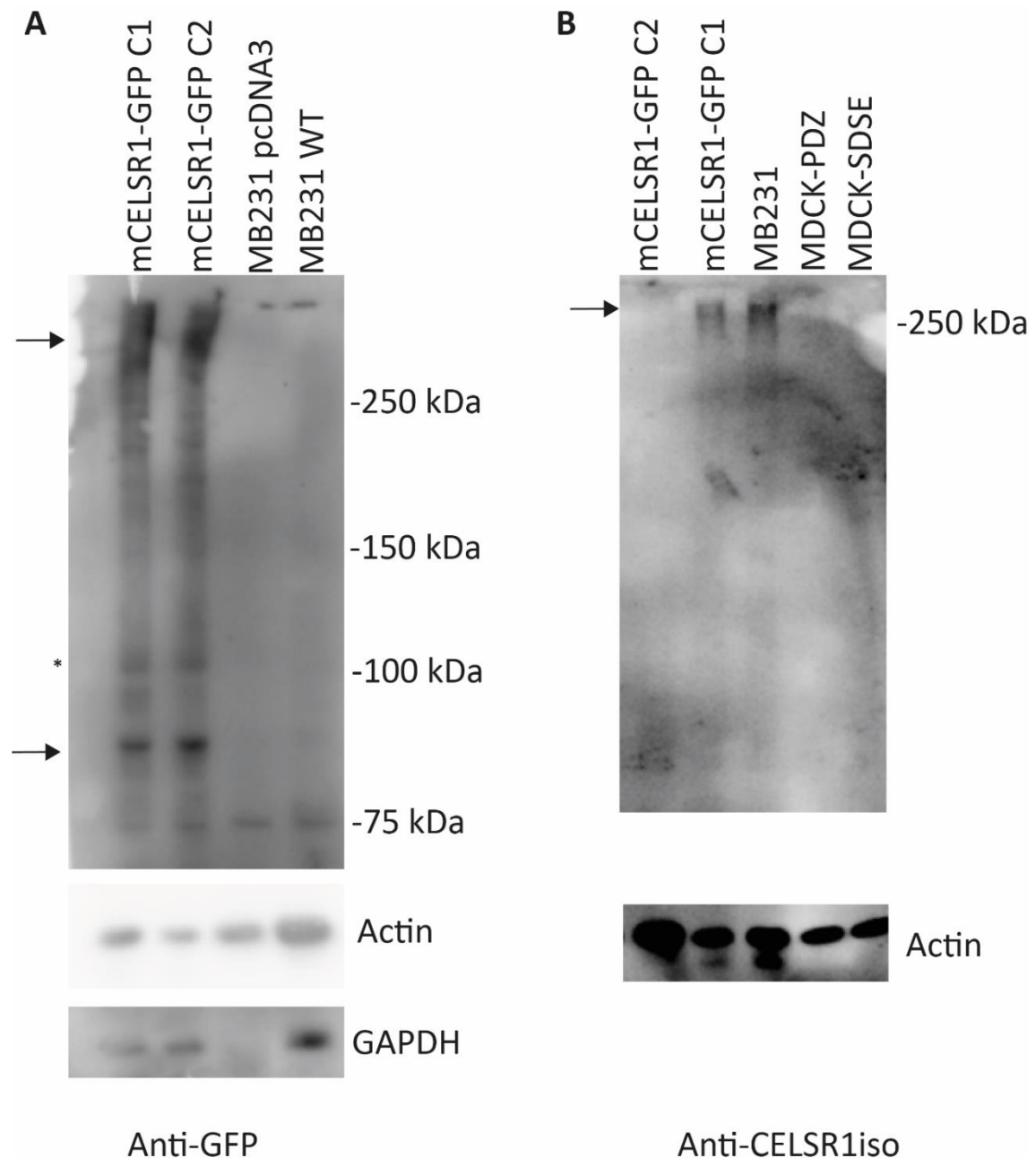


Figure 46 - Western blots of anti-GFP and anti-CELSR1iso antibodies with MDA-MB231 GOF cell samples. Western blot. Upper black arrow shows full length mCelsr1 GFP, asterisk shows cleaved product + GFP, lower black arrows show a probable p85 band. B. Black arrow indicates CELSR1iso bands. N=3 independent experiments

mCelsr1-expressing MDA-MB231 cells were significantly slower to close the scrape wound compared to control MDA-MB231-pcDNA3 control cells (Fig.47). Whilst control cells had mostly closed the gap after 24h as evidenced by the % cell-free area, mCelsr1-expressing MDA-MB231 cells were approximately half-way to scrape wound closure (Fig.48A). Only after 48h did mCelsr1-expressing 231 cells finally close the scrape wound (Fig.48B).

These data show that over-expression of mCelsr1 reduces the proliferative and migratory potential of the highly invasive TNBC basal-like MDA-MB231 cell line.

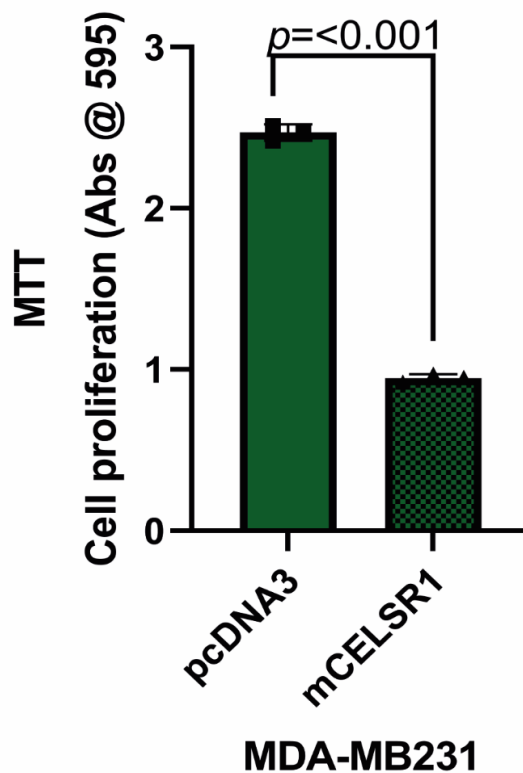


Figure 47 - MTT proliferation assay of MDA-MB231 cells transfected with a pcDNA3 empty vector (control) and with mCelsr1-GFP. There is a significant reduction in cell proliferation in mCelsr1-GFP transfected cells compared to pcDNA3 controls. n=5 independent experiments. Statistical analysis was done by unpaired students t-test. P-values are indicated.

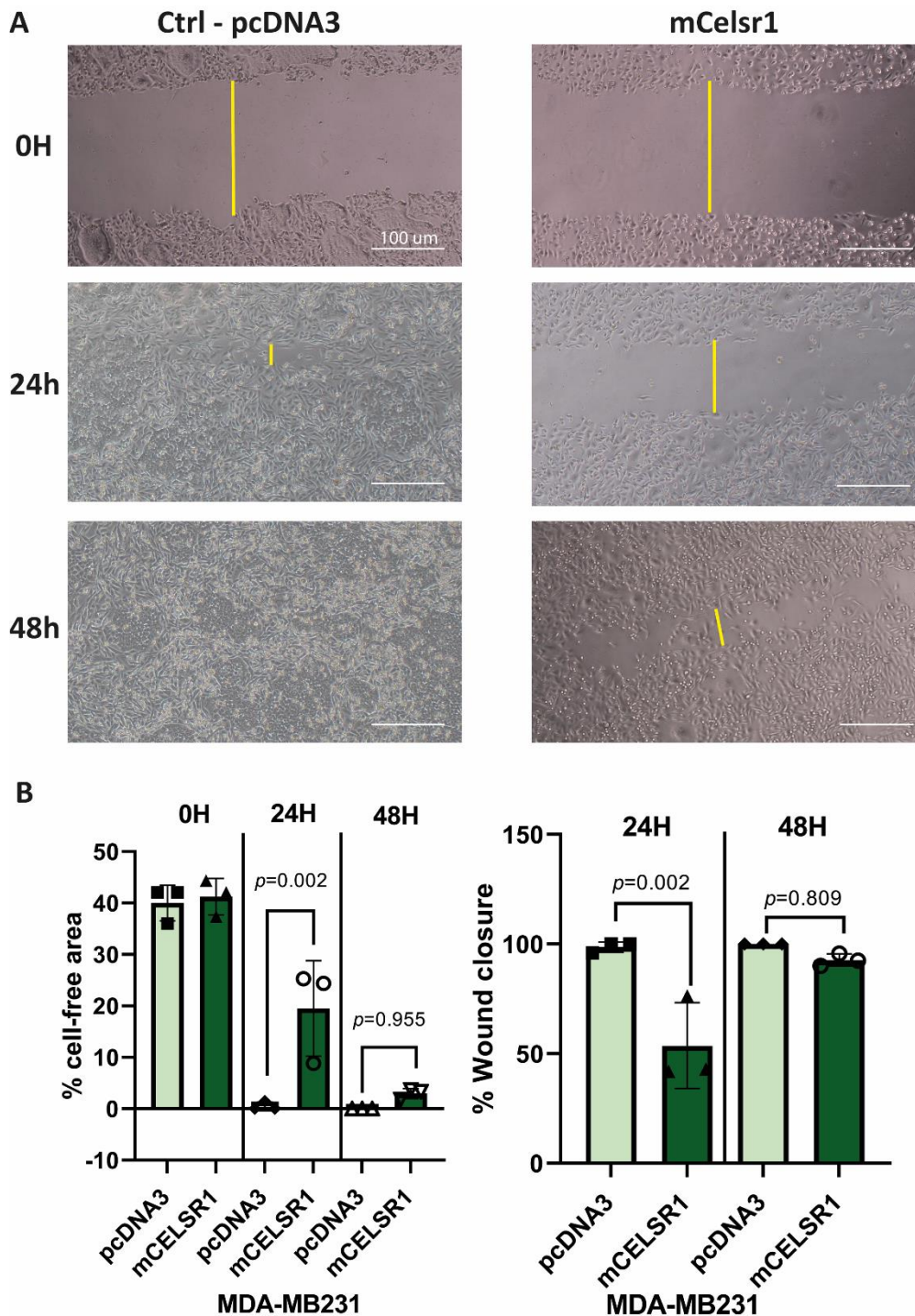


Figure 48 - Scratch assays conducted on MDA-MB231 cells transfected with mCelsr1-GFP. A. Representative brightfield images of the scratch assay in MDA-MB231 Ctrl-pcDNA3 (empty vector) and MDA-MB231 mCelsr1-GFP cells at 0-, 24- and 48-hours post scratch. Yellow lines indicated width of free cell-free area in the scratch area. **B.** (Left) Migration assay results showing cell free area at 0, 24 and 48h post-scratch. (Right) % wound (scratch space) closure after 24 and 48 hours compared to 0h. mCelsr1-GFP migrate significantly slower when compared to pcDNA3 cells. N=3 independent experiments. Statistical analysis was done by one-way ANOVA with Tukey's multiple comparisons test. P-values are indicated. Scale bar is 100 μ m.

6. DISCUSSION

6.1 Overview

Cell membrane receptors CELSR1 and FZD6 work together within PCP during embryonic development (Oozeer et al., 2017). In recent years several studies have suggested that the PCP receptor CELSR1 might function as a tumour suppressor in breast cancer, and its counterpart FZD6 as an oncogene (Corda et al., 2017; Geradts et al., 2016; Liao et al., 2012). This PhD project investigated the hypothesis that CELSR1 and FZD6 have opposing roles in breast cancer. First, bioinformatics was used to determine the significance of CELSR1 and FZD6 in large scale breast cancer patient datasets. Secondly, several human breast cancer cell lines were characterised to determine an optimal *in vitro* model to study PCP in breast cancer. Lastly, the significance of the PCP receptor CELSR1 in breast cancer was determined by functional assays. One novel finding of this thesis was through bioinformatics analyses in Chapter 1 where it has been revealed that *CELSR1* mRNA expression is increased in less invasive luminal type breast cancer but decreased in invasive basal type breast cancer. In addition, it was shown, that increased expression of *CELSR1* is associated with better patient survival, and notably *CELSR1* enriches gene sets involved in protection against metastasis. In Chapter 2 characterisation of breast cancer cell lines as *in vitro* models are mostly consistent with the bioinformatics data. Further novel findings were that mRNA and protein expression analysis suggest that *CELSR1* mRNA and protein expression was increased in less invasive luminal type cell lines and decreased in more invasive basal-type cell lines, whereas the opposite effect was found for *FZD6*. ICC with CELSR1 antibodies also revealed a cortical staining pattern in most luminal type cell lines. Finally, knockdown of *CELSR1* changes the phenotype of normal-like MCF10A cells. We observed a decrease in cell-cell adhesion at low density and the expression of markers associated with EMT. Functional assays have also shown that overexpression of mouse *Celsr1* in highly aggressive basal like MDA-MB231 cell lines reduced cell proliferation and cell motility. We conclude that CELSR1 is a tumour suppressor and raise the hypothesis that CELSR1 attenuates EMT, as evidenced by our experimental data. The manner in which CELSR1 achieves this will be the subject of future work.

6.2 Assessment of available human breast cancer cell lines as appropriate *in vitro* models for studying the role of CELSR1 and FZD6 in breast cancer

A major aim of this project was to characterise breast cancer cell lines as possible *in vitro* models to study the biological function of PCP in breast cancer. qPCR and Western analysis (using CELSR1sc and FZD6 antibodies) of breast cancer cell lines was found to reflect bioinformatics analysis of large-scale patient datasets (i.e, CELSR1 is highly expressed in the T47D cell line consistent with high CELSR1 expression in Luminal A subtype breast cancer, whereas FZD6 is expressed more strongly in invasive basal types, consistent with patient data. Moreover, phenotypically, the common cell lines derived from patients exhibit characteristics equivalent to their molecular subtype (Luminal, Basal), such as growth rate, motility and shape (Nguyen et al., 2018). qPCR data is mean of three experiments each with 4 technical replicates for common cell lines but needs to be addressed in MCF10A for both *CELSR1* and *FZD6* to complete the study. Western blots for MCF10A series cell lines with CELSR1-sc also needs to be repeated to ensure robust data. FZD6 protein levels will be tested in the MCF10A series to complete this study. Given the robust data collected, it can be concluded, however that the common cell lines reflect patient samples and thus are appropriate *in vitro* models. The common cell lines are considered appropriate *in vitro* models, due to the similarity of their molecular signature to major clinical breast cancer subclasses as already reported (Dai et al., 2017) . Furthermore, as mentioned above, qPCR and western blots confirm *in silico* data from patient datasets, in that the common cell lines reflect a clinical scenario. This is further discussed in the discussion section. However, the common cell lines do have the limitation in that they come from different metastatic sites but not the primary tumour. On one hand this could mean that they are representative of a variety of sizes and types, however these cell lines have a completely different genetic makeup compared to the MCF10A series which have the same genetic background, i.e., are derived from the MCF10A parental line. Therefore, the common cell lines are not very representative of cancer progression as it would occur *in vivo* (Chapter 1 section 1.11 and Fig.8). Another limitation of these common cell lines is that they are all invasive since they are all derived from metastatic sites albeit with lower and higher invasiveness. The MCF10A progression series offers a useful alternative in this

respect because these cell lines have the same genetic background. There has been a plethora of studies in the past looking at and arguing which cell lines might or might not be ideal models of breast cancer, whether for studying biological function or novel drugs. Jiang et al. (2016) compared the molecular profiles of breast cancer cell lines to breast tumour patients and scored the cell lines based on how representative they were of actual patient tumours in a clinical setting (Jiang et al., 2016). These authors have shown the T47D cell line as one of the most similar to actual tumours (Jiang et al., 2016): we have used T47D as a model of Luminal A breast cancer. We can therefore conclude that this cell line was an appropriate choice for a model of Luminal A breast cancer which is supported by the qPCR, Western and ICC data using CELSR1-sc antibody. The BT474 cell lines are representative of a Luminal B subtype, reflecting what is usually observed in breast cancer patients, i.e., expression of Luminal B markers (Dai et al., 2017; Holliday & Speirs, 2011; K. Liu et al., 2019). Interestingly, recent studies using advanced sequencing and molecular profiling technologies have reported that MDA-MB231 cells, which have been categorised as basal-like based in previous publications (Dai et al., 2017; K. Liu et al., 2019), may not be basal like at all (K. Liu et al., 2019; Prat et al., 2010; Robinson et al., 2017). There have also been reports that some cell lines used to study metastatic cancer do not reflect the profile of real metastatic samples obtained from cancer patients when compared against the MET500 database (metastatic breast cancer patient database) (K. Liu et al., 2019; Robinson et al., 2017). Nevertheless, other studies have reported that these cell lines mostly have the biological features of invasive breast cancer, so are still regarded as good models and are widely used and reported in the literature (Dai et al., 2017; Nguyen et al., 2018). MDA-MB436 cell lines were also reported to have a similar molecular profile to actual tumours derived from breast cancer patients (Chavez et al., 2010; Stephens et al., 2009). Overall, the common cell lines chosen for this project appear to be appropriate models but choosing more cell lines to represent a wider spectrum of breast tumours would have improved the study. Cells such as MDA-MB438/458, which have been reported to be closer to real tumours in their molecular profile could be used in the future (Holliday & Speirs, 2011). Cell lines representing HER2+ only tumours such as SK-BR3 could have also been more widely

used and it would have been useful in hindsight to have studied more than one cell line representing Luminal A and Luminal B breast cancers.

As mentioned above the MCF10A progression series cell lines might be more useful *in vitro* models to study PCP proteins in breast cancer. This is because they come from a single parental cell line (MCF10A) and therefore have the same genetic makeup (Santner et al., 2001; Soule et al., 1990; B. Tang et al., 2003). However, the biggest advantage of using these cell lines over the common cell lines described above, is that they allow one to model and assess any desired changes from normal to atypical epithelium all the way to low and finally high-grade invasive breast cancer (Puleo & Polyak, 2021; Santner et al., 2001; Soule et al., 1990). This is where the common cell lines are lacking, owing to their site of origin as mentioned above (Holliday & Speirs, 2011). Another limitation of using cell lines derived from patients is the lack of a control cell line which is not tumorigenic. Finite lifespan cell lines or primary cancer cells are not always available or are costly to purchase (Holliday & Speirs, 2011). Additionally, all the common cell lines utilised here are already metastatic cell lines albeit with varying levels of invasiveness. While they are representative in terms of molecular subtypes (i.e., ER+ Luminal A to triple negative basal) they do not adequately represent benign breast cancer, such as DCIS. This has limited this study since our hypothesis about CELSR1 was deduced from published works which identified CELSR1 primarily in *in situ* carcinomas, not metastatic sites (Geradts et al., 2016; Liao et al., 2012). This does not discredit our study, but rather increases the sample spectrum giving greater depth and insight into different types of breast cancer (i.e., representing different metastatic sites as mentioned in section 1.11). Even so, it would be better to use cell lines for functional studies which represent *in situ* carcinomas as well as atypical epithelia. The MCF10A progression series might be more suitable *in vitro* models therefore (Puleo & Polyak, 2021; Santner et al., 2001; Soule et al., 1990). In this study, the experimental data obtained using the MCF10A series cell lines is consistent with the bioinformatics data. In the more aggressive Ca1 cell lines CELSR1 expression was downregulated or had disappeared (WB and ICC-CELSR1-sc Figs.21, 30 and 31). However, not all reports on this cell line series have been favourable (Y. Qu et al., 2015). One argument against is the expression of both luminal and basal markers in the parental MCF10A cells, which challenges their origin/type. Studies

suggest that MCF10As might be a basal type of cell line expressing luminal markers or a luminal cell line in the process of EMT (Y. Qu et al., 2015; Sarrió et al., 2008). Only MCF10A cells grown in 3D in Matrigel (e.g., Fig.38) expressed markers similar to the human mammary gland (Y. Qu et al., 2015). The study of Qu et al. (2015) concluded that tissue culture conditions affect the markers expressed by the MCF10A cells and their true identity is still unknown.

Nevertheless, the common cell lines remain valuable models as they are highly representative of the molecular subtypes of breast cancer used in clinical assessment, unlike the MCF10A series. Thus, we can conclude that the common and MCF10A series cell lines complement each other and as long as their individual limitations are taken into account when drawing conclusions from data generated. To conclude, one aim of this project, which was to characterise relevant breast cancer cell lines to act as potential *in vitro* models to study PCP in breast cancer has been accomplished but further experiments are needed to complete the study.

6.3 What is the role of CELSR1 in breast cancer?

PCP genes are generally switched off in adulthood and only reactivated during certain disease states. One example is the lung during Idiopathic Pulmonary Arterial Hypertension, where it has been shown that the WNT/PCP pathway plays a significant role (Laumanns et al., 2009). Another example is where *Vangl2* enhances the severity of nephrotoxic nephritis in mice (Papakrivopoulou et al., 2018). PCP proteins are also expressed in specific healthy tissues (Hadjantonakis et al., 1997; Ewald et al., 2012). In case of the breast, this includes during puberty, pregnancy, and involution (Ewald et al., 2012; Morales et al., 2012). It is well known that cell polarity, namely apico-basal polarity is lost in cancer and some of its components re-utilised by cancer cells in favour of cancer progression (Gandalovičová et al., 2016). PCP components have been reported to play significant roles in breast cancer including VANGL2 and FZD6 (Corda et al., 2017; Corda & Sala, 2017; Hatakeyama et al., 2014; Puvirajesinghe et al., 2016). FZD6 has already been well characterised as an oncogene in previous studies of breast cancer (Corda et al., 2017; Corda & Sala, 2017). CELSR1 has been studied in other

cancers, such as ovarian cancer and glioma, where it has also been suggested to function as an oncogene (G. Wang et al., 2020; Wei et al., 2021). In breast cancer however CELSR1 is predicted to be a tumour suppressor (Geradts et al., 2016; Liao et al., 2012; Terkelsen et al., 2021). One recent study has shown that CELSR1 is found at high concentration in extracellular vesicles within the interstitial fluid of Luminal type breast tumours compared to basal type tumours echoing with our study where CELSR1 is found upregulated in luminal type breast cancer compared to basal like (Terkelsen et al., 2021). FZD6 has been found to act as an oncogene in breast cancer as well as in other cancers (Corda & Sala, 2017). As this project moved forwards the focus at the functional level was on CELSR1 rather than FZD6 and this is reflected in the discussion section below.

6.3.1 Does CELSR1 play multiple roles in breast cancer progression?

6.3.1.1 CELSR1 is differentially expressed in Luminal vs Basal breast cancer cell lines

In silico analyses here (Chapter 1) have shown that indeed, CELSR1 seems to have a significant role in breast cancer. GEPIA2 and UALCAN data show that *CELSR1* mRNA expression is significantly higher in breast tumours compared to normal healthy tissue. The differences in significance between *CELSR1* and *FZD6* mRNA expression point to CELSR1 being more important than FZD6. A limiting factor here is that we did not have access to or a knowledge of a large-scale cohort which would involve non-invasive breast cancer data. Hence bioinformatics analysis from the TCGA data was only possible using invasive breast cancer data. Normal (healthy) breast tissue samples are included in these GEPIA2/UALCAN datasets (but not in datasets obtained from cBioPortal) as well as invasive cancers, although samples such as DCIS or other benign types were not specified unless individual analysis would have been carried out. Perhaps in the future a database or large-scale study including a greater spectrum of samples will become available allowing for more comprehensive cancer bioinformatics. Using the TCGA datasets which were made up of invasive luminal A, B and basal type breast cancers, copy number analyses partly agree with previously published data, showing that *CELSR1* copy number is lost in invasive breast cancer (Geradts et al., 2016; Liao et al., 2012). Although Geradts et al. (2012) and Liao et al. (2016) showed that *CELSR1* copy number is increased in pure (non-invasive) DCIS and

decreases in mixed (invasive) DCIS, they did not report on mRNA expression. Additionally, these studies have only looked at one specific – DCIS – type of breast cancer without further molecular classification (i.e., without specifying whether the samples were Luminal, basal etc.). These studies while providing a strong basis for this project, do not provide a greater insight into the biological function of CELSR1 in breast cancer. These aspects were aimed to be expanded upon in this project, by investigating CELSR1 expression *in vitro* using gene/protein expression analysis assays, ICC, spheroid, and functional assays.

CELSR1 is located on the long arm of chromosome 22 (*Chromosome 22: 46,360,834-46,537,620 - Region in Detail - Homo_sapiens - Ensembl Genome Browser 109*, n.d.). Parts of chromosome 22 are known to undergo copy number changes and recombination events such as deletions resulting in various disorders, one of which is DiGeorge syndrome (Bailey et al., 2002; McDonald-McGinn & Sullivan, 2011; Yu et al., 2012). *CELSR1* copy number changes were reported to be significantly different in non-invasive compared to invasive DCIS type breast cancer in the key study which first suggested *CELSR1* CNVs in various types of DCIS (Liao et al., 2012). The study of Liao et. al. does not specify the molecular subtypes of the DCIS cases, so it is not possible to directly compare our bioinformatics and *in vitro* data with these studies, except invasiveness. Studies have shown that copy number changes (CNV) on chromosome 22 contribute to oncogenic transformation of other cancers, such as ovarian cancer (Benetkiewicz et al., 2005). Using the TCGA datasets, copy number vs mRNA expression data for *CELSR1* and *FZD6* support the hypothesis that these two receptors play opposing roles in breast cancer. Interestingly though when *CELSR1* copy number is gained, mRNA expression does not increase, rather a decrease in expression can be seen (Fig. 12B). This is uncommon but not unheard of, as this phenomenon has been previously observed with other genes both in tumours and cancer cell lines, through analysing large-scale patient and cell line databases, such as CCLE and TCGA (Gamazon & Stranger, 2015; Shao et al., 2019). However, it must be noted that the GAIN of copy number sample set is highly variable in relation to mRNA expression with a wide standard deviation. Similarly, DIPLOID and partial (SHAL DEL) deletions exhibit a wide standard deviation (SD). Therefore, one cannot be sure whether in all these cases CNVs are directly linked to mRNA expression. More

detailed analysis of individual cases would need to be conducted in order to answer this question. On the whole, CNVs tend to be linked to large chromosomal regions rather than individual gene loci and hence it has been suggested that CNVs might not be reflected at the mRNA expression level for any specific gene in a deleted/amplified chromosomal region (Perry, 2009). CNVs might also result in loss of certain transcription factor binding domains i.e., promoter/enhancer regions upstream of the *CELSR1* locus and hence no or lower levels of *CELSR1* mRNA is produced (Perry, 2009). On the other hand, *FZD6* CNVs seem to better reflect mRNA expression levels and there is less variability for SHAL DEL and DIPLOID groups although SD is broad as for *CELSR1* in the GAIN of copy number cohort. These data suggest that gene amplifications lead to more variability in mRNA levels. To improve the analysis, it might be useful in the future to repeat them on individual subtypes (Luminal A/B, Her2+ and Basal), to provide greater insight particularly because Fig.12D shows that the Luminal A subtype is overrepresented in the TCGA dataset.

Survival analyses via KM plotter also supports the hypothesis that *CELSR1* might be a tumour suppressor in breast cancer. The results generated by KM plotter show that different expression levels of *CELSR1/FZD6* have a significantly positive or a negative effect on survival, respectively (Fig. 12C). Survival data for *FZD6* has been published previously (Corda et al., 2017; Corda & Sala, 2017) and is consistent with our data. *CELSR1* survival analysis has, to the best of our knowledge, not been published before. This piece of data is key since it provides direct clinical evidence that higher expression of *CELSR1* is linked to a better prognosis for breast cancer patients. Additionally, this data is more representative as KM plotter pulls raw data from other large-scale datasets than only TCGA as in previous analyses (Lánczky & Győrffy, 2021). It should be noted that (N) is greatest up to 150 months, so any correlations after this time should be interpreted with caution as (N) is very low and data may constitute outliers.

The analysis next focused on *CELSR1/FZD6* mRNA expression levels and their effect on patient survival in individual subtypes of breast cancer (Luminal to Basal – Fig. 13). Fig. 13A shows that high *CELSR1* mRNA expression was more strongly associated with better patient survival in luminal A sub-

types and that expression level versus better patient survival differed between breast cancer subtypes i.e., in HER2+ and Basal subtypes. Conversely, *FZD6* expression level was consistent across the different sub-types and significantly different for basal type breast cancer, which is consistent with *FZD6* acting as an oncogene as reported by Corda et.al (2017). As mentioned, *CELSR1* expression assessed in this study by qPCR (Fig.23), while significantly different in all subtypes, is highest in Luminal subtypes. Expression then rapidly drops in HER2+ and Basal subtypes. As mentioned earlier, Geradts et. al. (2012) and Liao et.al. (2016) only look at DCIS without further classification, however they did report that *CELSR1* copy number is gained in non-invasive DCIS and lost in invasive DCIS. Our data is therefore consistent with their report in that less aggressive breast cancer shows *CELSR1* copy number gains compared to more aggressive breast cancer. Survival analyses across different subtypes of breast cancer has revealed lower association of *CELSR1* in progression to more aggressive subtypes (Fig.13C). The increasing P values from the bioinformatics analyses demonstrate that *CELSR1* does not have a significant effect on patient survival in the Luminal B, HER2+ and Basal subtypes of breast cancer. Notably, the greatest association for better patient survival is now with low *CELSR1* expression. This apparent 'switch' needs to be investigated in more detail using new patient samples of equal (N) but it is tempting to speculate that the role of *CELSR1* changes from luminal A to luminal B sub-types. A couple of studies have reported *CELSR1* acts as an oncogene in Glioma and Ovarian cancer (G. Wang et al., 2020; Wei et al., 2021). Wang et. al. (2020) has shown that *CELSR1* is overexpressed in Glioma and acts as an oncogene by interacting with certain miRNAs. It might be possible that while in less invasive breast cancer *CELSR1* has a protective effect, in more invasive subtypes it has an opposite effect. However, the idea of *CELSR1* being a 'double agent' is a novel one in breast cancer and would be the subject of a new and future study. In conclusion the loss of *CELSR1* as observed via *CELSR1*-sc staining is consistent with the hypothesis that *CELSR1* expression negatively impacts invasive potential of breast cancer cells.

6.3.2 CELSR1 antibody staining of fixed cells shows inconsistencies between antibodies but for CELSR1-sc the immunocytochemistry data reflects the Western blot data

ICC with CELSR1-iso antibody revealed interesting and unexpected staining patterns in breast cancer cell lines. While CELSR1sc (commercial antibody) staining revealed an expected cortical staining pattern co-localising with actin in healthy MCF10A breast cancer cell lines, the isoform specific antibody (CELSR1iso) revealed unusual bridge like structures connecting between cells but also exhibited a wrapping effect around the nucleus (Fig.26). However, CELSR1iso antibody staining using ICC is potentially non-specific as suggested by *CELSR1* KD in MCF10A cells, therefore it is highly likely that the CELSR1iso antibody does not label CELSR1 protein in fixed cultured cells. In the future new antibodies will have to be made to more specifically assess the distribution of CELSR1-PDZ in breast cancer cell lines and tissues.

In Luminal type breast cancer cell lines CELSR1-sc staining exhibits a cortical staining pattern, while in basal like breast cancer cell lines CELSR1-sc seems to be inside the cell as unidentified puncta (Fig.27, n= 3 independent staining experiments). Similarly, in the MCF10A progression series CELSR1sc antibody staining reveals cortical enrichment in the least invasive cell lines (Neo-T to DCIS.COM) but became less intense and was eventually lost in the invasive Ca1 cell lines. Agreeing with western blot data, ICC in both common cell lines and MCF10A series shows that CELSR1 is progressively lost in invasive breast cancer. This data suggests that while in normal MCF10A and luminal/pre-cancerous cell lines CELSR1 retains its location at the plasma membrane where it can function normally in basal like cell lines CELSR1 is either lost from the plasma membrane or protein expression is too low to be visualised by our fluorescent microscope. We conclude therefore that CELSR1 function is suppressed in basal like/highly metastatic breast cancer cell lines. This is a novel finding, as to the best of our knowledge, has not been published before.

6.3.3 CELSR1-iso staining overlaps with the EMT marker, vimentin

shRNA KD of CELSR1 in MCF10A cells suggests that CELSR1-iso antibody is not specific for CELSR1 epitopes in fixed cultured cells (Fig.39). It was interesting however that the filamentous

pattern of CELSR1iso antibody staining structures co-localised with vimentin antibody staining (Fig.41). In invasive MDA-MB-231 cells CELSR1iso antibody-stained filamentous structures but also large puncta which also co-stained with vimentin (Fig.28). It is also interesting that in the MCF10A series, CELSR1-iso staining became highly filamentous in the most invasive cell types (Fig.31). Again, co-localising with vimentin but exhibiting a broader filamentous pattern. The Ca1.D staining pattern for example suggests that the CELSR1-iso antibody does not cross-react to vimentin but it is possible that it is recognising a vimentin binding protein.

Vimentin is a type III intermediate filament, which has been of growing interest because of its involvement in metastatic processes (Z. Chen et al., 2021). Vimentin is also of interest as it is associated with epithelial-mesenchymal transition (EMT). EMT is a normal physiological process in embryonic development by which cells attain migratory abilities and become more plastic, however cancer cells use this process to drive metastasis (Z. Chen et al., 2021). Therefore, vimentin is an important marker of invasive type cancers (C.-Y. Liu et al., 2015). Research has shown that vimentin is upregulated in the most invasive, basal TN breast cancer (81.2%) compared to Luminal A breast cancer (29.1%) (T. Qu et al., 2019). Studies have also shown that increased expression of vimentin is linked to poor prognosis and that vimentin is most highly expressed in TN breast cancer than non-TN breast cancer (Javir et al., 2020; Su et al., 2018). A larger scale study on patient samples (n~650) has shown that vimentin was found in >90% TNBC samples and radically lowered relapse free survival in breast cancer patients (Winter et al., 2021). A study looking at how vimentin regulates integrin-ligand interactions could hold possible answers to the identity of the filamentous structures revealed by CELSR1iso antibody staining observed in breast cancer cell lines (J. Kim et al., 2016). The study of Kim et. al. (2016) raised the hypothesis that H-Ras signalling could cause vimentin to translocate from the plasma membrane to the nucleus resulting in very similar nuclear 'enwrapment' as we see in this study of CELSR1iso antibody staining in fixed cells (Figs.26-31) (J. Kim et al., 2016). Thus, it would be of interest in the future to understand what protein epitope(s) CELSR1-iso antibody binds to in fixed cultured cells.

Immunostaining of basal-like MDA-MB231 cells reveals that CELSR1-iso antibody recognises a protein that is localised in punctate structures inside these invasive cells, which are also marked with vimentin (Fig.28). We tried using markers for various vesicles to discern the identity of these punctate structures but without success. We used a LAMP1 antibody for lysosomes, a CD63 antibody as a marker for exosomes, an EEA1 antibody as an early endosome marker and a cytokeratin antibody as an additional intermediate filament marker. However, none of these markers were informative. The possible identity of this unidentified vesicle was only deciphered further through an undergraduate project student (UH). Suspecting the puncta were part of the Golgi, MDA-MB231 cells were treated with Vinblastine (a chemotherapeutic drug that disrupts the Golgi) and the puncta became blown out, like a corn kernel changing into popcorn (Appendix, Fig.1) (Ismaeel & Formstone, personal communication 2023). Publications in the past have shown that certain intracellular signalling molecules can bind to vimentin and interact with components of the Golgi at the same time (Bloom & Brashear, 1989; Y. S. Gao et al., 2002; Y.-S. Gao & Sztul, 2001). These publications show that not only does vimentin have the capacity to bind other proteins/signalling molecules but also affect the regulation of the cytoskeleton in response to such binding. Stunningly, it has also been shown that Scribble, a principal component of apico-basal polarity, can also bind vimentin (Phua et al., 2009). What is more interesting though, is that the study has shown that only PDZ domain-containing scribble binds vimentin (Phua et al., 2009). Vimentin is not known to contain specific domains for PDZ binding; however, the study has suggested that perhaps vimentin may contain a special loop structure to facilitate such binding (Phua et al., 2009). Nevertheless, these studies show that vimentin has an inclination to bind proteins containing a PDZ domain. One possibility therefore is that CELSR1-iso antibody cross-reacts with SCRIBBLE. This can be tested in the future using SCRIB KD cancer cells ((Milgrom-Hoffman & Humbert, 2018).

In sub section 6.2.1 CELSR1iso antibody staining in fixed cells was discussed. During this part of the study, we saw that in MCF10A series vimentin expression also intensifies with increasing invasiveness, i.e., in MCF10A normal-like cell lines vimentin expression is null whereas it becomes present in the more aggressive cell lines (Fig.31). This is an indication of EMT in these cell lines, as

vimentin is a marker for EMT (C.-Y. Liu et al., 2015; Winter et al., 2021). One study has found that when NUMB, a negative regulator of EMT in TN breast cancer, is knocked down this causes an increase in vimentin expression indicating EMT and an invasive phenotype in MCF10A cells (Zhang et al., 2016). NUMB links to the Notch signalling pathway which has parallels with CELSR1 function in embryonic development and in PCP in terms of asymmetric localisation, cell organisation and fate determination in *Drosophila* sensory organs (Barad et al., 2011; Rawls & Wolff, 2003; Upadhyay et al., 2013). Like PCP, Numb is also involved in asymmetric cell division in various cell types in both *Drosophila* and vertebrates (Katanaev et al., 2018; Knoblich et al., 1995; Llimargas & Lawrence, 2001; Shen et al., 2002) This has been nicely shown in the development of the *Drosophila* eye, where Numb is expressed in R3/R4 photoreceptors during PCP establishment (Katanaev et al., 2018). This study has also shown that disruption of Numb during this process causes PCP defects, additionally when Numb was knocked-down, 20% ommatidia displayed PCP defects (Katanaev et al., 2018). These findings shown that Numb/Notch work together with PCP and are both required for correct asymmetric cell division. We did not investigate vimentin expression in common cell lines nor in knockdown cell lines, although that CELSR1-iso staining labels more CELSR1 KD MCF10A cells compared to WT is a strong indication that expression of vimentin will follow the same pattern in KO cell lines. The association of CELSR1iso staining with vimentin together with the increased proportion of CELSR1iso ICC in MCF10 shCad3 cell lines raises the hypothesis therefore that CELSR1 knockdown in MCF10A epithelial cells give rise to EMT. Future work will seek to test this hypothesis.

6.3.4 – Does the CELSR1 PDZ isoform play an important role in breast cancer?

Western blot analyses with CELSR1-iso antibody did consistently show the same 400KDa band which was absent in CELSR1-shRNA KD cells (Fig.39) supporting its specificity.

Western blot data has revealed differences in the expression profiles of CELSR1 using the CELSR1iso antibody compared to the CEL:SR1sc antibody. This suggests that CELSR1 (PDZ) could be a potential biomarker for DCIS sub-types. This is important because as already mentioned there is no specific treatment for various types of DCIS, since there is a lack of biomarkers to distinguish between

invasive and non-invasive DCIS. Distinguishing between DCIS that will be invasive from benign types is important. RT-PCR and Sanger sequencing of the CELSR1 C-terminal splicing in control and breast cancer cell lines has raised the hypothesis that CELSR1-PDZ itself exists as multiple variants.

Importantly, our RT-PCR analysis of the CELSR1 C-terminal cytoplasmic tail region revealed a duplication of the PDZ sequence in the 3'UTR of CELSR1 (Fig.23). This duplication has not been highlighted in the literature so far. This data might hold some answers to the dual allele hypothesis since more duplications and rearrangements might be going on upstream in the 3'UTR. It has already been mentioned that chromosome 22q where CELSR1 locus is located is prone to recombination events. The duplication of CELSR1 specifically around the alternative spliced region however is highly interesting. BLAST searches of gene databases revealed that this duplication emerged during the evolution of the Great Apes. Our primers did not reach more upstream so more in-depth analysis of the CELSR1 sequence will be carried out in the future using the RACE method to analyse further stretches of sequence. This duplication took on greater significance with our discovery, through Sanger sequencing of C-terminal tail RT-PCR products, of a novel alternatively spliced PDZ variant of CELSR1, which we have termed CELSR1 PDZ+ (plus). This is a version of the PDZ variant with the characteristic C-terminal GSNETSI amino acid sequence albeit with additional upstream nucleotides of unknown origin as shown in red in Appendix, Fig.2. Initially we thought this variant is cancer specific but upon conducting Sanger sequencing with human foetal spinal cord cDNA we discovered the same variant, suggesting it is found in other tissues as well. BLAST searches failed to locate this variant in any genomic or mRNA expression database. The puzzle was to understand where the novel nucleotides came from. Searches of the intron between the penultimate exon and the C-terminal alternatively spliced exons failed to identify additional alternatively spliced coding regions for the novel GRCGTSVSPQ amino acid domain. It was finally understood that the novel sequence could be derived if nucleotide changes were made within the most 5' PDZ sequence, including mutation of the TGA stop. Loss of the TGA codon would result in a read through of coding sequence into the second PDZ motif as illustrated in Fig.23. The next outstanding question is the origin of this novel mRNA as well as its function and significance in both development and cancer. To understand this better

genomic DNA will be amplified using rapid amplification of cDNA ends (RACE) to identify the gene locus and an extended mRNA. This will enable us to do generate FISH probes for chromosomal location and understand if other changes in coding sequence compared to CELSR1 sequence on NCBI.

We have discovered an evolutionarily conserved PDZ variant of *CELSR1* as well as another previously unknown PDZ+ variant. This raises further questions, especially when it comes to antibody specificity (for example of the CELSR1iso antibody which has been raised against the PDZ domain of CELSR1). Better knowledge of the *CELSR1* sequence will enable us to make more specific antibodies, qPCR probes and shRNAs to investigate the significance and biological function of individual variants in breast cancer. Next steps would involve sequencing breast cancer patient samples to assess these PDZ variant as well as conducting gain-of-function assays with variant-specific constructs.

6.3.5 Functional studies support a role for CELSR1 as a tumour suppressor

In order to begin to assess the function of CELSR1 in breast cancer and to discern its tumour suppressive functions, we performed both gain-of-function and loss-of-function experiments,

To test the hypothesis that loss of CELSR1 (as demonstrated by CELSR1-sc staining) in more invasive cell lines contributes to their invasive potential we added back Celsr1 protein by transfection of a mouse *Celsr1*, tagged with GFP, into highly aggressive basal like TN MDA-MB231 breast cancer cell lines. Western blots confirmed the successful stable transfection of *Celsr1* (a GFP antibody highlighted multiple bands in Westerns compared to control cells; Fig.46, n=3 independent Westerns). We expected Celsr1 to localise at cell-cell contacts as a result of its homophilic recognition at the cell surface, instead Celsr1 showed intracellular punctate staining in MDA-MB231 cells, suggesting that it predominantly localised to intracellular vesicles. However, light microscopy of cultured mCelsr1-expressing MDA-MB231 cells revealed an intriguing local clustering of cells, often along their long axis, compared to the control as seen in Fig.45, in n=3 independent clones. This phenotype requires further investigation to understand whether low levels of mCelsr1 protein are present at the cell membrane to drive cell-cell organisation or if internal mCelsr1 signalling alters cell-cell adhesion or cell-matrix adhesion more generally. Migration assays using each of the three independent stably expressing

clones with three technical replicates also revealed that mCelsr1-MDA-MB231 breast cancer cell lines migrated slower compared to pcDNA3 empty vector controls. The MTT assay, which measures cell proliferation further showed significantly lower cell proliferation in MDA-MB231-mCelsr1 expressing cells compared to controls, again for each of the three independent clones and using 5 technical replicates for each clone. These assays are consistent with CELSR1 acting as a tumour suppressor in aggressive breast cancer, however there are a few limitations with these experiments. Firstly, the MTT assay is an indirect measurement of cell proliferation as it quantifies metabolic activity, additionally there are concerns about the toxicity of the assay reagents and non-specific factors included in the reduction of the MTT reagent. In the future more specific methods of assaying cell proliferation should be used. For example, this might be the ATP assay which is a marker of viable cells and is considered superior to the MTT assay in specificity and ease of use. The Ki-67 proliferation assay is another example of a more specific assay since Ki-67 is directly associated with proliferation and is expressed through the cell cycle. Another limitation is the use of a mouse *Celsr1* construct instead of a human construct. Mouse *Celsr1* is very similar to human *CELSR1* and because of this many studies on PCP cited in this work have used mice as model organisms. However, mCelsr1 protein is processed differently to human in that it exists as p85 and p400. In the future transfection of a human *CELSR1* construct would be more ideal. Another limitation of these experiments was the use of only one type of invasive cell line. Additional experiments with MDA-MB436 cells and MCF10A series Ca1A, D,H cells would be useful in the future. Altogether, the gain-of-function data support a role for CELSR1 as a tumour suppressor, but further experiments are needed to extend the study and provide mechanistic data.

To further investigate the role of CELSR1 to identify shRNA tools to knockdown CELSR1 and to investigate the potential as a tumour suppressor we conducted loss-of function assays in MCF10A cells as well as luminal B type BT474 cells. We successfully stably knocked down CELSR1 as evidenced by loss of CELSR1-sc antibody staining in western blots, but only for one of two shRNAs employed, the Cad3-specific shRNA. *CELSR1* shRNA-expressing MCF10A cells displayed reduced cell-cell contacts at low density. This suggests a link between CELSR1 and the formation of early stable cell-cell adhesions.

ShRNA-MCF10A cells looked more spindle shaped than WT cells at low density, which is usually more typical of invasive cells. The cells also seemed to grow slower compared to their WT counterparts (personal observation), suggesting that cell motility might not have been affected but this would have to be assessed in the future using scratch assays. It is also relevant here to reiterate that CELSR1-iso antibody staining which co-localised with vimentin, increased when CELSR1 was lost in MCF10A cells further indicating a more mesenchymal phenotype in these cells. Why we observed small numbers of vimentin expressing WT MCF10A cells is unclear. Future work will identify further CELSR1-specific shRNAs and generation of a control shRNA MCF10A cell line to complete 2D functional assays in MCF10A cells, as were performed for CELSR1 gain-of-function. MCF10A cells undergoing shRNA knockdown will also be characterised more fully with markers for luminal as well as myoepithelial cells so better understand the impact of loss of CELSR1. Unfortunately, CELSR1 knockdown was unsuccessful in the Luminal B-type BT474 cell line which expresses high levels of CELSR1-PDZ protein. Ideally in future we will need to knockdown CELSR1 in Luminal A ER+ (T47D) type as well as MCF10A series NeoT, both express high levels of CELSR1 protein. However, it will also be interesting to knockdown CELSR1 in HER2+ cells and particularly we would want to specifically knockdown CELSR1-PDZ isoform which is strongly expressed in DCIS types. Knockdown of CELSR1 in ER+ and HER2+ DCIS types would also be more clinically relevant, since *in silico* data has shown that CELSR1 expression is highly expressed in Luminal A/B breast cancer. Therefore, knockdown of CELSR1 in these cell lines will produce more robust and clinically relevant data, which would enable us to link CELSR1 function to a specific molecular profile of breast cancer which exemplifies the patient state. Such cell lines might be T47D cells and SK-BR3+, which are Luminal A and HER2+, respectively.

6.3.6 3D functional assays

Multiple 3D assays were trialled in order to identify a suitable 3D model with which to test both gain- and loss-of function of CELSR1 in breast cancer cell lines in an environment that would mimic a more *in vivo* situation (Jensen & Teng, 2020). 2D surfaces such as cell culture flasks and plates are not natural environments for cells to grow, which forces them to adapt to such an environment

by changing their morphology and sometimes gene expression (Jensen & Teng, 2020). Hence, 3D assays especially in cancer research are being widely used and developed in order to create more sophisticated methods for cancer modelling. It was reported that 3D mammospheres also can be representative of inter and intra-tumour heterogeneity as is observed in real breast tumours (Smart et al., 2013). This means that 3D spheroids are a promising, relatively inexpensive alternative to *in vivo* research albeit without the ability to study organ-specific metastasis. We trialled a several published methods of 3D spheroid assays and assessed their utility. for ICC and fluorescent microscopy. The favoured methods were the alginate bead method as well as the Matrigel on-top culture. We used Luminal A and B type breast cancer cell lines but also basal like MDA-MB231 cells, however the spheroids were lost during handling and ICC processing of the latter, due to their weak and unstable cell-cell adhesions , as has been reported elsewhere (Smart et al., 2013). Hence no processing for ICC was achievable with basal type cell lines. (Smart et al., 2013)We also encounter issues with obtaining high quality images. This is because we did not have access to a confocal microscope, only a widefield Apotome fluorescent microscope. Thus, for future functional assays a confocal microscope will need to be used for fluorescent imaging of 3D spheroids made from *Celstr1/CELSR1* gain-of function and loss-of function cells. These assays are important as *CELSR1* acts in 3D in tissue organisation. To decipher its role as a tumour suppressor we will need to investigate the mechanisms in 3D.

6.3.7 Enrichment analysis suggest oncogenic/metastatic and tumour protective pathways downstream of FZD6 and CELSR1 receptor signalling respectively

Gene enrichment analyses conducted *in silico* suggested potential signalling roles for *CELSR1* and *FZD6* in breast cancer. *In silico* analyses showed that *CELSR1* positively enriches gene sets which might be linked to protection against breast cancer metastasis, and negatively enriched gene sets which might be linked to breast cancer invasiveness, consistent with the experimental data and patient database analyses reported in this thesis. However, one caveat of this work was that the patient samples the enrichment data was derived from were not from specific breast cancer sub-types but the broad spectrum of invasive breast cancers derived from different sub-types.

Positively enriched gene sets involved in protective pathways included the early estrogen response gene set. Estrogen response especially early is associated with better prognosis of Luminal type breast cancers (Oshi et al., 2020; Takeshita et al., 2022). and a better prognosis and therefore survival of breast cancer patients with ER+/HER2- breast cancer i.e. Luminal A types (Oshi et al., 2020), where we find CELSR1 is highly expressed (by qPCR and CELSR1-sc Westerns). Gene sets involved in mitotic spindle regulation were also upregulated and as mentioned before are of interest as CELSR1 plays a role in mitotic spindle orientation (Oozer et al., 2017). Dysfunction in mitotic spindle orientation can promote tissue multi-layering and thus CELSR1 may protect against this by ensuring mitotic spindle alignment maintains tissue organisation. Deregulation of mitotic spindle orientation is well characterised in breast cancer oncogenesis and progression (Gulluni et al., 2017). However, it is also possible that increased CELSR1 expression might derail the mitotic spindle and promote cell multi-layering. Interestingly MYC targets and oxidative phosphorylation were enriched as well, however these pathways are known to contribute to metastasis rather than protect against it (Evans et al., 2021; Fallah et al., 2017; J. Xu et al., 2010). As mentioned earlier some publications reported that CELSR1 acts as an oncogene in some cancers and our own bioinformatics analysis suggested a potential 'switch' in function from 'protector' to 'enabler' in benign subtypes of breast cancer with more invasive potential. Thus, investigation of 'if' and 'how' CELSR1 utilises these pathways in breast cancer will be important in the future.

Negatively enriched pathways included gene sets linked to oncogenesis and metastasis. Of main interest were gene sets involved in EMT and angiogenesis. These two processes are well characterised hallmarks of cancer and key to the process of metastasis (Hanahan & Weinberg, 2000, 2011). Negative enrichment might suggest that CELSR1 negatively impacts EMT which is consistent with experimental data. A role for CELSR1 in the branching of tubular structures suggests that CELSR1 should also impact blood vessel branching (Zhan et al., 2016). A role for CELSR1 in EMT can be tested using gain and loss of function but whether CELSR1 impacts angiogenesis to hinder or promote breast cancer progression will need 3D co-culture experiments of breast cancer cells and blood vessels.

Overall, the negative enrichment data suggests that CELSR1 might have tumour suppressive effects by negatively regulating pro-metastatic signalling.

Gene set enrichment analysis with *FZD6* has shown the positive enrichment of gene sets related to oncogenic and metastatic pathways. This data is in line with previously published work which has shown that *FZD6* is an oncogene (Corda et al., 2017; Corda & Sala, 2017). Negatively enriched gene sets in the *FZD6* breast cancer dataset did not involve many signalling pathways directly related to regulating the tumour microenvironment. This means that *FZD6* might not inhibit protective pathways (including *CELSR1*) but only promotes those pathways that are involved in oncogenesis and metastasis, as reported. Conversely, *CELSR1* both inhibits pro-metastatic pathways and at the same time is involved in positive enrichment of protective signalling pathways. These enrichment data provides a basis for future investigations into the signalling activity of *CELSR1* in breast cancer.

6.3.8 Investigation of *CELSR1* expression experimentally in patient samples

This thesis reports experimental data that is based on breast cancer cells *in vitro* and provides evidence that *CELSR1* and *FZD6* play opposing roles in breast cancer, with *CELSR1* acting in this case to limit progression onto invasiveness. The next step is to investigate *CELSR1* in patient samples. Our study highlights the need to assess specific sub-types of breast cancer in isolation both in patient databases and experimentally. Patient samples of different types need to be investigated and RNA and protein expression of *CELSR1* and *FZD6* tested in the same samples, as we have reported here *in vitro*. RT-PCR analysis will also be necessary on an initially limited patient sample set to establish the importance of C-terminal slicing variants in *CELSR1* cancer biology. These experiments will provide us with a direct clinical insight into how *CELSR1* is expressed in real tumours. Going forwards should patient samples prove successful, possibly patient specific breast cancer organoids could be useful to fully understand how *CELSR1* protects against cancer progression.

As previously mentioned, we will also need to generate new antibodies for the CELSR1 PDZ variants and design variant specific TaqMan probes for qPCR to understand if C-terminal spliced products play a specific and important role in CELSR1 function in breast cancer. This is exciting as Western blots suggest that CELSR1-PDZ might be an important biomarker to distinguish less invasive luminal DCIS type breast cancers from more invasive types. We will also aim to conduct more robust analysis on the MCF10A series, including qPCR, as well as incorporate other cell lines for more representative data. Additionally, we will also aim to perfect the 3D spheroid system and set-up organoids in our lab. This will enable us to do more robust cancer modelling and as well as being a more accurate method to study PCP in breast cancer.

6.4 Conclusion

This study supports the hypothesis that CELSR1 has a significant role in human breast cancer. We have shown that CELSR1 is overexpressed in breast cancer patients with Luminal A breast cancer but is repressed in more invasive breast cancer whereas, in the same patient samples, the opposite is the case for FZD6. These patient analyses were reinforced by *in vitro* studies using two different sets of model breast cancer cell lines. Notably, CELSR1 is lost from the plasma membrane in more invasive breast cancer cell lines *in vitro*. We have also provided data to suggest that CELSR1 can act as a tumour suppressor *in vitro* i.e. Celsr1 over-expression attenuated the invasive characteristics of basal like invasive breast cancer cell lines whereas loss-of-function of CELSR1 in normal breast epithelial cells led to reduced cell-cell connections at low density and increased levels of a marker associated with vimentin and thus EMT. We believe we have identified a novel CELSR1-PDZ variant in humans, of unknown origin and function, which will be necessary to investigate more fully in the future in both breast cancer and in foetal development. In conclusion, this thesis concludes that CELSR1 acts as a tumour suppressor in breast cancer but may also play distinct roles and possibly opposing roles during specific stages of breast cancer progression. Further studies are needed to better understand its biological function in breast cancer and beyond.

References

- Agarwala, R., Barrett, T., Beck, J., Benson, D. A., Bollin, C., Bolton, E., Bourexis, D., Brister, J. R., Bryant, S. H., Canese, K., Cavanaugh, M., Charowhas, C., Clark, K., Dondoshansky, I., Feolo, M., Fitzpatrick, L., Funk, K., Geer, L. Y., Gorelenkov, V., ... Zbicz, K. (2018). Database resources of the National Center for Biotechnology Information. *Nucleic Acids Research*.
<https://doi.org/10.1093/nar/gkx1095>
- Aggarwal, V., Tuli, H. S., Varol, A., Thakral, F., Yerer, M. B., Sak, K., Varol, M., Jain, A., Khan, M. A., & Sethi, G. (2019). Role of Reactive Oxygen Species in Cancer Progression: Molecular Mechanisms and Recent Advancements. *Biomolecules*, *9*(11), 735. <https://doi.org/10.3390/BIOM9110735>
- Aigner, K., Dampier, B., Descovich, L., Mikula, M., Sultan, A., Schreiber, M., Mikulits, W., Brabletz, T., Strand, D., Obrist, P., Sommergruber, W., Schweifer, N., Wernitznig, A., Beug, H., Foisner, R., & Eger, A. (2007). The transcription factor ZEB1 (deltaEF1) promotes tumour cell dedifferentiation by repressing master regulators of epithelial polarity. *Oncogene*, *26*(49), 6979–6988. <https://doi.org/10.1038/SJ.ONC.1210508>
- Allinen, M., Beroukhim, R., Cai, L., Brennan, C., Lahti-Domenici, J., Huang, H., Porter, D., Hu, M., Chin, L., Richardson, A., Schnitt, S., Sellers, W. R., & Polyak, K. (2004). Molecular characterization of the tumor microenvironment in breast cancer. *Cancer Cell*, *6*(1), 17–32.
<https://doi.org/10.1016/j.ccr.2004.06.010>
- Alluri, P., & Newman, L. A. (2014). Basal-like and Triple Negative Breast Cancers: Searching For Positives Among Many Negatives. *Surgical Oncology Clinics of North America*, *23*(3), 567.
<https://doi.org/10.1016/J.SOC.2014.03.003>
- Alrefaei, A. F. (2021). Frizzled receptors (FZD) play multiple cellular roles in development, in diseases, and as potential therapeutic targets. *Journal of King Saud University - Science*, *33*(8), 101613.
<https://doi.org/10.1016/J.JKSUS.2021.101613>
- Andre, P., Song, H., Kim, W., Kispert, A., & Yang, Y. (2015). Wnt5a and Wnt11 regulate mammalian anterior-posterior axis elongation. *Development (Cambridge)*, *142*(8), 1516–1527.
<https://doi.org/10.1242/DEV.119065/-/DC1>
- Andrew, D. J., & Ewald, A. J. (2010). Morphogenesis of epithelial tubes: Insights into tube formation, elongation, and elaboration. *Developmental Biology*, *341*(1), 34–55.
<https://doi.org/10.1016/J.YDBIO.2009.09.024>
- Anti-Fade Mounting Medium - Jackson ImmunoResearch*. (n.d.). Retrieved 3 March 2023, from
<https://www.jacksonimmuno.com/technical/products/protocols/anti-fade>
- Aw, W. Y., & Devenport, D. (2017). Planar cell polarity: global inputs establishing cellular asymmetry. *Current Opinion in Cell Biology*, *44*, 110–116. <https://doi.org/10.1016/J.CEB.2016.08.002>
- Axelrod, J. D. (2020). Planar cell polarity signaling in the development of left–right asymmetry. *Current Opinion in Cell Biology*, *62*, 61–69. <https://doi.org/10.1016/J.CEB.2019.09.002>
- Bailey, J. A., Yavor, A. M., Viggiano, L., Misceo, D., Horvath, J. E., Archidiacono, N., Schwartz, S., Rocchi, M., & Eichler, E. E. (2002). Human-specific duplication and mosaic transcripts: the recent paralogous structure of chromosome 22. *American Journal of Human Genetics*, *70*(1), 83–100. <https://doi.org/10.1086/338458>

- Balogh, G. A., Heulings, R., Mailo, D. A., Russo, P. A., Sheriff, F., Russo, I. H., Moral, R., & Russo, J. (2006). Genomic signature induced by pregnancy in the human breast. *International Journal of Oncology*, 28(2), 399–410. <https://doi.org/10.3892/IJO.28.2.399/HTML>
- Barad, O., Hornstein, E., & Barkai, N. (2011). Robust selection of sensory organ precursors by the Notch-Delta pathway. *Current Opinion in Cell Biology*, 23(6), 663–667. <https://doi.org/10.1016/J.CEB.2011.09.005>
- Barberà, M. J., Puig, I., Domínguez, D., Julien-Grille, S., Guaita-Esteruelas, S., Peiró, S., Baulida, J., Francí, C., Dedhar, S., Larue, L., & García De Herreros, A. (2004). Regulation of Snail transcription during epithelial to mesenchymal transition of tumor cells. *Oncogene*, 23(44), 7345–7354. <https://doi.org/10.1038/SJ.ONC.1207990>
- Barnes, C. J., & Kumar, R. (2004). Biology of the epidermal growth factor receptor family. *Cancer Treatment and Research*, 119, 1–13. https://doi.org/10.1007/1-4020-7847-1_1
- Barrow, J. (2011). Wnt/planar cell polarity signaling: an important mechanism to coordinate growth and patterning in the limb. *Organogenesis*, 7(4), 260–266. <https://doi.org/10.4161/org.7.4.19049>
- Basta, L. P., Sil, P., Jones, R. A., Little, K. A., Hayward-Lara, G., & Devenport, D. (2023). Celsr1 and Celsr2 exhibit distinct adhesive interactions and contributions to planar cell polarity. *Frontiers in Cell and Developmental Biology*, 10, 2398. <https://doi.org/10.3389/FCELL.2022.1064907/BIBTEX>
- Bazley, L. A., & Gullick, W. J. (2005). The epidermal growth factor receptor family. *Endocrine-Related Cancer*, 12(Supplement_1), S17–S27. <https://doi.org/10.1677/ERC.1.01032>
- Beleut, M., Rajaram, R. D., Caikovski, M., Ayyanan, A., Germano, D., Choi, Y., Schneider, P., & Brisken, C. (2010). Two distinct mechanisms underlie progesterone-induced proliferation in the mammary gland. *Proceedings of the National Academy of Sciences of the United States of America*, 107(7), 2989–2994. <https://doi.org/10.1073/PNAS.0915148107>
- Belting, M., Ahamed, J., & Ruf, W. (2005). Signaling of the Tissue Factor Coagulation Pathway in Angiogenesis and Cancer. *Arteriosclerosis, Thrombosis, and Vascular Biology*, 25(8), 1545–1550. <https://doi.org/10.1161/01.ATV.0000171155.05809.BF>
- Benetkiewicz, M., Wang, Y., Schaner, M., Wang, P., Mantripragada, K. K., Buckley, P. G., Kristensen, G., Børresen-Dale, A. L., & Dumanski, J. P. (2005). High-resolution gene copy number and expression profiling of human chromosome 22 in ovarian carcinomas. *Genes, Chromosomes & Cancer*, 42(3), 228–237. <https://doi.org/10.1002/GCC.20128>
- Bhargava, R., Beriwal, S., Dabbs, D. J., Ozbek, U., Soran, A., Johnson, R. R., Brufsky, A. M., Lembersky, B. C., & Ahrendt, G. M. (2010). Immunohistochemical surrogate markers of breast cancer molecular classes predicts response to neoadjuvant chemotherapy: a single institutional experience with 359 cases. *Cancer*, 116(6), 1431–1439. <https://doi.org/10.1002/CNCR.24876>
- Bloom, G. S., & Brashear, T. A. (1989). A Novel 58-kDa Protein Associates with the Golgi Apparatus and Microtubules. *Journal of Biological Chemistry*, 264(27), 16083–16092. [https://doi.org/10.1016/S0021-9258\(18\)71590-1](https://doi.org/10.1016/S0021-9258(18)71590-1)
- Bombonati, A., & Sgroi, D. C. (2011). The molecular pathology of breast cancer progression. *J Pathol*, 223(2), 307–317. <https://doi.org/10.1002/path.2808>

- Brennan, K., Offiah, G., McSherry, E. A., & Hopkins, A. M. (2010). Tight junctions: A barrier to the initiation and progression of breast cancer? *Journal of Biomedicine and Biotechnology*, 2010. <https://doi.org/10.1155/2010/460607>
- Brisken, C., Park, S., Vass, T., Lydon, J. P., O'Malley, B. W., & Weinberg, R. A. (1998). A paracrine role for the epithelial progesterone receptor in mammary gland development. *Proceedings of the National Academy of Sciences of the United States of America*, 95(9), 5076. <https://doi.org/10.1073/PNAS.95.9.5076>
- Brzoska, H. L., d'Esposito, A. M., Kolatsi-Joannou, M., Patel, V., Igarashi, P., Lei, Y., Finnell, R. H., Lythgoe, M. F., Woolf, A. S., Papakrivopoulou, E., & Long, D. A. (2016). Planar cell polarity genes *Celsr1* and *Vangl2* are necessary for kidney growth, differentiation, and rostrocaudal patterning. *Kidney Int*, 90(6), 1274–1284. <https://doi.org/10.1016/j.kint.2016.07.011>
- BT-474 - HTB-20 | ATCC. (n.d.). Retrieved 1 July 2023, from <https://www.atcc.org/products/htb-20>
- Burstein, H. J., Polyak, K., Wong, J. S., Lester, S. C., & Kaelin, C. M. (2004). Ductal carcinoma in situ of the breast. *N Engl J Med*, 350(14), 1430–1441. <https://doi.org/10.1056/NEJMra031301>
- Butler, M. T., & Wallingford, J. B. (2017). Planar cell polarity in development and disease. *Nat Rev Mol Cell Biol*, 18(6), 375–388. <https://doi.org/10.1038/nrm.2017.11>
- Cameron, D., Piccart-Gebhart, M. J., Gelber, R. D., Procter, M., Goldhirsch, A., de Azambuja, E., Castro, G., Untch, M., Smith, I., Gianni, L., Baselga, J., Al-Sakaff, N., Lauer, S., McFadden, E., Leyland-Jones, B., Bell, R., Dowsett, M., & Jackisch, C. (2017). 11 years' follow-up of trastuzumab after adjuvant chemotherapy in HER2-positive early breast cancer: final analysis of the HERceptin Adjuvant (HERA) trial. *Lancet (London, England)*, 389(10075), 1195–1205. [https://doi.org/10.1016/S0140-6736\(16\)32616-2](https://doi.org/10.1016/S0140-6736(16)32616-2)
- Cantilena, S., Pastorino, F., Pezzolo, A., Chayka, O., Pistoia, V., Ponzoni, M., & Sala, A. (2011). Frizzled receptor 6 marks rare, highly tumourigenic stem-like cells in mouse and human neuroblastomas. *Oncotarget*, 2(12), 976–983. <https://doi.org/10.18632/oncotarget.410>
- Carey, L. A. (2010). Through a glass darkly: advances in understanding breast cancer biology, 2000-2010. *Clinical Breast Cancer*, 10(3), 188–195. <https://doi.org/10.3816/CBC.2010.N.026>
- Carraro, D. M., Elias, E. V., & Andrade, V. P. (2014). Ductal carcinoma in situ of the breast: morphological and molecular features implicated in progression. *Bioscience Reports*, 34(1), 19–28. <https://doi.org/10.1042/BSR20130077>
- Casal, J., Lawrence, P. A., & Struhl, G. (2006). Two separate molecular systems, Dachshous/Fat and Starry night/Frizzled, act independently to confer planar cell polarity. *Development (Cambridge, England)*, 133(22), 4561–4572. <https://doi.org/10.1242/DEV.02641>
- Cavo, M., Caria, M., Pulsoni, I., Beltrame, F., Fato, M., & Scaglione, S. (2018). A new cell-laden 3D Alginate-Matrigel hydrogel resembles human breast cancer cell malignant morphology, spread and invasion capability observed 'in vivo'. *Sci Rep*, 8(1), 5333. <https://doi.org/10.1038/s41598-018-23250-4>
- Cerami, E., Gao, J., Dogrusoz, U., Gross, B. E., Sumer, S. O., Aksoy, B. A., Jacobsen, A., Byrne, C. J., Heuer, M. L., Larsson, E., Antipin, Y., Reva, B., Goldberg, A. P., Sander, C., & Schultz, N. (2012). The cBio Cancer Genomics Portal: An open platform for exploring multidimensional cancer genomics data. *Cancer Discovery*. <https://doi.org/10.1158/2159-8290.CD-12-0095>

- Cetera, M., Leybova, L., Joyce, B., & Devenport, D. (2018). Counter-rotational cell flows drive morphological and cell fate asymmetries in mammalian hair follicles. *Nat Cell Biol*, *20*(5), 541–552. <https://doi.org/10.1038/s41556-018-0082-7>
- Chandrashekar, D. S., Bashel, B., Balasubramanya, S. A. H., Creighton, C. J., Ponce-Rodriguez, I., Chakravarthi, B. V. S. K., & Varambally, S. (2017). UALCAN: A Portal for Facilitating Tumor Subgroup Gene Expression and Survival Analyses. *Neoplasia (New York, N.Y.)*, *19*(8), 649–658. <https://doi.org/10.1016/J.NEO.2017.05.002>
- Chandrashekar, D. S., Karthikeyan, S. K., Korla, P. K., Patel, H., Shovon, A. R., Athar, M., Netto, G. J., Qin, Z. S., Kumar, S., Manne, U., Crieghton, C. J., & Varambally, S. (2022). UALCAN: An update to the integrated cancer data analysis platform. *Neoplasia (New York, N.Y.)*, *25*, 18–27. <https://doi.org/10.1016/J.NEO.2022.01.001>
- Chapman, R. S., Lourenco, P. C., Tonner, E., Flint, D. J., Selbert, S., Takeda, K., Akira, S., Clarke, A. R., & Watson, C. J. (1999). Suppression of epithelial apoptosis and delayed mammary gland involution in mice with a conditional knockout of Stat3. *Genes & Development*, *13*(19), 2604. <https://doi.org/10.1101/GAD.13.19.2604>
- Chavez, K. J., Garimella, S. V., & Lipkowitz, S. (2010). Triple Negative Breast Cancer Cell Lines: One Tool in the Search for Better Treatment of Triple Negative Breast Cancer. *Breast Disease*, *32*(1–2), 35. <https://doi.org/10.3233/BD-2010-0307>
- Chen, W. S., Antic, D., Matis, M., Logan, C. Y., Povelones, M., Anderson, G. A., Nusse, R., & Axelrod, J. D. (2008). Asymmetric Homotypic Interactions of the Atypical Cadherin Flamingo Mediate Intercellular Polarity Signaling. *Cell*, *133*(6), 1093–1105. <https://doi.org/10.1016/j.cell.2008.04.048>
- Chen, Z., Fang, Z., & Ma, J. (2021). Regulatory mechanisms and clinical significance of vimentin in breast cancer. *Biomedicine & Pharmacotherapy*, *133*, 111068. <https://doi.org/10.1016/J.BIOPHA.2020.111068>
- Chromosome 22: 46,360,834-46,537,620 - Region in detail - Homo_sapiens - Ensembl genome browser 109.* (n.d.). Retrieved 10 July 2023, from https://www.ensembl.org/Homo_sapiens/Location/View?db=core;g=ENSG00000075275;r=22:46360834-46537620
- Clarkson, R. W. E., Boland, M. P., Kritikou, E. A., Lee, J. M., Freeman, T. C., Tiffen, P. G., & Watson, C. J. (2006). The genes induced by signal transducer and activators of transcription (STAT)3 and STAT5 in mammary epithelial cells define the roles of these STATs in mammary development. *Molecular Endocrinology (Baltimore, Md.)*, *20*(3), 675–685. <https://doi.org/10.1210/ME.2005-0392>
- Clarkson, R. W. E., & Watson, C. J. (2003). Microarray analysis of the involution switch. *Journal of Mammary Gland Biology and Neoplasia*, *8*(3), 309–319. <https://doi.org/10.1023/B:JOMG.0000010031.53310.92>
- Colleoni, M., Rotmensz, N., Maisonneuve, P., Mastropasqua, M. G., Luini, A., Veronesi, P., Intra, M., Montagna, E., Canello, G., Cardillo, A., Mazza, M., Perri, G., Iorfida, M., Pruneri, G., Goldhirsch, A., & Viale, G. (2012). Outcome of special types of luminal breast cancer. *Annals of Oncology*, *23*(6), 1428–1436. <https://doi.org/10.1093/annonc/mdr461>

- Copp, A. J., Stanier, P., & Greene, N. D. (2013). Neural tube defects: recent advances, unsolved questions, and controversies. *Lancet Neurol*, *12*(8), 799–810. [https://doi.org/10.1016/S1474-4422\(13\)70110-8](https://doi.org/10.1016/S1474-4422(13)70110-8)
- Corda, G., & Sala, A. (2017). Non-canonical WNT/PCP signalling in cancer: Fzd6 takes centre stage. *Oncogenesis*, *6*(7), e364. <https://doi.org/10.1038/oncsis.2017.69>
- Corda, G., Sala, G., Lattanzio, R., Iezzi, M., Sallese, M., Fragassi, G., Lamolinara, A., Mirza, H., Barcaroli, D., Ermler, S., Silva, E., Yasaei, H., Newbold, R. F., Vagnarelli, P., Mottolose, M., Natali, P. G., Perracchio, L., Quist, J., Grigoriadis, A., ... Sala, A. (2017). Functional and prognostic significance of the genomic amplification of frizzled 6 (FZD6) in breast cancer. *J Pathol*, *241*(3), 350–361. <https://doi.org/10.1002/path.4841>
- Creamer, B. A., Sakamoto, K., Schmidt, J. W., Triplett, A. A., Moriggl, R., & Wagner, K.-U. (2010). Stat5 promotes survival of mammary epithelial cells through transcriptional activation of a distinct promoter in Akt1. *Molecular and Cellular Biology*, *30*(12), 2957–2970. <https://doi.org/10.1128/MCB.00851-09>
- Creeden, J. F., Nanavaty, N. S., Einloth, K. R., Gillman, C. E., Stanbery, L., Hamouda, D. M., Dworkin, L., & Nemunaitis, J. (2021). Homologous recombination proficiency in ovarian and breast cancer patients. *BMC Cancer* *2021* *21:1*, *21*(1), 1–12. <https://doi.org/10.1186/S12885-021-08863-9>
- Creighton, C. J. (2012). The molecular profile of luminal B breast cancer. *Biologics : Targets & Therapy*, *6*, 289. <https://doi.org/10.2147/BTT.S29923>
- Criscitello, C., Azim, H. A., Schouten, P. C., Linn, S. C., & Sotiriou, C. (2012). Understanding the biology of triple-negative breast cancer. *Annals of Oncology : Official Journal of the European Society for Medical Oncology*, *23* Suppl 6(SUPPL. 6). <https://doi.org/10.1093/ANNONC/MDS188>
- CRUK. (2017). *Breast cancer statistics*. <https://www.cancerresearchuk.org/health-professional/cancer-statistics/statistics-by-cancer-type/breast-cancer#heading-Zero>
- Cui, Y., Riedlinger, G., Miyoshi, K., Tang, W., Li, C., Deng, C.-X., Robinson, G. W., & Hennighausen, L. (2004). Inactivation of Stat5 in Mouse Mammary Epithelium during Pregnancy Reveals Distinct Functions in Cell Proliferation, Survival, and Differentiation. *Molecular and Cellular Biology*, *24*(18), 8037. <https://doi.org/10.1128/MCB.24.18.8037-8047.2004>
- Curtin, J. A., Quint, E., Tsipouri, V., Arkell, R. M., Cattanach, B., Copp, A. J., Henderson, D. J., Spurr, N., Stanier, P., Fisher, E. M., Nolan, P. M., Steel, K. P., Brown, S. D., Gray, I. C., & Murdoch, J. N. (2003). Mutation of Celsr1 disrupts planar polarity of inner ear hair cells and causes severe neural tube defects in the mouse. *Curr Biol*, *13*(13), 1129–1133. <http://www.ncbi.nlm.nih.gov/pubmed/12842012>
- Curtis, C., Shah, S. P., Chin, S. F., Turashvili, G., Rueda, O. M., Dunning, M. J., Speed, D., Lynch, A. G., Samarajiwa, S., Yuan, Y., Gräf, S., Ha, G., Haffari, G., Bashashati, A., Russell, R., McKinney, S., Aparicio, S., Brenton, J. D., Ellis, I., ... Caldas, C. (2012). The genomic and transcriptomic architecture of 2,000 breast tumours reveals novel subgroups. *Nature*. <https://doi.org/10.1038/nature10983>
- Dahan, I., Yearim, A., Touboul, Y., & Ravid, S. (2012). The tumor suppressor Lgl1 regulates NMII-A cellular distribution and focal adhesion morphology to optimize cell migration. *Molecular Biology of the Cell*, *23*(4), 591–601. <https://doi.org/10.1091/MBC.E11-01-0015>

- Dai, X., Cheng, H., Bai, Z., & Li, J. (2017). Breast Cancer Cell Line Classification and Its Relevance with Breast Tumor Subtyping. *Journal of Cancer*, *8*(16), 3131. <https://doi.org/10.7150/JCA.18457>
- Darvin, P., Toor, S. M., Sasidharan Nair, V., & Elkord, E. (2018). Immune checkpoint inhibitors: recent progress and potential biomarkers. *Experimental & Molecular Medicine*, *50*(12). <https://doi.org/10.1038/S12276-018-0191-1>
- Daulat, A. M., & Borg, J. P. (2017). Wnt/Planar Cell Polarity Signaling: New Opportunities for Cancer Treatment. *Trends Cancer*, *3*(2), 113–125. <https://doi.org/10.1016/j.trecan.2017.01.001>
- Daulat, A. M., Finetti, P., Revinski, D., Silveira Wagner, M., Camoin, L., Audebert, S., Birnbaum, D., Kodjabachian, L., Borg, J. P., & Bertucci, F. (2019). ECT2 associated to PRICKLE1 are poor-prognosis markers in triple-negative breast cancer. *Br J Cancer*, *120*(9), 931–940. <https://doi.org/10.1038/s41416-019-0448-z>
- Davey, C. F., Mathewson, A. W., & Moens, C. B. (2016). PCP Signaling between Migrating Neurons and their Planar-Polarized Neuroepithelial Environment Controls Filopodial Dynamics and Directional Migration. *PLOS Genetics*, *12*(3), e1005934. <https://doi.org/10.1371/JOURNAL.PGEN.1005934>
- Davey, C. F., & Moens, C. B. (2017). Planar cell polarity in moving cells: think globally, act locally. *Development*, *144*(2), 187–200. <https://doi.org/10.1242/dev.122804>
- Davies, A., Formstone, C., Mason, I., & Lewis, J. (2005). Planar polarity of hair cells in the chick inner ear is correlated with polarized distribution of c-flamingo-1 protein. *Dev Dyn*, *233*(3), 998–1005. <https://doi.org/10.1002/dvdy.20376>
- D’Cruz, C. M., Moody, S. E., Master, S. R., Hartman, J. L., Keiper, E. A., Imielinski, M. B., Cox, J. D., Wang, J. Y., Ha, S. I., Keister, B. A., & Chodosh, L. A. (2002). Persistent parity-induced changes in growth factors, TGF-beta3, and differentiation in the rodent mammary gland. *Molecular Endocrinology (Baltimore, Md.)*, *16*(9), 2034–2051. <https://doi.org/10.1210/ME.2002-0073>
- Devenport, D. (2014). The cell biology of planar cell polarity. *J Cell Biol*, *207*(2), 171–179. <https://doi.org/10.1083/jcb.201408039>
- Devenport, D., & Fuchs, E. (2008). Planar polarization in embryonic epidermis orchestrates global asymmetric morphogenesis of hair follicles. *Nat Cell Biol*, *10*(11), 1257–1268. <https://doi.org/10.1038/ncb1784>
- Devenport, D., Oristian, D., Heller, E., & Fuchs, E. (2011). Mitotic internalization of planar cell polarity proteins preserves tissue polarity. *Nature Cell Biology*, *13*(8), 893–902. <https://doi.org/10.1038/NCB2284>
- Dijksterhuis, J. P., Petersen, J., Schulte, G., Schulte, G., & of Receptor Biology, S. (2014). WNT/Frizzled signalling: receptor–ligand selectivity with focus on FZD-G protein signalling and its physiological relevance: IUPHAR Review 3. *British Journal of Pharmacology*, *171*(5), 1195–1209. <https://doi.org/10.1111/BPH.12364>
- Dong, B., Vold, S., Olvera-Jaramillo, C., & Chang, H. (2018). Functional redundancy of frizzled 3 and frizzled 6 in planar cell polarity control of mouse hair follicles. *Development (Cambridge)*, *145*(19). <https://doi.org/10.1242/DEV.168468/264581/AM/FUNCTIONAL-REDUNDANCY-OF-FRIZZLED-3-AND-FRIZZLED-6>
- Dow, L. E., Kauffman, J. S., Caddy, J., Peterson, A. S., Jane, S. M., Russell, S. M., & Humbert, P. O. (2006). The tumour-suppressor Scribble dictates cell polarity during directed epithelial

- migration: regulation of Rho GTPase recruitment to the leading edge. *Oncogene* 2007 26:16, 26(16), 2272–2282. <https://doi.org/10.1038/sj.onc.1210016>
- Duggal, S., Robin, J., & Julian, T. B. (2013). Ductal carcinoma in situ: an overview. *Expert Rev Anticancer Ther*, 13(8), 955–962. <https://doi.org/10.1586/14737140.2013.820557>
- Eaton, S. (1997). Planar polarization of Drosophila and vertebrate epithelia. *Curr Opin Cell Biol*, 9(6), 860–866. <http://www.ncbi.nlm.nih.gov/pubmed/9425352>
- Ellis, M. J., Tao, Y., Luo, J., A'Hern, R., Evans, D. B., Bhatnagar, A. S., Chaudri Ross, H. A., Von Kameke, A., Miller, W. R., Smith, I., Eiermann, W., & Dowsett, M. (2008). Outcome prediction for estrogen receptor-positive breast cancer based on postneoadjuvant endocrine therapy tumor characteristics. *Journal of the National Cancer Institute*, 100(19), 1380–1388. <https://doi.org/10.1093/JNCI/DJN309>
- Elsum, I. A., Humbert, P. O., Humbert, P., Thompson, E. W., Simpson, K. A. B. M. J., Williams, E. D., Vargas, D. 3 A., Bates, O., & Zaman, M. H. (2013). Localization, Not Important in All Tumor-Suppressing Properties: A Lesson Learnt from Scribble. *Cells Tissues Organs*, 198(1), 1–11. <https://doi.org/10.1159/000348423>
- Emens, L. A. (2018). Breast Cancer Immunotherapy: Facts and Hopes. *Clinical Cancer Research : An Official Journal of the American Association for Cancer Research*, 24(3), 511–520. <https://doi.org/10.1158/1078-0432.CCR-16-3001>
- ERBB2 Gene - GeneCards | ERBB2 Protein | ERBB2 Antibody*. (n.d.). Retrieved 3 June 2023, from <https://www.genecards.org/cgi-bin/carddisp.pl?gene=ERBB2&keywords=her2>
- Esserman, L. J., Perou, C., Cheang, M., DeMichele, A., Carey, L., Veer, L. J. van 't, Gray, J., Petricoin, E., Conway, K., Hylton, N., & Berry, D. (2009). Breast cancer molecular profiles and tumor response of neoadjuvant doxorubicin and paclitaxel: The I-SPY TRIAL (CALGB 150007/150012, ACRIIN 6657). https://doi.org/10.1200/Jco.2009.27.18_suppl.Lba515, 27(18_suppl), LBA515–LBA515. https://doi.org/10.1200/JCO.2009.27.18_SUPPL.LBA515
- Eubelen, M., Bostaille, N., Cabochette, P., Gauquier, A., Tebabi, P., Dumitru, A. C., Koehler, M., Gut, P., Alsteens, D., Stainier, D. Y. R., Garcia-Pino, A., & Vanhollebeke, B. (2018). A molecular mechanism for Wnt ligand-specific signaling. *Science*. <https://doi.org/10.1126/science.aat1178>
- Evans, K. W., Yuca, E., Scott, S. S., Zhao, M., Arango, N. P., Cruz Pico, C. X., Saridogan, T., Shariati, M., Class, C. A., Bristow, C. A., Vellano, C. P., Zheng, X., Gonzalez-Angulo, A. M., Su, X., Tapia, C., Chen, K., Akcakanat, A., Lim, B., Tripathy, D., ... Meric-Bernstam, F. (2021). Oxidative Phosphorylation Is a Metabolic Vulnerability in Chemotherapy-Resistant Triple-Negative Breast Cancer. *Cancer Research*, 81(21), 5572. <https://doi.org/10.1158/0008-5472.CAN-20-3242>
- Ewald, A. J., Brenot, A., Duong, M., Chan, B. S., & Werb, Z. (2008). Collective Epithelial Migration and Cell Rearrangements Drive Mammary Branching Morphogenesis. *Developmental Cell*, 14(4), 570–581. <https://doi.org/10.1016/J.DEVCEL.2008.03.003>
- Ewald, A. J., Huebner, R. J., Palsdottir, H., Lee, J. K., Perez, M. J., Jorgens, D. M., Tauscher, A. N., Cheung, K. J., Werb, Z., & Auer, M. (2012). Mammary collective cell migration involves transient loss of epithelial features and individual cell migration within the epithelium. *Journal of Cell Science*, 125(11), 2638–2654. <https://doi.org/10.1242/JCS.096875/-/DC1>
- Fallah, Y., Brundage, J., Allegakoen, P., & Shajahan-Haq, A. N. (2017). MYC-Driven Pathways in Breast Cancer Subtypes. *Biomolecules*, 7(3). <https://doi.org/10.3390/BIOM7030053>

- Fantozzi, A., Gruber, D. C., Pisarsky, L., Heck, C., Kunita, A., Yilmaz, M., Meyer-Schaller, N., Cornille, K., Hopfer, U., Bentires-Alj, M., & Christofori, G. (2014). VEGF-mediated angiogenesis links EMT-induced cancer stemness to tumor initiation. *Cancer Research*, *74*(5), 1566–1575. <https://doi.org/10.1158/0008-5472.CAN-13-1641/651065/AM/VEGF-MEDIATED-ANGIOGENESIS-LINKS-EMT-INDUCED>
- Fata, J. E., Leco, K. J., Voura, E. B., Yu, H.-Y. E., Waterhouse, P., Murphy, G., Moorehead, R. A., & Khokha, R. (2001). Accelerated apoptosis in the Timp-3-deficient mammary gland. *Journal of Clinical Investigation*, *108*(6), 831. <https://doi.org/10.1172/JCI13171>
- Feigin, M. E., Akshinthala, S. D., Araki, K., Rosenberg, A. Z., Muthuswamy, L. B., Martin, B., Lehmann, B. D., Berman, H. K., Pietenpol, J. A., Cardiff, R. D., & Muthuswamy, S. K. (2014). Mislocalization of the cell polarity protein scribble promotes mammary tumorigenesis and is associated with basal breast cancer. *Cancer Research*, *74*(11), 3180–3194. <https://doi.org/10.1158/0008-5472.CAN-13-3415>
- Feiguin, F., Hannus, M., Mlodzik, M., & Eaton, S. (2001). The Ankyrin Repeat Protein Diego Mediates Frizzled-Dependent Planar Polarization. *Developmental Cell*, *1*(1), 93–101. [https://doi.org/10.1016/S1534-5807\(01\)00010-7](https://doi.org/10.1016/S1534-5807(01)00010-7)
- Fenteany, G., Janmey, P. A., & Stossel, T. P. (2000). Signaling pathways and cell mechanics involved in wound closure by epithelial cell sheets. *Current Biology*, *10*(14), 831–838. [https://doi.org/10.1016/S0960-9822\(00\)00579-0](https://doi.org/10.1016/S0960-9822(00)00579-0)
- Fernandez-Valdivia, R., Mukherjee, A., Creighton, C. J., Buser, A. C., DeMayo, F. J., Edwards, D. P., & Lydon, J. P. (2008). Transcriptional response of the murine mammary gland to acute progesterone exposure. *Endocrinology*, *149*(12), 6236–6250. <https://doi.org/10.1210/EN.2008-0768>
- Fernandez-Valdivia, R., Mukherjee, A., Ying, Y., Li, J., Paquet, M., DeMayo, F. J., & Lydon, J. P. (2009). The RANKL signaling axis is sufficient to elicit ductal side-branching and alveologenesis in the mammary gland of the virgin mouse. *Developmental Biology*, *328*(1), 127–139. <https://doi.org/10.1016/J.YDBIO.2009.01.019>
- Formstone, C. J., & Mason, I. (2005). Expression of the Celsr/flamingo homologue, c-fmi1, in the early avian embryo indicates a conserved role in neural tube closure and additional roles in asymmetry and somitogenesis. *Developmental Dynamics : An Official Publication of the American Association of Anatomists*, *232*(2), 408–413. <https://doi.org/10.1002/DVDY.20228>
- Formstone, C. J., Moxon, C., Murdoch, J., Little, P., & Mason, I. (2010). Basal enrichment within neuroepithelia suggests novel function(s) for Celsr1 protein. *Molecular and Cellular Neuroscience*. <https://doi.org/10.1016/j.mcn.2010.03.008>
- Foulkes, W. D., Brunet, J. S., Stefansson, I. M., Straume, O., Chappuis, P. O., Bégin, L. R., Hamel, N., Goffin, J. R., Wong, N., Trudel, M., Kapusta, L., Porter, P., & Akslen, L. A. (2004). The prognostic implication of the basal-like (cyclin E high/p27 low/p53+/glomeruloid-microvascular-proliferation+) phenotype of BRCA1-related breast cancer. *Cancer Research*, *64*(3), 830–835. <https://doi.org/10.1158/0008-5472.CAN-03-2970>
- Galiè, M. (2019). RAS as Supporting Actor in Breast Cancer. *Frontiers in Oncology*, *9*, 1199. <https://doi.org/10.3389/FONC.2019.01199/BIBTEX>
- Gamazon, E. R., & Stranger, B. E. (2015). The impact of human copy number variation on gene expression. *Briefings in Functional Genomics*, *14*(5), 352. <https://doi.org/10.1093/BFGP/ELV017>

- Gammons, M., & Bienz, M. (2018). Multiprotein complexes governing Wnt signal transduction. In *Current Opinion in Cell Biology*. <https://doi.org/10.1016/j.ceb.2017.10.008>
- Gandalovičová, A., Vomastek, T., Rosel, D., & Brábek, J. (2016). Cell polarity signaling in the plasticity of cancer cell invasiveness. *Oncotarget*. <https://doi.org/10.18632/oncotarget.7214>
- Gao, B. (2012). Wnt Regulation of Planar Cell Polarity (PCP). In *Current Topics in Developmental Biology*. <https://doi.org/10.1016/B978-0-12-394592-1.00008-9>
- Gao, B., & Yang, Y. (2013). Planar cell polarity in vertebrate limb morphogenesis. *Curr Opin Genet Dev*, 23(4), 438–444. <https://doi.org/10.1016/j.gde.2013.05.003>
- Gao, J., Aksoy, B. A., Dogrusoz, U., Dresdner, G., Gross, B., Sumer, S. O., Sun, Y., Jacobsen, A., Sinha, R., Larsson, E., Cerami, E., Sander, C., & Schultz, N. (2013). Integrative analysis of complex cancer genomics and clinical profiles using the cBioPortal. *Science Signaling*. <https://doi.org/10.1126/scisignal.2004088>
- Gao, Y. S., Vrieling, A., MacKenzie, R., & Sztul, E. (2002). A novel type of regulation of the vimentin intermediate filament cytoskeleton by a Golgi protein. *European Journal of Cell Biology*, 81(7), 391–401. <https://doi.org/10.1078/0171-9335-00260>
- Gao, Y.-S., & Sztul, E. (2001). A Novel Interaction of the Golgi Complex with the Vimentin Intermediate Filament Cytoskeleton. In *The Journal of Cell Biology* (Vol. 152, Issue 5). <http://www.jcb.org/cgi/content/full/152/5/877>
- Gemmete, J. J., & Mukherji, S. K. (2011). Trastuzumab (herceptin). *AJNR. American Journal of Neuroradiology*, 32(8), 1373–1374. <https://doi.org/10.3174/AJNR.A2619>
- Gene: *CELSR1* (ENSG00000075275) - Summary - Homo_sapiens - Ensembl genome browser 110. (n.d.). Retrieved 19 July 2023, from https://www.ensembl.org/Homo_sapiens/Gene/Summary?db=core;g=ENSG00000075275;r=22:46360834-46537620
- Gene: *FZD6* (ENSG00000164930) - Splice variants - Homo_sapiens - Ensembl genome browser 110. (n.d.). Retrieved 17 July 2023, from https://www.ensembl.org/Homo_sapiens/Gene/Splice?db=core;g=ENSG00000164930;r=8:103298433-103332866
- Geradts, J., Groth, J., Wu, Y., & Jin, G. (2016). Validation of an oligo-gene signature for the prognostic stratification of ductal carcinoma in situ (DCIS). *Breast Cancer Res Treat*, 157(3), 447–459. <https://doi.org/10.1007/s10549-016-3838-4>
- Gey, G. O., Coffmann, W. D., & Kubieck, M. T. (1952). Tissue culture studies of the proliferative capacity for cervical carcinoma and normal epithelium. *Cancer Res*, 12, 264–265.
- Ghimire, S. R., & Deans, M. R. (2019). Frizzled3 and Frizzled6 Cooperate with Vangl2 to Direct Cochlear Innervation by type II Spiral Ganglion Neurons. *Journal of Neuroscience*, 39(41), 8013–8023. <https://doi.org/10.1523/JNEUROSCI.1740-19.2019>
- Goldhirsch, A., Wood, W. C., Coates, A. S., Gelber, R. D., Thürlimann, B., & Senn, H. J. (2011). Strategies for subtypes—dealing with the diversity of breast cancer: highlights of the St Gallen International Expert Consensus on the Primary Therapy of Early Breast Cancer 2011. *Annals of Oncology*, 22(8), 1736. <https://doi.org/10.1093/ANNONC/MDR304>
- Gonzalez, A. L., Luciana, L., Nevé, C. Le, Valantin, J., Francols, L., Gadot, N., Vanbelle, C., Davignon, L., & Broutier, L. (2021). Staining and High-Resolution Imaging of Three-Dimensional Organoid and

- Spheroid Models. *Journal of Visualized Experiments : JoVE*, 2021(169).
<https://doi.org/10.3791/62280>
- González-Mariscal, L., Miranda, J., Gallego-Gutiérrez, H., Cano-Cortina, M., & Amaya, E. (2020). Relationship between apical junction proteins, gene expression and cancer. *Biochimica et Biophysica Acta (BBA) - Biomembranes*, 1862(9), 183278.
<https://doi.org/10.1016/J.BBAMEM.2020.183278>
- Grumolato, L., Liu, G., Mong, P., Mudbhary, R., Biswas, R., Arroyave, R., Vijayakumar, S., Economides, A. N., & Aaronson, S. A. (2010). Canonical and noncanonical Wnts use a common mechanism to activate completely unrelated coreceptors. *Genes and Development*.
<https://doi.org/10.1101/gad.1957710>
- Gudjonsson, T., Adriance, M. C., Sternlicht, M. D., Petersen, O. W., & Bissell, M. J. (2005). Myoepithelial Cells: Their Origin and Function in Breast Morphogenesis and Neoplasia. *Journal of Mammary Gland Biology and Neoplasia*, 10(3), 261–272. <https://doi.org/10.1007/S10911-005-9586-4/METRICS>
- Gulluni, F., Martini, M., De Santis, M. C., Campa, C. C., Ghigo, A., Margaria, J. P., Ciraolo, E., Franco, I., Ala, U., Annaratone, L., Disalvatore, D., Bertalot, G., Viale, G., Noatynska, A., Compagno, M., Sigismund, S., Montemurro, F., Thelen, M., Fan, F., ... Hirsch, E. (2017). Mitotic Spindle Assembly and Genomic Stability in Breast Cancer Require PI3K-C2 α Scaffolding Function. *Cancer Cell*, 32(4), 444–459.e7. <https://doi.org/10.1016/J.CCELL.2017.09.002>
- Gutierrez, C., & Schiff, R. (2011). HER 2: Biology, Detection, and Clinical Implications. *Archives of Pathology & Laboratory Medicine*, 135(1), 55. <https://doi.org/10.1043/2010-0454-RAR.1>
- Habas, R., Kato, Y., & He, X. (2001). Wnt/Frizzled activation of Rho regulates vertebrate gastrulation and requires a novel formin homology protein Daam1. *Cell*, 107(7), 843–854.
[https://doi.org/10.1016/S0092-8674\(01\)00614-6](https://doi.org/10.1016/S0092-8674(01)00614-6)
- Halaoui, R., & McCaffrey, L. (2015). Rewiring cell polarity signaling in cancer. *Oncogene*, 34(8), 939–950. <https://doi.org/10.1038/onc.2014.59>
- Halim, C. E., Deng, S., Ong, M. S., & Yap, C. T. (2020). Involvement of STAT5 in Oncogenesis. *Biomedicines*, 8(9). <https://doi.org/10.3390/BIOMEDICINES8090316>
- Han, Y., Liu, D., & Li, L. (2020). PD-1/PD-L1 pathway: current researches in cancer. *American Journal of Cancer Research*, 10(3), 727. [/pmc/articles/PMC7136921/](https://pmc/articles/PMC7136921/)
- Han, Y., Watling, D., Rogers, N. C., & Stark, G. R. (1997). JAK2 and STAT5, but not JAK1 and STAT1, are required for prolactin-induced beta-lactoglobulin transcription. *Molecular Endocrinology (Baltimore, Md.)*, 11(8), 1180–1188. <https://doi.org/10.1210/MEND.11.8.9952>
- Hanahan, D., & Weinberg, R. A. (2000). The hallmarks of cancer. *Cell*, 100(1), 57–70.
<http://www.ncbi.nlm.nih.gov/pubmed/10647931>
- Hanahan, D., & Weinberg, R. A. (2011). Hallmarks of cancer: The next generation. *Cell*, 144(5), 646–674. <https://doi.org/10.1016/J.CELL.2011.02.013/ATTACHMENT/68024D79-3A9C-46C4-930B-640934F11E2E/MMC1.PDF>
- Hardin, J., Lynch, A., Loveless, T., & Pettitt, J. (2013). Cadherins and their partners in the nematode worm *Caenorhabditis elegans*. In *Progress in Molecular Biology and Translational Science*.
<https://doi.org/10.1016/B978-0-12-394311-8.00011-X>

- Hare, S. H., & Harvey, A. J. (2017). mTOR function and therapeutic targeting in breast cancer. *American Journal of Cancer Research*, 7(3), 383. /pmc/articles/PMC5385631/
- Hatakeyama, J., Wald, J. H., Printsev, I., Ho, H. Y. H., & Carraway, K. L. (2014). Vangl1 and Vangl2: planar cell polarity components with a developing role in cancer. *Endocrine-Related Cancer*, 21(5), 345–356. <https://doi.org/10.1530/ERC-14-0141>
- Heiden, M. G. V., Cantley, L. C., & Thompson, C. B. (2009). Understanding the Warburg Effect: The Metabolic Requirements of Cell Proliferation. *Science (New York, N.Y.)*, 324(5930), 1029. <https://doi.org/10.1126/SCIENCE.1160809>
- Heitz, F., Harter, P., Lueck, H. J., Fissler-Eckhoff, A., Lorenz-Salehi, F., Scheil-Bertram, S., Traut, A., & Bois, A. du. (2009). Triple-negative and HER2-overexpressing breast cancers exhibit an elevated risk and an earlier occurrence of cerebral metastases. *European Journal of Cancer (Oxford, England : 1990)*, 45(16), 2792–2798. <https://doi.org/10.1016/J.EJCA.2009.06.027>
- Hobbs, C., & Formstone, C. J. (2022). Planar cell polarity proteins determine basal cell height in the later stage embryonic mouse epidermis'. *Wellcome Open Research*, 7, 138. <https://doi.org/10.12688/WELLCOMEOPENRES.17733.2>
- Hollern, D. P., Swiatnicki, M. R., Rennhack, J. P., Misesk, S. A., Matson, B. C., McAuliff, A., Gallo, K. A., Caron, K. M., & Andrechek, E. R. (2019). E2F1 Drives Breast Cancer Metastasis by Regulating the Target Gene FGF13 and Altering Cell Migration. *Scientific Reports 2019 9:1*, 9(1), 1–13. <https://doi.org/10.1038/s41598-019-47218-0>
- Holliday, D. L., & Speirs, V. (2011). Choosing the right cell line for breast cancer research. *Breast Cancer Research*, 13(4), 1–7. <https://doi.org/10.1186/BCR2889/COMMENTS>
- Hummel, D., Becks, A., Men, H., Bryda, E. C., Glasco, D. M., & Chandrasekhar, A. (2022). Celsr1 suppresses Wnt5a-mediated chemoattraction to prevent incorrect rostral migration of facial branchiomotor neurons. *Development (Cambridge, England)*, 149(22). <https://doi.org/10.1242/DEV.200553>
- Humphries, A. C., & Mlodzik, M. (2018). From instruction to output: Wnt/PCP signaling in development and cancer. *Curr Opin Cell Biol*, 51, 110–116. <https://doi.org/10.1016/j.ceb.2017.12.005>
- Imbalzano, K. M., Tatarkova, I., Imbalzano, A. N., & Nickerson, J. A. (2009). Increasingly transformed MCF-10A cells have a progressively tumor-like phenotype in three-dimensional basement membrane culture. *Cancer Cell International*, 9(1), 1–11. <https://doi.org/10.1186/1475-2867-9-7/FIGURES/9>
- Ismaeel, E., & Formstone, C. (2023). *Understanding the role of planar cell polarity Celsr1 protein in the protection against breast cancer metastasis (Unpublished)*.
- Jaiswal, D., Cowley, N., Bian, Z., Zheng, G., Claffey, K. P., & Hoshino, K. (2017a). Stiffness analysis of 3D spheroids using microtweezers. *PLoS One*, 12(11), e0188346. <https://doi.org/10.1371/journal.pone.0188346>
- Jaiswal, D., Cowley, N., Bian, Z., Zheng, G., Claffey, K. P., & Hoshino, K. (2017b). Stiffness analysis of 3D spheroids using microtweezers. *PLoS ONE*, 12(11). <https://doi.org/10.1371/JOURNAL.PONE.0188346>
- Javed, A., & Lteif, A. (2013a). Development of the Human Breast. *Seminars in Plastic Surgery*, 27(1), 5. <https://doi.org/10.1055/S-0033-1343989>

- Javed, A., & Lteif, A. (2013b). Development of the Human Breast. *Seminars in Plastic Surgery*, 27(1), 5. <https://doi.org/10.1055/S-0033-1343989>
- Javir, G., Joshi, K., Khedkar, V., & Rojatar, S. (2020). 6 α -Hydroxy-4[14], 10[15]-guainadien-8 β , 12-olide induced cell cycle arrest via modulation of EMT and Wnt/ β -catenin pathway in HER-2 positive breast cancer cells. *The Journal of Steroid Biochemistry and Molecular Biology*, 197, 105514. <https://doi.org/10.1016/J.JSBMB.2019.105514>
- Jensen, C., & Teng, Y. (2020). Is It Time to Start Transitioning From 2D to 3D Cell Culture? *Frontiers in Molecular Biosciences*, 7, 513823. <https://doi.org/10.3389/FMOLB.2020.00033/BIBTEX>
- Jiang, G., Zhang, S., Yazdanparast, A., Li, M., Pawar, A. V., Liu, Y., Inavolu, S. M., & Cheng, L. (2016). Comprehensive comparison of molecular portraits between cell lines and tumors in breast cancer. *BMC Genomics*, 17(7), 281–301. <https://doi.org/10.1186/S12864-016-2911-Z/TABLES/3>
- Kalluri, R., & Weinberg, R. A. (2009). The basics of epithelial-mesenchymal transition. *The Journal of Clinical Investigation*, 119(6), 1420. <https://doi.org/10.1172/JCI39104>
- Kamdje, A. H. N., Kamga, P. T., Simo, R. T., Vecchio, L., Etet, P. F. S., Muller, J. M., Bassi, G., Lukong, E., Goel, R. K., Amvene, J. M., & Krampera, M. (2017). Developmental pathways associated with cancer metastasis: Notch, Wnt, and Hedgehog. In *Cancer Biology and Medicine*. <https://doi.org/10.20892/j.issn.2095-3941.2016.0032>
- Kao, J., Salari, K., Bocanegra, M., Choi, Y. La, Girard, L., Gandhi, J., Kwei, K. A., Hernandez-Boussard, T., Wang, P., Gazdar, A. F., Minna, J. D., & Pollack, J. R. (2009). Molecular Profiling of Breast Cancer Cell Lines Defines Relevant Tumor Models and Provides a Resource for Cancer Gene Discovery. *PLOS ONE*, 4(7), e6146. <https://doi.org/10.1371/JOURNAL.PONE.0006146>
- Kashyap, A., Zimmerman, T., Ergül, N., Bosserhoff, A., Hartman, U., Alla, V., Bataille, F., Galle, P. R., Strand, S., & Strand, D. (2012). The human Lgl polarity gene, Hugel-2, induces MET and suppresses Snail tumorigenesis. *Oncogene* 2013 32:11, 32(11), 1396–1407. <https://doi.org/10.1038/onc.2012.162>
- Katanaev, V. L., Egger-Adam, D., & Tomlinson, A. (2018). Antagonistic PCP Signaling Pathways in the developing Drosophila eye. *Sci Rep*, 8(1), 5741. <https://doi.org/10.1038/s41598-018-24053-3>
- Katoh, M. (2005). WNT/PCP signaling pathway and human cancer (review). *Oncol Rep*, 14(6), 1583–1588. <http://www.ncbi.nlm.nih.gov/pubmed/16273260>
- Katoh, M. (2017). Canonical and non-canonical WNT signaling in cancer stem cells and their niches: Cellular heterogeneity, omics reprogramming, targeted therapy and tumor plasticity (Review). In *International Journal of Oncology*. <https://doi.org/10.3892/ijo.2017.4129>
- Kennecke, H., Yerushalmi, R., Woods, R., Cheang, M. C. U., Voduc, D., Speers, C. H., Nielsen, T. O., & Gelmon, K. (2010). Metastatic behavior of breast cancer subtypes. *Journal of Clinical Oncology*, 28(20), 3271–3277. <https://doi.org/10.1200/JCO.2009.25.9820>
- Kessenbrock, K., Smith, P., Steenbeek, S. C., Pervolarakis, N., Kumar, R., Minami, Y., Goga, A., Hinck, L., & Werb, Z. (2017). Diverse regulation of mammary epithelial growth and branching morphogenesis through noncanonical Wnt signaling. *Proc Natl Acad Sci U S A*, 114(12), 3121–3126. <https://doi.org/10.1073/pnas.1701464114>
- Kiliç, Y., Çelebiler, A. C., & Sakizli, M. (2014). Selecting housekeeping genes as references for the normalization of quantitative PCR data in breast cancer. *Clinical and Translational Oncology*. <https://doi.org/10.1007/s12094-013-1058-5>

- Kim, J., Yang, C., Kim, E. J., Jang, J., Kim, S. J., Kang, S. M., Kim, M. G., Jung, H., Park, D., & Kim, C. (2016). Vimentin filaments regulate integrin-ligand interactions by binding to the cytoplasmic tail of integrin β 3. *Journal of Cell Science*, *129*(10), 2030–2042. <https://doi.org/10.1242/JCS.180315/260303/AM/VIMENTIN-FILAMENTS-REGULATE-INTEGRIN-LIGAND>
- Kim, R. K., Suh, Y., Yoo, K. C., Cui, Y. H., Kim, H., Kim, M. J., Kim, I. G., & Lee, S. J. (2015). Activation of KRAS promotes the mesenchymal features of basal-type breast cancer. *Experimental & Molecular Medicine* *2015* *47*:1, *47*(1), e137–e137. <https://doi.org/10.1038/emm.2014.99>
- King, T. D., Zhang, W., Suto, M. J., & Li, Y. (2012). Frizzled7 as an emerging target for cancer therapy. *Cell Signal*, *24*(4), 846–851. <https://doi.org/10.1016/j.cellsig.2011.12.009>
- Klaus, A., & Birchmeier, W. (2008). Wnt signalling and its impact on development and cancer. *Nat Rev Cancer*, *8*(5), 387–398. <https://doi.org/10.1038/nrc2389>
- Knoblich, J. A., Jan, L. Y., & Jan, Y. N. (1995). Asymmetric segregation of Numb and Prospero during cell division. *Nature* *1995* *377*:6550, *377*(6550), 624–627. <https://doi.org/10.1038/377624a0>
- Koundouros, N., & Poulgiannis, G. (2019). Reprogramming of fatty acid metabolism in cancer. *British Journal of Cancer* *2019* *122*:1, *122*(1), 4–22. <https://doi.org/10.1038/s41416-019-0650-z>
- Koval, A., Purvanov, V., Egger-Adam, D., & Katanaev, V. L. (2011). Yellow submarine of the Wnt/Frizzled signaling: Submerging from the G protein harbor to the targets. *Biochemical Pharmacology*. <https://doi.org/10.1016/j.bcp.2011.06.005>
- Kreike, B., van Kouwenhove, M., Horlings, H., Weigelt, B., Peterse, H., Bartelink, H., & van de Vijver, M. J. (2007). Gene expression profiling and histopathological characterization of triple-negative/basal-like breast carcinomas. *Breast Cancer Research*, *9*(5). <https://doi.org/10.1186/BCR1771/FIGURES/1>
- Kunimoto, K., Bayly, R. D., Vldar, E. K., Vonderfecht, T., Gallagher, A. R., & Axelrod, J. D. (2017). Disruption of Core Planar Cell Polarity Signaling Regulates Renal Tubule Morphogenesis but Is Not Cystogenic. *Curr Biol*, *27*(20), 3120-3131 e4. <https://doi.org/10.1016/j.cub.2017.09.011>
- Lánczky, A., & Gyórfy, B. (2021). Web-Based Survival Analysis Tool Tailored for Medical Research (KMplot): Development and Implementation. *J Med Internet Res* *2021*;23(7):E27633 <https://www.jmir.org/2021/7/E27633>, *23*(7), e27633. <https://doi.org/10.2196/27633>
- Laumanns, I. P., Fink, L., Wilhelm, J., Wolff, J. C., Mitnacht-Kraus, R., Graef-Hoehst, S., Stein, M. M., Bohle, R. M., Klepetko, W., Hoda, M. A. R., Schermuly, R. T., Grimminger, F., Seeger, W., & Voswinckel, R. (2009). The noncanonical WNT pathway is operative in idiopathic pulmonary arterial hypertension. *American Journal of Respiratory Cell and Molecular Biology*, *40*(6), 683–691. <https://doi.org/10.1165/rcmb.2008-0153OC>
- Lawrence, P. A. (1975). The structure and properties of a compartment border: the intersegmental boundary in *Oncopeltus*. *CIBA FOUND.SYMP*. <https://doi.org/10.1002/9780470720110.ch2>
- Lawrence, P. A. (2001). Wingless signalling: more about the Wingless morphogen. *Current Biology : CB*, *11*(16). [https://doi.org/10.1016/S0960-9822\(01\)00380-3](https://doi.org/10.1016/S0960-9822(01)00380-3)
- Lawrence, P. A., & Green, S. M. (1975). The anatomy of a compartment border: The intersegmental boundary in *oncopeltus*. *Journal of Cell Biology*. <https://doi.org/10.1083/jcb.65.2.373>

- Lee, H. J., & Zheng, J. J. (2010). PDZ domains and their binding partners: structure, specificity, and modification. *Cell Communication and Signaling* 2010 8:1, 8(1), 1–18. <https://doi.org/10.1186/1478-811X-8-8>
- Li, C., Nguyen, V., Clark, K. N., Zahed, T., Sharkas, S., Filipp, F. V., & Boiko, A. D. (2019). Down-regulation of FZD3 receptor suppresses growth and metastasis of human melanoma independently of canonical WNT signaling. *Proc Natl Acad Sci U S A*. <https://doi.org/10.1073/pnas.1813802116>
- Li, M., Liu, X., Ribinson, G., Bar-Peled, U., Wagner, K. U., Young, W. S., Hennighausen, L., & Furth, P. A. (1997). Mammary-derived signals activate programmed cell death during the first stage of mammary gland involution. *Proceedings of the National Academy of Sciences of the United States of America*, 94(7), 3425–3430. <https://doi.org/10.1073/PNAS.94.7.3425>
- Li, Z., Dong, X., Wang, Z., Liu, W., Deng, N., Ding, Y., Tang, L., Hla, T., Zeng, R., Li, L., & Wu, D. (2005). Regulation of PTEN by Rho small GTPases. *Nature Cell Biology*, 7(4), 399–404. <https://doi.org/10.1038/NCB1236>
- Liao, S., Desouki, M. M., Gaile, D. P., Shepherd, L., Nowak, N. J., Conroy, J., Barry, W. T., & Geradts, J. (2012). Differential copy number aberrations in novel candidate genes associated with progression from in situ to invasive ductal carcinoma of the breast. *Genes Chromosomes Cancer*, 51(12), 1067–1078. <https://doi.org/10.1002/gcc.21991>
- Lindqvist, M., Horn, Z., Bryja, V., Schulte, G., Papachristou, P., Ajima, R., Dyberg, C., Arenas, E., Yamaguchi, T. P., Lagercrantz, H., & Ringstedt, T. (2010). Vang-like protein 2 and Rac1 interact to regulate adherens junctions. *Journal of Cell Science*, 123(Pt 3), 472–483. <https://doi.org/10.1242/JCS.048074>
- Liu, C.-Y., Lin, H.-H., Tang, M.-J., Wang, Y.-K., Liu, C.-Y., Lin, H.-H., Tang, M.-J., & Wang, Y.-K. (2015). Vimentin contributes to epithelial-mesenchymal transition cancer cell mechanics by mediating cytoskeletal organization and focal adhesion maturation. *Oncotarget*, 6(18), 15966–15983. <https://doi.org/10.18632/ONCOTARGET.3862>
- Liu, J., Lichtenberg, T., Hoadley, K. A., Poisson, L. M., Lazar, A. J., Cherniack, A. D., Kovatich, A. J., Benz, C. C., Levine, D. A., Lee, A. v, Omberg, L., Wolf, D. M., Shriver, C. D., Thorsson, V., & Hu, H. (2018). An Integrated TCGA Pan-Cancer Clinical Data Resource to Drive High-Quality Survival Outcome Analytics. *Cell*, 173(2), 400-416.e11. <https://doi.org/10.1016/j.cell.2018.02.052>
- Liu, K., Newbury, P. A., Glicksberg, B. S., Zeng, W. Z. D., Paithankar, S., Andrechek, E. R., & Chen, B. (2019). Evaluating cell lines as models for metastatic breast cancer through integrative analysis of genomic data. *Nature Communications* 2019 10:1, 10(1), 1–12. <https://doi.org/10.1038/s41467-019-10148-6>
- Llimargas, M., & Lawrence, P. A. (2001). Seven Wnt homologues in *Drosophila*: a case study of the developing tracheae. *Proceedings of the National Academy of Sciences of the United States of America*, 98(25), 14487–14492. <https://doi.org/10.1073/PNAS.251304398>
- Loi, S., Sotiriou, C., Haibe-Kains, B., Lallemand, F., Conus, N. M., Piccart, M. J., Speed, T. P., & McArthur, G. A. (2009). Gene expression profiling identifies activated growth factor signaling in poor prognosis (Luminal-B) estrogen receptor positive breast cancer. *BMC Medical Genomics*, 2. <https://doi.org/10.1186/1755-8794-2-37>

- Luga, V., Zhang, L., Vilorio-Petit, A. M., Ogunjimi, A. A., Inanlou, M. R., Chiu, E., Buchanan, M., Hosein, A. N., Basik, M., & Wrana, J. L. (2012). Exosomes mediate stromal mobilization of autocrine Wnt-PCP signaling in breast cancer cell migration. *Cell*, *151*(7), 1542–1556. <https://doi.org/10.1016/j.cell.2012.11.024>
- Lüönd, F., Sugiyama, N., Bill, R., Bornes, L., Hager, C., Tang, F., Santacrose, N., Beisel, C., Ivanek, R., Bürglin, T., Tiede, S., van Rheenen, J., & Christofori, G. (2021). Distinct contributions of partial and full EMT to breast cancer malignancy. *Developmental Cell*, *56*(23), 3203–3221.e11. <https://doi.org/10.1016/J.DEVCEL.2021.11.006>
- Lydon, J. P., DeMayo, F. J., Funk, C. R., Mani, S. K., Hughes, A. R., Montgomery, C. A., Shyamala, G., Conneely, O. M., & O'Malley, B. W. (1995). Mice lacking progesterone receptor exhibit pleiotropic reproductive abnormalities. *Genes & Development*, *9*(18), 2266–2278. <https://doi.org/10.1101/GAD.9.18.2266>
- MacDonald, B. T., Tamai, K., & He, X. (2009). Wnt/ β -Catenin Signaling: Components, Mechanisms, and Diseases. In *Developmental Cell*. <https://doi.org/10.1016/j.devcel.2009.06.016>
- Macias, H., & Hinck, L. (2012). Mammary Gland Development. *Wiley Interdisciplinary Reviews. Developmental Biology*, *1*(4), 533. <https://doi.org/10.1002/WDEV.35>
- MacMillan, C. D., Leong, H. S., Dales, D. W., Robertson, A. E., Lewis, J. D., Chambers, A. F., & Tuck, A. B. (2014). Stage of breast cancer progression influences cellular response to activation of the WNT/planar cell polarity pathway. *Scientific Reports*, *4*. <https://doi.org/10.1038/SREP06315>
- Manore, S. G., Doheny, D. L., Wong, G. L., & Lo, H. W. (2022). IL-6/JAK/STAT3 Signaling in Breast Cancer Metastasis: Biology and Treatment. *Frontiers in Oncology*, *12*, 862. <https://doi.org/10.3389/FONC.2022.866014/BIBTEX>
- Marconi, G. D., Fonticoli, L., Rajan, T. S., Pierdomenico, S. D., Trubiani, O., Pizzicannella, J., & Diomedea, F. (2021). Epithelial-Mesenchymal Transition (EMT): The Type-2 EMT in Wound Healing, Tissue Regeneration and Organ Fibrosis. *Cells*, *10*(7). <https://doi.org/10.3390/CELLS10071587>
- Matsumoto, S., Fumoto, K., Okamoto, T., Kaibuchi, K., & Kikuchi, A. (2010). Binding of APC and dishevelled mediates Wnt5a-regulated focal adhesion dynamics in migrating cells. *The EMBO Journal*, *29*(7), 1192–1204. <https://doi.org/10.1038/EMBOJ.2010.26>
- Matthews, H. K., Marchant, L., Carmona-Fontaine, C., Kuriyama, S., Larraín, J., Holt, M. R., Parsons, M., & Mayor, R. (2008). Directional migration of neural crest cells in vivo is regulated by Syndecan-4/Rac1 and non-canonical Wnt signaling/RhoA. *Development*, *135*(10), 1771–1780. <https://doi.org/10.1242/DEV.017350>
- Maung, S. M., & Jenny, A. (2011). Planar cell polarity in Drosophila. *Organogenesis*, *7*(3), 165–179. <https://doi.org/10.4161/org.7.3.18143>
- McDaniel, S. M., Rumer, K. K., Biroc, S. L., Metz, R. P., Singh, M., Porter, W., & Schedin, P. (2006). Remodeling of the Mammary Microenvironment after Lactation Promotes Breast Tumor Cell Metastasis. *The American Journal of Pathology*, *168*(2), 608. <https://doi.org/10.2353/AJPATH.2006.050677>
- McDonald-McGinn, D. M., & Sullivan, K. E. (2011). Chromosome 22q11.2 deletion syndrome (DiGeorge syndrome/velocardiofacial syndrome). *Medicine*, *90*(1), 1–18. <https://doi.org/10.1097/MD.0B013E3182060469>

- McGreevy, E. M., Vijayraghavan, D., Davidson, L. A., & Hildebrand, J. D. (2015). Shroom3 functions downstream of planar cell polarity to regulate myosin II distribution and cellular organization during neural tube closure. *Biology Open*, *4*(2), 186–196. <https://doi.org/10.1242/BIO.20149589>
- MDA-MB-231 - HTB-26 | ATCC. (n.d.). Retrieved 1 July 2023, from <https://www.atcc.org/products/htb-26>
- MDA-MB-436 - HTB-130 | ATCC. (n.d.). Retrieved 1 July 2023, from <https://www.atcc.org/products/htb-130>
- Mercogliano, M. F., Bruni, S., Elizalde, P. v., & Schillaci, R. (2020). Tumor Necrosis Factor α Blockade: An Opportunity to Tackle Breast Cancer. *Frontiers in Oncology*, *10*, 584. <https://doi.org/10.3389/FONC.2020.00584/BIBTEX>
- Micalizzi, D. S., Farabaugh, S. M., & Ford, H. L. (2010). Epithelial-mesenchymal transition in cancer: Parallels between normal development and tumor progression. In *Journal of Mammary Gland Biology and Neoplasia*. <https://doi.org/10.1007/s10911-010-9178-9>
- Milgrom-Hoffman, M., & Humbert, P. O. (2018). Regulation of cellular and PCP signalling by the Scribble polarity module. *Seminars in Cell & Developmental Biology*, *81*, 33–45. <https://doi.org/10.1016/J.SEMCDB.2017.11.021>
- Moasser, M. M. (2007). The oncogene HER2: its signaling and transforming functions and its role in human cancer pathogenesis. *Oncogene*, *26*(45), 6469–6487. <https://doi.org/10.1038/SJ.ONC.1210477>
- Mootha, V. K., Lindgren, C. M., Eriksson, K. F., Subramanian, A., Sihag, S., Lehar, J., Puigserver, P., Carlsson, E., Ridderstråle, M., Laurila, E., Houstis, N., Daly, M. J., Patterson, N., Mesirov, J. P., Golub, T. R., Tamayo, P., Spiegelman, B., Lander, E. S., Hirschhorn, J. N., ... Groop, L. C. (2003). PGC-1 α -responsive genes involved in oxidative phosphorylation are coordinately downregulated in human diabetes. *Nature Genetics* *2003* *34*:3, *34*(3), 267–273. <https://doi.org/10.1038/ng1180>
- Morales, F. C., Hayashi, Y., Van Pelt, C. S., & Georgescu, M. M. (2012). NHERF1/EBP50 controls lactation by establishing basal membrane polarity complexes with prolactin receptor. *Cell Death & Disease*, *3*(9). <https://doi.org/10.1038/CDDIS.2012.131>
- Morgan, R. K., Anderson, G. R., Araç, D., Aust, G., Balenga, N., Boucard, A., Bridges, J. P., Engel, F. B., Formstone, C. J., Glitsch, M. D., Gray, R. S., Hall, R. A., Hsiao, C. C., Kim, H. Y., Knierim, A. B., Kusuluri, D. K., Leon, K., Liebscher, I., Piao, X., ... Mogha, A. (2019). The expanding functional roles and signaling mechanisms of adhesion g protein-coupled receptors. In *Annals of the New York Academy of Sciences*. <https://doi.org/10.1111/nyas.14094>
- Muggerud, A. A., Hallett, M., Johnsen, H., Kleivi, K., Zhou, W., Tahmasebpoor, S., Amini, R. M., Botling, J., Borresen-Dale, A. L., Sorlie, T., & Warnberg, F. (2010). Molecular diversity in ductal carcinoma in situ (DCIS) and early invasive breast cancer. *Mol Oncol*, *4*(4), 357–368. <https://doi.org/10.1016/j.molonc.2010.06.007>
- Mukherjee, A., Soyal, S. M., Li, J., Ying, Y., He, B., DeMayo, F. J., & Lydon, J. P. (2010). Targeting RANKL to a specific subset of murine mammary epithelial cells induces ordered branching morphogenesis and alveologenesis in the absence of progesterone receptor expression. *The FASEB Journal*, *24*(11), 4408. <https://doi.org/10.1096/FJ.10-157982>

- Munoz-Soriano, V., Belacortu, Y., & Paricio, N. (2012). Planar cell polarity signaling in collective cell movements during morphogenesis and disease. *Curr Genomics*, *13*(8), 609–622. <https://doi.org/10.2174/138920212803759721>
- Muthuswamy, S. K., & Xue, B. (2012). Cell polarity as a regulator of cancer cell behavior plasticity. *Annu Rev Cell Dev Biol*, *28*, 599–625. <https://doi.org/10.1146/annurev-cellbio-092910-154244>
- Muz, B., Puente, P. de la, Azab, F., & Azab, A. K. (2015). The role of hypoxia in cancer progression, angiogenesis, metastasis, and resistance to therapy. *Hypoxia*, *3*, 83. <https://doi.org/10.2147/HP.S93413>
- Navajas Acedo, J., Voas, M. G., Alexander, R., Woolley, T., Unruh, J. R., Li, H., Moens, C., & Piotrowski, T. (2019). PCP and Wnt pathway components act in parallel during zebrafish mechanosensory hair cell orientation. *Nature Communications* *2019 10:1*, *10*(1), 1–17. <https://doi.org/10.1038/s41467-019-12005-y>
- Naz, G., Pasternack, S. M., Perrin, C., Mattheisen, M., Refke, M., Khan, S., Gul, A., Simons, M., Ahmad, W., & Betz, R. C. (2012). FZD6 encoding the Wnt receptor frizzled 6 is mutated in autosomal-recessive nail dysplasia. *Br J Dermatol*, *166*(5), 1088–1094. <https://doi.org/10.1111/j.1365-2133.2011.10800.x>
- Neta, G., Brenner, A. V., Sturgis, E. M., Pfeiffer, R. M., Hutchinson, A. A., Aschebrook-Kilfoy, B., Yeager, M., Xu, L., Wheeler, W., Abend, M., Ron, E., Tucker, M. A., Chanock, S. J., & Sigurdson, A. J. (2011). Common genetic variants related to genomic integrity and risk of papillary thyroid cancer. *Carcinogenesis*, *32*(8), 1231–1237. <https://doi.org/10.1093/carcin/bgr100>
- Neumann, N. M., Perrone, M. C., Veldhuis, J. H., Huebner, R. J., Zhan, H., Devreotes, P. N., Brodland, G. W., & Ewald, A. J. (2018). Coordination of Receptor Tyrosine Kinase Signaling and Interfacial Tension Dynamics Drives Radial Intercalation and Tube Elongation. *Developmental Cell*. <https://doi.org/10.1016/j.devcel.2018.03.011>
- Neve, R. M., Chin, K., Fridlyand, J., Yeh, J., Baehner, F. L., Fevr, T., Clark, L., Bayani, N., Coppe, J. P., Tong, F., Speed, T., Spellman, P. T., DeVries, S., Lapuk, A., Wang, N. J., Kuo, W. L., Stilwell, J. L., Pinkel, D., Albertson, D. G., ... Gray, J. W. (2006). A collection of breast cancer cell lines for the study of functionally distinct cancer subtypes. *Cancer Cell*, *10*(6), 515–527. <https://doi.org/10.1016/J.CCR.2006.10.008>
- Neville, M. C., & Monks, J. (2018). The cell biology of the lactating mammary epithelium. In *Encyclopedia of Reproduction*. <https://doi.org/10.1016/B978-0-12-801238-3.64419-7>
- Nguyen, Q. H., Pervolarakis, N., Blake, K., Ma, D., Davis, R. T., James, N., Phung, A. T., Willey, E., Kumar, R., Jabart, E., Driver, I., Rock, J., Goga, A., Khan, S. A., Lawson, D. A., Werb, Z., & Kessenbrock, K. (2018). Profiling human breast epithelial cells using single cell RNA sequencing identifies cell diversity. *Nature Communications* *2018 9:1*, *9*(1), 1–12. <https://doi.org/10.1038/s41467-018-04334-1>
- Nicoletto, R. E., & Ofner, C. M. (2022). Cytotoxic mechanisms of doxorubicin at clinically relevant concentrations in breast cancer cells. *Cancer Chemotherapy and Pharmacology*, *89*(3), 285–311. <https://doi.org/10.1007/S00280-022-04400-Y>
- Nikolopoulou, E., Galea, G. L., Rolo, A., Greene, N. D., & Copp, A. J. (2017). Neural tube closure: cellular, molecular and biomechanical mechanisms. *Development*, *144*(4), 552–566. <https://doi.org/10.1242/dev.145904>

- Nishimura, T., & Takeichi, M. (2008). Shroom3-mediated recruitment of Rho kinases to the apical cell junctions regulates epithelial and neuroepithelial planar remodeling. *Development*, *135*(8), 1493–1502. <https://doi.org/10.1242/DEV.019646>
- Ochoa-Espinosa, A., & Affolter, M. (2012). Branching Morphogenesis: From Cells to Organs and Back. *Cold Spring Harbor Perspectives in Biology*, *4*(10). <https://doi.org/10.1101/CSHPERSPECT.A008243>
- O'Neill, A. K., Gallegos, L. L., Justilien, V., Garcia, E. L., Leitges, M., Fields, A. P., Hall, R. A., & Newton, A. C. (2011). Protein kinase C α promotes cell migration through a PDZ-dependent interaction with its novel substrate discs large homolog 1 (DLG1). *The Journal of Biological Chemistry*, *286*(50), 43559–43568. <https://doi.org/10.1074/JBC.M111.294603>
- Oozeer, F., Yates, L. L., Dean, C., & Formstone, C. J. (2017). A role for core planar polarity proteins in cell contact-mediated orientation of planar cell division across the mammalian embryonic skin. *Sci Rep*, *7*(1), 1880. <https://doi.org/10.1038/s41598-017-01971-2>
- Oshi, M., Tokumaru, Y., Angarita, F. A., Yan, L., Matsuyama, R., Endo, I., & Takabe, K. (2020). Degree of Early Estrogen Response Predict Survival after Endocrine Therapy in Primary and Metastatic ER-Positive Breast Cancer. *Cancers*, *12*(12), 1–16. <https://doi.org/10.3390/CANCERS12123557>
- Ossipova, O., Chu, C. W., Fillatre, J., Brott, B. K., Itoh, K., & Sokol, S. Y. (2015). The involvement of PCP proteins in radial cell intercalations during *Xenopus* embryonic development. *Developmental Biology*. <https://doi.org/10.1016/j.ydbio.2015.06.013>
- Paik, S., Shak, S., Tang, G., Kim, C., Baker, J., Cronin, M., Baehner, F. L., Walker, M. G., Watson, D., Park, T., Hiller, W., Fisher, E. R., Wickerham, D. L., Bryant, J., & Wolmark, N. (2004). A multigene assay to predict recurrence of tamoxifen-treated, node-negative breast cancer. *The New England Journal of Medicine*, *351*(27), 2817–2826. <https://doi.org/10.1056/NEJMOA041588>
- Panousopoulou, E., Hobbs, C., Mason, I., Green, J. B., & Formstone, C. J. (2016). Epiboly generates the epidermal basal monolayer and spreads the nascent mammalian skin to enclose the embryonic body. *J Cell Sci*, *129*(9), 1915–1927. <https://doi.org/10.1242/jcs.180703>
- Papakrivopoulou, E., Vasilopoulou, E., Lindenmeyer, M. T., Pacheco, S., Brzóška, H., Price, K. L., Kolatsi-Joannou, M., White, K. E., Henderson, D. J., Dean, C. H., Cohen, C. D., Salama, A. D., Woolf, A. S., & Long, D. A. (2018). Vangl2, a planar cell polarity molecule, is implicated in irreversible and reversible kidney glomerular injury. *The Journal of Pathology*, *246*(4), 485–496. <https://doi.org/10.1002/PATH.5158>
- Park, M., Kim, D., Ko, S., Kim, A., Mo, K., & Yoon, H. (2022). Breast Cancer Metastasis: Mechanisms and Therapeutic Implications. *International Journal of Molecular Sciences 2022, Vol. 23, Page 6806*, *23*(12), 6806. <https://doi.org/10.3390/IJMS23126806>
- Park, W. J., Liu, J., Sharp, E. J., & Adler, P. N. (1996). The *Drosophila* tissue polarity gene inturnd acts cell autonomously and encodes a novel protein. *Development*, *122*(3), 961–969. <http://www.ncbi.nlm.nih.gov/pubmed/8631273>
- Parker, P. J., Justilien, V., Riou, P., Linch, M., & Fields, A. P. (2014). Atypical Protein Kinase C ι as a human oncogene and therapeutic target. *Biochemical Pharmacology*, *88*(1), 1. <https://doi.org/10.1016/J.BCP.2013.10.023>
- Péchoux, C., Gudjonsson, T., Rønnev-Jessen, L., Bissell, M. J., & Petersen, O. W. (1999). Human Mammary Luminal Epithelial Cells Contain Progenitors to Myoepithelial Cells. *Developmental Biology*, *206*(1), 88–99. <https://doi.org/10.1006/DBIO.1998.9133>

- Perry, G. H. (2009). The evolutionary significance of copy number variation in the human genome. *Cytogenetic and Genome Research*, 123(1–4), 283. <https://doi.org/10.1159/000184719>
- Phua, D. C. Y., Humbert, P. O., & Hunziker, W. (2009). Vimentin regulates scribble activity by protecting it from proteasomal degradation. *Molecular Biology of the Cell*, 20(12), 2841–2855. https://doi.org/10.1091/MBC.E08-02-0199/SUPPL_FILE/SUPMOVIESLEGEND.TXT
- Pohl, S. G., Brook, N., Agostino, M., Arfuso, F., Kumar, A. P., & Dharmarajan, A. (2017). Wnt signaling in triple-negative breast cancer. *Oncogenesis*, 6(4), e310. <https://doi.org/10.1038/oncsis.2017.14>
- Prat, A., Parker, J. S., Karginova, O., Fan, C., Livasy, C., Herschkowitz, J. I., He, X., & Perou, C. M. (2010). Phenotypic and molecular characterization of the claudin-low intrinsic subtype of breast cancer. *Breast Cancer Research*, 12(5), 1–18. <https://doi.org/10.1186/BCR2635/FIGURES/7>
- Provance, O. K., & Lewis-Wambi, J. (2019). Deciphering the role of interferon alpha signaling and microenvironment crosstalk in inflammatory breast cancer. *Breast Cancer Research*, 21(1), 1–10. <https://doi.org/10.1186/S13058-019-1140-1/FIGURES/3>
- Puleo, J., & Polyak, K. (2021). The MCF10 Model of Breast Tumor Progression. *Cancer Research*, 81(16), 4183–4185. <https://doi.org/10.1158/0008-5472.CAN-21-1939>
- Puvirajesinghe, T. M., Bertucci, F., Jain, A., Scerbo, P., Belotti, E., Audebert, S., Sebbagh, M., Lopez, M., Brech, A., Finetti, P., Charafe-Jauffret, E., Chaffanet, M., Castellano, R., Restouin, A., Marchetto, S., Collette, Y., Gonçalves, A., Macara, I., Birnbaum, D., ... Borg, J. P. (2016). Identification of p62/SQSTM1 as a component of non-canonical Wnt VANGL2-JNK signalling in breast cancer. *Nature Communications*, 7. <https://doi.org/10.1038/NCOMM510318>
- Qu, T., Zhao, Y., Chen, Y., Jin, S., Fang, Y., Jin, X., Sun, L., & Ma, Y. (2019). Down-regulated MAC30 expression inhibits breast cancer cell invasion and EMT by suppressing Wnt/ β -catenin and PI3K/Akt signaling pathways. *International Journal of Clinical and Experimental Pathology*, 12(5), 1888. <https://pubmed.ncbi.nlm.nih.gov/31111111/>
- Qu, Y., Glasco, D. M., Zhou, L., Sawant, A., Ravni, A., Fritsch, B., Damrau, C., Murdoch, J. N., Evans, S., Pfaff, S. L., Formstone, C., Goffinet, A. M., Chandrasekhar, A., & Tissir, F. (2010). Atypical cadherins Celsr1-3 differentially regulate migration of facial branchiomotor neurons in mice. *The Journal of Neuroscience : The Official Journal of the Society for Neuroscience*, 30(28), 9392–9401. <https://doi.org/10.1523/JNEUROSCI.0124-10.2010>
- Qu, Y., Han, B., Yu, Y., Yao, W., Bose, S., Karlan, B. Y., Giuliano, A. E., & Cui, X. (2015). Evaluation of MCF10A as a Reliable Model for Normal Human Mammary Epithelial Cells. *PLoS ONE*, 10(7). <https://doi.org/10.1371/JOURNAL.PONE.0131285>
- Rakha, E. A., Elsheikh, S. E., Aleskandarany, M. A., Habashi, H. O., Green, A. R., Powe, D. G., El-Sayed, M. E., Benhasouna, A., Brunet, J. S., Akslen, L. A., Evans, A. J., Blamey, R., Reis-Filho, J. S., Foulkes, W. D., & Ellis, I. O. (2009). Triple-negative breast cancer: distinguishing between basal and nonbasal subtypes. *Clinical Cancer Research : An Official Journal of the American Association for Cancer Research*, 15(7), 2302–2310. <https://doi.org/10.1158/1078-0432.CCR-08-2132>
- Rawls, A. S., & Wolff, T. (2003). Strabismus requires Flamingo and Prickle function to regulate tissue polarity in the Drosophila eye. *Development*, 130(9), 1877–1887. <https://www.ncbi.nlm.nih.gov/pubmed/12642492>

- RCSB PDB - 7SZ8: Crystal structure of human CELSR1 EC4-7. (n.d.). Retrieved 18 April 2023, from <https://www.rcsb.org/structure/7SZ8>
- Reis-Filho, J. S., Weigelt, B., Fumagalli, D., & Sotiriou, C. (2010). Molecular profiling: moving away from tumor philately. *Science Translational Medicine*, 2(47). <https://doi.org/10.1126/SCITRANSLMED.3001329>
- Robinson, D. R., Wu, Y. M., Lonigro, R. J., Vats, P., Cobain, E., Everett, J., Cao, X., Rabban, E., Kumar-Sinha, C., Raymond, V., Schuetze, S., Alva, A., Siddiqui, J., Chugh, R., Worden, F., Zalupski, M. M., Innis, J., Mody, R. J., Tomlins, S. A., ... Chinnaiyan, A. M. (2017). Integrative Clinical Genomics of Metastatic Cancer. *Nature*, 548(7667), 297. <https://doi.org/10.1038/NATURE23306>
- Ross, J. S., Fletcher, J. A., Linette, G. P., Stec, J., Clark, E., Ayers, M., Symmans, W. F., Pusztai, L., & Bloom, K. J. (2003). The Her-2/neu gene and protein in breast cancer 2003: biomarker and target of therapy. *The Oncologist*, 8(4), 307–325. <https://doi.org/10.1634/THEONCOLOGIST.8-4-307>
- Santner, S. J., Dawson, P. J., Tait, L., Soule, H. D., Eliason, J., Mohamed, A. N., Wolman, S. R., Heppner, G. H., & Miller, F. R. (2001). Malignant MCF10CA1 cell lines derived from premalignant human breast epithelial MCF10AT cells. In *Breast Cancer Research and Treatment* (Vol. 65).
- Saramaki, O. R., Porkka, K. P., Vessella, R. L., & Visakorpi, T. (2006). Genetic aberrations in prostate cancer by microarray analysis. *Int J Cancer*, 119(6), 1322–1329. <https://doi.org/10.1002/ijc.21976>
- Sarrió, D., Rodriguez-Pinilla, S. M., Hardisson, D., Cano, A., Moreno-Bueno, G., & Palacios, J. (2008). Epithelial-mesenchymal transition in breast cancer relates to the basal-like phenotype. *Cancer Research*, 68(4), 989–997. <https://doi.org/10.1158/0008-5472.CAN-07-2017>
- Schedin, P. (2006). Pregnancy-associated breast cancer and metastasis. *Nature Reviews Cancer* 2006 6:4, 6(4), 281–291. <https://doi.org/10.1038/nrc1839>
- Schindelin, J., Arganda-Carreras, I., Frise, E., Kaynig, V., Longair, M., Pietzsch, T., Preibisch, S., Rueden, C., Saalfeld, S., Schmid, B., Tinevez, J. Y., White, D. J., Hartenstein, V., Eliceiri, K., Tomancak, P., & Cardona, A. (2012). Fiji: An open-source platform for biological-image analysis. In *Nature Methods*. <https://doi.org/10.1038/nmeth.2019>
- Schramek, D., Leibbrandt, A., Sigl, V., Kenner, L., Pospisilik, J. A., Lee, H. J., Hanada, R., Joshi, P. A., Aliprantis, A., Glimcher, L., Pasparakis, M., Khokha, R., Ormandy, C. J., Widschwendter, M., Schett, G., & Penninger, J. M. (2010). Osteoclast differentiation factor RANKL controls development of progesterin-driven mammary cancer. *Nature* 2010 468:7320, 468(7320), 98–102. <https://doi.org/10.1038/nature09387>
- Schulte, G., & Wright, S. C. (2018). Frizzleds as GPCRs – More Conventional Than We Thought! In *Trends in Pharmacological Sciences*. <https://doi.org/10.1016/j.tips.2018.07.001>
- Sebbagh, M., & Borg, J. P. (2014). Insight into planar cell polarity. *Exp Cell Res*, 328(2), 284–295. <https://doi.org/10.1016/j.yexcr.2014.09.005>
- Sepich, D. S., Usmani, M., Pawlicki, S., & Solnica-Krezel, L. (2011). Wnt/PCP signaling controls intracellular position of MTOCs during gastrulation convergence and extension movements. *Development*. <https://doi.org/10.1242/dev.053959>

- Sero, J. E., Sailem, H. Z., Ardy, R. C., Almuttaqi, H., Zhang, T., & Bakal, C. (2015). Cell shape and the microenvironment regulate nuclear translocation of NF- κ B in breast epithelial and tumor cells. *Molecular Systems Biology*. <https://doi.org/10.15252/msb.20145644>
- SFRP1 Gene - GeneCards | SFRP1 Protein | SFRP1 Antibody*. (n.d.). Retrieved 18 June 2023, from <https://www.genecards.org/cgi-bin/carddisp.pl?gene=SFRP1&keywords=sfrp1>
- Shao, X., Lv, N., Liao, J., Long, J., Xue, R., Ai, N., Xu, D., & Fan, X. (2019). Copy number variation is highly correlated with differential gene expression: A pan-cancer study. *BMC Medical Genetics*, 20(1), 1–14. <https://doi.org/10.1186/S12881-019-0909-5/FIGURES/6>
- Shen, Q., Zhong, W., Jan, Y. N., & Temple, S. (2002). Asymmetric Numb distribution is critical for asymmetric cell division of mouse cerebral cortical stem cells and neuroblasts. *Development*, 129(20), 4843–4853. <https://doi.org/10.1242/DEV.129.20.4843>
- Shi, D., Komatsu, K., Hirao, M., Toyooka, Y., Koyama, H., Tissir, F., Goffinet, A. M., Uemura, T., & Fujimori, T. (2014). Celsr1 is required for the generation of polarity at multiple levels of the mouse oviduct. *Development (Cambridge)*. <https://doi.org/10.1242/dev.115659>
- SHROOM3 Gene - GeneCards | SHRM3 Protein | SHRM3 Antibody*. (n.d.). Retrieved 18 June 2023, from <https://www.genecards.org/cgi-bin/carddisp.pl?gene=SHROOM3&keywords=shroom3>
- Simmons G. E., Jr., Pandey, S., Nedeljkovic-Kurepa, A., Saxena, M., Wang, A., & Pruitt, K. (2014). Frizzled 7 expression is positively regulated by SIRT1 and beta-catenin in breast cancer cells. *PLoS One*, 9(6), e98861. <https://doi.org/10.1371/journal.pone.0098861>
- Simons, M., & Mlodzik, M. (2008). Planar cell polarity signaling: from fly development to human disease. *Annu Rev Genet*, 42, 517–540. <https://doi.org/10.1146/annurev.genet.42.110807.091432>
- Sittaramane, V., Pan, X., Glasco, D. M., Huang, P., Gurung, S., Bock, A., Li, S., Wang, H., Kawakami, K., Matisse, M. P., & Chandrasekhar, A. (2013). The PCP protein Vangl2 regulates migration of hindbrain motor neurons by acting in floor plate cells, and independently of cilia function. *Developmental Biology*, 382(2), 400–412. <https://doi.org/10.1016/J.YDBIO.2013.08.017>
- Smart, C. E., Morrison, B. J., Saunus, J. M., Vargas, A. C., Keith, P., Reid, L., Wockner, L., Amiri, M. A., Sarkar, D., Simpson, P. T., Clarke, C., Schmidt, C. W., Reynolds, B. A., Lakhani, S. R., & Lopez, J. A. (2013). In Vitro Analysis of Breast Cancer Cell Line Tumourspheres and Primary Human Breast Epithelia Mammospheres Demonstrates Inter- and Intrasphere Heterogeneity. *PLoS ONE*, 8(6), 64388. <https://doi.org/10.1371/JOURNAL.PONE.0064388>
- Snaebjornsson, M. T., Janaki-Raman, S., & Schulze, A. (2020). Greasing the Wheels of the Cancer Machine: The Role of Lipid Metabolism in Cancer. *Cell Metabolism*, 31(1), 62–76. <https://doi.org/10.1016/J.CMET.2019.11.010>
- Sokol, S. Y. (2015). Spatial and temporal aspects of Wnt signaling and planar cell polarity during vertebrate embryonic development. In *Seminars in Cell and Developmental Biology*. <https://doi.org/10.1016/j.semcdb.2015.05.002>
- Sotiriou, C., Neo, S. Y., McShane, L. M., Korn, E. L., Long, P. M., Jazaeri, A., Martiat, P., Fox, S. B., Harris, A. L., & Liu, E. T. (2003). Breast cancer classification and prognosis based on gene expression profiles from a population-based study. *Proceedings of the National Academy of Sciences of the United States of America*, 100(18), 10393–10398. https://doi.org/10.1073/PNAS.1732912100/SUPPL_FILE/2912TABLE2.XLS

- Soule, H., Maloney, T., Wolman, S., Peterson, W. D., Brenz, R., Mcgrath, C., Russo, J., Pauley, R., Jones, R., & Brooks, S. (1990). Isolation and characterization of a spontaneously immortalized human breast epithelial cell line, MCF-10. *Cancer Research*.
- Stephens, P. J., McBride, D. J., Lin, M. L., Varela, I., Pleasance, E. D., Simpson, J. T., Stebbings, L. A., Leroy, C., Edkins, S., Mudie, L. J., Greenman, C. D., Jia, M., Latimer, C., Teague, J. W., Lau, K. W., Burton, J., Quail, M. A., Swerdlow, H., Churcher, C., ... Stratton, M. R. (2009). Complex landscapes of somatic rearrangement in human breast cancer genomes. *Nature*, *462*(7276), 1005–1010. <https://doi.org/10.1038/NATURE08645>
- Strutt, D. (2009). Gradients and the specification of planar polarity in the insect cuticle. *Cold Spring Harb Perspect Biol*, *1*(5), a000489. <https://doi.org/10.1101/cshperspect.a000489>
- Stubbs, J. L., Davidson, L., Keller, R., & Kintner, C. (2006). Radial intercalation of ciliated cells during *Xenopus* skin development. *Development*. <https://doi.org/10.1242/dev.02417>
- Su, Y., Hopfinger, N. R., Nguyen, T. D., Pogash, T. J., Santucci-Pereira, J., & Russo, J. (2018). Epigenetic reprogramming of epithelial mesenchymal transition in triple negative breast cancer cells with DNA methyltransferase and histone deacetylase inhibitors. *Journal of Experimental and Clinical Cancer Research*, *37*(1), 1–18. <https://doi.org/10.1186/S13046-018-0988-8/FIGURES/8>
- Suarez-Arnedo, A., Torres Figueroa, F., Clavijo, C., Arbeláez, P., Cruz, J. C., & Muñoz-Camargo, C. (2020). An image J plugin for the high throughput image analysis of in vitro scratch wound healing assays. *PLOS ONE*, *15*(7), e0232565.
- Subramanian, A., Tamayo, P., Mootha, V. K., Mukherjee, S., Ebert, B. L., Gillette, M. A., Paulovich, A., Pomeroy, S. L., Golub, T. R., Lander, E. S., & Mesirov, J. P. (2005). Gene set enrichment analysis: A knowledge-based approach for interpreting genome-wide expression profiles. *Proceedings of the National Academy of Sciences of the United States of America*, *102*(43), 15545–15550. https://doi.org/10.1073/PNAS.0506580102/SUPPL_FILE/06580FIG7.JPG
- Sun, Y., Wang, W., & Zhao, C. (2021). Frizzled Receptors in Tumors, Focusing on Signaling, Roles, Modulation Mechanisms, and Targeted Therapies. *Oncology Research*, *28*(6), 661. <https://doi.org/10.3727/096504020X16014648664459>
- Sympson, C. J., Talhouk, R. S., Alexander, C. M., Chin, J. R., Clift, S. M., Bissell, M. J., & Werb, Z. (1994). Targeted expression of stromelysin-1 in mammary gland provides evidence for a role of proteinases in branching morphogenesis and the requirement for an intact basement membrane for tissue-specific gene expression. *The Journal of Cell Biology*, *125*(3), 681–693. <https://doi.org/10.1083/JCB.125.3.681>
- T-47D - HTB-133 | ATCC. (n.d.). Retrieved 1 July 2023, from <https://www.atcc.org/products/htb-133>
- Takeshita, T., Tokumaru, Y., Oshi, M., Wu, R., Patel, A., Tian, W., Hatanaka, Y., Hatanaka, K. C., Yan, L., & Takabe, K. (2022). Clinical Relevance of Estrogen Reactivity in the Breast Cancer Microenvironment. *Frontiers in Oncology*, *12*, 2196. <https://doi.org/10.3389/FONC.2022.865024/BIBTEX>
- Tang, B., Vu, M., Booker, T., Santner, S. J., Miller, F. R., Anver, M. R., & Wakefield, L. M. (2003). TGF- β switches from tumor suppressor to prometastatic factor in a model of breast cancer progression. *Journal of Clinical Investigation*, *112*(7), 1116–1124. <https://doi.org/10.1172/JCI18899>

- Tang, X., Zhang, L., Ma, T., Wang, M., Li, B., Jiang, L., Yan, Y., & Guo, Y. (2020). Molecular mechanisms that regulate export of the planar cell-polarity protein Frizzled-6 out of the endoplasmic reticulum. *The Journal of Biological Chemistry*. <https://doi.org/10.1074/jbc.RA120.012835>
- Tang, Z., Kang, B., Li, C., Chen, T., & Zhang, Z. (2019). GEPIA2: an enhanced web server for large-scale expression profiling and interactive analysis. *Nucleic Acids Research*, *47*(W1), W556–W560. <https://doi.org/10.1093/NAR/GKZ430>
- Terkelsen, T., Pernemalm, M., Gromov, P., Børresen-Dale, A.-L., Krogh, A., Haakensen, V. D., Lethiø O, J., Papaleo, E., Gromova, I., & Papaleo, E. (2021). High-throughput proteomics of breast cancer interstitial fluid: identification of tumor subtype-specific serologically relevant biomarkers. *Molecular Oncology*, *15*, 429–461. <https://doi.org/10.1002/1878-0261.12850>
- Thrasivoulou, C., Millar, M., & Ahmed, A. (2013). Activation of Intracellular Calcium by Multiple Wnt Ligands and Translocation of β -Catenin into the Nucleus: A CONVERGENT MODEL OF Wnt/Ca²⁺ AND Wnt/ β -CATENIN PATHWAYS*. *The Journal of Biological Chemistry*, *288*(50), 35651. <https://doi.org/10.1074/JBC.M112.437913>
- Tilli, T. M., Castro, C. da S., Tuszynski, J. A., & Carels, N. (2016). A strategy to identify housekeeping genes suitable for analysis in breast cancer diseases. *BMC Genomics*. <https://doi.org/10.1186/s12864-016-2946-1>
- Tissir, F., & Goffinet, A. M. (2013). Shaping the nervous system: role of the core planar cell polarity genes. *Nat Rev Neurosci*, *14*(8), 525–535. <https://doi.org/10.1038/nrn3525>
- Tokumar, Y., Oshi, M., Katsuta, E., Yan, L., Satyananda, V., Matsushashi, N., Futamura, M., Akao, Y., Yoshida, K., & Takabe, K. (2020). KRAS signaling enriched triple negative breast cancer is associated with favorable tumor immune microenvironment and better survival. *American Journal of Cancer Research*, *10*(3), 897. [/pmc/articles/PMC7136911/](https://doi.org/10.1186/s12864-016-2946-1)
- Tran, B., & Bedard, P. L. (2011). Luminal-B breast cancer and novel therapeutic targets. *Breast Cancer Research*, *13*(6), 1–10. <https://doi.org/10.1186/BCR2904/TABLES/4>
- Tsutsui, S., Ohno, S., Murakami, S., Kataoka, A., Kinoshita, J., & Hachitanda, Y. (2003). Prognostic significance of the coexpression of p53 protein and c-erbB2 in breast cancer. *American Journal of Surgery*, *185*(2), 165–167. [https://doi.org/10.1016/S0002-9610\(02\)01203-5](https://doi.org/10.1016/S0002-9610(02)01203-5)
- Upadhyay, A., Kandachar, V., Zitserman, D., Tong, X., & Roegiers, F. (2013). Sanpodo controls sensory organ precursor fate by directing Notch trafficking and binding γ -secretase. *The Journal of Cell Biology*, *201*(3), 439–448. <https://doi.org/10.1083/JCB.201209023>
- Usman, S., Waseem, N. H., Nguyen, T. K. N., Mohsin, S., Jamal, A., Teh, M. T., & Waseem, A. (2021). Vimentin Is at the Heart of Epithelial Mesenchymal Transition (EMT) Mediated Metastasis. *Cancers*, *13*(19), 4985. <https://doi.org/10.3390/CANCERS13194985>
- Usui, T., Shima, Y., Shimada, Y., Hirano, S., Burgess, R. W., Schwarz, T. L., Takeichi, M., & Uemura, T. (1999). Flamingo, a seven-pass transmembrane cadherin, regulates planar cell polarity under the control of Frizzled. *Cell*, *98*(5), 585–595. <http://www.ncbi.nlm.nih.gov/pubmed/10490098>
- vanden Berg, A. L., & Sassoon, D. A. (2009). Non-canonical Wnt signaling regulates cell polarity in female reproductive tract development via van gogh-like 2. *Development (Cambridge, England)*, *136*(9), 1559–1570. <https://doi.org/10.1242/DEV.034066>
- VanderVorst, K., Dreyer, C. A., Hatakeyama, J., Bell, G. R. R., Learn, J. A., Berg, A. L., Hernandez, M., Lee, H., Collins, S. R., & Carraway, K. L. (2023). Vangl-dependent Wnt/planar cell polarity

- signaling mediates collective breast carcinoma motility and distant metastasis. *Breast Cancer Research* 2023 25:1, 25(1), 1–19. <https://doi.org/10.1186/S13058-023-01651-2>
- VanderVorst, K., Dreyer, C. A., Konopelski, S. E., Lee, H., Ho, H. H., & Carraway K. L., 3rd. (2019). Wnt/PCP Signaling Contribution to Carcinoma Collective Cell Migration and Metastasis. *Cancer Res*, 79(8), 1719–1729. <https://doi.org/10.1158/0008-5472.CAN-18-2757>
- VanderVorst, K., Hatakeyama, J., Berg, A., Lee, H., & Carraway K. L., 3rd. (2018). Cellular and molecular mechanisms underlying planar cell polarity pathway contributions to cancer malignancy. *Semin Cell Dev Biol*, 81, 78–87. <https://doi.org/10.1016/j.semcdb.2017.09.026>
- Veeman, M. T., Axelrod, J. D., & Moon, R. T. (2003). A second canon. Functions and mechanisms of beta-catenin-independent Wnt signaling. *Developmental Cell*, 5(3), 367–377. [https://doi.org/10.1016/S1534-5807\(03\)00266-1](https://doi.org/10.1016/S1534-5807(03)00266-1)
- Villasenor, A., Chong, D. C., Henkemeyer, M., & Cleaver, O. (2010). Epithelial dynamics of pancreatic branching morphogenesis. *Development*. <https://doi.org/10.1242/dev.052993>
- Wada, H., & Okamoto, H. (2009). Roles of noncanonical Wnt/PCP pathway genes in neuronal migration and neurulation in zebrafish. *Zebrafish*. <https://doi.org/10.1089/zeb.2008.0557>
- Wagner, K.-U., Krempler, A., Triplett, A. A., Qi, Y., George, N. M., Zhu, J., & Rui, H. (2004). Impaired alveologenesis and maintenance of secretory mammary epithelial cells in Jak2 conditional knockout mice. *Molecular and Cellular Biology*, 24(12), 5510–5520. <https://doi.org/10.1128/MCB.24.12.5510-5520.2004>
- Wald, J. H., Hatakeyama, J., Printsev, I., Cuevas, A., Fry, W. H. D., Saldana, M. J., Vandervorst, K., Rowson-Hodel, A., Angelastro, J. M., Sweeney, C., & Carraway, K. L. (2017). Suppression of planar cell polarity signaling and migration in glioblastoma by Nrdp1-mediated Dvl polyubiquitination. *Oncogene*, 36(36), 5158. <https://doi.org/10.1038/ONC.2017.126>
- Waldman, A. D., Fritz, J. M., & Lenardo, M. J. (2020). A guide to cancer immunotherapy: from T cell basic science to clinical practice. *Nature Reviews Immunology* 2020 20:11, 20(11), 651–668. <https://doi.org/10.1038/s41577-020-0306-5>
- Wang, G., Li, Y., Zhang, D., Zhao, S., Zhang, Q., Luo, C., Sun, X., & Zhang, B. (2020). CELSR1 Acts as an Oncogene Regulated by miR-199a-5p in Glioma. *Cancer Management and Research*, 12, 8857–8865. <https://doi.org/10.2147/CMAR.S258835>
- Wang, Y., Chang, H., Rattner, A., & Nathans, J. (2016). Frizzled Receptors in Development and Disease. In *Current Topics in Developmental Biology*. <https://doi.org/10.1016/bs.ctdb.2015.11.028>
- Wang, Y., & Zhou, B. P. (2011). Epithelial-mesenchymal transition in breast cancer progression and metastasis. *Chinese Journal of Cancer*, 30(9), 603. <https://doi.org/10.5732/CJC.011.10226>
- Waterhouse, A. M., Procter, J. B., Martin, D. M. A., Clamp, M., & Barton, G. J. (2009). Jalview Version 2-A multiple sequence alignment editor and analysis workbench. *Bioinformatics*. <https://doi.org/10.1093/bioinformatics/btp033>
- Watson, C. J., & Khaled, W. T. (2008). Mammary development in the embryo and adult: a journey of morphogenesis and commitment. *Development (Cambridge, England)*, 135(6), 995–1003. <https://doi.org/10.1242/DEV.005439>

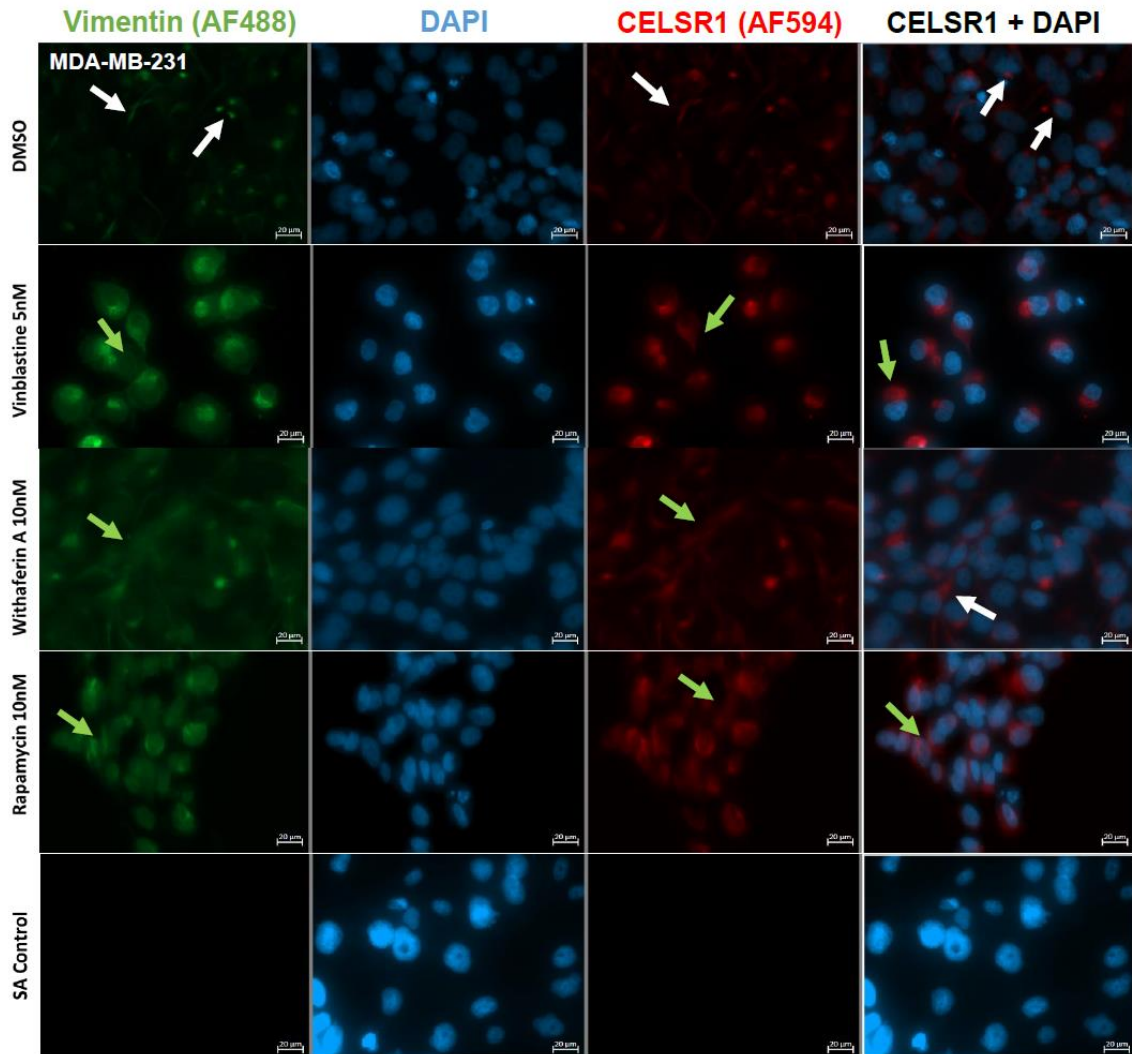
- Wei, S., Qi, L., & Wang, L. (2021). Overexpression of circ_CELSR1 facilitates paclitaxel resistance of ovarian cancer by regulating miR-149-5p/SIK2 axis. *Anti-Cancer Drugs*, 32(5), 496–507. <https://doi.org/10.1097/CAD.0000000000001058>
- Wellings, S. R., & Jensen, H. M. (1973). On the origin and progression of ductal carcinoma in the human breast. *J Natl Cancer Inst*, 50(5), 1111–1118. <http://www.ncbi.nlm.nih.gov/pubmed/4123242>
- Whiteman, E. L., Liu, C. J., Fearon, E. R., & Margolis, B. (2008). The transcription factor snail represses Crumbs3 expression and disrupts apico-basal polarity complexes. *Oncogene*, 27(27), 3875–3879. <https://doi.org/10.1038/ONC.2008.9>
- WHO. (2018). *Cancer*. <https://www.who.int/news-room/fact-sheets/detail/cancer>
- Williams, J. M., & Daniel, C. W. (1983). Mammary Ductal Elongation: Differentiation of Myoepithelium and Basal Lamina during Branching Morphogenesis. In *DEVELOPMENTAL BIOLOGY* (Vol. 97).
- Williams, M., Yen, W., Lu, X., & Sutherland, A. (2014). Distinct apical and basolateral mechanisms drive planar cell polarity-dependent convergent extension of the mouse neural plate. *Developmental Cell*, 29(1), 34–46. <https://doi.org/10.1016/j.devcel.2014.02.007>
- Wilson, P. D. (2011). Apico-basal polarity in polycystic kidney disease epithelia. *Biochimica et Biophysica Acta - Molecular Basis of Disease*. <https://doi.org/10.1016/j.bbadis.2011.05.008>
- Winter, M., Meignan, S., Völkel, P., Angrand, P. O., Chopin, V., Bidan, N., Toillon, R. A., Adriaenssens, E., Lagadec, C., & Le Bourhis, X. (2021). Vimentin Promotes the Aggressiveness of Triple Negative Breast Cancer Cells Surviving Chemotherapeutic Treatment. *Cells*, 10(6). <https://doi.org/10.3390/CELLS10061504>
- Wu, J., & Mlodzik, M. (2008). The frizzled extracellular domain is a ligand for Van Gogh/Stbm during nonautonomous planar cell polarity signaling. *Developmental Cell*, 15(3), 462–469. <https://doi.org/10.1016/J.DEVCEL.2008.08.004>
- Wu, J., & Mlodzik, M. (2017). Wnt/PCP Instructions for Cilia in Left-Right Asymmetry. In *Developmental Cell*. <https://doi.org/10.1016/j.devcel.2017.02.023>
- Wu, Q. L., Zierold, C., & Ranheim, E. A. (2009). Dysregulation of Frizzled 6 is a critical component of B-cell leukemogenesis in a mouse model of chronic lymphocytic leukemia. *Blood*, 113(13), 3031–3039. <https://doi.org/10.1182/blood-2008-06-163303>
- Xia, L., Tan, S., Zhou, Y., Lin, J., Wang, H., Oyang, L., Tian, Y., Liu, L., Su, M., Wang, H., Cao, D., & Liao, Q. (2018). Role of the NFκB-signaling pathway in cancer. *OncoTargets and Therapy*, 11, 2063. <https://doi.org/10.2147/OTT.S161109>
- Xu, C., Tian, G., Jiang, C., Xue, H., Kuerbanjiang, M., Sun, L., Gu, L., Zhou, H., Liu, Y., Zhang, Z., & Xu, Q. (2019). NPTX2 promotes colorectal cancer growth and liver metastasis by the activation of the canonical Wnt/beta-catenin pathway via FZD6. *Cell Death Dis*, 10(3), 217. <https://doi.org/10.1038/s41419-019-1467-7>
- Xu, J., Chen, Y., & Olopade, O. I. (2010). MYC and Breast Cancer. *Genes & Cancer*, 1(6), 629. <https://doi.org/10.1177/1947601910378691>
- Yan, Y., Xu, H., Wang, J., Wu, X., Wen, W., Liang, Y., Wang, L., Liu, F., & Du, X. (2019). Inhibition of breast cancer cells by targeting E2F-1 gene and expressing IL15 oncolytic adenovirus. *Bioscience Reports*, 39(7). <https://doi.org/10.1042/BSR20190384>

- Yang, J., Mani, S. A., Donaher, J. L., Ramaswamy, S., Itzykson, R. A., Come, C., Savagner, P., Gitelman, I., Richardson, A., & Weinberg, R. A. (2004). Twist, a master regulator of morphogenesis, plays an essential role in tumor metastasis. *Cell*, *117*(7), 927–939. <https://doi.org/10.1016/j.cell.2004.06.006>
- Yang, Y., & Mlodzik, M. (2015). Wnt-Frizzled/planar cell polarity signaling: cellular orientation by facing the wind (Wnt). *Annu Rev Cell Dev Biol*, *31*, 623–646. <https://doi.org/10.1146/annurev-cellbio-100814-125315>
- Yates, A. D., Achuthan, P., Akanni, W., Allen, J., Allen, J., Alvarez-Jarreta, J., Amode, M. R., Armean, I. M., Azov, A. G., Bennett, R., Bhai, J., Billis, K., Boddu, S., Marugán, J. C., Cummins, C., Davidson, C., Dodiya, K., Fatima, R., Gall, A., ... Flicek, P. (2020). Ensembl 2020. *Nucleic Acids Research*. <https://doi.org/10.1093/nar/gkz966>
- Yates, L. L., Papakrivopoulou, J., Long, D. A., Goggolidou, P., Connolly, J. O., Woolf, A. S., & Dean, C. H. (2010). The planar cell polarity gene Vangl2 is required for mammalian kidney-branching morphogenesis and glomerular maturation. *Hum Mol Genet*, *19*(23), 4663–4676. <https://doi.org/10.1093/hmg/ddq397>
- Yates, L. L., Schnatwinkel, C., Murdoch, J. N., Bogani, D., Formstone, C. J., Townsend, S., Greenfield, A., Niswander, L. A., & Dean, C. H. (2010). The PCP genes Celsr1 and Vangl2 are required for normal lung branching morphogenesis. *Hum Mol Genet*, *19*(11), 2251–2267. <https://doi.org/10.1093/hmg/ddq104>
- Yersal, O., & Barutca, S. (2014). Biological subtypes of breast cancer: Prognostic and therapeutic implications. *World Journal of Clinical Oncology*, *5*(3), 412. <https://doi.org/10.5306/WJCO.V5.I3.412>
- Yu, S., Graf, W. D., & Shprintzen, R. J. (2012). Genomic disorders on chromosome 22. *Current Opinion in Pediatrics*, *24*(6), 665–671. <https://doi.org/10.1097/MOP.0B013E328358ACD0>
- Yu, S., Kim, T., Yoo, K. H., & Kang, K. (2017). The T47D cell line is an ideal experimental model to elucidate the progesterone-specific effects of a luminal A subtype of breast cancer. *Biochemical and Biophysical Research Communications*, *486*(3), 752–758. <https://doi.org/10.1016/J.BBRC.2017.03.114>
- Zeng, C. M., Chen, Z., & Fu, L. (2018). Frizzled receptors as potential therapeutic targets in human cancers. In *International Journal of Molecular Sciences*. <https://doi.org/10.3390/ijms19051543>
- Zhan, Y. H., Luo, Q. C., Zhang, X. R., Xiao, N. A., Lu, C. X., Yue, C., Wang, N., & Ma, Q. L. (2016). CELSR1 Is a Positive Regulator of Endothelial Cell Migration and Angiogenesis. *Biochemistry. Biokhimiia*, *81*(6), 591–599. <https://doi.org/10.1134/S0006297916060055>
- Zhang, J., Shao, X., Sun, H., Liu, K., Ding, Z., Chen, J., Fang, L., Su, W., Hong, Y., Li, H., & Li, H. (2016). NUMB negatively regulates the epithelial-mesenchymal transition of triple-negative breast cancer by antagonizing Notch signaling. *Oncotarget*, *7*(38), 61036–61053. <https://doi.org/10.18632/ONCOTARGET.11062>
- Zhu, Y., Zhu, X., Tang, C., Guan, X., & Zhang, W. (2021a). Progress and challenges of immunotherapy in triple-negative breast cancer. *Biochimica et Biophysica Acta (BBA) - Reviews on Cancer*, *1876*(2), 188593. <https://doi.org/10.1016/J.BBCAN.2021.188593>
- Zhu, Y., Zhu, X., Tang, C., Guan, X., & Zhang, W. (2021b). Progress and challenges of immunotherapy in triple-negative breast cancer. *Biochimica et Biophysica Acta. Reviews on Cancer*, *1876*(2). <https://doi.org/10.1016/J.BBCAN.2021.188593>

Zou, Z., Tao, T., Li, H., & Zhu, X. (2020). MTOR signaling pathway and mTOR inhibitors in cancer: Progress and challenges. *Cell and Bioscience*, 10(1), 1–11. <https://doi.org/10.1186/S13578-020-00396-1/TABLES/2>

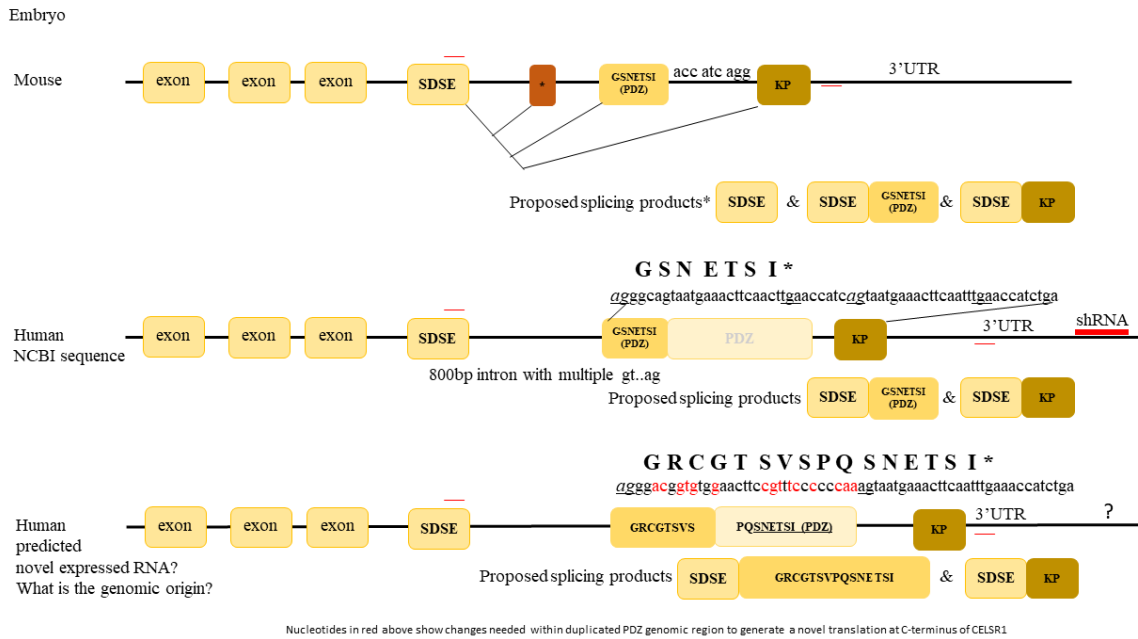
Appendix

Immunostaining of Vinblastine treated MDA-MB231 cells



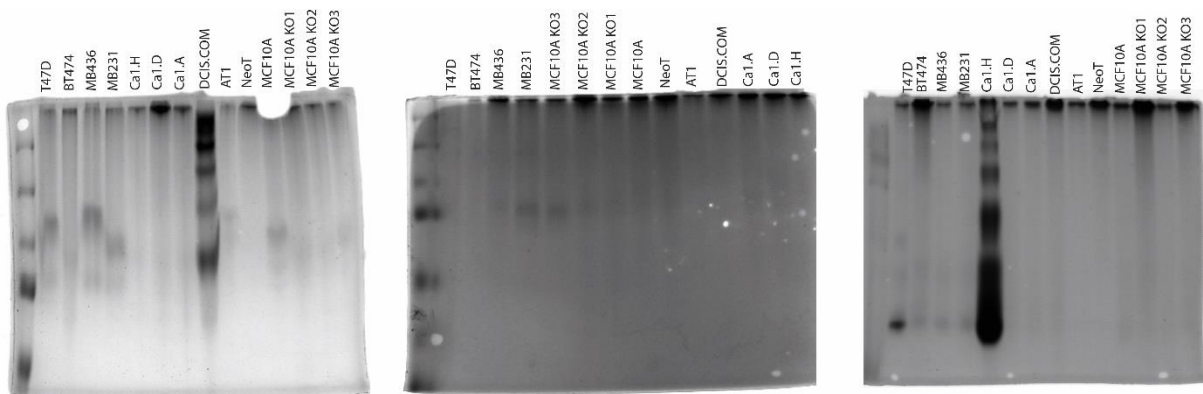
Afig 1 – MDA-MB2931 cells stained with DAPI and CELSR1iso. Top panel shows control with DMSO, staining observed punctate. 2nd row – Treatment with Vinblastine caused CELSR1iso staining to show a blown-out structure likely because of Golgi disruption. 3rd row - Treatment with Withaferin results in CELSR1iso staining looking filamentous. 4th row – Rapamycin treatment shows a more dispersed hallow structure of CELS R1iso staining. 5th row – Secondary antibody only controls. Created By : Ismael&Formstone(2023), personal communication)

Novel CELSR1 PDZ+ variant



AFig 2 – CELSR1 splice variants. Comparison of mouse and human Celsr1/CELSR1 variants and the different splicing products. Bottom diagram is showing the novel PDZ+ variant with the additional nucleotides shown in red and the novel splicing products shown below. Created by: Formstone (2023), personal communication

Coomassie Gels

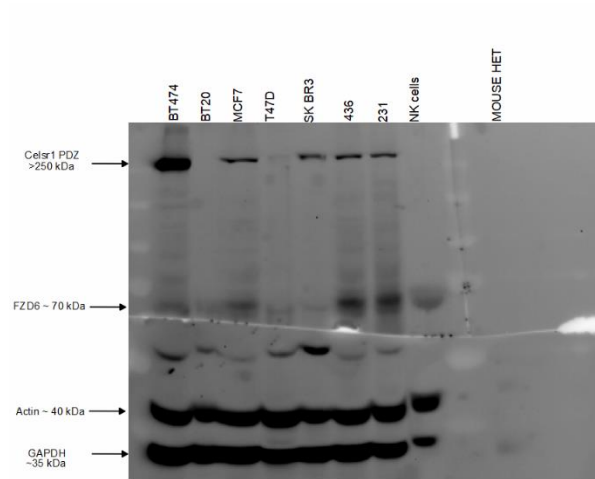


AFig 3 – Coomassie stained SDS-PAGE gels. The most recent SDS-PAGE gels stained with Coomassie brilliant blue showing the increasingly more sample aggregating at the top of the gel (left-right).

Western blot collection

2020

1.

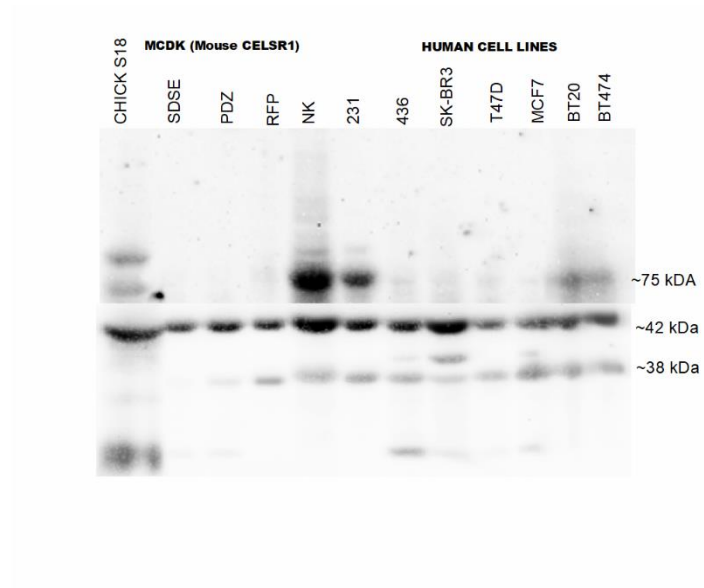


Afig 4 – WB1. Western blot with CELSR1iso antibody. Actin and GAPDH were used as loading controls. The blot was cut. NK cells are used as a control.

Antibodies:	CELSR1 PDZ (pB), FZD6
Blot cut?:	Yes
Incubation:	CELSR1 PDZ (pB) incubated separately. FZD6, Actin, GAPDH incubated together.
Controls:	NK cells

2021

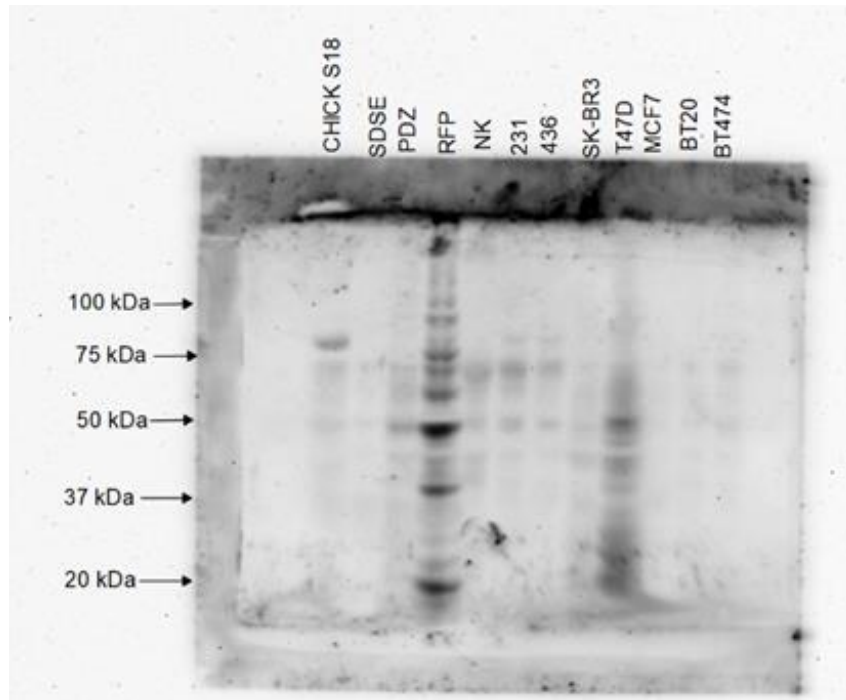
1.



Afig 5 – WB2. Western blot with CELSR1 EKL antibody. Actin and GAPDH were used as loading controls. Bands were non specific

Antibodies:	CELSR1 EKL (pA)
Blot cut?:	No
Incubation:	Primaries together. Secondaries for Actin/GAPDH separately.
Controls:	NK, RFP, PDZ, SDSE, ChickS18

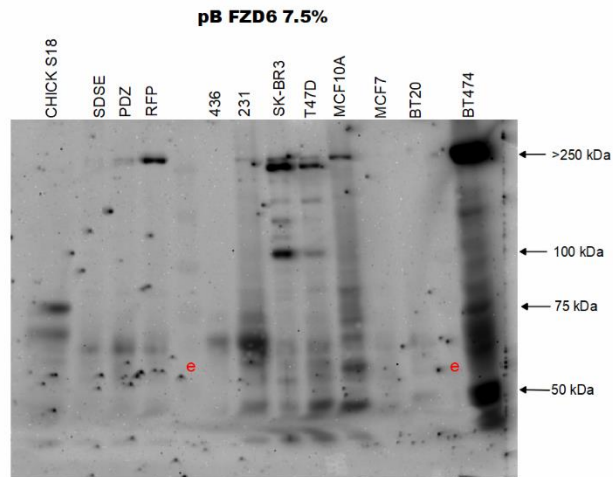
2.



Afig 6- WB3. Western blot with CELSR1 EKL antibody. Non specific bands.

Antibodies:	CELSR1 EKL (pA)/PDZ (pB)
Blot cut?:	No
Incubation:	Primaries incubated together
Controls:	NK, RFP, PDZ, SDSE, ChickS18

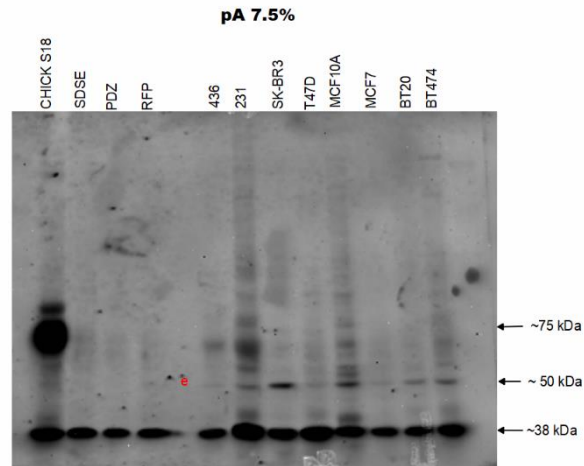
4.



A Fig 7 – WB4. Western blot with CELSR1iso antibody and FZD6 (CST) antibody. Controls did not work. e denotes an empty lane.

Antibodies:	CELSR1 PDZ (pB)
Blot cut?:	No
Incubation:	Primaries together. Actin/GAPDH secondaries together
Controls:	RFP, PDZ, SDSE, ChickS18

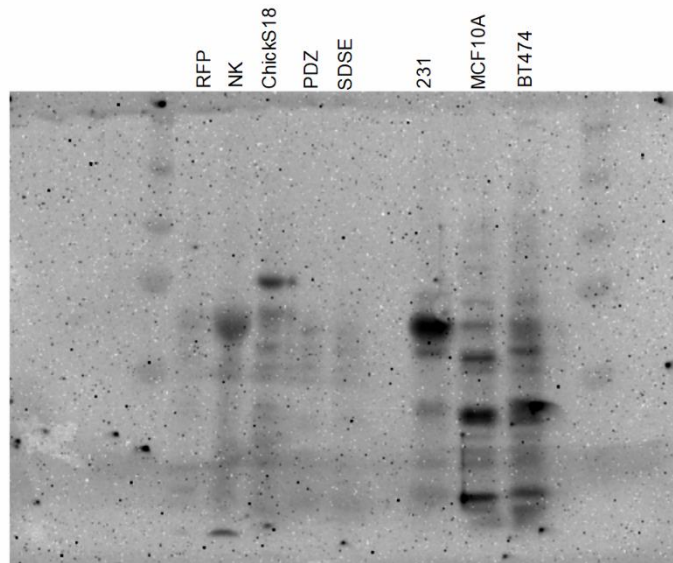
5.



AFig 8 – WB5. Western blot with CELSR1 EKL antibody. Actin and GAPDH were used as controls. CELSR1 staining was non-specific.

Antibodies:	anti-CELSR1 EKL(pA), actin, GAPDH
Blot cut?:	No
Incubation:	Primaries and secondaries together
Controls:	RFP, PDZ, SDSE, ChickS18

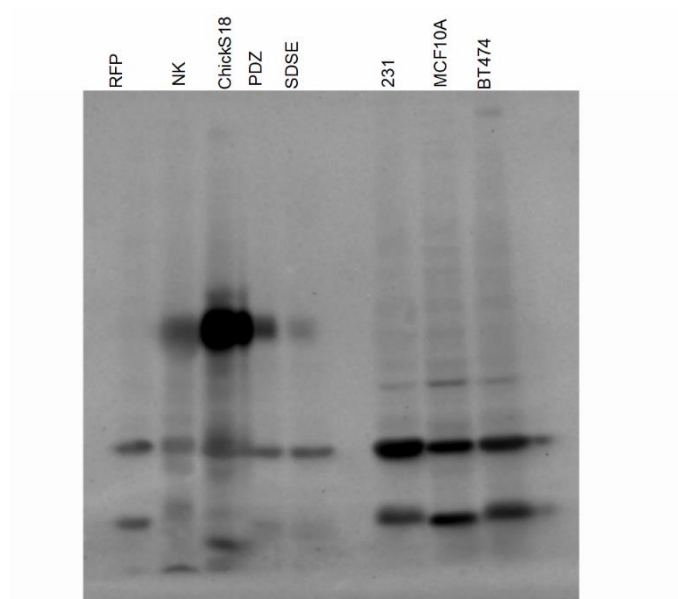
6.



AFig 9 – WB6. Western blot with CELSR1 EKL antibody. CELSR1 staining was non-specific

Antibodies:	anti-CELSR1 EKL (pA)
Blot cut?:	No
Incubation:	anti-CELSR1 EKL (pA) only
Controls:	SDSE, PDZ, ChickS18, NK, RFP

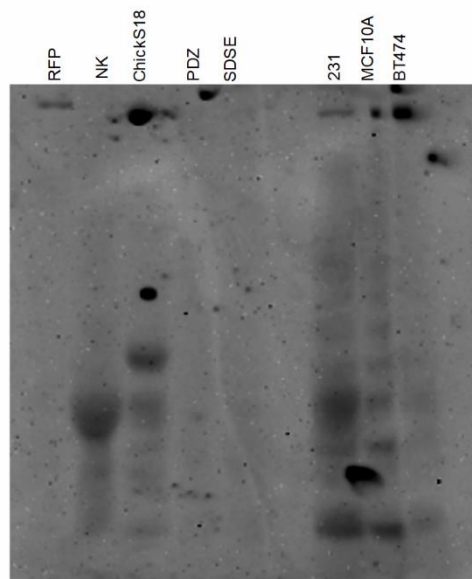
7.



Afig 10 – WB7. Western blot with CELSR1 EKL antibody. Actin and GAPDH were used as controls. CELSR1 staining was non-specific

Antibodies:	anti-CELSR1 EKL (pA)/Actin, GAPDH
Blot cut?:	No
Incubation:	Primaries together. Secondaries for actin/GAPDH separately.
Controls:	SDSE, PDZ, ChickS18, NK, RFP

8.

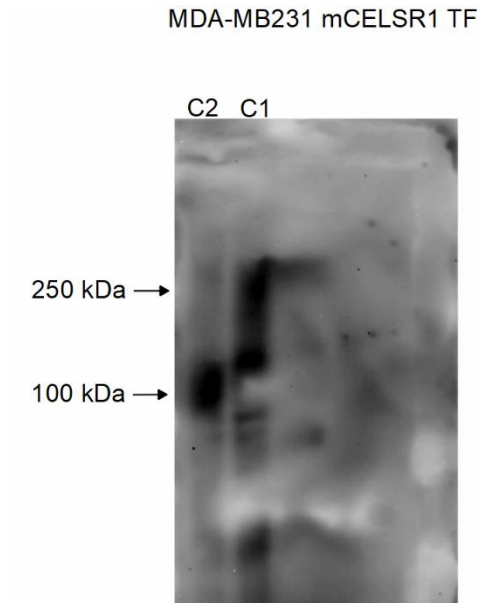


Afig 11 – WB8. Western blot with CELSR1 PDZ antibody. No controls were used so all CELSR1 related bands could be seen

Antibodies:	anti-CELSR1 PDZ (pB)
Blot cut?:	No
Incubation:	Primaries together. Actin/GAPDH secondaries incubated separately (did not work)
Controls:	SDSE, PDZ, ChickS18, NK, RFP

October

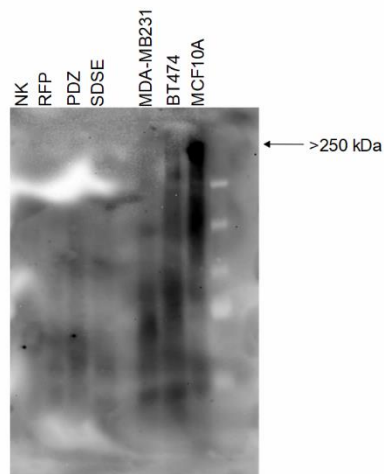
9.



A Fig 12 - WB9. Western blot of mCelsr1 MDA-MB231 cell lines with anti-GFP antibody. C1 and C2 denote the 2 individual clones. No controls were used

Antibodies:	anti-GFP
Blot cut?:	No
Incubation:	Whole blot incubated with anti-GFP only
Controls:	None

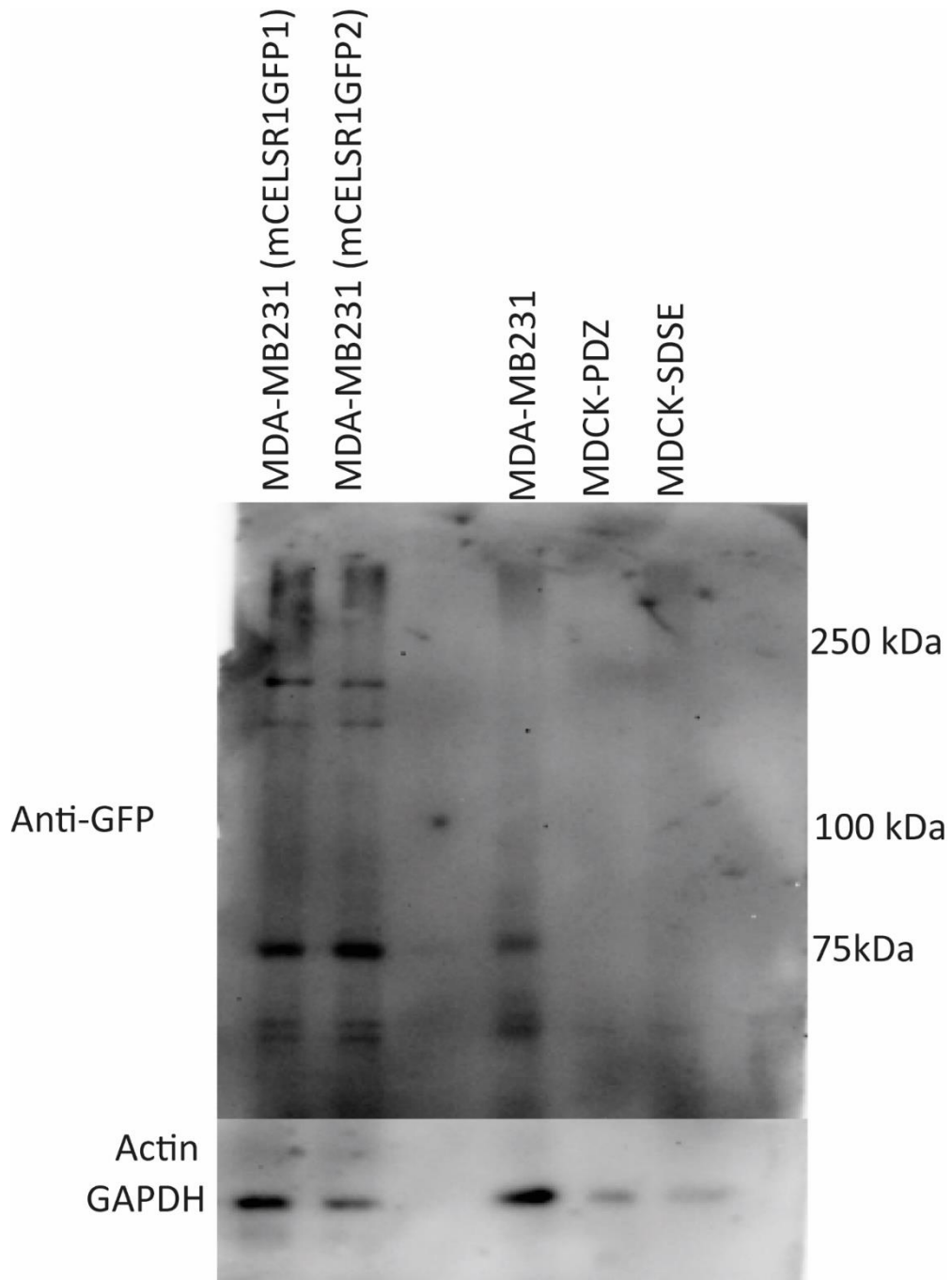
10.



A Fig 13 - WB10. First western blot with CELSR1sc antibody to test specificity

Antibodies:	CELSR1 (SC)
Blot cut?:	No
Incubation:	Whole blot incubated with anti-CELSR1 SC
Controls:	MCF10A, BT474, MDA-MB231

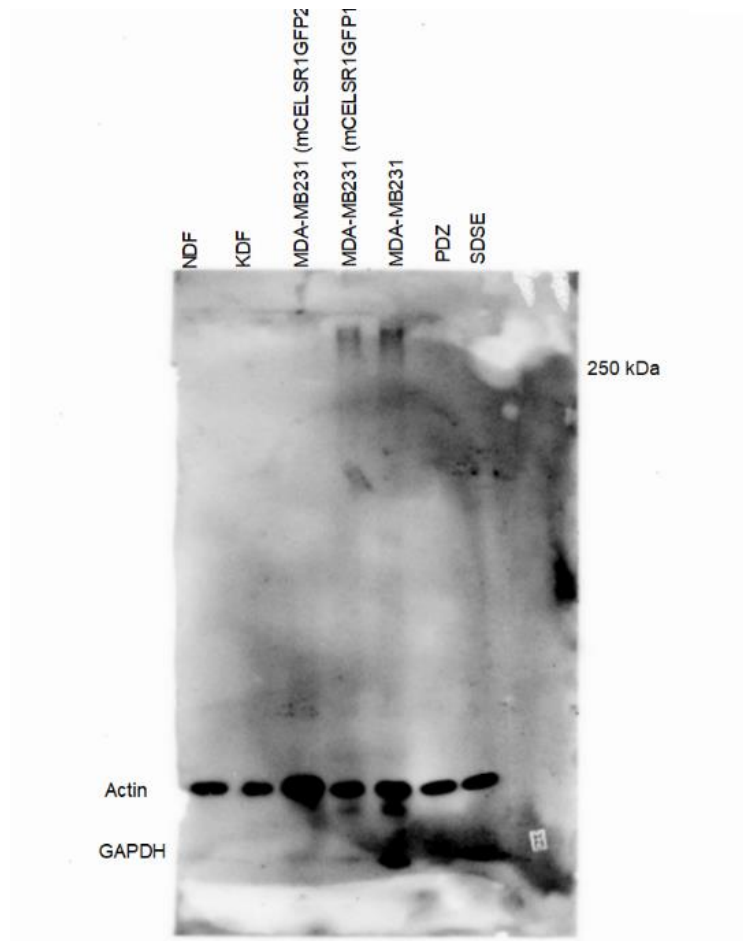
15.



Afig 14 – WB14. Western blot of mCelsr1 MDA-MB231 cell lines with anti-GFP antibody. Actin and GAPDH were used as loading controls.

Antibodies:	Anti-GFP
Blot cut?:	No
Incubation:	Primaries together. Secondaries for Actin/GAPDH separately
Controls:	SDSE/PDZ/ MDA-MB231

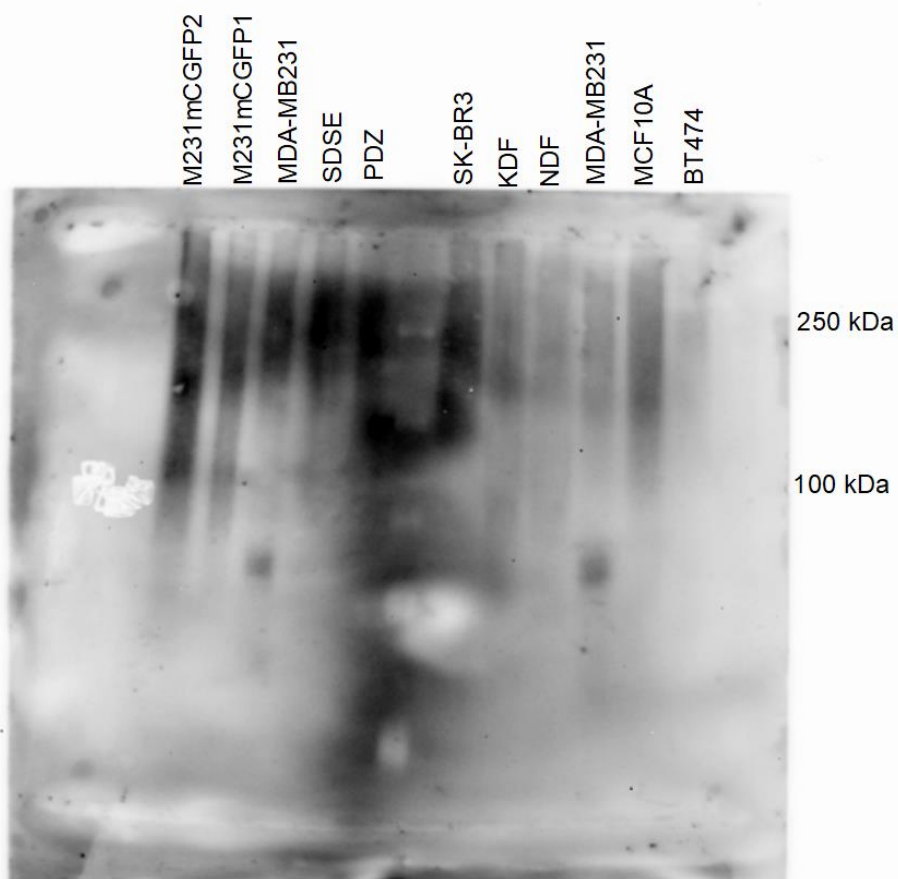
16.



Afig 15 – WB15. Western blot of mCelsr1 MDA-MB231 cell lines with anti-GFP antibody. Actin and GAPDH were used as loading controls.

Antibodies:	CELSR1-PDZ (pB), Actin, GAPDH
Blot cut?:	No
Incubation:	Primaries together. Secondaries for Actin/GAPDH separately
Controls:	PDZ/SDSE/MDA-MB231

17.

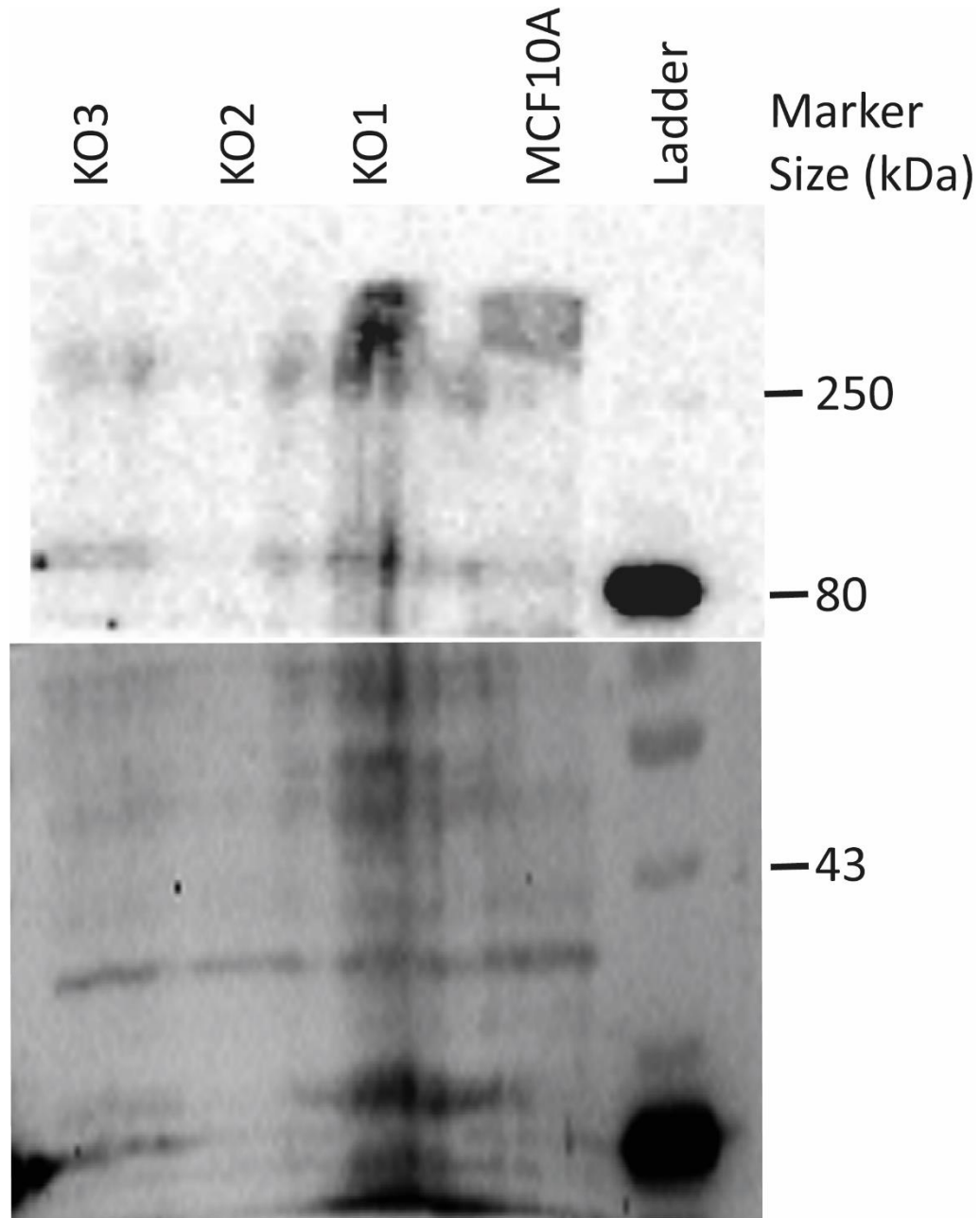


Afig 16 – WB16. Western blot with CELSR1iso antibody. No controls.

Antibodies:	CELSR1-PDZ (pB)
Blot cut?:	No
Incubation:	Primaries together. Actin/GAPDH separately.
Controls:	SDSE/PDZ/231/SK-BR3

2023

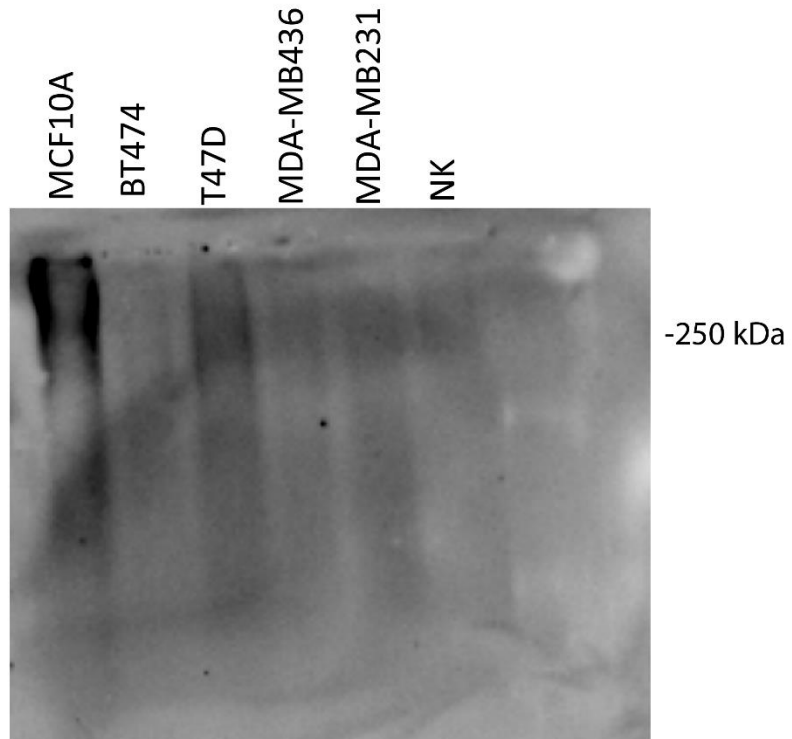
1.



Afig 17 - WB17. Western blot using CELSR1sc and actin as loading control. Semi-dry method used for transfer.

Antibodies:	CELSR1sc/Actin
Blot cut?:	Yes
Incubation:	Separately
Controls:	MCF10A

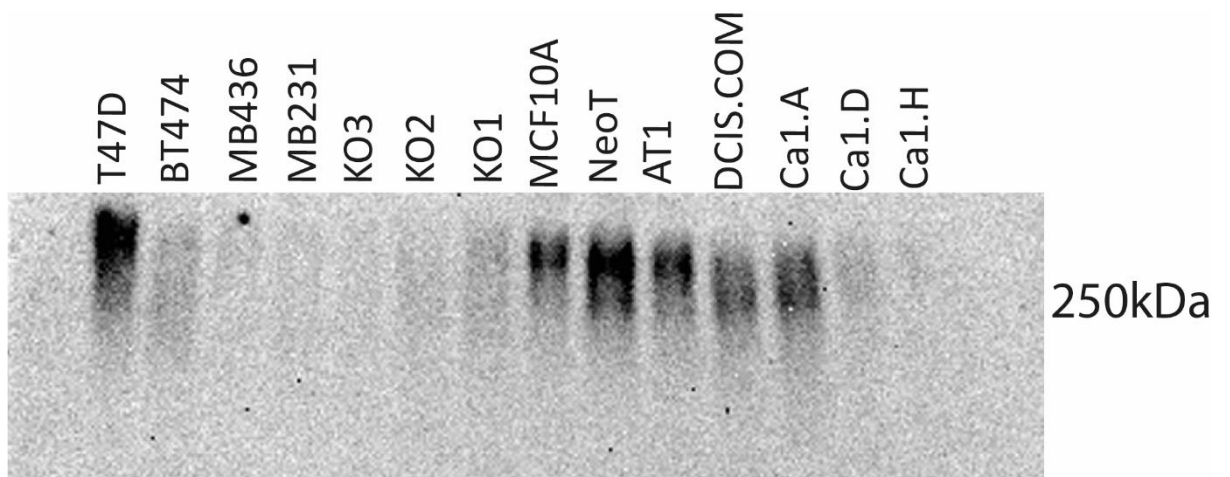
2.



A Fig 18 – WB18. Western blot using CELSR1sc. Semi-dry method used for transfer. Loading control did not work.

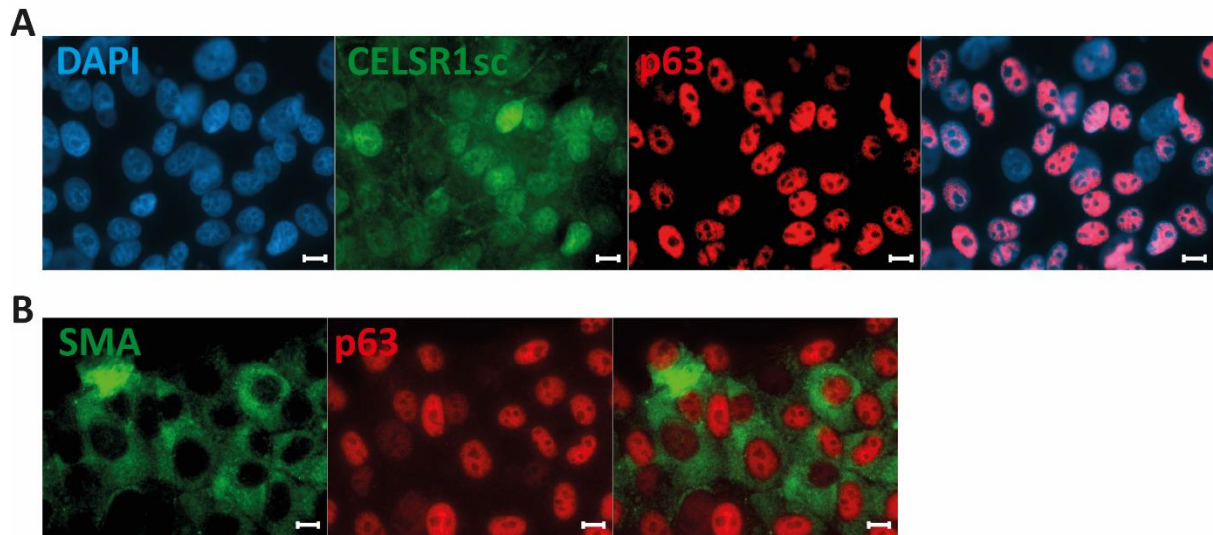
Antibodies:	CELSR1sc
Blot cut?:	Yes
Incubation:	Separately Semi-dry transfer
Controls:	MCF10A/NK

3.



Afig 19 – WB19. Western blot using CELSR1sc antibody. Controls did not work. Semi-dry transfer method was used.

Antibodies:	CELSR1sc
Blot cut?:	Yes
Incubation:	Separately Semi-dry transfer
Controls:	MCF10A/NK



AFig 20 – MCF10A cells express smooth muscle actin and P63. A. MCF10A cells express P63. B. MCF10A cells express SMA and P63.